

**MICROWAVE-ASSISTED EXTRACTION AND SYNTHESIS  
STUDIES AND THE SCALE-UP STUDY WITH THE AID OF  
FDTD SIMULATION**

**By**

**Jianming Dai**

**Department of Bioresource Engineering  
Macdonald Campus, McGill University  
Montreal, QC, Canada**

**February 2006**

**A thesis submitted to McGill University in partial fulfilment of the  
requirements of the degree of Doctor of Philosophy**

**© Jianming Dai 2006**



Library and  
Archives Canada

Bibliothèque et  
Archives Canada

Published Heritage  
Branch

Direction du  
Patrimoine de l'édition

395 Wellington Street  
Ottawa ON K1A 0N4  
Canada

395, rue Wellington  
Ottawa ON K1A 0N4  
Canada

*Your file    Votre référence*

*ISBN: 978-0-494-25123-2*

*Our file    Notre référence*

*ISBN: 978-0-494-25123-2*

#### NOTICE:

The author has granted a non-exclusive license allowing Library and Archives Canada to reproduce, publish, archive, preserve, conserve, communicate to the public by telecommunication or on the Internet, loan, distribute and sell theses worldwide, for commercial or non-commercial purposes, in microform, paper, electronic and/or any other formats.

The author retains copyright ownership and moral rights in this thesis. Neither the thesis nor substantial extracts from it may be printed or otherwise reproduced without the author's permission.

#### AVIS:

L'auteur a accordé une licence non exclusive permettant à la Bibliothèque et Archives Canada de reproduire, publier, archiver, sauvegarder, conserver, transmettre au public par télécommunication ou par l'Internet, prêter, distribuer et vendre des thèses partout dans le monde, à des fins commerciales ou autres, sur support microforme, papier, électronique et/ou autres formats.

L'auteur conserve la propriété du droit d'auteur et des droits moraux qui protègent cette thèse. Ni la thèse ni des extraits substantiels de celle-ci ne doivent être imprimés ou autrement reproduits sans son autorisation.

---

In compliance with the Canadian Privacy Act some supporting forms may have been removed from this thesis.

Conformément à la loi canadienne sur la protection de la vie privée, quelques formulaires secondaires ont été enlevés de cette thèse.

While these forms may be included in the document page count, their removal does not represent any loss of content from the thesis.

Bien que ces formulaires aient inclus dans la pagination, il n'y aura aucun contenu manquant.

  
**Canada**

**Suggested Short Title**

**MICROWAVE-ASSISTED EXTRACTION AND SYNTHESIS AND THE FDTD  
SIMULATED SCALE-UP**

## **ABSTRACT**

Jianming Dai

Ph.D. (Bioresource Engineering)

### **MICROWAVE-ASSISTED EXTRACTION AND SYNTHESIS STUDIES AND THE SCALE-UP STUDY WITH THE AID OF FDTD SIMULATION**

The research undertaken in this thesis includes microwave-assisted extraction (MAE), synthesis, and the investigation of the scale-up of the microwave-assisted processes with the numerical aid.

The main goal of this research is to study the various problems associated with the scale-up of the microwave-assisted extraction and synthesis processes. Laboratory studies were carried out to investigate the microwave-assisted extraction of known components from peppermint leaves and American ginseng. Various factors that influence the extraction processes were studied. Microwave-assisted extraction method was compared with conventional heating and room temperature extraction methods on the extraction of ginsenosides from American ginseng. Microwave-assisted extraction method was determined to have higher extraction rate than both room temperature extraction and reflux temperature extraction using hotplate heating indicating that there is acceleration factor in enhancing the extraction rate beyond the temperature influence.

In the study of synthesizing n-butyl paraben, microwave-assisted synthesis was observed to greatly increase the yield of n-butyl paraben in much shorter period of time compared to the classic synthesis method. A transition state theory was proposed to explain this rate enhancement. The study of the synthesis of parabens with different alcohol and the influencing factors on the synthesis of n-butyl paraben yield were also studied.

A visualization method was developed to determine the microwave distribution in a domestic microwave cavity. The method uses gypsum plate as carrier and



cobalt chloride as indicator. A simulation program was developed using the finite difference time domain (FDTD) approach and written in C programming language. The program was proved to be very versatile in different type of cavity simulation. Not only cavities with different dimensions and geometrical designs can be simulated, multiple magnetrons and various ways of magnetron placement can also be integrated into the simulation program. The detailed power distribution can be visualized in a 3-D plot, and the power distribution in each layer can be analyzed using the simulation result. The power distribution information will be very useful and necessary before any real equipment development.

## RÉSUMÉ

Jianming Dai

Ph.D. (Génie des bioressources)

### **Études des procédés d'extraction et de synthèse aux micro-ondes et modélisation de leurs applications à grande échelle à l'aide d'un simulateur DFDT**

Les travaux de recherche entrepris lors de cette étude couvrent les procédés d'extraction et de synthèse aux micro-ondes et le développement d'un modèle numérique pour leurs applications à grande échelle.

L'objectif principal de cette recherche était d'étudier les difficultés associées à l'utilisation des procédés d'extraction et de synthèse aux micro-ondes à l'échelle commerciale. Des essais en laboratoire ont été effectués pour étudier les facteurs affectant l'extraction des composés actifs du ginseng américain et de la menthe poivrée. L'extraction aux micro-ondes des ginsenosides du ginseng américain a été comparée à une procédure d'extraction à reflux, opérant à la même température, avec chauffage conventionnel et à une procédure d'extraction avec agitation conduite à la température de la pièce. Les résultats ont démontré que l'extraction aux micro-ondes permettait d'avoir des rendements plus élevés que les deux autres méthodes étudiées. Cette observation a révélé la présence d'un facteur accélérant des taux d'extraction au-delà de l'effet de la température. Des résultats similaires ont été observés lors des essais effectués sur la menthe poivrée.

Des essais ont été faits pour comparer la méthode de synthèse aux micro-ondes du n-butyle parabène à la méthode conventionnelle. Cette étude a démontré que l'utilisation des micro-ondes permettait d'accroître de façon marquée les rendements en n-butyle parabène tout en diminuant

considérablement les temps de réaction. Une théorie basée sur l'état transitoire a été proposée pour expliquer les phénomènes observés. Les résultats sur la synthèse des parabènes à l'aide de différents alcools ainsi que des facteurs affectant le processus sont aussi discutés.

Un simulateur numérique utilisant les différences finies à dimension temporelle (DFDT) a été conçu pour visualiser la distribution des micro-ondes et de l'énergie dans les cavités micro-ondes. Le modèle permet de prendre en compte plusieurs types de cavités de dimensions et de géométries variées ainsi que l'utilisation et l'emplacement d'une ou de plusieurs sources de micro-ondes. La simulation permet d'établir et de visualiser, à l'aide de graphique en trois dimensions, la distribution de la puissance à l'intérieur de la cavité. Des plaques de gypse contenant un indicateur au chlorure de cobalt et un four à micro-ondes domestique ont permis de valider les résultats du simulateur numérique. La connaissance de la distribution des micro-ondes est essentielle au développement d'appareils commerciaux performants.

## **ACKNOWLEDGEMENTS**

First of all, I wish to express my deep gratitude to my supervisor, Dr. G.S. Vijaya Raghavan, James McGill Professor, Department of Bioresource Engineering of McGill University for his guidance, support, and encouragement. Wonderful ideas can just sparkle during the conversation with him. My gratefulness is beyond any word can express.

Many thanks to Prof. V. Yaylayan, Department of Food Science and Agricultural Chemistry for allowing me to access his various experimental equipments and also for his constructive suggestions in the research work. I also wish to thank Prof. M. Ngadi, Department of Bioresource Engineering for allowing me to use his lab.

My deep gratitude goes to Prof. Zhun Liu, the research Institute of Elemento-organic Chemistry, Nankai University, Tianjin, China. His constructive advice and suggestions are valuable for this research work. I wish also to thank Ms. Chuanxiang Zhang, Prof. Guiling Sun, Prof. Weixiang Li, and Prof. Tianren Ji for their help.

Many thanks to Dr. Valérie Orsat, Dr. Yvan Gariepy and Dr. Sam Sotocinal for their help.

I am grateful to my parents and parents in law for their solid support no matter where I am. I would like to thank my wife, Mingfei Yuan for her support and encouragement. When I was sick, when I was stressed she was always ready to take care of me, to encourage me and to convince me that there is nothing I can not accomplish.

I wish to thank Amy Wong scholarship, Canadian International Development Agency (CIDA), and Natural Science and Engineering Research Council of Canada (NSERC) for their financial support.

## TABLE OF CONTENTS

<b>ABSTRACT</b> .....	i
<b>RÉSUMÉ</b> .....	iii
<b>ACKNOWLEDGEMENTS</b> .....	v
<b>TABLE OF CONTENTS</b> .....	vi
<b>LIST OF FIGURES</b> .....	xi
<b>LIST OF TABLES</b> .....	xxiii
<b>LIST OF SCHEMES</b> .....	xxv
<b>NOMENCLATURE</b> .....	xxvi
<b>CHAPTER I: GENERAL INTRODUCTION</b> .....	1
1.1 Background .....	1
1.2 Objectives .....	2
<b>CHAPTER II: LITERATURE REVIEW</b> .....	4
2. 1 Microwaves and microwave-matter interaction .....	4
2.2 Microwave-assisted Extraction (MAE) .....	6
2.2.1 A brief history of microwave-assisted extraction .....	7
2.2.2 Advantages of MAE over conventional extraction methods .....	8
2.2.3 Mechanism of microwave accelerating effect .....	13
2.2.4 Laboratory equipment for microwave-assisted extraction .....	15
2.2.5. The scale-up of microwave-assisted extraction .....	19
2.3 Microwave-assisted synthesis.....	20
2.3.1 General advantage of microwave-assisted synthesis .....	21
2.3.1.1 Rate enhancement .....	21
2.3.1.2 Improved yield .....	22
2.3.1.3 Selectivity .....	23
2.3.2 Basic types of microwave-assisted organic synthesis and possible mechanisms .....	24
2.3.2.1 Pressurized microwave-assisted organic synthesis .....	24
2.3.2.2 Open vessel microwave assisted synthesis .....	24
2.3.2.3 Solvent free reaction .....	25
2.4 Simulation of microwave energy distribution .....	25
2.4.1 Lambert's Law .....	26
2.4.2 Solving Maxwell's Equation .....	26
2.5 Summary .....	29
<b>CONNECTING STATEMENT 1</b> .....	30
<b>CHAPTER III: INVESTIGATION OF VARIOUS FACTORS ON THE EXTRACTION OF PEPPERMINT (<i>MENTHA PIPERITA</i> L.) LEAVES</b> .....	31
3.1 Abstract .....	31
3.2 Introduction .....	31

3.3 Material and Methods.....	32
3.3.1 Materials .....	32
3.3.2 Experimental Design .....	32
3.3.3 Extraction Procedures .....	34
3.3.4 GC analysis .....	34
3.3.5 Statistical analysis .....	35
3.4 Results and Discussion .....	35
3.5 Conclusion .....	40
3.6 Acknowledgment .....	41
3.7 References .....	41
CONNECTING STATEMENT 2 .....	43
<b>CHAPTER IV: INVESTIGATION OF DIFFERENT FACTORS ON THE EXTRACTION OF GINSENOSIDES FROM FRESH AMERICAN GINSENG (PANAX QUINQUEFOLIUM L.) ROOT</b>	<b>44</b>
4.1 Abstract .....	44
4.2 Introduction .....	44
4.3 MATERIAL AND METHODS .....	45
4.3.1 Materials .....	45
4.3.2 Experimental Design .....	45
4.3.3 Extraction Procedures.....	46
4.3.4 HPLC Analysis.....	46
4.3.5 Statistical analysis .....	47
4.4 Results and discussion .....	47
4.5 Conclusion .....	55
4.6 Acknowledgment .....	55
4.7 References .....	55
CONNECTING STATEMENT 3 .....	57
<b>CHAPTER V: EXTRACTION OF GINSENOSIDES FROM AMERICAN GINSENG (PANAX QUINQUEFOLIUM L.) ROOT WITH DIFFERENT EXTRACTION METHODS AND CHROMATOGRAPHIC ANALYSIS OF THE EXTRACTS</b>	<b>58</b>
5.1 Abstract .....	58
5.2 Introduction .....	58
5.3 Material and Methods .....	59
5.3.1 Fresh American Ginseng Roots .....	59
5.3.2 Ginsenosides Content of the American Ginseng Root .....	60
5.3.3 Extraction Procedures for Comparing Different Extraction Methods .....	60
5.3.4 HPLC Analysis .....	60
5.3.5 Calibration with Standards .....	61
5.3.6 Statistical Analysis .....	61
5.4 Results and Discussion .....	61

5.4.1 Extraction of ginsenosides with three extraction methods .....	61
5.4.2 Comparison of the extraction rates.....	64
5.4.3 Chromatographic Analysis.....	70
5.5 Conclusion .....	72
5.6 Acknowledgement .....	72
5.7 References .....	72
CONNECTING STATEMENT 4 .....	75
<b>CHAPTER VI: MICROWAVE-ASSISTED SYNTHESIS OF N-BUTYL PARABEN USING ZnCl<sub>2</sub> AS CATALYST .....</b>	<b>76</b>
6.1 Abstract .....	76
6.2 Introduction .....	76
6.3 Fundamentals of microwave-assisted synthesis.....	77
6.3.1 Microwaves .....	77
6.3.2 Microwave-matter interaction .....	77
6.3.3 Mechanism of Microwave-assisted synthesis .....	78
6.4 Material and methods .....	79
6.4.1 Materials .....	79
6.4.2 Experimental procedure.....	80
6.4.3 Microwave-assisted synthesis .....	80
6.4.4 Conventional heating method .....	80
6.4.5 GC analysis .....	80
6.5 Results and discussion .....	81
6.6 Conclusions .....	82
6.7 Acknowledgement .....	83
6.8 References .....	83
CONNECTING STATEMENT 5 .....	84
<b>CHAPTER VII: ZnCl<sub>2</sub> CATALYZED SYNTHESIS OF VARIOUS PARABENS UNDER MICROWAVE IRRADIATION .....</b>	<b>85</b>
7.1 Abstract .....	85
7.2 Introduction .....	85
7.3 Material and methods .....	86
7.3.1 Materials .....	86
7.3.2 Experimental procedure .....	86
7.3.3 Temperature profile .....	86
7.3.4 Synthesis of n-butyl paraben under controlled temperature ...	87
7.3.5 Reaction of p-hydroxybenzoic acid with different alcohols .....	87
7.3.6 Interaction of ZnCl <sub>2</sub> with microwaves.....	87
7.3.7 GC/MS analysis .....	87
7.3.7.1 GC/MS conditions.....	87
7.3.7.2 Calibration .....	88

7.4 Results and discussion .....	89
7.5 Conclusions .....	101
7.6 Acknowledgement .....	101
7.7 References .....	101
CONNECTING STATEMENT 6 .....	103
<b>CHAPTER VIII: INFLUENCE OF VARIOUS FACTORS ON THE SYNTHESIS OF N-BUTYL- PARABEN USING <math>ZnCl_2</math> AS CATALYST UNDER MICROWAVE IRRADIATION .....</b>	
8.1 Abstract .....	104
8.2 Introduction.....	104
8.3 Material and methods.....	105
8.3.1 Materials .....	105
8.3.2 Experimental procedure .....	105
8.3.3 A two-level study using an $L_8(2^7)$ orthogonal array .....	105
8.3.4 A four-level study using an $L_{16}(4^5)$ orthogonal array .....	106
8.3.5 GC/MS analysis .....	106
8.3.5.1 GC/MS conditions .....	106
8.3.5.2 Calibration .....	106
8.3.5.3 Determination of the conversion percentage.....	106
8.3.5.4 Statistical Analysis.....	107
8.4 Results and discussion .....	110
8.5 Conclusions .....	119
8.6 Acknowledgment .....	119
8.7 References .....	120
CONNECTING STATEMENT 7 .....	121
<b>CHAPTER IX: VISUALIZATION OF MICROWAVE ENERGY DISTRIBUTION IN A MULTIMODE MICROWAVE CAVITY USING <math>CoCl_2</math> ON GYPSUM PLATES .....</b>	
9.1. Abstract .....	122
9.2. Introduction .....	122
9.3. Principle of the Method .....	123
9.4. Material and Methods .....	124
9.4.1. Gypsum plate preparation.....	124
9.4.2. Experimental setup.....	125
9.4.3. Experimental procedures.....	126
9.5. Results and Discussion .....	127
9.6. Conclusions .....	134
9.6 Acknowledgment .....	134
9.7. References.....	134



CONNECTING STATEMENT 8 .....	136
<b>CHAPTER X: FDTD SIMULATION OF MICROWAVE DISTRIBUTION AND ASSIST IN THE DESIGN OF SCALED-UP MICROWAVE-ASSISTED EXTRACTION AND SYNTHESIS EQUIPMENT .....</b>	<b>137</b>
10.1. Abstract .....	137
10.2. Introduction .....	137
10.3. The Model .....	138
10.3.1. Maxwell's equations .....	138
10.3.2. The Yee scheme .....	140
10.3.3. Finite difference approximation and implementation in C language.....	141
10.3.4. The stability Criteria .....	143
10.3.5. Boundary conditions.....	144
10.3.6. Dielectric properties of the object simulated .....	144
10.3.7. Power dissipation .....	145
10.3.8 Power source .....	146
10.3.9. Programming using C language.....	147
10.4 Simulation of a domestic microwave oven .....	147
10.4.1 Power distribution with a lossy dielectric plate inserted in the cavity .....	148
10.4.2 Power dissipation into multiple lossy dielectric plates .....	152
10.4.3. E field distribution and the influence of lossy dielectric materials on the E field distributions .....	169
10.4.4. Experimental evaluation of the simulation .....	173
10.5. Simulation of an oven-type chemical reactor/extractor. ....	174
10.6 Simulation of a microwave chemical reactor/extractor .....	193
10.7 Conclusions.....	212
10.8 Acknowledgment .....	213
10.9 Reference .....	213
<b>CHAPTER XI: GENERAL CONCLUSION, CONTRIBUTION TO KNOWLEDGE AND RECOMMENDATIONS FOR FUTURE RESEARCH ....</b>	<b>216</b>
11.1 General conclusions 245e oven type of reactor with multiple magnetrons and glassware inside the cavity.....	216
11.2 Contribution to knowledge .....	218
11.3 Recommendations for future research .....	219
<b>REFERENCES.....</b>	<b>220</b>
Appendix 1.....	232
Appendix 2:.....	243
Appendix 3 .....	246:
Appendix 4 .....	249

## LIST OF FIGURES

Fig. 2.1	Locations of microwaves on the electromagnetic spectrum. ....	4
Fig. 2.2	Comparison of MAE with conventional extraction methods: Material A – large pieces (5-10 mm in diameter and 3-5 mm in thickness); Material B – unrefined powder (about 5 – 10 mesh); and Material C – Powder (50 mesh). Extraction conditions (sample 10 g): Heat reflux – sequential solvent 100 mL for 1.5 h, 80 mL for 1.5 h and 80 mL for 1.5 h; Ultrasonic extraction – solvent 200 mL in ultrasonic for 30 min followed by extraction at room temperature for 20 h; Soxhlet – solvent 200 mL for 10 h; Soxhlet-MAE – solvent 200 mL for 5 h by Soxhlet and residue with solvent 100 mL and MAE for 4 min; ERT – sample 3 g in solvent 30 mL extracted at room temperature for 20 h; MAE – solvent 100 mL in microwave irradiation for 4 min. ....	9
Fig. 2.3	Scanning electron micrograph of (A) Untreated fresh mint gland; (B) Soxhlet extraction for 6 hrs; (C) Microwave irradiation for 20 s .....	14
Fig. 2.4	Untreated leaf showing globular whole glands (10 $\mu$ m bar, 200 x magnification) .....	16
Fig. 2.5	Glands collapsed to varying degree in leaves extracted with hexane at 200 W, $\Delta T$ c. 10 $^{\circ}$ C (100 $\mu$ m bar, 100 x magnifications) .....	16
Fig. 2.6	Shrivelled collapsed glands in extractions carried out using ethanol at a constant temperature of 35 $^{\circ}$ C (10 $\mu$ m bar, 200 x magnifications).....	17
Fig. 2.7	Glands transformed into deeply sunken cavities after extraction in 90 mol% ethanol at 35 $^{\circ}$ C (100 $\mu$ m bar, 100 x magnification) .....	17
Fig. 2.8	Glands that have ruptured completely in isothermal extraction carried out with 90 mol% hexane at 35 $^{\circ}$ C (100 $\mu$ m bar, 100 x magnification) .....	18
Fig. 2.9	Schematic diagram of the microwave reactor for MAE .....	18
Fig. 2.10	Schematic view of focused microwave oven (a) and Multimode microwave oven (b) .....	19
Fig. 2.11	A schematic diagram of a scaled-up microwave-assisted extraction equipment .....	20

Fig. 3.1 Influence of extraction methods on the amount of menthone, menthofuran, and menthol extracted .....	38
Fig. 3.2 Influence of solvents on the amount of menthone, menthofuran, and menthol extracted .....	38
Fig. 3.3 Influence of extraction time on the amount of menthone, menthofuran, and menthol extracted.....	39
Fig. 3.4 Influence of sample/solvent ratio on the amount of menthone, menthofuran, and menthol extracted .....	39
Fig. 3.5 Contribution of different factors on the extraction efficacy: (a) menthone (b) menthofuran, and (c) menthol; A: Extraction method, B: Solvent, C: Extraction time, D: Sample/solvent ratio .....	40
Fig. 4.1 HPLC chromatograph of aqueous methanol extracts of American ginseng root .....	49
Fig. 4.2 Influence of extraction methods on the amount of ginsenosides extracted .....	50
Fig. 4.3 Influence of solvents on the amount of ginsenosides extracted .....	52
Fig. 4.4 Influence of sample/solvent ratio on the amount of ginsenosides extracted .....	52
Fig. 4.5 Influence of extraction time on the amount of ginsenosides extracted .....	53
Fig. 4.6 Influence of the size of sample particles on the amount of ginsenosides extracted .....	53
Fig. 4.7 Contribution of different factors on the extraction. A - Re; B - mRb1; C - Rb1; D – Total ginsenosides .....	54
Figure 5.1 Extraction of ginsenoside Re by three extraction methods.....	62
Figure 5.2 Extraction of ginsenoside mRb1 by three extraction methods.....	63
Figure 5.3 Extraction of ginsenoside Rb1 by three extraction methods.....	63
Figure 5.4 Extraction of total ginsenosides represented the Re, mRb1 and Rb1 by three extraction methods .....	64

Fig. 5.5 Linear regression of the natural log of residue amount of ginsenoside Re in the sample vs. extraction time for MAE, RTE and RFX extraction methods .....	66
Fig. 5.6 Linear regression of lnA vs. extraction time for ginsenoside mRb1 using the three extraction methods .....	67
Fig. 5.7 Linear regression of lnA vs. extraction time for ginsenoside Rb1 using the three extraction methods. ....	67
Fig. 5.8 Linear regression of lnA vs. extraction time for total ginsenosides using the three extraction methods. ....	68
Figure 5.9 Chromatographs of ginseng root extracts obtained using different extraction methods and extraction times .....	71
Fig. 7.1 Calibration curve for n-butyl paraben from 0.02mg/mL to 20 mg/mL .....	88
Fig. 7.2 Calibration curve for p-hydroxybenzoic acid from 0.02mg/mL to 20 mg/mL .....	89
Fig. 7.3 Temperature profile of the synthesis of n-butyl paraben: a) with ZnCl <sub>2</sub> as catalyst; b) without catalyst. b) Microwave power level: 50% (Full power 600W). .... c)	91
Fig. 7.4 Temperature profile of 2 mL of n-butanol with the addition of 0.1g of ZnCl <sub>2</sub> under microwaves of 300W .....	92
Fig. 7.5 Temperature profile of 1.38g of p-hydroxybenzoic acid with the addition of 0.07g of ZnCl <sub>2</sub> under microwaves of 300W .....	92
Fig. 7.6 Decomposition of p-hydroxybenzoic acid during the ZnCl <sub>2</sub> catalyzed synthesis of n-butyl-paraben when temperature reaches over 150 °C. Phenol as the product of decomposition of p-hydroxybenzoic acid; n-butyl paraben was also obtained.....	93
Fig. 7.7 Microwave-assisted heating of p-hydroxylbenoic acid with the addition of ZnCl <sub>2</sub> . Phenyl-4-hydroxybenzoate was obtained during the heating.....	93
Fig. 7.8 Temperature profile of 5 mL of n-butanol under microwaves of 300W without the addition of ZnCl <sub>2</sub> .....	95
Fig. 7.9 Temperature profile of 5g of p-hydroxybenzoic acid under microwaves of 300W without the addition of ZnCl <sub>2</sub> .....	95

Fig. 7.10 Temperature profile of 5g of $\text{ZnCl}_2$ under microwaves of 300W .....	96
Fig. 7.11 Synthesis of n-butyl-paraben with temperature controlled at 100 °C for 2 min, microwave power level was set at 50% (300W) during the temperature control. ....	96
Fig. 7.12 Synthesis of n-butyl-paraben with temperature controlled at 120 °C for 2 min, microwave power level was set at 50% (300W) during the temperature control. ....	97
Fig. 7.13 Synthesis of 2-methyl-1-propyl-paraben with temperature controlled at 120 °C for 2 minutes. Microwave power level was set at 50% (300W) during the temperature control.....	97
Fig. 7.14 Synthesis of 1-propyl-paraben with temperature controlled at 120 °C for 2 minutes. Microwave power level was set at 50% (300W) during the temperature control.....	98
Fig.7.15 Synthesis of ethyl paraben with temperature controlled at 120 °C for 2 min. Microwave power level was set at 50% (300W) during the temperature control.....	98
Fig. 7.16 Synthesis of sec-butanol paraben with $\text{ZnCl}_2$ as catalyst under microwave irradiation (300W, 2 minutes) .....	99
Fig. 7.17 Synthesis of sec-butanol paraben using conc. $\text{H}_2\text{SO}_4$ (0.01 mL) as catalyst under microwave irradiation (300W, 2 minutes). ....	99
Fig. 7.18 Synthesis of 1-octyl paraben with $\text{ZnCl}_2$ as catalyst under microwave irradiation (300W, 2 minutes). 2-octene and n-octyl ether were detected.....	100
Fig. 7.19 Microwave-assisted heating of n-octanol with the addition of $\text{ZnCl}_2$ under microwave power of 300W for 2 min.....	100
Fig. 8.1. Calibration curve for n-butyl paraben from 0.02mg/mL to 20 mg/mL .....	107
Fig. 8.2. Calibration curve for p-hydroxybenzoic acid from 0.02mg/mL to 20 mg/mL.....	108
Fig. 8.3 Temperature profile during the synthesis of n-butylparaben under microwave irradiation using $\text{ZnCl}_2$ as catalyst.....	113

Fig. 8.4 GC chromatograph and MS spectroscopy result of run No. 15 of Table 8.7 indicating the majority of p-hydroxybenzoic acid was decomposed into phenol.....	113
Fig. 8.5. GC chromatograph and MS spectroscopy result of run No. 8 of Table 8.7. Relatively high conversion rate was obtained and at this temperature the acid starts to decompose to phenol. ....	114
Fig. 8.6. Contribution of different factors on the percentage conversion rate of the n-butyl paraben .....	114
Fig. 8.7. Influence of reaction time on paraben yield. The letters in the bracket under each category is the Duncan grouping symbols at ( $\alpha=0.10$ ); Means with the same letter are not significantly different. ....	115
Fig. 8.8. Influence of Microwave Power on paraben yield. The letters in the bracket under each category is the Duncan grouping symbols at ( $\alpha=0.10$ ); Means with the same letter are not significantly different.....	115
Fig. 8.9. Influence of acid/alcohol mol ratio on paraben yield. The letters in the bracket under each category is the Duncan grouping symbols at ( $\alpha=0.10$ ); Means with the same letter are not significantly different. ....	116
Fig. 8.10. Influence of the amount of catalyst on paraben yield. The letters in the bracket under each category is the Duncan grouping symbols at ( $\alpha=0.05$ ); Means with the same letter are not significantly different. ....	116
Fig. 9.1. The stands used for holding the plates at both vertical and horizontal positions. The stands were made from acrylic plate.....	125
Fig. 9.2. Single plate vertical orientation facing the magnetron. Locations 1 through 9 corresponding to the distance to the magnetron from 4 to 36 cm with 4 cm increment. ....	128
Fig. 9.3. Multiple plates vertical oriented facing the magnetron. Plates were loaded at locations 1, 5 and 9, corresponding to the distance to the magnetron of 4, 20, and 36 cm. ....	129
Fig. 9.4. Multiple plates vertical oriented parallel to the magnetron. Plates were loaded at locations 1, 5 and 9, corresponding	

to the distance to the back wall of 4, 20, and 36 cm.....	130
Fig. 9.5. Multiple-horizontal oriented loading. Locations 1 though 5 correspond to the distance to the bottom of the cavity of 5 to 25 cm with 5 cm increment.....	130
Fig. 9.6. Single plate horizontally oriented in a reflection free cavity. Locations 1 and 3 correspond to the distance of 5 and 15 cm to the bottom.....	132
Fig. 9.7. Single plate horizontally oriented at location 1 corresponding 5 cm to the bottom of the cavity .....	132
Fig. 10.1. The Yee cell that shows the relative location of E and H field in 3D .....	139
Fig. 10.2. The dimension of the microwave cavity simulated and the location of microwave entry port .....	150
Fig. 10.3. The Cartesian 3-D meshing of the microwave oven. The number of grids is: 97 x 97 x 56, the size of the cell is: 4.845 x 4.845 x 4.821 mm. The power entry is 1 x 18 x 9.....	150
Fig. 10.4. The nine locations of the lossy dielectric plate in the microwave oven:	
H-1: Horizontal placement of the plate 9 cell grid above oven bottom, corresponding to the location range of 4.5-5 cm above the bottom	
H-2: Horizontal placement of the plate 29 cell grid above oven bottom, corresponding to 14.5-15cm above the bottom	
H-3: Horizontal placement of the plate 47 cell grid above oven bottom corresponding to 24.5-25 cm above the bottom	
V-F-1: Vertical placement facing the power entrance port, 9 cells from the power entrance wall corresponding to a range of 4.5-5 cm	
V-F-2: Vertical placement facing the power entrance port, 29 cells from the power entrance wall corresponding to a range of 14.5-15 cm	
V-F-3: Vertical placement facing the power entrance port, 47 cells from the power entrance wall corresponding to a range of 24.5-25 cm	
V-P-1: Vertical placement parallel to the power entrance port, 9 cells from the back wall corresponding to a range of 4.5-5 cm	
V-P-2: Vertical placement facing the power entrance port, 29 cells from the back wall corresponding to a range of 14.5-15 cm	
V-P-3: Vertical placement facing the power entrance port, 47 cells from the back wall corresponding to a range of 24.5-25 cm .....	155

Fig. 10.5. The power dissipation on the lossy dielectric plate with dielectric constant:  $\epsilon' = 20$  and dielectric loss factor  $\epsilon'' = 5$ . Simulation was run using an AMD Athlon 3800 dual core personal computer with 1Gb DDR400 PC-3200 computer. Simulation time is 5 min. On the figures, the scale in color map is normalized to 1 s of microwave application at 1KW of incident power. The color map has a unit of joule. Since it is normalized to 1 s, it can also be an energy dissipation rate with the unit of W.

- H-1: Horizontal placement of the plate 9 cell grid above oven bottom, corresponding to the location range of 4.5-5 cm above the bottom
- H-2: Horizontal placement of the plate 29 cell grid above oven bottom, corresponding to 14.5-15cm above the bottom
- H-3: Horizontal placement of the plate 47 cell grid above oven bottom corresponding to 24.5-25 cm above the bottom
- V-F-1: Vertical placement facing the power entrance port, 9 cells from the power entrance wall corresponding to a range of 4.5-5 cm
- V-F-2: Vertical placement facing the power entrance port, 29 cells from the power entrance wall corresponding to a range of 14.5-15 cm
- V-F-3: Vertical placement facing the power entrance port, 47 cells from the power entrance wall corresponding to a range of 24.5-25 cm
- V-P-1: Vertical placement parallel to the power entrance port, 9 cells from the back wall corresponding to a range of 4.5-5 cm
- V-P-2: Vertical placement facing the power entrance port, 29 cells from the back wall corresponding to a range of 14.5-15 cm
- V-P-3: Vertical placement facing the power entrance port, 47 cells from the back wall corresponding to a range of 24.5-25 cm

..... 159

Fig. 10.6. The 2D view of Fig. 10.5 to assist in the observation of the pattern and to compare with the experimental results

- H-1: Horizontal placement of the plate 9 cell grid above oven bottom, corresponding to the location range of 4.5-5 cm above the bottom
- H-2: Horizontal placement of the plate 29 cell grid above oven bottom, corresponding to 14.5-15cm above the bottom
- H-3: Horizontal placement of the plate 47 cell grid above oven bottom corresponding to 24.5-25 cm above the bottom
- V-F-1: Vertical placement facing the power entrance port, 9 cells from the power entrance wall corresponding to a range of 4.5-5 cm
- V-F-2: Vertical placement facing the power entrance port, 29 cells from the power entrance wall corresponding to a range of 14.5-15 cm
- V-F-3: Vertical placement facing the power entrance port, 47 cells from the power entrance wall corresponding to a range of 24.5-25 cm



V-P-1: Vertical placement parallel to the power entrance port, 9 cells from the back wall corresponding to a range of 4.5-5 cm	
V-P-2: Vertical placement facing the power entrance port, 29 cells from the back wall corresponding to a range of 14.5-15 cm	
V-P-3: Vertical placement facing the power entrance port, 47 cells from the back wall corresponding to a range of 24.5-25 cm	
.....	163
Fig. 10.7. The study of power dissipation when multiple lossy dielectric plates simultaneously exist in a microwave oven.....	165
Fig. 10.8. Power dissipation into lossy dielectric plates ( $\epsilon' = 20$ ; $\epsilon'' = 5$ ) when 5 horizontally placed plates simultaneously exist in the cavity .....	167
Fig. 10.9. E field distribution in the empty cavity after 3000 timesteps ( $2.79 \times 10^{-7}$ s). Total meshing number: $97 \times 97 \times 56$ cells. Simulation was run using an AMD Athlon 3800 dual core personal computer with 1Gb DDR400 PC-3200 memory. Simulation time was 5 min. The XY plane is 5 cm from the bottom of the cavity; XY plane is 5 cm from the back wall of the cavity YZ plane is 5 cm from the power entry port wall. ....	169
Fig. 10.10. E field distribution in the cavity with a single lossy dielectric plate ( $\epsilon' = 20$ ; $\epsilon'' = 5$ ) horizontally placed 5 cm from the bottom of the cavity. Results were obtained after 3000 timesteps ( $2.79 \times 10^{-7}$ s) of run using an AMD Athlon 3800 dual core personal computer with 1Gb DDR400 PC-3200 memory. Simulation time was 5 min. XY plane is 5 cm from the bottom of the cavity XY plane is 5 cm from the back wall of the cavity YZ plane is 5 cm from the power entry port wall.....	170
Fig. 10.11. E field distribution in the cavity with five lossy dielectric plates ( $\epsilon' = 20$ ; $\epsilon'' = 5$ ) simultaneously exist. Results were obtained after 3000 timesteps ( $2.79 \times 10^{-7}$ s) of run using an AMD Athlon 3800 dual core personal computer with 1Gb DDR400 PC-3200 memory. Simulation time was 5 min. XY plane is 5 cm from the bottom of the cavity XY plane is 5 cm from the back wall of the cavity YZ plane is 5 cm from the power entry port wall. ....	171
Fig. 10.12. Single plate horizontally oriented at location 1 corresponding 5 cm to the bottom of the cavity. A Panasonic microwave oven $47 \times 47 \times 27$ cm in dimension and 1 KW power output. Pattern obtained after 3 min of heating at full power Level .....	173

- Fig. 10.13. Multiple-horizontal oriented loading. Locations 1 through 5 correspond to the distance to the bottom of the cavity of 5 to 25 cm with 5 cm increment. A Panasonic microwave oven 47 x 47 x 27 cm in dimension and 1 KW power output. Pattern obtained after 9 min of heating at full power level..... 174
- Fig. 10.14. Single plate horizontally oriented at location 1 corresponding 5 cm to the bottom of a reflection free cavity created by adding power absorption materials around the walls. A Panasonic microwave oven 47 x 47 x 27 cm in dimension and 1 KW power output. Pattern obtained after 10 min of heating at full power level..... 175
- Fig. 10.15. Oven-type chemical reactor. The oven has a dimension of 80 x 80 x 60 cm. Three magnetrons are used and each of the gives a power output of 1 KW. The diameter of the glass container is 70 cm and the height is 50 cm giving a total volume of 192 liters and the applicable capacity of about 100 liters when half filled..... 176
- Fig. 10.16. The E field distribution and power dissipation at different depth into the reactor container. The container was filled with 30 cm in depth of low loss dielectric reactant with  $\epsilon' = 5$  and  $\epsilon'' = 1$ . Total meshing number of the whole cavity is: 164 x 164 x 123 cells. Results obtained after 3000 timesteps ( $2.79 \times 10^{-7}$  s). Simulation was run using an AMD Athlon 3800 dual core personal computer with 1Gb DDR400 PC-3200 memory. Simulation time was 2hr 10 min.
- A: the top layer of the reactant corresponding to 30 cm from the bottom of the cavity.
  - B: 15 cm from the bottom of the cavity.
  - C: 3 cm from the bottom of the cavity. .... 179
- Fig. 10.17. The E field distribution and power dissipation at different depth into the reactor container. The container was filled with 30 cm in depth of medium loss dielectric reactant with  $\epsilon' = 20$  and  $\epsilon'' = 5$ . Total meshing number of the whole cavity is: 164 x 164 x 123 cells. Results obtained after 3000 timesteps ( $2.79 \times 10^{-7}$  s). Simulation was run using an AMD Athlon 3800 dual core personal computer with 1Gb DDR400 PC-3200 memory. Simulation time was 2hr 10 min.
- A: the top layer of the reactant corresponding to 30 cm from the bottom of the cavity.
  - B: 15 cm from the bottom of the cavity.
  - C: 3 cm from the bottom of the cavity. .... 181

Fig. 10.18. The E field distribution and power dissipation at different depth into the reactor container. The container was filled with 30 cm in depth of High loss dielectric reactant with  $\epsilon' = 80$  and  $\epsilon'' = 15$ . Total meshing number of the whole cavity is:  $164 \times 164 \times 123$  cells. Results obtained after 3000 timesteps ( $2.79 \times 10^{-7}$  s). Simulation was run using an AMD Athlon 3800 dual core personal computer with 1Gb DDR400 PC-3200 memory. Simulation time was 2hr 10 min.

- A: the top layer of the reactant corresponding to 30 cm from the bottom of the cavity.
- B: 15 cm from the bottom of the cavity.
- C: 3 cm from the bottom of the cavity. .... 183

Fig. 10.19. The E field distribution and power dissipation at different distance from the X direction (YZ plane) into the reactor container. The container was filled with 30 cm in depth of low loss dielectric reactant with  $\epsilon' = 5$  and  $\epsilon'' = 1$ . Total meshing number of the whole cavity is:  $164 \times 164 \times 123$  cells. Results obtained after 3000 timesteps ( $2.79 \times 10^{-7}$  s). Simulation was run using an AMD Athlon 3800 dual core personal computer with 1Gb DDR400 PC-3200 memory. Simulation time was 2hr 10 min.

- A: YZ plane 5 cm from the container side wall into the container
- B: YZ plane 10 cm from the container side wall into the container
- C: YZ plane in the middle of the container corresponding to 36cm from the container side wall ..... 186

Fig. 10.20. The E field distribution and power dissipation at different distance from the X direction (YZ plane) into the reactor container. The container was filled with 30 cm in depth of medium loss dielectric reactant with  $\epsilon' = 20$  and  $\epsilon'' = 5$ . Total meshing number of the whole cavity is:  $164 \times 164 \times 123$  cells. Results obtained after 3000 timesteps ( $2.79 \times 10^{-7}$  s). Simulation was run using an AMD Athlon 3800 dual core personal computer with 1Gb DDR400 PC-3200 memory. Simulation time was 2hr 10 min.

- A: YZ plane 5 cm from the container side wall into the container
- B: YZ plane 10 cm from the container side wall into the container
- C: YZ plane in the middle of the container corresponding to 36cm from the container side wall ..... 188

Fig. 10.21. The E field distribution and power dissipation at different distance from the X direction (YZ plane) into the reactor container.

The container was filled with 30 cm in depth of high loss dielectric reactant with  $\epsilon' = 80$  and  $\epsilon'' = 15$ . Total meshing number of the whole cavity is: 164 x 164 x 123 cells. Results obtained after 3000 timesteps ( $2.79 \times 10^{-7}$  s). Simulation was run using an AMD Athlon 3800 dual core personal computer with 1Gb DDR400 PC-3200 memory. Simulation time was 2hr 10 min.

- A: YZ plane 5 cm from the container side wall into the container
- B: YZ plane 10 cm from the container side wall into the container
- C: YZ plane in the middle of the container  
corresponding to 36cm from the container side wall .....190

Fig. 10.22. Power dissipations in each horizontal layer from the top to the bottom for low loss, medium loss and high loss reactants. ....193

Fig. 10.23. Power dissipations in each circular layer in the radius direction for low loss, medium loss and high loss reactants..... 193

Fig. 10.24. A microwave-assisted chemical reactor/extractor. The dimension is: 0.6 x 0.6 x 1.8 m. Totally 8 magnetrons (1 KW of each) were used with two of them on each vertical wall. The 4 lower power entry ports are located 15-19 cm from the bottom and the 4 upper power entry ports are located 35-39 cm from the bottom. ....194

Fig. 10.25. E field distribution and power dissipation at different depth of the reactor container. The container was filled with 100 cm in depth of low loss dielectric reactant with  $\epsilon' = 5$  and  $\epsilon'' = 1$ . Total meshing number of the whole cavity is: 123 x 123 x 371 cells. Results obtained after 3000 timesteps ( $2.79 \times 10^{-7}$  s). Simulation was run using an AMD Athlon 3800 dual core personal computer with 1Gb DDR400 PC-3200 memory. Simulation time was 2hr 50 min.

- A: 5 cm from the bottom
- B: 17 cm from the bottom
- C: 35 cm from the bottom
- D: 45 cm from the bottom
- E: 75 cm from the bottom ..... 199

Fig. 10.26. The E field distribution and power dissipation at different distance from the Y direction (XZ plane) into the reactor container. The container was filled with 100 cm in depth of low loss dielectric reactant with  $\epsilon' = 5$  and  $\epsilon'' = 1$ . Total meshing number of the whole cavity is: 123 x 123 x 371 cells. Results obtained after 3000 timesteps ( $2.79 \times 10^{-7}$  s). Simulation was run using an AMD Athlon 3800 dual core personal computer with 1Gb DDR400 PC-3200 memory. Simulation time was 2hr 50 min.

- A: XZ plane 2.5 cm from the container side wall into the container

B: XZ plane 5 cm from the container side wall into the container	
C: XZ plane 15 cm from the container side wall into the container	
D: XZ plane 25 cm from the container side wall into the container	
E: XZ plane in the middle of the container corresponding to 35cm from the container side wall	202

Fig. 10.27. E field distribution and power dissipation at different depth of the reactor container. The container was filled with 100 cm in depth of medium loss dielectric reactant with  $\epsilon' = 20$  and  $\epsilon'' = 5$ . Total meshing number of the whole cavity is: 123 x 123 x 371 cells. Results obtained after 3000 timesteps ( $2.79 \times 10^{-7}$  s). Simulation was run using an AMD Athlon 3800 dual core personal computer with 1Gb DDR400 PC-3200 memory. Simulation time was 2hr 50 min.

A: 5 cm from the bottom	
B: 12.5 cm from the bottom	
C: 17 cm from the bottom	
D: 35 cm from the bottom	
E: 75 cm from the bottom	205

Fig. 10.28. The E field distribution and power dissipation at different distance from the Y direction (XZ plane) into the reactor container. The container was filled with 100 cm in depth of medium loss dielectric reactant with  $\epsilon' = 20$  and  $\epsilon'' = 5$ . Total meshing number of the whole cavity is: 123 x 123 x 371 cells. Results obtained after 3000 timesteps ( $2.79 \times 10^{-7}$  s). Simulation was run using an AMD Athlon 3800 dual core personal computer with 1Gb DDR400 PC-3200 memory. Simulation time was 2hr 50 min.

A: XZ plane 2.5 cm from the container side wall into the container	
B: XZ plane 5 cm from the container side wall into the container	
C: XZ plane 15 cm from the container side wall into the container	
D: XZ plane in the middle of the container corresponding to 35cm from the container side wall	208

Fig. 10.29. Power dissipations in each horizontal layer for low loss, medium loss and high loss reactants.....209

Fig. 10.30. Power dissipation in different layers of squares from inner to outer. The power dissipation value is normalized to the square with a side of 17cm .....209

Fig. 10.31. A cylindrical microwave chemical reactor/extractor with 8 magnetrons..... 211

## LIST OF TABLES

Table 2.1. Comparison of the extraction of getiopicroside from gentian by MAE with two Soxhlet extraction methods – the yields and the quality of the product. ....	12
Table 2.2 Comparison of the components by MAE and steam distillation method (Pare, 1995). ....	13
Table 2.3. Effect of various solvent and heating systems on the peltate glands during extraction of peppermint oil.....	19
Table 2.4. Comparison of microwave-assisted synthesis and classic method. The microwave-assisted synthesis was carried out in a sealed TEFLON vessel using a domestic microwave oven (adapted from Gedye, et al., 1986). ....	21
Table 2.5. Cyclization of monotrifluoroacetylated o-arylenediamines (Bougrin, et al., 2001) .....	22
Table 2.6. Synthesis of TCP protected $\alpha$ -amino- $\beta$ -lactams (Bose, et al., 1996) .....	23
Table 3.1 Factors and levels used in the investigation. ....	33
Table 3.2 Orthogonal experimental design table .....	33
Table 3.3 DUNCAN analysis results for the different levels in the various factors investigated for menthone, menthofuran and menthol, the different letters in each column means they are significantly different ( $\alpha=0.05$ ).....	36
Table 4.1 Factors and levels of the experimental design .....	47
Table 4.2 Orthogonal experimental design table .....	48
Table 4.3 DUNCAN analysis results for the different levels in the various factors investigated for different ginsenosides, the different letters in each column means they are significantly different. ....	51
Table 5.1 Linear regression results of $\ln A - t$ relationships .....	69
Table 5.2 The extraction rate enhancement factor RFX vs. RTE and MAE vs. RFX.....	70

Table 6.1. Interaction of microwaves and catalyst .....	81
Table 8.1. Factors and levels used in the investigation. ....	108
Table 8.2. $L_8(2^7)$ array of experimental design .....	109
Table 8.3. Factors and levels in the four-level study .....	109
Table 8.4. $L_{16}(4^5)$ orthogonal array experimental design .....	110
Table 8.5 Percentage conversion results of the two-level study .....	117
Table 8.6 ANOVA procedure results of the two-level study .....	118
Table 8.7 Percentage conversion of the four-level study.....	118
Table 8.8 ANOVA procedure results of the four level study.....	119
Table 10.1. Power dissipation into the lossy dielectric plates at different locations. The dielectric constant is 20 and the loss factor is 5. Results were obtained from the 3000 iteration simulation but normalized to the total energy dissipation within 1 s. The total input power to the cavity is 1KW. ....	165
Table 10.2. Power dissipation into the lossy dielectric plates at different locations. The dielectric constant of is 20 and the loss factor is 5. Results were obtained from the 3000 iteration simulation but normalized to the total energy dissipation within 1 s. The total input power to the cavity is 1KW. ....	165
Table 10.3. Power dissipation into the lossy dielectric plates at different locations in the existence of 5 horizontally placed plates as shown in Fig. 10.7. The dielectric constant of the plates is 20 and the Loss factor is 5. Results were obtained from the 3000 iteration simulation normalized to 1 s. The total input power to the cavity is 1KW.....	169

## LIST OF SCHEMES

Scheme 2.1 Cyclization of monotrifluoroacetylated o-arylenediamines .....	22
Scheme 2.2. Synthesis of TCP protected $\alpha$ -amino- $\beta$ -lactams. TCP=tetrachlorophthaloyl; NMM=N-methylmorpholine; MWI=microwave irradiation, R"=PhOCH <sub>2</sub> .....	23
Scheme 2.3. Appearance of a dipolar transition state during the reaction; the presence of dipolar transition state causes the lower activation energy by microwaves than conventional heating (Loupy, 2004).....	25
Scheme 6.1. The synthesis of parabens (cat.=catalyst such as PTSA, H <sub>2</sub> SO <sub>4</sub> ). .....	77
Scheme 6.2. Appearance of a dipolar transition state during the reaction; the presence of dipolar transition state causes the lower activation energy by microwaves than conventional heating (Loupy, 2004).....	79
Scheme 6.3. Mechanism of acid catalyzed esterification reaction .....	81
Scheme 6.4. ZnCl <sub>2</sub> catalyzed esterification reaction .....	82
Scheme 7.1 Mechanism of ZnCl <sub>2</sub> catalyzed synthesis of parabens.....	101



## NOMENCLATURE

$\epsilon^*$	The complex relative permittivity
$\epsilon'$	Dielectric constant
$\epsilon''$	Dielectric loss factor
$\epsilon_0$	Dielectric constant in vacuum
$P_v$	The energy development per unit volume ( $W/m^3$ )
$P_{abs}$	Power absorption in the lossy dielectric materials
$Q$	The energy dissipation in certain cell
$f$	Frequency (Hz)
$\epsilon_0$	The absolute permittivity of vacuum (F/m)
$ E $	Electric strength inside the load (V/m)
$P_d$	Penetration depth
$\mu_0$	Magnetic permittivity in vacuum
$\mu'$	The relative magnetic permittivity
$J$	Current density
$\sigma$	The effective conductivity
$\omega$	The angular speed of light
$P_0$	Incident power
$P_d$	The energy at the distance of $d$
$\alpha$	The attenuation factor
$D$	The vector flux density
$E$	The vector electric field strength
$H$	The vector magnetic field strength
$c_0$	Light speed in free space
$Contri_i$	The contribution of the $i^{th}$ factor
$F_i$	The F value of the $i^{th}$ factor
$A$	The amount of principles of interest
$k$	A constant in the extraction rate equation
$\Delta c$	Concentration gradient
$c_s$	The concentration of the principles in the sample

$C_{\text{sol}}$	The concentration of the extracted principle in the solution
$V_{\text{sample}}$	The volume of solvents that enter the sample
$V_{\text{sol}}$	The volume of the solution
$A_0$	The original amount of principle in the sample
$A_{\text{extr}}$	The amount of principle extracted
$P_{\text{out}}$	The power output of the magnetron
$P_{\text{simulation1}}$	The total simulated dissipated power

# CHAPTER I

## GENERAL INTRODUCTION

### 1.1 Background

Microwaves are electromagnetic waves with frequencies in the range of 300 MHz to 30 GHz. Besides their intensive applications in RADAR and telecommunications as carriers of signals, microwave energy has found its way into many other areas such as drying and food processing (Tulasidas *et al.*, 1993; Hulls, 1982; Mudgett, 1989; Decareau, 1983).

In 1986, Ganzler *et al.*, first introduced microwave energy in the extraction system for crude fat, vicine, convicine, and gossypol from seeds, foods and feeds using organic solvents. With only 3.5 minutes of microwave irradiation, the yields of these compounds were comparable to those obtained with a 3-hr Soxhlet extraction. This accelerated microwave-assisted extraction of organic compounds was also demonstrated for other materials (Ganzler and Salgo, 1987; Ganzler *et al.*, 1990). Paré *et al.* (1991) compared microwave-assisted extraction with steam distillation for producing essential oil from fresh peppermint (*Mentha x piperita*). The extraction was carried out with hexane as solvent. With a 40 s microwave irradiation (2450 MHz) at 625 W, the yield was 0.371%, compared to 0.227% for a 2-hr steam distillation. Paré *et al.*, (1991) calculated that using the microwave-assisted extraction method would result in a 94% increase in net profit in the production of essential oil from peppermint. Accumulated facts on the tremendously high efficiency of this technique, in terms of extremely short processing time, low solvent and energy consumption, better yields, and higher quality compared to conventional methods (Gao, 1997; Mattina *et al.*, 1997; Hao *et al.*, 2000; Huang *et al.*, 2000; Lee *et al.*, 2000; Li and Jin, 2000; Liu *et al.*, 2000; Pan *et al.*, 2000; Seifert *et al.*, 2000) suggest that microwave-assisted

extraction is a promising alternative to conventional extraction methods in the industrial production of natural products.

Microwave-assisted synthesis is also reported to have increased reaction rate as compared to the classic organic synthesis methods (Bougrin, et al., 2005; Gedye, et al., 1986; Zhong, et al., 2006; Wu, 2006; Moghaddam, et al., 2005; Guillot, et al., 2005, Williams, et al., 200; Dai, et al., 1999). Besides, microwave-assisted synthesis can also improve the yield of those reactions that are difficult to obtain satisfactory yield and to have selectivity of the final product when isomers are formed during the reaction (Dai and Raghavan, 2005; Li and Yan, 2005; Nanjunda Swamy, et al., 2006; Grieco, et al., 2003; Alterman and Hallberg, 2000; Langa, et al., 1997; Bose, et al., 1996; Vega, et al., 1996; Perreux and Loupy, 2001).

Although the microwave technology showed great advantage over conventional methods in either extraction or organic synthesis, they are still mainly limited to the laboratory applications. Many factors restricting the scale-up process of the microwave-assisted extraction and synthesis processes. Among these factors, the most important ones are the non-uniform power distribution and limited penetration depth. These factors have to be known before any effort in designing the scale-up equipments for the microwave-assisted extraction or synthesis equipments. A numerical simulation for the microwave-power distribution will be the most affordable and practical way to study the problems associated with the scale-up of microwave-assisted extraction and synthesis processes.

## **1.2 Objectives**

The main objective of this research is to identify and solve various problems, especially the energy distribution problem during the scale up of the microwave-assisted extraction and synthesis processes. Besides the numerical simulation approaches, detailed laboratory study on the microwave-assisted extraction and synthesis need to be investigated. To accomplish this main goal, the following specific steps will be pursued:

- 1) Laboratory study of the microwave-assisted extraction process and investigate various factors that affect the extraction rate and final extract yield.
- 2) Laboratory study of microwave-assisted organic synthesis reaction and the influencing factors on the synthesis yield and to understand the mechanisms behind the microwave-assisted synthesis process.
- 3) Development of methods that can experimentally or numerically determine microwave energy distribution within given cavity as well as the proposed designed scale-up cavities for microwave-assisted extraction and synthesis processes.

## CHAPTER II

### LITERATURE REVIEW

#### 2. 1 Microwaves and microwave-matter interaction

Microwaves are electromagnetic waves with frequencies in the range of 300 MHz and 30 GHz located between infrared and radio frequency on the electromagnetic spectrum as shown in Fig. 2.1. Since this frequency range is extensively used in RADAR transmission and telecommunications, regulations were made to limit the frequencies that can be used for Industry, scientific, and medicinal purpose (ISM frequencies) (Stuerga and Delmotte, 2002). The frequencies of 2450 MHz and 915 MHz, are frequently employed in the industrial use. 2450 MHz is used for domestic microwave ovens and the microwave-assisted extraction equipments.

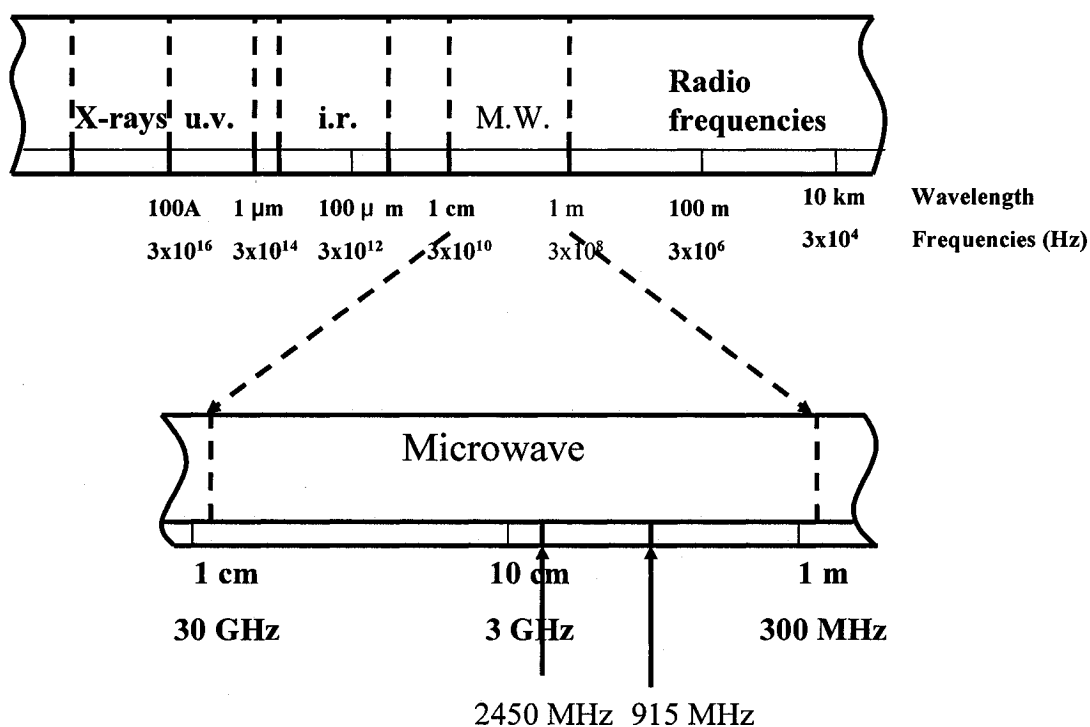


Fig. 2.1. Locations of microwaves on the electromagnetic spectrum.

The energy level of microwaves corresponds to the rotational energy level of polar molecules. Therefore the interaction of microwave energy with matter is through the dielectric rotation of the molecules. The friction between the fast rotating molecules causes a fast and volumetric heating. This is the most significant character that microwave heating differs from the conventional heating methods.

From the heating mechanism, it is easy to understand that only those molecules that can couple with the microwave field can be heated with microwave energy. Electrically, the complex relative permittivity ( $\epsilon^*$ ) is used to describe the interaction of microwaves and matter. The complex relative permittivity ( $\epsilon^*$ ) can be expressed as:

$$\epsilon^* = \epsilon' - j\epsilon'' \quad (2.1)$$

Where  $\epsilon'$  is the dielectric constant and  $\epsilon''$  the loss factor. The dielectric constant describes the capability of molecules to be polarized by electric field and the loss factor measures the efficiency of molecules to convert microwave energy into heat (Mingos and Baghurst, 1991). The following equation is used to calculate the energy absorption:

$$P_v = 2\pi f \epsilon_0 \epsilon'' |E|^2 \quad (2.2)$$

Where:  $P_v$  is the energy developed per unit volume ( $\text{W/m}^3$ )

$f$  is the frequency (Hz)

$\epsilon_0$  is the absolute permittivity of vacuum ( $\text{F/m}$ )

$|E|$  is the electric field strength inside the load ( $\text{V/m}$ ).

As can be seen the power dissipated in a certain volume is proportional to the loss factor of the matter. This property of microwave-matter interaction could possibly bring some new character into the extraction mechanism.

Another important concept associated with microwave-matter interaction is the penetration depth ( $D_p$ ), which is defined as the depth into a sample where the microwave power drops to  $1/e$  of its transmitted value. The penetration depth is a function of dielectric constant and loss factor:

$$D_p = \frac{1}{2\pi f} \sqrt{\frac{2}{\mu_0 \varepsilon_0 \varepsilon'} \left( \sqrt{1 + \left( \frac{\varepsilon''}{\varepsilon'} \right)^2} - 1 \right)} \quad (2.3)$$

Penetration depth is one of the restricting factors in the scale-up of microwave assisted extraction process.

## 2.2 Microwave-assisted Extraction (MAE)

Extraction is a solid/liquid separation technique, during which the chemical components in the solids are extracted into the liquid, and are subsequently recovered by removing the solvents. The basic mechanism involved in the separation process is diffusion caused by a concentration gradient inside the sample and the solvent. Therefore, the extraction rate can be accelerated by a few methods, e.g. refreshing solvents, stirring, and increased temperature. By refreshing the solvents from time to time, the concentration gradient can be kept at maximum and this is especially important when the concentration in the sample drops to a certain level. By stirring, the higher concentration zone close to the sample can be mixed with the far zone with relatively low concentration, therefore increasing the concentration gradient between the inner part of sample and the immediate neighbouring solvent. The increased temperature on the other hand increases the kinetic constant leading to the extraction rate increase. Based on these mechanisms, various classic extraction methods are developed, e.g. Soxhlet extraction, tumbling and shaking, reflux extraction. Even though these methods were widely used for sample preparation, and some methods are used as standard method for sample extraction, they are very low efficient extraction methods in terms of extraction time, quality of extracts, solvent and energy



consumption (Pare, et al. 1991; Pare, 1994,1995; Pan, et al., 2000; Mattina, et al., 1997). Therefore, there is a need to improve the extraction processes with a new method. Microwave-assisted extraction is a promising alternative to the conventional extraction methods.

Microwave-assisted extraction is an extraction method based on conventional solvent-immersion extraction. The new character evolved in the microwave-assisted extraction is the introduction of microwave energy into the extraction system. Due to the special microwave-matter interaction pattern, the extraction was reported to be very efficient (Mattina, et al., 1997; Gao, 1997; Seifert, et al. 2000; Hao, et al. 2000; Liu, et al. 2000; Huang, et al. 2000; Pan, et al. 2000; Li and Jin, 2000; Lee, et al. 2000).

#### 2.2.1 A brief history of microwave-assisted extraction

A reliable device for generating fixed frequency microwaves was developed at the University of Birmingham as part of RADAR development during World War II (Mingos and Baghurst, 1991). In the 1950s, domestic and commercial applications of microwave in heating and cooking appeared in the US. The application of microwave in chemistry is a result of the wide spread of domestic microwave oven in the 1970s. In 1975, Abu-Samra et al. first applied microwave in wet-ashing biological samples for element analysis. Even though the great accelerating effect was observed as compared to the conventional digestion methods, not enough attention was paid and the application was limited to the digestion for inorganic analysis. In 1986, microwave was first applied in organic extraction by Ganzler et al. for extracting various types of compounds from soil, seeds, food and feed with organic solvents. And at the same year, Gedye et al. (1986) applied microwave energy in organic synthesis. The great accelerating effect of microwave energy brought to the various areas of chemistry; which chemists in various areas soon applied the technique to the various fields, e.g. food, environment, geological, biology, etc. (Stripp and Bogen, 1989; Kalra, 1989; Ding, et al. 1991; Cesare, et al. 1995; Zlotorzynski, 1995; Kovacs, et al., 1998; Wang, et al. 1997; Pastor, et al. 1997).

### 2.2.2 Advantages of MAE over conventional extraction methods

In microwave-assisted extraction system, microwave energy replaces the hotplate as the energy supply to heat up the extraction process. The most significant result from this change is the dramatic accelerating effect in extraction rate.

Ganzler et al. (1986) reported the extraction of crude fat, vicine, convicine, and gossypol from seeds, foods and feeds with microwave-assisted extraction method and conventional Soxhlet extraction method. The results showed that with 3.5 minutes microwave irradiation, the yields of these compounds are comparable with those obtained with 3-hr Soxhlet extraction.

Pare (1995) compared the microwave-assisted extraction method with the steam distillation for producing essential oil from fresh peppermint. The extraction was carried out with hexane as solvent. With 40 s microwave irradiation at 625 W, the yield is 0.371% as compared to the 2-hr steam distillation of 0.277%. Therefore, he suggested a method by using the microwave-assisted extraction method, the production of essential oil from peppermint can increase a net profit to 94%.

Seifert et al. (2000) reported the extraction of Getiopicroside from gentian root with microwave-assisted extraction method and two Soxhlet extraction methods. The results showed that with 90s microwave irradiation at 2 kW, a comparative yield was obtained with 1 hr Soxhlet extraction at both 50 °C and 100 °C. In another example he showed for extracting isoquercitrin from equisetum ar-verse, 60 s microwave irradiation at 2 kW resulting in comparable yield with 1 hr Soxhlet extraction. Pan, et al. (2000) observed a more pronounced microwave accelerating effect when comparing six extraction methods for extracting glycyrrhizic acid from licorice. The results are shown in Figure 2.2. As can be seen, to obtain similar yields, heat reflux extraction needs 4.5 h, ultrasonic extraction 30 minutes plus 20 hrs' room temperature extraction, Soxhlet 10 h, Soxhlet 5.07 h, extraction at room temperature (ERT) 20 h, while MAE needs only 4 minutes. The dramatic acceleration effect of microwave-assisted extraction suggests a great reduction in energy consumption, a faster production cycle or

smaller process equipment if this technique is used in an industrial production set up.

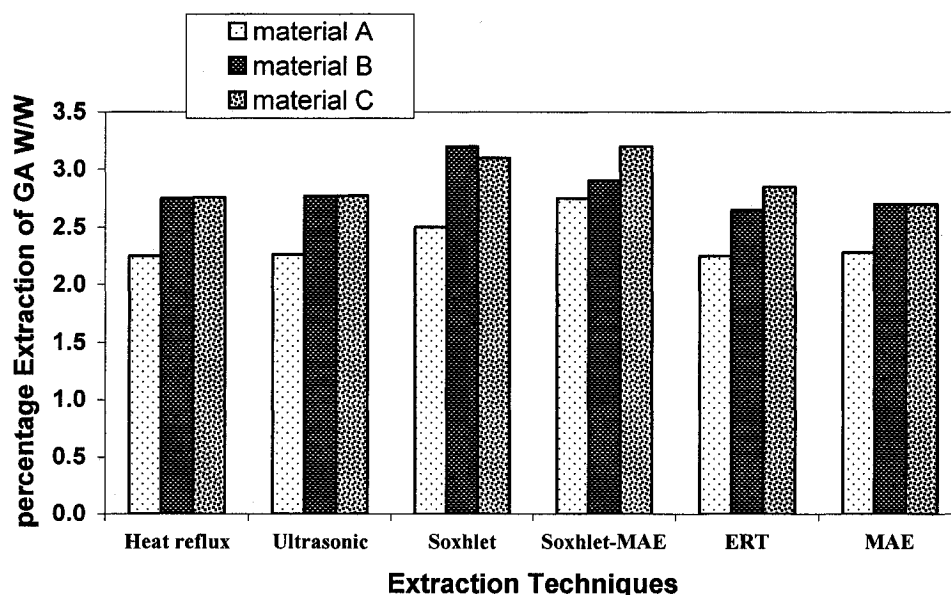


Fig. 2. 2 Comparison of MAE with conventional extraction methods: Material A – large pieces (5-10 mm in diameter and 3-5 mm in thickness); Material B – unrefined powder (about 5 – 10 mesh); and Material C – Powder (50 mesh). Extraction conditions (sample 10 g): Heat reflux – sequential solvent 100 mL for 1.5 h, 80 mL for 1.5 h and 80 mL for 1.5 h; Ultrasonic extraction – solvent 200 mL in ultrasonic for 30 min followed by extraction at room temperature for 20 h; Soxhlet – solvent 200 mL for 10 h; Soxhlet-MAE – solvent 200 mL for 5 h by Soxhlet and residue with solvent 100 mL and MAE for 4 min; ERT – sample 3 g in solvent 30 mL extracted at room temperature for 20 h; MAE – solvent 100 mL in microwave irradiation for 4 min.

Besides the great acceleration effect, microwave-assisted extraction can also improve the product quality as a result of short processing time or due to the special characteristics of microwave bringing to the extraction method. In the

extracts there are target components and undesired components. The ideal result would be to have only target components and no undesired components; in practice this can never be obtained. However, it is possible to increase the content of target components and lower the undesired components by changing the extraction conditions or using different extraction methods. Microwave-assisted extraction is one approach in which it is possible to obtain products of increased quality. As shown in the examples mentioned above, microwave-assisted extraction can greatly accelerate the extraction rate for the recovery of certain components. The fast process allows target components to be extracted in minutes or even seconds. However, within such short time, most of the undesired components still remain in the sample matrix. Therefore the quality of the product can be improved and the cost for purifying the production will be consequently lowered. The results obtained in our previous work for extracting AZRL from neem seed and leaves proved this to be true. It shows that for both neem seed and leaves, the content of AZRL (target components) reaches highest within 30 s and 60 s of microwave irradiation and decrease after that due to the extraction of undesired components from the sample (Dai, et al., 1999).

When target components are heat sensitive, microwave-assisted extraction exhibit as an excellent alternative to conventional extraction methods either due to the short process time or due to another special characteristic of microwave-assisted extraction based on the property of the components. In one case, heat sensitive components will decompose when exposed to heat for a long time. The short extraction time and consequently short exposure time to high temperature will help to obtain better quality product. The study of Seifert et al. (2000) in extracting getiopicroside from gentian with MAE and Soxhlet extraction at 50 °C and 100 °C clearly shows this advantage of microwave-assisted extraction. The results of the extraction are summarized in Table 2.1 (Seifert, et al. 2000). As can be seen in the two Soxhlet extraction, with the increase of extraction time, the content of the target component increase at first and then decrease with the extraction time indicating decomposition of the component. The colour delta value also measures the amount decomposed. By using microwave-assisted

extraction, the decomposition can be avoided while obtaining an acceptable yield. The colour Delta E also suggests that the product obtained by MAE is better than those obtained through long processing time.

For heat sensitive components, in another case, the components are extremely unstable when heated therefore completely decomposes in a short time when subjected to high temperatures. A MAE process with nonpolar solvent will help keep these components while maintaining high extraction rate. As we mentioned earlier, extraction is mainly a diffusion process and the increase in temperature will help increase the diffusion rate. However in conventional methods, you can either use high temperature to obtain a high extraction rate but at the price of losing the target components, or protect the components in a lower temperature but a long process time. In microwave-assisted extraction, both rapid extraction and no decomposition of target components can be achieved by a special character of microwave heating. As we described before, only those dipoles can couple with the microwave energy and generate heat within them. Nonpolar solvent such as hexane therefore can not couple with microwave energy and can not absorb microwave energy. During the extraction process, microwave energy will heat the sample which has high content of water in it therefore raise the temperature of the sample. The raised temperature consequently leads to a high diffusion rate of the target components to the solvent. Once the heat sensitive component reaches the solvent, the solvent with lower temperature will protect the components from decomposition. Therefore, MAE becomes an ideal extraction model, with high temperature spots to guarantee the high extraction rate and low temperature environment to protect the heat sensitive components. The study on the MAE and steam distillation for oil production showed the significance of MAE method (Pare 1995). Garlic contains many components that are highly sensitive to heat and when steam distillation is used for producing garlic oil, many of the components are decomposed as shown in Table 2.2 (Pare, 1995). While with microwave extraction, even energy is applied and the sample is subjected to temperature

rise during extraction, its heat sensitive components are extracted without decomposition.

Besides all the above mentioned advantages of microwave assisted extraction over the conventional methods, it was also suggested to be solvent saving, clean production, higher recovery (Pan, et al., 2000; Pare, 1995; Pare and Belanger, 1994, 1997; LeBlanc, 1999). Therefore if this technique can be applied in the industrial production, all these characteristics of the MAE will lead to efficient production method.

Table 2.1. Comparison of the extraction of getiopicroside from gentian by MAE with two Soxhlet extraction methods – the yields and the quality of the product.

Microwave-Assisted Extraction				
Extraction time (s)	15	30	60	90
Target component Concentration (ppm)	1510	1570	1870	1994
Colour Delta E*	38.6	42.1	47.2	54.9
Soxhlet Extraction at 50 °C				
Extraction time (h)	0.5	1	3	6
Target component Concentration (ppm)	1500	1880	1690	1300
Colour Delta E*	50.1	53.8	58.3	61.2
Soxhlet Extraction at 100 °C				
Extraction time (h)	0.5	1	3	6
Target component Concentration (ppm)	1620	2200	2030	1700
Colour Delta E*	61.6	70.3	74.9	79.0

Colour Delta E is measured by Chromameter instrument calibrated with pure colourless solvent blend used for the extraction. Delta E indicates a vectorial calibration of clarity, green to red colour and blue to yellow colour. This value is 1 for clear, water-white liquids and reaches a value in excess of 100 for very dark brown liquids.

Table 2.2 Comparison of the components by MAE and steam distillation method (Pare, 1995).

Composition of Garlic Extracts (%)										
Microwave Irradiation (30 s; in CH <sub>2</sub> Cl <sub>2</sub> )			Steam Distillation (2 hrs)							
A*	B	C	A*	D	E	F	G	H	I	J
22.2	28.4	49.4	14.7	5.80	45.9	9.92	8.96	4.84	5.96	3.94

\* Component A is the only component that is common to both extracts

### 2.2.3 Mechanism of microwave accelerating effect

From the previous section, we can see that the most significant character of microwave-assisted extraction is the acceleration rate in the extraction process. As compared to the conventional room temperature extraction and the reflux temperature extraction, the introduction of microwave energy into the system results in an acceleration effect up to 300 times. To date there is no widely accepted explanation on the accelerating effect. Attempts in explaining the special effect is made by Pare et al. (1991) using peppermint as an example. In their experiment, fresh mint leaf is extracted with a non-polar solvent under microwave irradiation and using Soxhlet extraction. Scanning electron micrographs was obtained for the glands of fresh untreated sample, the sample extracted with hexane by Soxhlet extraction for 6 hrs, and the sample in hexane subjected to microwave-irradiation for 20 s (See Figure 2.3, Pare and Belanger, 1994). The picture showed that with soxhlet extraction for 6hrs, the only cause is the shrinkage of the gland, while with the 40 s microwave irradiation, the gland was completely destroyed. Therefore they explain the special accelerating effect as follows: "the microwave rays travel freely through the microwave-transparent medium and are allowed to reach the inner glandular and vascular systems" and "the result is a sudden rise in temperature inside the material. That rise is more pronounced in the glandular and vascular system. The temperature keeps rising until the internal pressure exceeds the capacity of the expansion of the cells walls

thus creating explosion at the cell level. The substances that were located in the cells are then free to flow out of the cells. They migrate to the surrounding medium.” Therefore the extraction could be finished in extremely short period of time, say, less than a minute. While in the case of Soxhlet extraction, they suggest the content in the glandular system and vascular system can only reach the solvent through a diffusion mechanism, thus very slow.

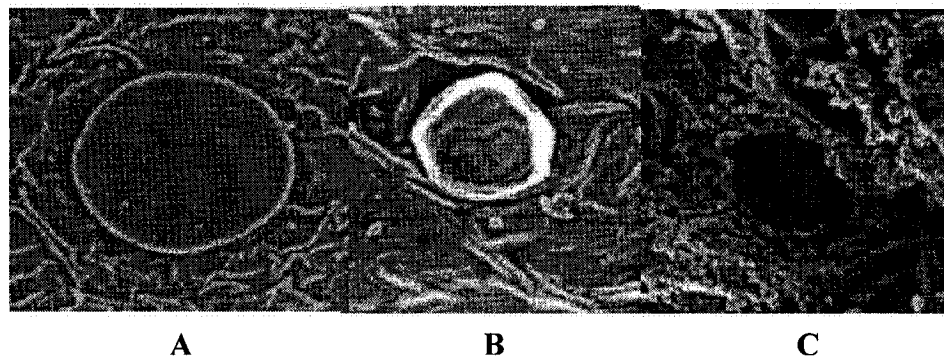


Fig. 2. 3 Scanning electron micrograph of (A) Untreated fresh mint gland; (B) Soxhlet extraction for 6 hrs; (C) Microwave irradiation for 20 s

Similar study was carried out by Spiro and Chen (1995) with the aid of scanning electron micrographic tools but showed a contradictory result. The extraction methods were: MAE with hexane (200 W,  $\Delta T = 10^\circ\text{C}$ ); hexane at a constant temperature of  $35^\circ\text{C}$ ; ethanol at a constant temperature of  $35^\circ\text{C}$ ; 90 mol% of ethanol at a constant temperature of  $35^\circ\text{C}$ ; and 90 mol% hexane at a constant temperature of  $35^\circ\text{C}$ . The scanning electron micrographs of the untreated and samples after various methods of extraction are shown in Figures 2.4 – 2.8 and the statistical results are shown in Table 2.3 (Spiro and Chen, 1995). According to the electron micrographs and the statistical numbers of the number of glands affected during the extraction processes, Spiro and Chen (1995) suggested that the damages caused to the glands were due to the solvents rather than the microwave heating. Even though the explosion of the glands may lead to the rapid extraction, solvents played a more important role. Furthermore, the accelerating effects observed in the extraction of root samples



seeds can not be explained by the gland rupture mechanism. More studies are needed to reveal the real reason behind the special accelerating effect of microwave-assisted extraction method. But this does not prevent the application of this technology in the industrial production.

#### 2.2.4 Laboratory equipment for microwave-assisted extraction

Most of the earlier works on microwave-assisted extraction work were carried out with the modified microwave oven (Ganzler, et al. 1986; Craveiro, et al., 1989; Jean, et al. 1992; Spiro and Chen, 1995; Chen and Spiro, 1994, 1995). Due to the much lower cost as compared to the commercial ones, and to the fact the functions are comparable with some of the commercial ones, this modification method is still used even in the most recent report (Pan, et al. 2000). Figure 2.9 shows the modified microwave oven as used by Pan et al. (2000). However, commercial microwave-assisted chemistry apparatus did bring some new features such as focus microwave apparatus produced by former Prolabo corp. (France) and pressurized close vessel extraction equipments produced by CEM corporation (Matthews, NC, USA) or ATS Scientific Inc. (Burlington, ON, Canada).

Modified domestic microwave oven or commercial microwave-assisted extraction apparatus fall into two basic types: multimode cavity or monomode focused microwave as shown in Figures 2.10a and b (Letellier and Budzinski, 1999). In the monomode focused microwave-assisted extraction apparatus, vessel is placed in the waveguide where focused microwave is applied to the extraction vessel. With this method, a very high energy density can be obtained but the size of the sample is limited. An apparatus based on a multimode cavity in nature is the same as a domestic microwave oven. The large size in the cavity can provide more space for the extraction vessel and allows some new features as pressurized close-vessel extraction benefiting from the higher temperature it can reach. Considering the size it can reach, a multimode cavity type is preferred for the scaling-up of the microwave-assisted extraction equipments.

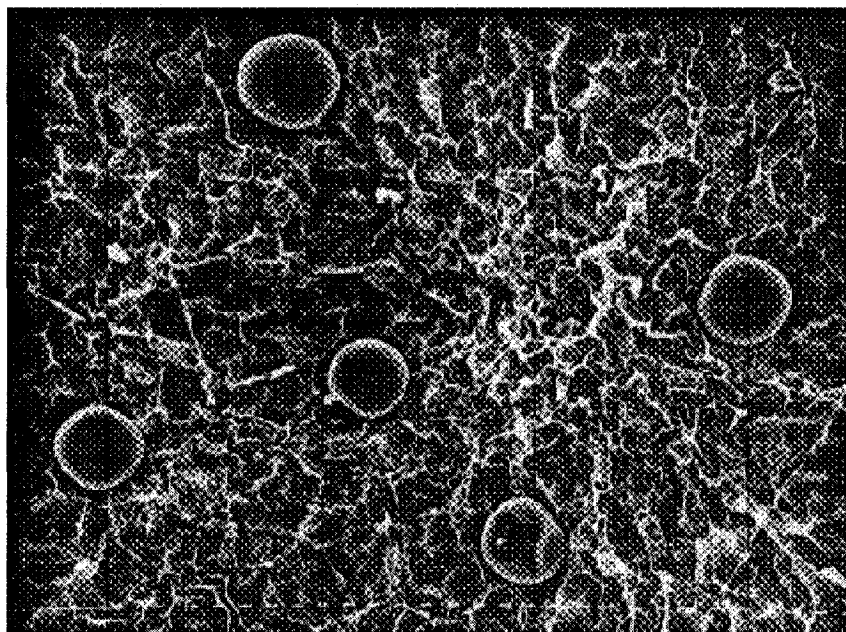


Fig. 2. 4 Untreated leaf showing globular whole glands (10  $\mu\text{m}$  bar, 200 x magnification)

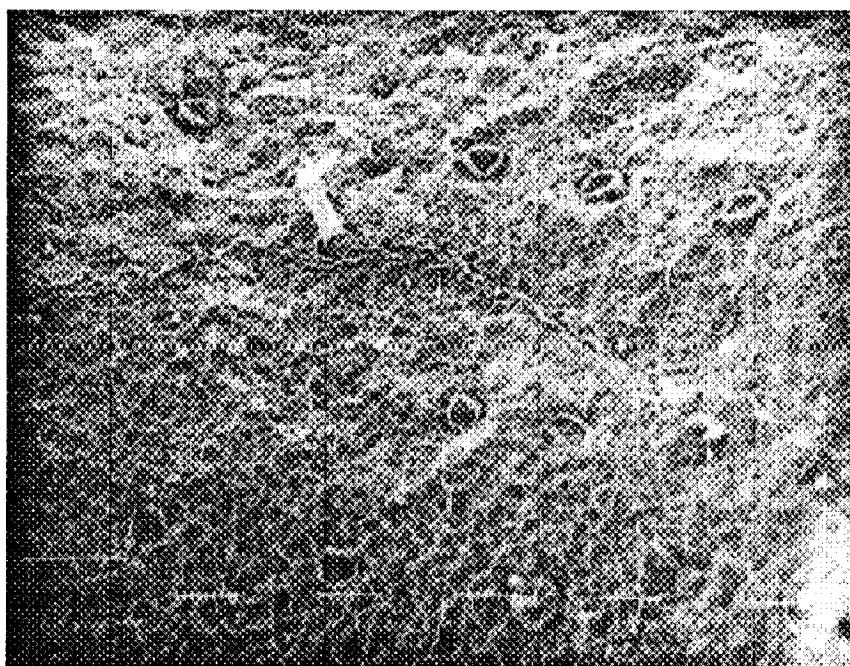


Fig. 2. 5 Glands collapsed to varying degree in leaves extracted with hexane at 200 W,  $\Delta T$  c. 10  $^{\circ}\text{C}$  (100  $\mu\text{m}$  bar, 100 x magnifications)

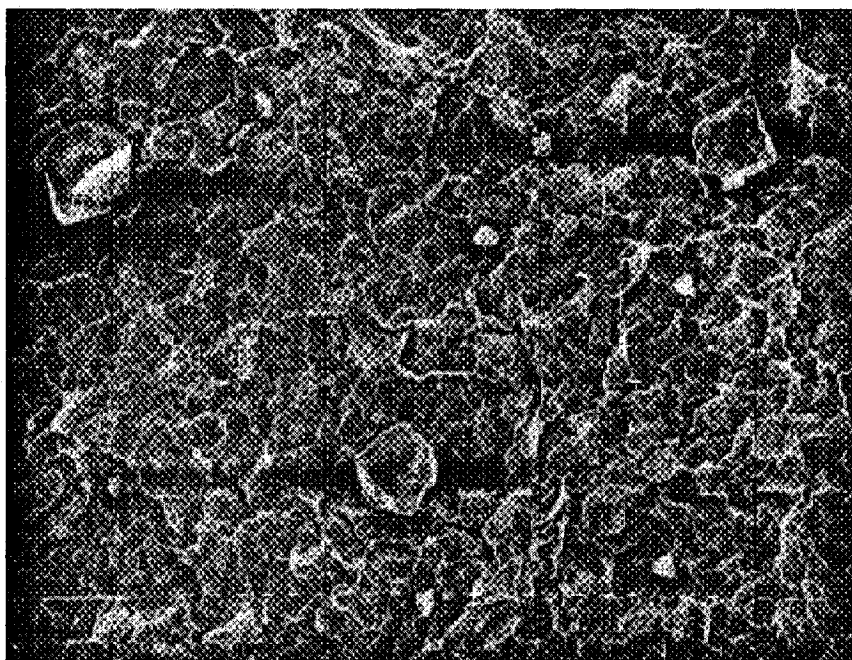


Fig. 2. 6 Shrivelled collapsed glands in extractions carried out using ethanol at a constant temperature of 35 °C (10  $\mu$ m bar, 200 x magnifications)

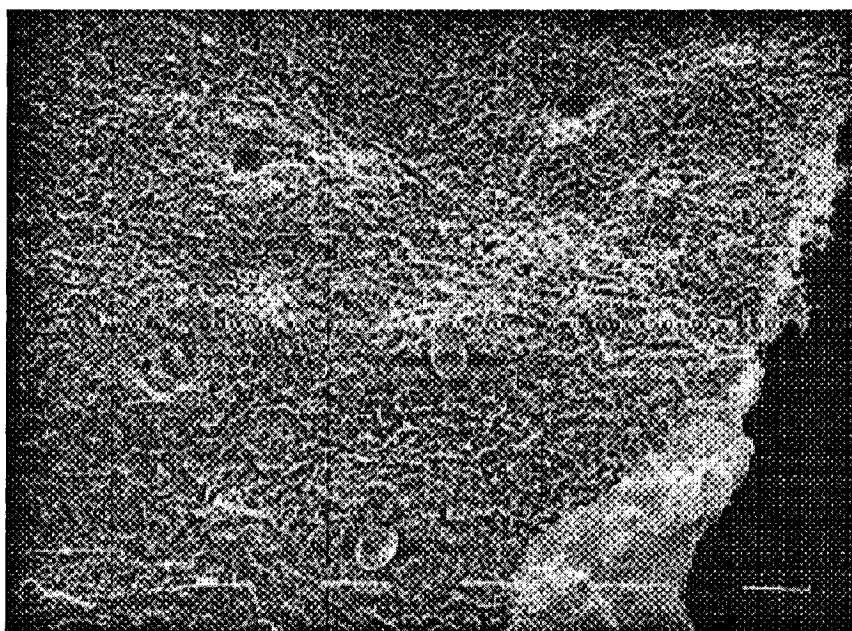


Fig. 2. 7 Glands transformed into deeply sunken cavities after extraction in 90 mol% ethanol at 35 °C (100  $\mu$ m bar, 100 x magnification)



Fig. 2. 8 Glands that have ruptured completely in isothermal extraction carried out with 90 mol% hexane at 35 °C (100  $\mu$ m bar, 100 x magnification)

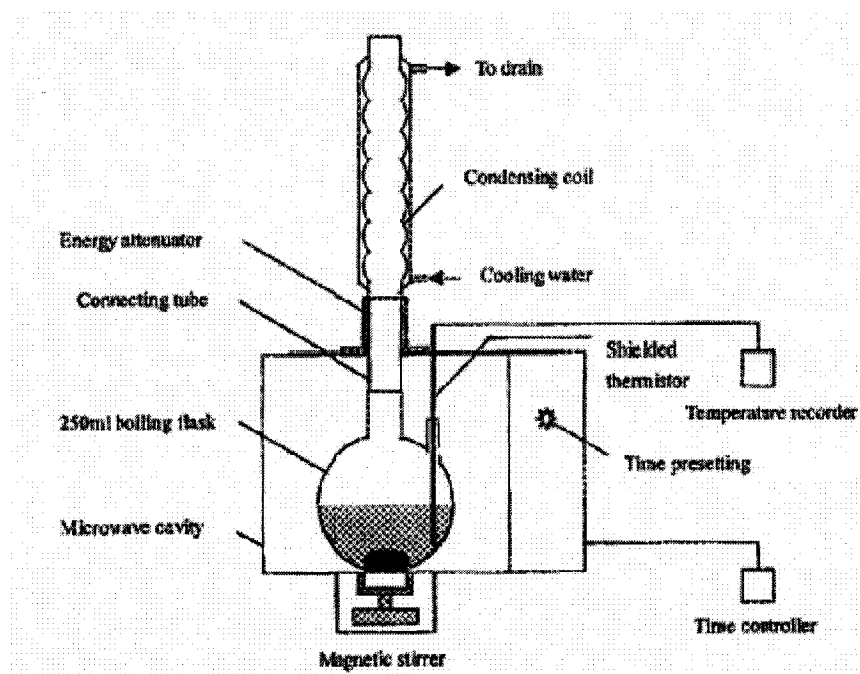
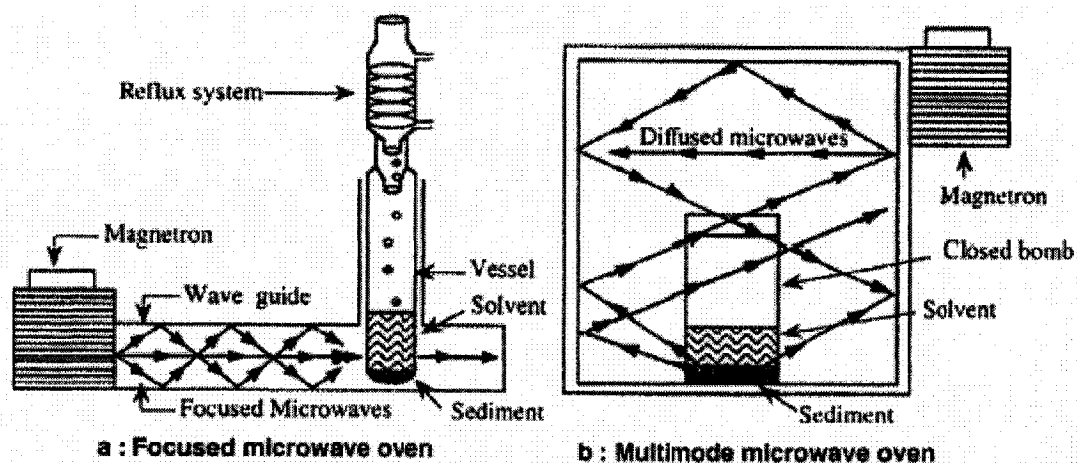


Fig. 2. 9 Schematic diagram of the microwave reactor for MAE

Table 2.3. Effect of various solvent and heating systems on the peltate glands during extraction of peppermint oil.

Extraction conditions	Number of glands				
	Globular whole glands	Slightly deformed and sunken glands	Deeply sunken glands	Broken glands	Percentage of damaged glands <sup>a</sup>
Untreated leaf	77	77			50
Hexane at 35 °C	3	359			99
Ethanol at 35 °C		64		7	100
90 mol% ethanol at 35 °C		18	132		100
90 mol% hexane at 35 °C	13		100	133	95
Microwave/200 W/hexane	26	142		4	85
Microwave/200 W/ethanol	1	221 <sup>b</sup>		7	99



**Fig. 2. 10.** Schematic view of focused microwave oven (a) and Multimode microwave oven (b)

#### 2.2.5. The scale-up of microwave-assisted extraction

Although the technique has been successfully used for 15 years and laboratory study showing promising industrial potentials, the industrialization of this technology seems very slow. Environment Technology Centre (ETC) of Environment Canada made the first step in the scale-up of this technology. The diagram of the equipment is shown in Figure 2.11 (ETC web). As can be seen,

the system is a continuous process where materials and solvents are pumped into the TEFLON tube located in a microwave cavity. In the cavity, microwave-assisted extraction occurs. This flowing continuous process enable this technique to be scaled up to 0.5 tonne/hr with microwave power of 6 kW. Analysis of the system shows that the continuous-flow-pipe system used in this equipment suggests that it can only be applied when the temperature is below the boiling point, preferably nonpolar solvent for the extraction with a mechanism suggested by Pare (1991, 1995). However, in most cases, the extraction need to be carried out in reflux conditions for a process of a few minutes to even hours (Mattina, et al., 1997; Pan et al. 2000; Bousquet, 1997; Li, et al. 2000), where the equipment can not be applied. In those cases a batch-type microwave-assisted extraction equipped with a condenser is more advantageous.

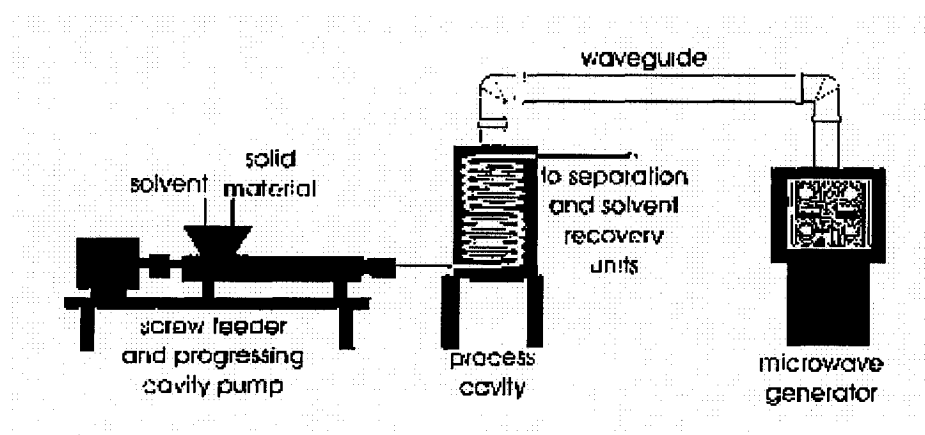


Fig. 2. 11 A schematic diagram of a scaled-up microwave-assisted extraction equipment

### 2.3 Microwave-assisted synthesis

Similar to microwave-assisted extraction, microwave-assisted organic synthesis is also a result of the wide spread of domestic microwave oven. Gedye et al. (1986) pioneered the application of microwaves in organic synthesis in sealed TEFLON vessels under pressurized conditions. Up to 240 times of acceleration was achieved compared to the classic synthesis method. A lot of research has been done after the first publication in this area. To date, there are

more than 1500 publications on the subject of microwave-assisted organic synthesis by performing a thorough search using the Chemical Abstract database. The synthesis covered most type of reactions that can be done using classic synthesis methods.

Table 2.4. Comparison of microwave-assisted synthesis and classic method. The microwave-assisted synthesis was carried out in a sealed TEFLON vessel using a domestic microwave oven (adapted from Gedye, et al., 1986).

Compound synthesized	Procedure followed	Reaction time	Recovery		Rate (MW)
			(Product)	(Reagent)	Rate (classic)
Esterification of benzoic acid with methanol					
C <sub>6</sub> H <sub>5</sub> COOCH <sub>3</sub>	Classic	8 hr.	74%	19%	96
C <sub>6</sub> H <sub>5</sub> COOCH <sub>3</sub>	Microwave	5 min	76%	11%	
Esterification of benzoic acid with propanol					
C <sub>6</sub> H <sub>5</sub> COOC <sub>3</sub> H <sub>7</sub>	Classic	7.5 hr.	89%	7%	25
C <sub>6</sub> H <sub>5</sub> COOC <sub>3</sub> H <sub>7</sub>	Microwave	18 min	86%	11%	
Esterification of benzoic acid with n-butanol					
C <sub>6</sub> H <sub>5</sub> COOC <sub>4</sub> H <sub>9</sub>	Classic	1 hr	82%	12%	8
C <sub>6</sub> H <sub>5</sub> COOC <sub>4</sub> H <sub>9</sub>	Microwave	7.5 min	79%	7%	
S <sub>N</sub> <sup>2</sup> reaction of 4-cyanophenoxide ion with benzyl chloride					
C <sub>6</sub> H <sub>5</sub> OCH <sub>2</sub> C <sub>6</sub> H <sub>5</sub>	Classic	12 hr.	72%	-	240
C <sub>6</sub> H <sub>5</sub> OCH <sub>2</sub> C <sub>6</sub> H <sub>5</sub>	Microwave	3 min	74%	-	
C <sub>6</sub> H <sub>5</sub> OCH <sub>2</sub> C <sub>6</sub> H <sub>5</sub>	Classic	16 hr.	89%	-	240
C <sub>6</sub> H <sub>5</sub> OCH <sub>2</sub> C <sub>6</sub> H <sub>5</sub>	Microwave	4 min	93%	-	

### 2.3.1 General advantage of microwave-assisted synthesis

#### 2.3.1.1 Rate enhancement

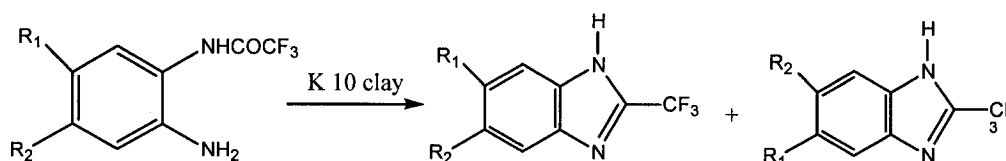
The fast reaction rate using microwave-assisted synthesis method was the main reason that it attracted so much attention. Many of the published literatures claimed that there is rate enhancement over classic synthesis methods (Bougrin,

et al., 2005; Gedye, et al., 1986; Zhong, et al., 2006; Wu, 2006; Moghaddam, et al., 2005; Guillot, et al., 2005)

Table 2.4 shows that microwave-assisted synthesis can greatly enhance the reaction rate of the esterification reaction of benzoic acid and different alcohols. With the increase in the carbon chain, the rate of enhancement gets lower. Very high enhancement was obtained for the  $S_N^2$  reaction.

### 2.3.1.2 Improved yield

In certain types of reactions, it is very hard to obtain satisfactory yield even after long period of time under classical synthesis conditions; however, high yield is possible in microwave-assisted synthesis method (Li and Yan, 2005; Nanjunda Swamy, et al., 2006; Grieco, et al., 2003; Altermin and Hallberg, 2000)



Scheme 2.1 Cyclization of monotrifluoroacetylated o-arylenediamines

Table 2.5. Cyclization of monotrifluoroacetylated o-arylenediamines (Bougrin, et al., 2001)

R1	R2	Temp. (°C)	Yield (%)	Δ (20 h)
			MW 2 min	
H	H	125	87	23
H	CH3	127	84	19
NO2	H	134	95	28

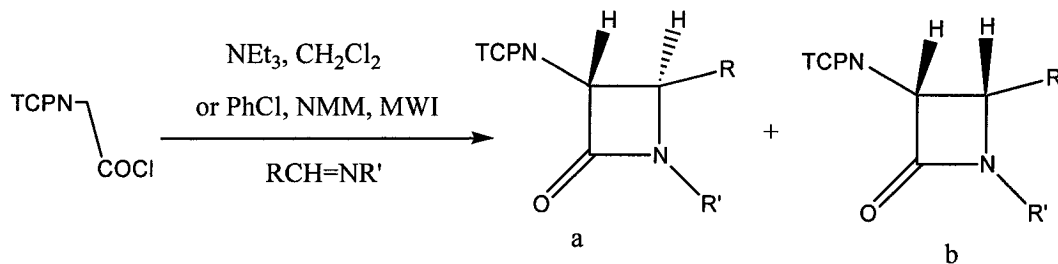
During the reaction published by Bougrin, et al. (2001), with conventional heating methods, even after 20 h of heating, the yield is no more than 30%. However with 2 min of microwave-assisted synthesis using montmorillonite K10,



more than 80% of yield was obtained and for the one with NO<sub>2</sub> the yield reaches 95%.

### 2.3.1.3 Selectivity

In many chemical reactions, different isomers are the products obtained instead of a single product. Microwave-assisted synthesis was reported to affect the formation of isomers of some reactions (Langa, et al., 1997; Bose, et al., 1996; Vega, et al., 1996; Perreux and Loupy, 2001). Selectivity in obtaining different ratio of isomers reported by Bose, et al. (1996) was presented in Scheme 2.2 and Table 2.6. It can be seen that using microwave-assisted synthesis, the isomer obtained after the reaction is completely different from the ones obtained through classic ways for most of these reactions.



Scheme 2.2. Synthesis of TCP protected  $\alpha$ -amino- $\beta$ -lactams.

TCP=tetrachlorophthaloyl; NMM=N-methylmorpholine; MWI=microwave irradiation, R'=PhOCH<sub>2</sub>

Table 2.6. Synthesis of TCP protected  $\alpha$ -amino- $\beta$ -lactams (Bose, et al., 1996)

No.	R	R'	Yield (%) <sup>*</sup>	a : b (MWI)	a : b Classic
1	Ph	p-methoxyphenyl	83 (57)	100 : 0	55 : 45
2	p-methoxyphenyl	p-methoxyphenyl	98 (52)	100 : 0	10 : 90
3	stytyl	p-methoxyphenyl	99 (77)	0:100	0 :100
4	furyl	p-methoxyphenyl	90 (53)	100: 0	20:80
5	Ph	benzyl	83	80: 20	/

\* Yields in the parenthesis are the ones obtained by the classic procedure

## 2.3.2 Basic types of microwave-assisted organic synthesis and possible mechanisms

### 2.3.2.1 Pressurized microwave-assisted organic synthesis

The earliest application of microwave energy in the organic synthesis is performed in a closed TEFLON vessel using a domestic microwave oven (Gedye, et al., 1986; Giguere, et al., 1986). In the closed TEFLON reactor, the vessel itself is transparent to microwaves. Microwaves can therefore be applied directly to the reactants. With the elevated pressure, the temperature can be much higher than in normal conditions. It can be approximated that an increase of 10 °C will cause the reaction rate double. As a result the reaction rate can be greatly enhanced.

### 2.3.2.2 Open vessel microwave assisted synthesis

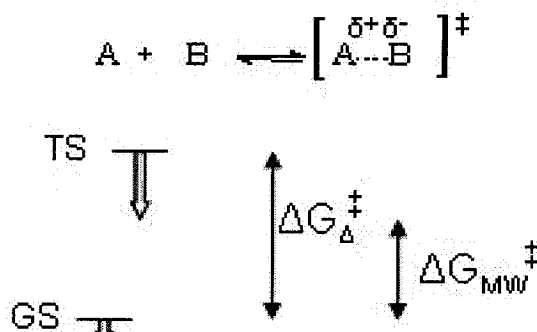
In an open vessel microwave-assisted synthesis, the temperature is determined by the boiling point of the reactants similar to the ones in the classic synthesis method. However, there are still many microwave-assisted chemical reactions having the greatly enhanced rate than classic organic synthesis (Bougrin, et al., 2005). The possible reason and mechanism involved in the open vessel microwave-assisted synthesis proposed by Loupy (2004) is illustrated in Scheme 2.3.

During the reaction, the appearance of a dipolar transition state makes it easier to couple with microwaves; as a result the free activation energy is reduced leading to a faster reaction. A few factors determine whether there will be athermal effect of microwaves. a). Polarity of the transition state: If the polarity of the transition state is higher than that of the ground level, then there is a strong possibility of athermal effect. b). Magnitude of the activation energy: fast reactions under conventional heating methods has a relatively small magnitude of the free energy; when microwaves are used, the space for magnitude reduction is limited, as a result the athermal effect will be limited if there will be

any. c). Rate determining step: if the formation of the dipolar transition state is the rate determining step, and if it meets other conditions, then athermal effect is likely to appear.

### 2.3.2.3 Solvent free reaction

The solvent free microwave-assisted synthesis is also called dry reaction or green reaction. By impregnating the reactant on solid supports such as aluminas, silicas, zeolites and clays, it can eliminate the use of solvents (Bougrin, et al., 2005). Great rate enhancement and yield improvement were reported using the dry reaction (Ding, et al., 1993; Zhu, et al., 1994; Villemin, et al., 1994, 1998; Varma and Kumer, 1999).



Scheme 2.3 Appearance of a dipolar transition state during the reaction; the presence of dipolar transition state causes the lower activation energy by microwaves than conventional heating (Loupy, 2004).

## 2.4 Simulation of microwave energy distribution

Two basic types are used for the simulation of energy distribution in a multimode cavity, i.e. using the Lambert's Law and solving the Maxwell equation. Both methods have been successfully applied in their corresponding problems solving situations (van Remmen, et al., 1996; Nykvist and Decareau, 1976; Fu

and Metaxas, 1994; Harms, et al. 1996; Meredith, 1994; Zhou, et al. 1995; Ma, et al., 1995).

#### 2.4.1 Lambert's Law

Lambert's law deals with the one dimensional penetration of microwave power into materials. It is expressed as:

$$P_d = P_o \exp(-2\alpha d) \quad (2.4)$$

Where:

$\alpha$  is the attenuation factor and

$$\alpha = \frac{2\pi}{\lambda} \sqrt{\epsilon' \frac{\sqrt{1 + \left(\frac{\epsilon''}{\epsilon'}\right)^2} - 1}{2}}$$

$P_d$  The energy at the distance of  $d$

$P_o$  is the incident energy

$\lambda$  is the wavelength

It can be seen that this is a very simple approach for simulation of the energy distribution. It is applicable only when the sample can be regarded as infinite in thickness, therefore it has very limited applications. In order to get a more accurate simulation for a more complex problem, or to get the energy distribution in a multimode cavity, solving Maxwell's equation provide a better solution.

#### 2.4.2 Solving Maxwell's Equation

Finite element and Finite Difference Time Domain (FDTD) are two commonly used methods for solving Maxwell's equation to get the energy

distribution in a complex object or within a multimode cavity and both methods are capable of simulating power density distribution in 3-D (Fu and Metaxas, 1994; Harms, et al. 1996; Meredith, 1994; Zhou, et al. 1995; Ma, et al., 1995). The finite element method is suitable for arbitrarily shaped inhomogeneous objects and this method requires the solution of a sparse matrix which may be very complicated. While FDTD is a very straight forward method that can readily model inhomogeneous and anisotropic materials as well as arbitrarily shaped geometries; it can also provide both time and frequency domain analyses which are important to microwave heating problems like field distribution, scattering parameters and dissipated power distribution for various materials and geometries (Harms, et al., 1996; Mittra and Harms, 1993). In our study, FDTD method will be used.

Time-dependent Maxwell's equations are:

$$\frac{\partial \mathbf{D}}{\partial t} = \nabla \times \mathbf{H} \quad (2.5)$$

$$\mathbf{D} = \epsilon \mathbf{E} \quad (2.6)$$

$$\frac{\partial \mathbf{H}}{\partial t} = \frac{1}{\mu_o} \nabla \times \mathbf{E} . \quad (2.7)$$

Where  $\mathbf{D}$ ,  $\mathbf{E}$  and  $\mathbf{H}$  are vectors in three dimensions and  $\mathbf{D}$  is the flux density. Pollard and Booton (2000) suggest that  $\mathbf{E}$  is normalized to

$$\tilde{\mathbf{E}} = \sqrt{\frac{\epsilon_o}{\mu_o}} \mathbf{E} \quad (2.8)$$

Therefore Equations 2.5 – 2.7 become

$$\frac{\partial \tilde{\mathbf{D}}}{\partial t} = \frac{1}{\sqrt{\epsilon_o \mu_o}} \cdot \nabla \times \mathbf{H} \quad (2.9)$$

$$\mathbf{D} = \epsilon \tilde{\mathbf{E}} \quad (2.10)$$

$$\frac{\partial \mathbf{H}}{\partial t} = - \frac{1}{\sqrt{\epsilon_o \mu_o}} \cdot \nabla \times \tilde{\mathbf{E}} \quad (2.11)$$

From equations 2.9 and 2.11, six scalar equations can be produced:

$$\frac{\partial \tilde{D}_x}{\partial t} = \frac{1}{\sqrt{\epsilon_o \mu_o}} \left( \frac{\partial H_z}{\partial y} - \frac{\partial H_y}{\partial z} \right) \quad (2.12a)$$

$$\frac{\partial \tilde{D}_y}{\partial t} = \frac{1}{\sqrt{\epsilon_o \mu_o}} \left( \frac{\partial H_x}{\partial z} - \frac{\partial H_z}{\partial x} \right) \quad (2.12b)$$

$$\frac{\partial \tilde{D}_z}{\partial t} = \frac{1}{\sqrt{\epsilon_o \mu_o}} \left( \frac{\partial H_y}{\partial x} - \frac{\partial H_x}{\partial y} \right) \quad (2.12c)$$

$$\frac{\partial H_x}{\partial t} = \frac{1}{\sqrt{\epsilon_o \mu_o}} \left( \frac{\partial \tilde{E}_y}{\partial z} - \frac{\partial \tilde{E}_z}{\partial y} \right) \quad (2.12d)$$

$$\frac{\partial H_y}{\partial t} = \frac{1}{\sqrt{\epsilon_o \mu_o}} \left( \frac{\partial \tilde{E}_z}{\partial x} - \frac{\partial \tilde{E}_x}{\partial z} \right) \quad (2.12e)$$

$$\frac{\partial H_z}{\partial t} = \frac{1}{\sqrt{\epsilon_o \mu_o}} \left( \frac{\partial \tilde{E}_x}{\partial y} - \frac{\partial \tilde{E}_y}{\partial x} \right) \quad (2.12f)$$

Finite difference approximations of Equations 2.12c, f result in:

$$\begin{aligned} D_z^{n+1/2}(i, j, k+1/2) &= D_z^{n-1/2}(i, j, k+1/2) \\ &+ \frac{\Delta t}{\Delta x \cdot \sqrt{\epsilon_o \mu_o}} (H_y^n(i+1/2, j, k+1/2) - H_y^n(i-1/2, j, k+1/2) \\ &- H_x^n(i, j+1/2, k+1/2) + H_x^n(i, j-1/2, k+1/2)) \end{aligned} \quad (2.13)$$

$$\begin{aligned} H_z^{n+1}(i+1/2, j+1, k) &= D_z^n(i+1/2, j+1/2, k) \\ &+ \frac{\Delta t}{\Delta x \cdot \sqrt{\epsilon_o \mu_o}} (E_y^{n+1/2}(i+1, j+1/2, k) - E_y^{n+1/2}(i, j+1/2, k) \\ &- E_x^{n+1/2}(i+1/2, j+1, k) + H_x^{n+1/2}(i+1/2, j, k)) \end{aligned} \quad (2.14)$$

The finite difference approximations and the computer equations of the rest of equations are similar.

The stable conditions are (Kunz and Luebbers, 1993):

$$v\Delta t \leq \frac{\Delta u}{\sqrt{d}} \quad (2.15)$$

And in the above computer equations, Sullivan (2000) used

$$\Delta t = \frac{\Delta x}{2 \cdot c_o} \quad (2.16)$$

so that

$$\frac{1}{\sqrt{\epsilon_o \mu_o}} \frac{\Delta t}{\Delta x} = 1/2 \quad (2.17)$$

## 2.5 Summary

In this chapter, the basic knowledge about microwave and microwave-matter interaction, microwave-assisted extraction and microwave-assisted synthesis were reviewed. Advantages of microwave-assisted extraction in extracting natural products, the possible explanations of the microwave accelerating effect were reviewed. The review indicates that microwave-assisted extraction technique has high potential for the industrial production of natural products. The status of its application in industry is briefly reviewed, showing that a different approach for the scale-up should be taken to make this technology more versatile. Microwave-assisted synthesis showed great advantages over classic synthesis methods in many organic reactions. However most of them are still applicable only in the laboratories. Basic methods for the simulation of microwave energy distribution, especially FDTD method are briefly introduced. This will be the basic knowledge for numerical study of the problems associated with the scale-up of this technique.

## CONNECTING STATEMENT 1

Background information was provided with the main goal and specific objectives specified in Chapter I. A comprehensive literature review in the field of microwave-assisted extraction and synthesis was provided in Chapter II. In the chapter, specific extraction study on the extraction of peppermint leaves will be presented. Microwave-assisted extraction is also studied in this chapter.

Manuscript has been prepared to be submitted to *journal of natural product*:

**Jianming Dai\*, G.S.Vijaya Raghavan\* and V. A. Yaylayan\*\*, Investigation of various factors on the extraction of peppermint (*Mentha piperita* L.) leaves. To be submitted to Journal of natural product.**

\*Department of Bioresource Engineering, McGill University, 21,111 Lakeshore road, Ste-Anne-de-Bellevue, QC, H9X 3V9

\*\*Department of Food Science and Agricultural Chemistry, McGill University, 21,111 Lakeshore road, Ste-Anne-de-Bellevue, QC, H9X 3V9

Contributions made by different authors are as follows:

The first author, the Ph.D. student did the experimental work and prepared the manuscript; the second author is the supervisor who guided the research work; the third author provided the laboratory equipment and guidance during the experimental process.



# CHAPTER III

## INVESTIGATION OF VARIOUS FACTORS ON THE EXTRACTION OF PEPPERMINT (*MENTHA PIPERITA* L.) LEAVES

### 3.1 Abstract

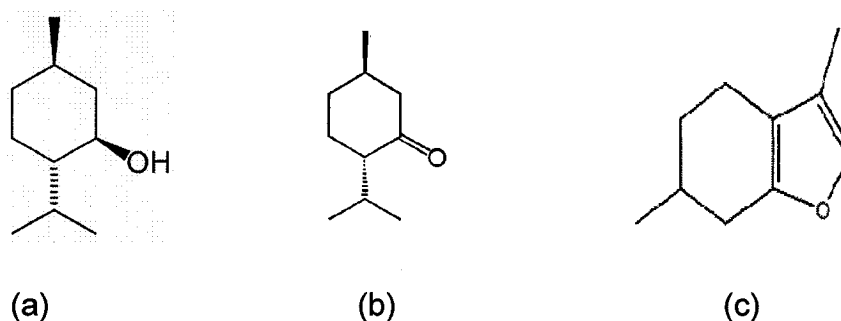
Ingredients from peppermint leaves are widely used in the food industry as food additives and natural flavours. The traditional way to obtain these ingredients is steam distillation, a long and energy consuming process. The use of solvent extraction could greatly reduce the process time and energy consumption. The objective of this paper is to investigate the influence of various factors on the efficacy of extracting peppermint leaves.

### 3.2 Introduction

Peppermint oil has been widely used in food, beverage, cosmetic, health and tobacco industries (Yazdani, 2002; Dulebohn, 2002; Harada, 2002; Guntert, Carmines, 2002). The major components of peppermint oil include mentol, menthone and menthofuran (Scheme 3.1). The peppermint oil is reported to have anti-oxidant properties (Ribeiro, 2002; Ljubojevic, 2000; Stangler, 2001), antibacterial activity (Arakawa, 2000) and is one of the most important constituents of some over-the-counter remedies in Europe for irritable bowel syndrome (Pittler and Ernst, 1998; Lis-Balchin and Hart, 1999). Steam distillation is traditionally used to produce essential oil from the aerial part of the peppermint plant (Yazdani, 2002; Pino, 2002; Ammann, 2002). In spite of its simplicity and non-solvent-involvement, steam distillation is time consuming and requires a lot of energy. Most importantly, the high temperature and high moisture volume obtained during the process may cause the modification of the flavor in the essential oil (Spiro and Chen, 1995).

Solvent extraction is one of the most commonly used methods in obtaining constituents from plant sources. The extraction process does not necessarily

require high temperature, therefore provides a milder condition in obtaining the essential oils from peppermint plant. In terms of time required, the extraction process can be influenced by many factors such as solvent, temperature, and sample to solvent ratio. Furthermore, the extraction process may be accelerated by the addition of different energy sources such as ultrasonic or microwave energy.



Scheme 3.1. Major components from peppermint oil. (a) menthol; (b) menthone; (c) menthofuran

Microwave-assisted extraction (MAE) is a technique developed in late 1980s. It is reported to greatly reduce the extraction time and especially useful for extracting natural products from plant origins (Dai et al., 1999; Ganzler et al., 1986; Pan et al., 2000; Pastor et al., 1997; Paré, 1994). For the extraction of peppermint using non-polar solvent, the extraction is 180 times faster than stream distillation (Paré, 1994). In this paper the influence of various factors on the extraction of essential oils from peppermint leaves are investigated. Microwave-assisted extraction is compared with different methods on the extraction efficacy.

### 3.3 Material and Methods

#### 3.3.1 Materials

Peppermint (*Mentha piperita* L.) used in this study was obtained from Ontario, Canada. The plant was grown in the greenhouse during the winter and

planted in the garden in summer. The peppermint plant of June was used in this study. The leaves were removed from the petiole before the experiment.

Table 3.1 Factors and levels used in the investigation.

Levels	Factors			
	A Extr. method	B Solvent	C Time (min)	D Sample/Sol.
1	Room temperature extr. (RTE)	EtOH	5	2g/20mL
2	Reflux extr. (RFX)	Hexane	10	2g/40mL
3	Microwave-assisted extr. (MAE)	EtOH/Hexane = 7/3	30	2g/60mL
4	Ultrasonic extr. (UE)	EtOH/Hexane = 3/7	60	2g/80mL

Table 3.2 Orthogonal experimental design table

Runs	Treatments				
	A	B	C	D	error
1	1	1	1	1	1
2	1	2	2	2	2
3	1	3	3	3	3
4	1	4	4	4	4
5	2	1	2	3	4
6	2	2	1	4	3
7	2	3	4	1	2
8	2	4	3	2	1
9	3	1	3	4	2
10	3	2	4	3	1
11	3	3	1	2	4
12	3	4	2	1	3
13	4	1	4	2	3
14	4	2	3	1	4
15	4	3	2	4	1
16	4	4	1	3	2

Note: Factors and levels in this table corresponding to the values noted in Table 3.1.

### 3.3.2 Experimental Design

Four factors, each at four levels were studied for their influence on the extraction of menthone and menthol (Table 3.1). To accomplish this, an

orthogonal experimental design was used (Table 3.2). Each treatment was replicated twice.

### 3.3.3 Extraction Procedures

1). *Room Temperature Extraction (RTE)*. Two grams of intact peppermint leaves was placed in a 100 mL conical flask, followed by the addition of required amount of selected solvent. The extraction was carried at room temperature under magnetic stirring for required period of time. 2). *Reflux Temperature Extraction (RFX)*. The procedure was almost the same as that of the RTE, except that it was carried out under the reflux temperature of the solvent using a hotplate. No stirring was needed. 3). *Microwave-Assisted Extraction (MAE)*. Two grams of sample was placed in the quartz extraction vessel of the Prolabo Synthewave 402 (focused microwave-assisted extraction/synthesis equipment at atmospheric pressure, Fontenay-Sous-Bois, Cesex, France) followed by the addition of required amount of certain solvent. The extraction was carried out at a fixed power level of 150 W during the entire extraction period. 4). *Ultrasonic Extraction (UE)*. The procedure was almost the same as that of RTE, except that it was carried out in the water bath of the ultrasonic equipment.

### 3.3.4. GC analysis

A gas chromatography (HP 5890, USA) equipped with an FID detector was used for the analysis of the extracts. A DB5 column (30 m, 0.25 mm i.d. and 0.25  $\mu$ m film) was used. The temperatures of the injector and the detector were 120 and 140 °C, respectively. The temperature of the oven was kept at 100 °C at all times during the separation. Helium was used as carrier gas at a flow rate of 1.8 mL/min through the column. The equipment was running in a split mode at a split ratio of 1/20. For quantification, menthol and menthone standards (Sigma Chemical Co., St. Louis, MO, USA) were used to establish the calibration curve ranging from 0.064 to 0.64 mg/mL and 0.1 to 1 mg/mL, respectively. The amount of menthofuran was calculated using the calibration curve of menthol.

### 3.3.5 Statistical analysis

SAS software was used to perform the ANOVA procedure for each factor, and GLM DUNCAN analysis was carried out for each level under the same factor. The contribution to total effect is calculated as:

$$Contr_i = F_i / \sum_{i=1}^n F_i \quad (1)$$

Where:  $Contr_i$  is the contribution of the  $i^{th}$  factor,  $F_i$  is the F value of the  $i^{th}$  factor, and  $n$  is the total number of factors.

## 3.4 Results and Discussion

The influence of four factors, viz., extraction methods, solvents, extraction time, and sample to solvent ratio on the extraction of three major constituents, menthone, menthofuran and menthol are shown in Figs. 3.1 through 3.4. The results of DUNCAN analysis for different components are presented in Table 3.3. As shown in Fig. 3.1 and Table 3.3, there are no significant difference between the MAE and the RFX for the extraction of menthone, but both of them are significantly higher than the ones obtained using UE. The UE value is significantly higher than the RTE one. Other than menthofuran and menthol, the extraction efficacy of the four methods significantly differs from each other and follow the order of  $MAE > RFX > UE > RTE$ .

The essential oil is located only in the peltate glands or trichomes of the peppermint leaves (Maffei, et al., 1989; McCaskill et al., 1992; Spiro and Chen, 1995). If the glands are kept intact during the extraction process, the extraction process is mainly a diffusion based process, during which the increased temperature leads to a higher diffusion rate. Therefore it is quite understandable that MAE and RFX have higher extraction rates than RTE or UE. It is observed that during the UE process, the temperature slightly increased, causing the UE procedure to proceed faster than the RTE process. Besides the influence of

temperature on the diffusion-based process, increased temperature could lead to the break down of the gland, causing the rapid release of the essential oil into the solvents. Pare (1991) suggested that the application of microwave energy in combination with a nonpolar solvent could cause the break down of the cell. Controversial reports on the breaking down of the gland suggest that it is caused by the solvent rather than microwave effect. Considering the non-significance between MAE and RFX on menthone and the slightly higher yield of MAE over RFX on menthofuran and menthol instead of the 180 times acceleration of MAE over steam distillation as reported by Pare (1991), we believe here the difference is caused by the overheating during the MAE process. This is further proved by the influence of solvent as shown in Fig. 3.2 and Table 3.3.

Table 3.3 DUNCAN analysis results for the different levels in the various factors investigated for menthone, menthofuran and menthol, the different letters in each column means they are significantly different ( $\alpha=0.05$ ).

Levels	Factors											
	A			B			C			D		
	Extr. method			Solvent			Extr. time			Sample/Solvent		
	I <sup>1</sup>	II <sup>2</sup>	III <sup>3</sup>	I	II	III	I	II	III	I	II	III
1	c	d	d	b	b	a	c	c	c	b	bc	b
2	a	b	b	c	c	b	b	b	b	b	c	b
3	b	c	c	b	b	a	a	a	a	a	ab	b
4	a	a	a	a	a	a	b	b	b	a	a	a

Note: <sup>1</sup> Menthone; <sup>2</sup> Menthofuran; <sup>3</sup> Menthol

Figure 3.2 showed that hexane gives the lowest yield for the extraction of all three of the compounds. Also, it informs us that the best solvent for the extraction of all the individual components is an Ethanol/Hexane mixture with a ratio of 3/7. This is consistent with Spiro and Chen's (1995) conclusions. Their work showed that using hexane as solvent, either under 35 °C or using microwave energy, none or only small amounts of the gland was broken.

However when using 90 mol% hexane, more than half of the glands were broken and the rest were deeply shrunken. Therefore, solvent is a more important factor than microwave energy in the break down of the glands containing the essential oil. 70% (v/v) of hexane provides the highest yield in this study for all three components, and 30% (v/v) hexane has similar effects as the pure ethanol.

The influence of extraction time on the extraction yield is shown in Fig. 3.3. For all the three components, the yield increases rapidly from 5 minutes to 10 minutes followed by a slower increases until the 30 minute mark, followed by a drop in yield from 30 to 60 minutes. Maximum yield was obtained at 30 minutes. Further increase in extraction time probably leads to the decomposition of the component which may be mainly due to the RFX and MAE processes. Steam distillation has even higher temperature than these two processes, therefore it is reasonable to believe the exposure to higher temperature over long period of time during the steam distillation process will alter the chemical composition thus modify the flavor. Solvent extraction with shorter time or even slightly lower temperature than the boiling temperatures of the solvent is preferable in the industrial processes.

Sample to solvent ratio was also studied as one of the influencing factors (Fig. 3.4 and Table 3.3). For menthone and menthofuran, the 60 mL solvent and 80 mL solvent did not make any difference but these values are higher than the 40 mL and 20 mL solvents. Other than menthol, which has the highest amount in the three components, the highest amount was obtained with 80 mL of solvent.

The ANOVA result shows that all factors have a significant effect at 95% confidence level on the extraction of each individual component. The contribution of each individual factor on the total effect is plotted in Fig. 3.5 a, b, c. For all three components, extraction methods are the most important factor among all factors studied. The second most important factor in extracting menthone and menthofuran is solvent but it is extraction time for menthol. Sample to solvent ratio is the least important factor for the extraction of all three components.

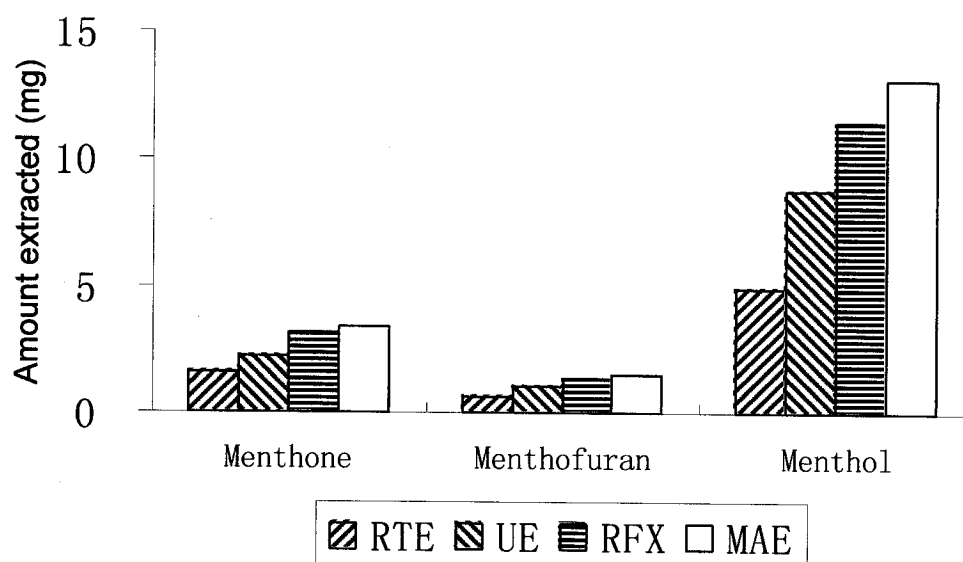


Fig. 3.1 Influence of extraction methods on the amount of menthone, menthofuran, and menthol extracted

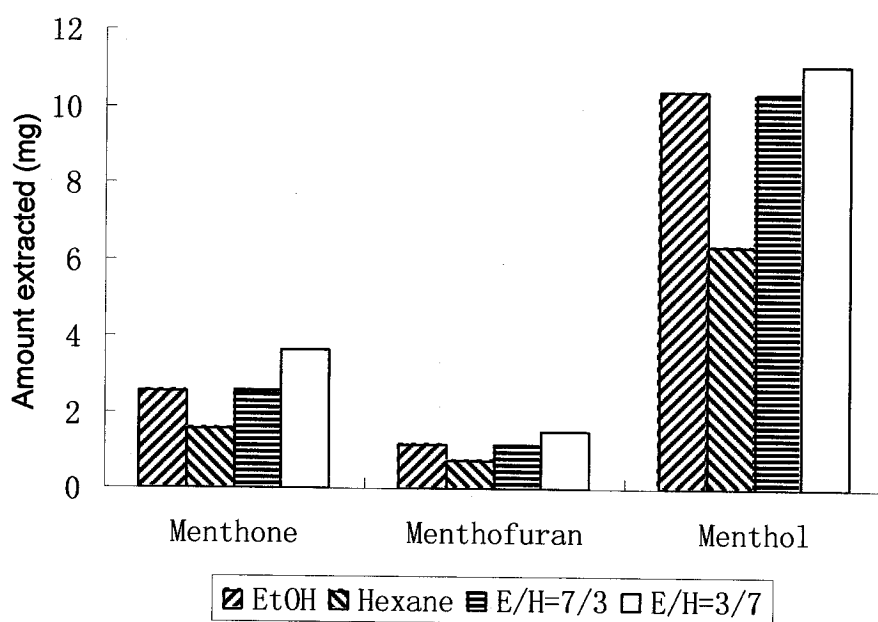


Fig. 3.2 Influence of solvents on the amount of menthone, menthofuran, and menthol extracted



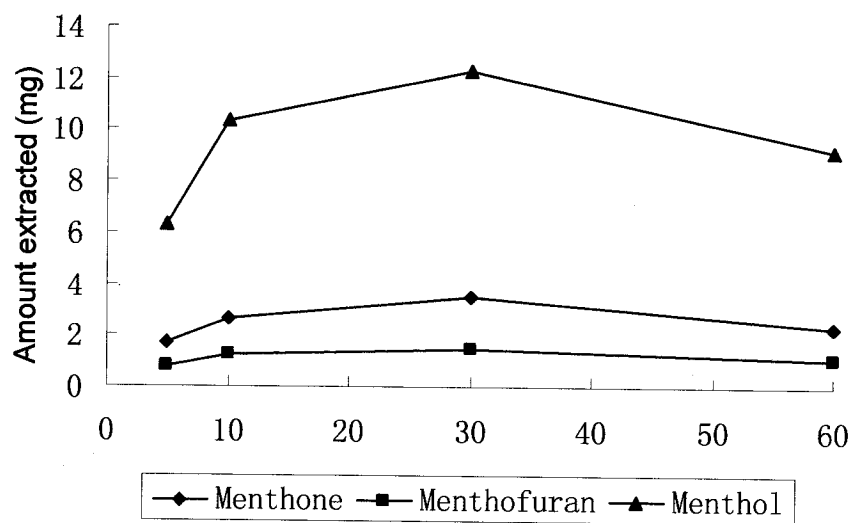


Fig. 3.3 Influence of extraction time on the amount of menthone, menthofuran, and menthol extracted

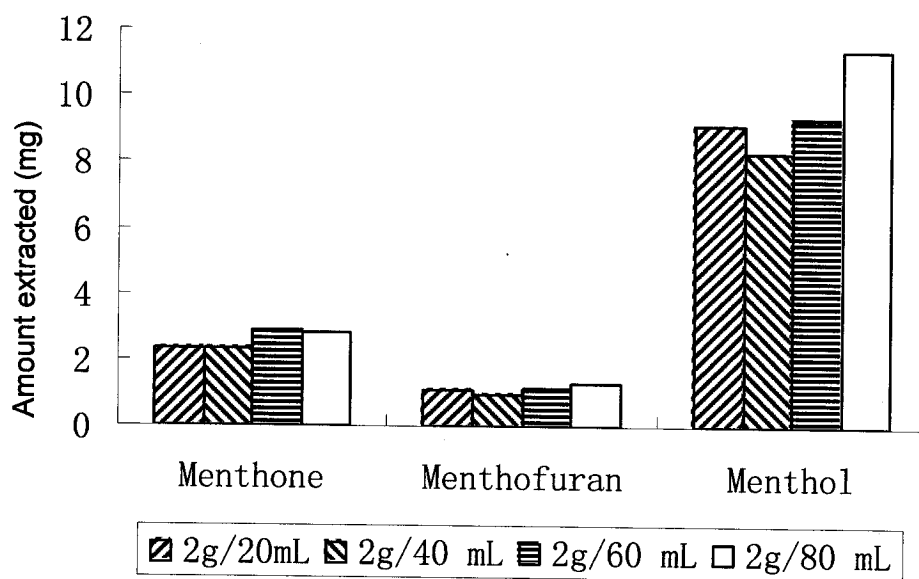


Fig. 3.4 Influence of sample/solvent ratio on the amount of menthone, menthofuran, and menthol extracted

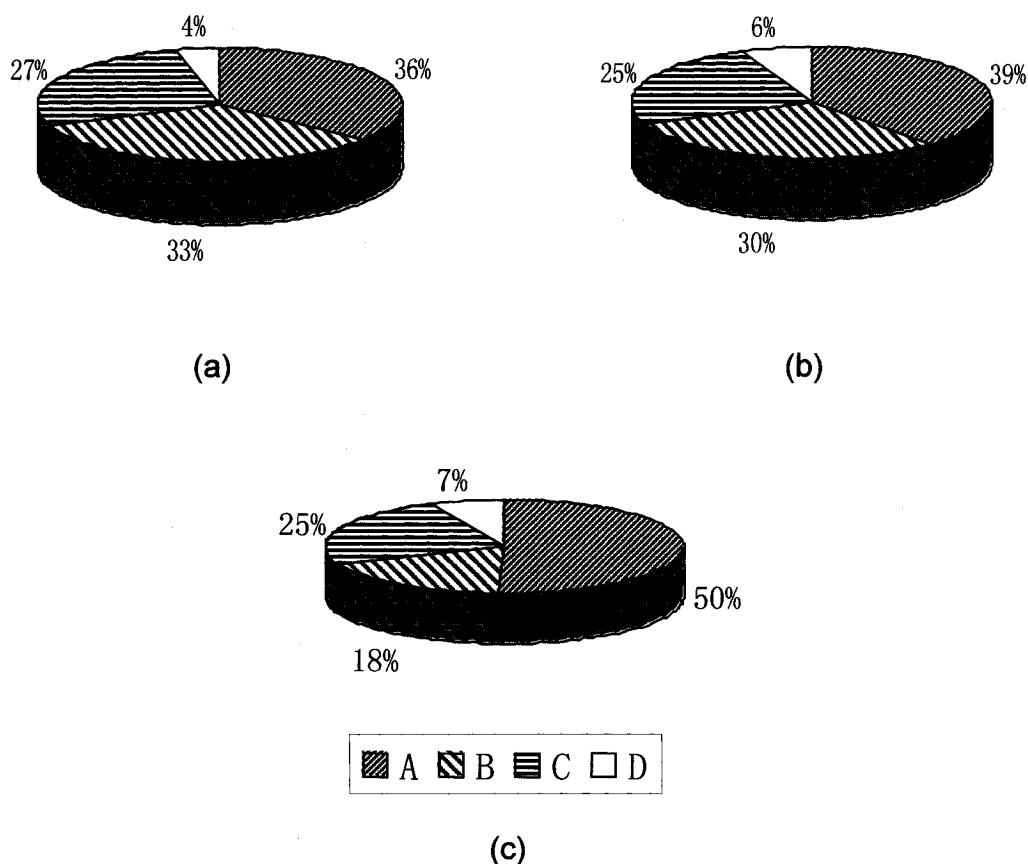


Fig. 3.5 Contribution of different factors on the extraction efficacy: (a) menthone (b) menthofuran, and (c) menthol; A: Extraction method, B: Solvent, C: Extraction time, D: Sample/solvent ratio

### 3.5 Conclusion

All factors studied significantly influence the extraction of menthone, menthofuran and menthol from peppermint leaves. Extraction method is the most important factor followed by either solvent or extraction time, depending on the components. Sample to solvent ratio is the least important factor in the extraction therefore lower amounts of solvent can be used in the industrial processes. Microwave-assisted extraction was observed to have an acceleration effect over RFX which may be due to the superheating effect during MAE rather than the mechanism proposed by Pare (1991). Solvent mixture is believed to be the factor that causes the break down of the glands.

### 3.6 Acknowledgment

The authors wish to acknowledge the Natural Science and Engineering Research Council of Canada (NSERC) and Canadian International Development Agency (CIDA) for their financial support.

### 3.7 References

- Ammann, A.; Hinz, D.C.; Addleman, R. S.; Wai, C.M. and Wenclawiak, B.W. 1999. Superheated water extraction, steam distillation, and SFE of peppermint oil. *Fresenius' Journal of Analytical Chemistry*. 364(7), 650-653.
- Arakawa, T. and Osawa, K. 2000. Pharmacological study and application to food of mint flavor-antibacterial and antiallergic principles. *Aroma Research*. 1(1), 20-23.
- Brun, N.; Colson, M.; Perrin, A. and Voirin, B. 1991. Chemical and morphological studies of the effects of aging on monoterpene composition in menthe-piperita leaves. *Canadian journal of botany*. 69(10), 2271-2278.
- Carmines, E. L. 2002. Evaluation of the potential effects of ingredients added to cigarettes. Part 1: Cigarette design, testing approach, and review of results. *Food and Chemical Toxicology*. 40(1), 77-91.
- Dai, J.; Yaylayan, V.A.; Raghavan, G. S. V. and Pare, J. R. 1999. Extraction and colorimetric determination of azadirachtin related limonoids in the neem seed kernel. *J. Agric. Food Chem*. 47, 3738-3742
- Dulebohn, J.I. and Carlotti, R. J. 2002. Soy milk-juice beverage. PCT Int. Appl. WO0249459 20 pp.
- Ganzler, K.; Salgo, A. and Valko, K. 1986. Microwave extraction: a novel sample preparation method for chromatography." *Journal of Chromatography*. 371, 299-306.
- Guntert, M.; Krammer, G.; Lambrecht, S.; Sommer, H.; Surburg, H. and Werkhoff, P. 2001. Flavor chemistry of peppermint oil (*Mentha piperita* L.). *ACS Symposium Series*. 794(Aroma Active Compounds in Foods), 119-137.
- Harada, S.; Ohara, H. and Nishimura, O. 2002. Method for modification of mentha essential oil. *Jpn. Kokai Tokkyo Koho*. JP 2002038187 6 pp.
- Ljubojevic, S. 2000. Antioxidative activity of ethanol extract of mint, sage, vitamin E and synthetic antioxidant BHT. Prague 2000, International Symposium

- & Exhibition on Environmental Contamination in Central & Eastern Europe, Proceedings, 5th, Prague, Czech Republic, Sept. 12-14, 2000, p1492-1497.
- Maffei, M.; Chialva, F. and Sacco, T. 1989. Glandular trichomes and essential oils in developing peppermint leaves I. variation of peltate trichome number and terpene distribution within leaves. *New phytologist*. 111(4), 707-716.
- Ribeiro, M. A.; Martins, M. M.; Esquivel, M. M.; Bernardo-Gil, M. G. 2002. Peppermint supercritical CO<sub>2</sub> extraction. Influence of extraction conditions on the antioxidant activity of the residues. *Informacion Tecnologica*. 13(3), 185-190.
- Pan, X.; Liu, H.; Jia, G.; and Shu, Y. 2000. Microwave-assisted extraction of glycyrrhizic acid from licorice root. *Biochem. Eng. J.* 5(3), 173-177.
- Paré, J. R. J. and Bélanger, J. M. R. 1994. Microwave-Assisted Process (MAP): a new tool for the analytical laboratory. *Trends Anal. Chem.* 13, 176-184.
- Pastor, A.; Vazquez, E.; Ciscar, R. and de la Guardia, M. 1997. Efficiency of the microwave-assisted extraction of hydrocarbons and pesticides from sediments. *Anal. Chim. Acta*. 344(3), 241-249.
- Pittler, M. H. and Ernst, E. 1998. Peppermint Oil for Irritable Bowel Syndrome: A Critical Review and Metaanalysis. *The American journal of gastroenterology*. 93 (7), 1131 – 1135.
- Pino, J. A.; Borges, P.; Martinez, M. A.; Vargas, M.; Flores, H.; Del Campo, S.T. M. and Fuentes, V. 2002. Essential oil of *Mentha piperita* L. grown in Jalisco. *Journal of Essential Oil Research*. 14(3), 189-190.
- Spiro, M. and Chen, S.S. 1995. Kinetics of isothermal and microwave extraction of essential oil constituents of peppermint leaves into several solvent systems. *Flavour and fragrance journal*. 10, 259-272.
- Stangler, H.S.; Hadolin, M.; Knez, Z. and Bauman, D. 2001. Antioxidant and emulsification efficiency of active components of Labiatae. Zbornik Referatov s Posvetovanja Slovenski Kemijski Dnevi, Maribor, Slovenia, Sept. 20-21, 2001(Part 2), 856d/1-856d/6.
- Yazdani, D.; Jamshidi, A. H. and Mojab, F. 2002. Comparison on menthol content of cultivated peppermint at different regions of Iran. *Faslnamah-i Giyahan-i Daruyi*. 1(3), 73-77, 93.

## CONNECTING STATEMENT 2

Chapter III studied the influence of various factors on the extraction of peppermint leaves. Microwave-assisted extraction is one of the levels of factors studied using an orthogonal experimental design. Rate enhancement was observed during the extraction compared to the extraction under other extraction methods especially under reflux conditions. In this chapter, similar method will be used to study the extraction of different ginsenosides from American ginseng.

Manuscript has been prepared to be submitted to *journal of Agricultural and food Chemistry*:

**Jianming Dai, G.S.Vijaya Raghavan and M. Ngadi, Investigation of Different Factors on the Extraction of Ginsenosides from Fresh American Ginseng (*Panax quinquefolium* L.) Root.**

Department of Bioresource Engineering, McGill University, 21,111 Lakeshore road, Ste-Anne-de-Bellevue, QC, H9X 3V9

Contributions made by different authors are as follows:

The first author, the Ph.D. student did the experimental work and prepared the manuscript; the second author is the supervisor who guided the research work; the third author provided the laboratory equipment and guidance during the experimental process.

## CHAPTER IV

### INVESTIGATION OF DIFFERENT FACTORS ON THE EXTRACTION OF GINSENOSIDES FROM FRESH AMERICAN GINSENG (*PANAX QUINQUEFOLIUM* L.) ROOT

#### 4.1 Abstract

The influence of various factors, i.e. extraction method, solvent, solvent to sample ratio, extraction time, and the size of sample particles on the extraction of ginsenosides Re, mRb1, Rb1 and total ginsenosides from fresh American ginseng root was studied. Results showed that for different ginsenosides, different factors influence extraction differently. Microwave-assisted extraction (MAE) was compared with other extraction methods, and no sign of special acceleration effect was observed.

Keywords: Microwave, extraction, ginseng, ginsenosides, orthogonal experimental design

#### 4.2 Introduction

American ginseng (*Panax quinquefolium* L.) is an important medicinal herb in North America. Many nutraceutical products have been developed from the extracts of American ginseng root in which the dammarane saponins, generally referred as ginsenosides, are believed to be the active constituents (Li et al., 1996). The major neutral components include ginsenosides Rb1, Rb2, Rc, Rd, Re, Rg1 and main malonyl ones are mRb1, mRb2, mRc, mRd (Ren and Chen, 1999). Among all these ginsenosides, Rb1 and Re accounts for 70 – 80% of the total ginsenosides for the ginseng from British Columbia, Canada (Li et al., 1996). Ren and Chen (1999) also reported the HPLC chromatographs of aqueous ethanol extracts of ginseng root from Jilin, P.R. China indicating Re, mRb1 and Rb1 contribute to more than 90% of total ginsenosides.

Most of the American ginseng are sold in whole dried products, a portion of them have been processed into nutraceutical products using the extracts from ginseng root. The extraction of dry ginseng root by conventional heating is a slow process (Ryu et al., 1979; Sung et al., 1985). Various factors such as solvent, sample to solvent ratio, sample particle size, and extraction time may influence the extraction process. Microwave-assisted Extraction (MAE) is a solvent extraction technology using microwave as power source of energy input in the cavity. Due to the special mechanism in heating and unknown mechanisms, this technology was reported to greatly reduce the time needed for the process (Dai et al. 1999; Ganzler et al. 1986; Pan et al., 2000; Pastor et al., 1997). Furthermore, new extraction technology as microwave-assisted extraction (MAE) may shorten the extraction time. The objectives of this study are to investigate how various factors affect the extraction of ginsenosides from fresh American ginseng root and to compare MAE method with other extraction methods.

#### **4.3 MATERIAL AND METHODS**

##### **4.3.1 Materials**

Roots of four year old American ginseng (*P. quinquefolium* L.) were provided by Agricultural Canada(ON, Canada). The fresh ginseng root samples were stored in the cold room at 4 °C. Before extraction, samples were washed and carefully peeled off the skin then cut or blended to the desired size.

##### **4.3.2 Experimental Design**

Five factors, each at four levels were studied for their influence on the extraction of ginsenosides Re, mRb1, Rb1 and total ginsenosides (see Table 4.1). To accomplish this, an orthogonal experimental design was used (see Table 4.2). Two replicates were obtained for each run.

#### 4.3.3 Extraction Procedures

1). Room Temperature Extraction (*RTE*). 2 g of ginseng in required size was placed in a 100 mL conical flask, followed by the addition of required amount of certain solvent. The extraction was carried at room temperature under magnetic stirring for required period of time. 2). Reflux Extraction (*RFX*). The procedure was almost the same as that of the *RTE*, except that it was carried out under reflux temperature of the solvent using a hotplate. No stirring was needed. 3). Microwave-assisted Extraction (*MAE*). 2 g of sample was placed in the quartz extraction vessel of the Prolabo Synthewave 402 (focused microwave-assisted extraction/synthesis equipment at atmospheric pressure, Fontenay-Sous-Bois, Ceseex, France) followed by the addition of required amount of certain solvent. The extraction was carried using 90 W fixed power at all the extraction period. 4). Ultrasonic Extraction (*UE*). The procedure was almost the same as that of *RTE*, except that it was carried out in the water bath of the ultrasonic equipment.

#### 4.3.4 HPLC Analysis

Varian ProStar liquid chromatograph (Walnut Creek, CA, USA) equipped with a ProStar 410 autosampler, a ProStar 220 pumping system and ProStar 330 photodiode array/UV detector was used. Separations were carried out using a reverse phase MicroSorb-MV<sup>TM</sup> 5  $\mu$ m C<sub>18</sub> column (25 x 4.6 mm). Mobile phases were: (A) water, (B) phosphate buffer at PH 5.82, and (C) acetonitrile HPLC grade, Fisher Scientific, Montreal Canada) using the following gradient: 0-6 min, 0%A, 73-66% B, 27-34% C; 6-9 min, 0%A, 66% B, 34% C; 9-12 min, 0% A, 66-60% B, 34-40% C; 12-17 min, 0% A, 60-40% B, 40-60% C; 17-21 min, 0% A, 40-15% B, 60-85% C; 21-28 min, 0% A, 15% B, 85% C. The flow rate was 1.0 ml/min until 17 min and 1.3 ml/min until 28 min. The chromatographs were obtained at 203 nm. For quantification, standard ginsenosides Re and Rb1 (Sigma Chemical Co. (St. Louis, MO, USA) were used to obtain the calibration curve ranging from 0.02 to 0.5 mg/mL. The amount of mRb1 was quantified using the calibration curve of Rb1.



#### 4.3.5 Statistical analysis

SAS software was used to perform the ANOVA procedure for each factor, and DUNCAN for each level under the same factor. The contribution to total effect is calculated as:

$$Contribution\% = \frac{F_i}{\sum_{i=1}^N F_i} \quad (4.1)$$

Where:  $F_i$  is the F value of the  $i^{\text{th}}$  factor, and  $\sum_{i=1}^N F_i$  is the sum of all the F values.

Table 4.1 Factors and levels of the experimental design

Levels	Factors				
	A Extr. method	B Solvent (MeOH:H <sub>2</sub> O)	C Sample/ Sol.	D Time (min)	E Size (mm <sup>3</sup> )
1	Room temperature extr. (RTE)	MeOH	2g/10mL	1 min	Blend
2	Reflux extr. (RFX)	7:3	2g/20mL	10 min	1x1x1
3	Microwave-assisted extr. (MAE)	1:1	2g/40mL	30 min	3x3x3
4	Ultrasonic extr. (UE)	3:7	2g/60mL	60 min	5x5x5

#### 4.4 Results and Discussion

The influence of five factors, i.e., extraction methods, solvents, solvent to sample ratio, extraction time and sample particle size on the extraction of three major ginsenosides and the total ginsenosides are presented in Figs. 4.2 through 4.6 and the DUNCAN analysis results for different ginsenosides are presented in Table 3. As shown in Fig. 4.2, for the extraction of Re, there are no significant difference between MAE, RFX and RTE but they are significantly higher than UE. For mRb1, no significant difference was observed between MAE and RTE, and between RFX and UE with the later group higher than the former one. The influence of extraction methods on the yield is the same for the Rb1 and total ginsenosides represented by the sum of these three major ones. The sequence of the influence is RFX > UE > MAE > RTE. The total ginsenoside is represented

in this paper by the sum of the three major ginsenosides, Re, mRb1 and Rb1 because these three ginsenosides consist more than 90% of the total ginsenosides as indicated in the chromatograph of the extracts (Fig. 4.1). This is consistent with Ren and Chen (1999).

Table 4.2 Orthogonal experimental design table

Runs	Treatments				
	A	B	C	D	E
1	1	1	1	1	1
2	1	2	2	2	2
3	1	3	3	3	3
4	1	4	4	4	4
5	2	1	2	3	4
6	2	2	1	4	3
7	2	3	4	1	2
8	2	4	3	2	1
9	3	1	3	4	2
10	3	2	4	3	1
11	3	3	1	2	4
12	3	4	2	1	3
13	4	1	4	2	3
14	4	2	3	1	4
15	4	3	2	4	1
16	4	4	1	3	2

Note: factors and levels in this table corresponds to that in Table 4.1.

Microwave-assisted extraction method is a solvent extraction method using microwave energy. The microwave energy is believed to have double roles; to increase the temperature thus increasing the diffusion rate and to create localized super heating effect causing the dramatical increase in extraction rate (Paré and Bélanger, 1994). The latter reason is believed to have special accelerating effect on the extraction of natural products. However in this paper, no advantage was observed in the extraction of ginsenosides from fresh American ginseng root other than the heating effect. The reason might be that fresh ginseng root does not have the microwave-favorable micro structure that causes localized super heating. It is also possible that the over heating during the MAE process degrade the ginsenosides. Ultrasonic extraction in this study showed similar effect as that of the reflux extraction.

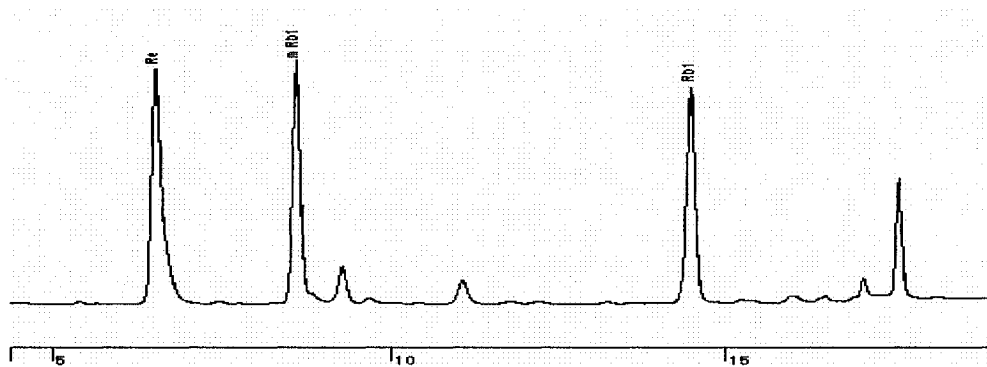


Fig. 4.1 HPLC chromatograph of aqueous methanol extracts of American ginseng root

Aqueous methanol with different ratios was recommended to extract the ginsenosides from dry ginseng root (Li, et al., 1996; Ren and Chen, 1996). In this paper, pure methanol and aqueous methanol with different water to methanol ratios was investigated. As shown in Fig. 4.3, and the DUNCAN results in Table 4.3, there is no significant difference between pure methanol and 70% aqueous methanol in extracting Re, but significantly higher than 50% and 30% aqueous methanol. But this trend reversed for the extraction of mRb1 with the latter group higher than the former one. However in the case of Rb1, pure methanol is significantly better than all the aqueous ones where there is no significant difference between the rest three solvents and this also applies to the total ginsenosides. In the extraction process, as far as total ginsenosides are concerned, methanol is the solvent recommended. However, considering the cost, if aqueous methanol is to be used, concentrations ranging from 30% to 70% do not make any difference, aqueous methanol with lower methanol ratios will lead to lower cost. For the extraction of mRb1, the more dilute aqueous methanol is more advantageous. Another factor to be considered is that while using more dilute aqueous methanol solvent, higher amount of polysaccharides is extracted which may affect the separation process after the extraction.

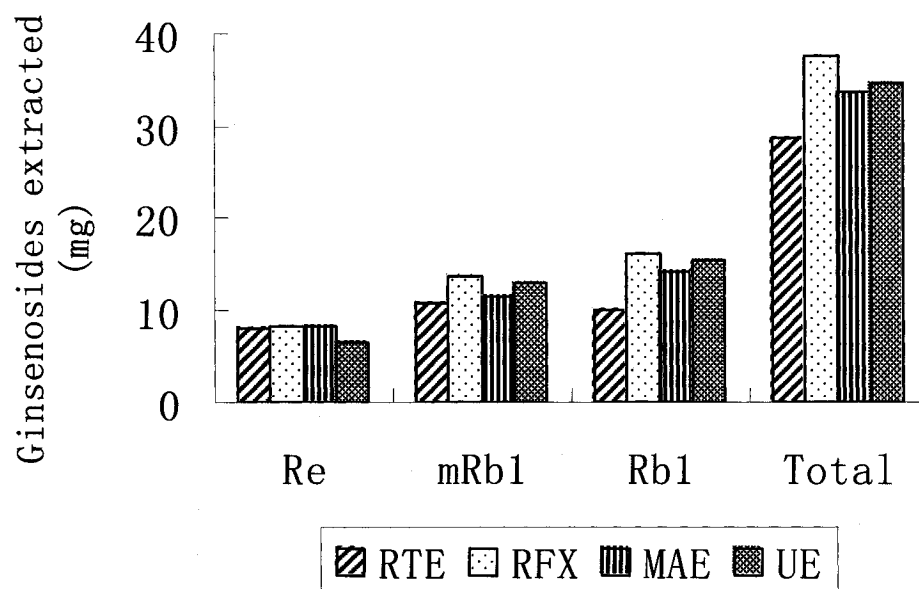


Fig. 4.2 Influence of extraction methods on the amount of ginsenosides extracted

Sample to solvent ratio was also studied as one of the influencing factors (See Fig. 4.4 and Table 4.3). The general trend is that 2 g in 60 mL of solvent has the best performance for all ginsenosides including the total ginsenosides and the 2 g in 10 mL solvent has the lowest. In the middle, the significance depends on the amount of each ginsenosides. Re has lowest amount and there is no significant difference between 2g in 20 mL or in 40 mL; the mRb1 has a little higher amount than Re and the 2g in 40 mL falls in between the 20 mL and 60 mL. With further increase of the amount, for Rb1, significant difference was observed between each of the levels. The total ginsenosides has the same trend with the Rb1. This phenomenon is quite understandable when single extraction was performed. The degree of saturation which can be defined by the ratio of concentration and the saturate concentration of the solute in the solvent may affect the kinetics of the diffusion based extraction process.

The influence of extraction time on the extraction yield is shown in Fig. 4.5. For all the three major ginsenosides, with only 10 min extraction maximum amount was reached. Further extension of the extraction time did not increase the amount of ginsenosides extracted. For the total ginsenosides, statistical

DUNCAN result indicated that there is no significant difference between 30 min and 60 min extraction. Even though there is significant difference between 10 min and 30 min, the 30 minute obtained less amount than 10 min, indicating that longer extraction time is not necessary.

For diffusion based extraction process, the size of sample particle is the crucial factor that determines the extraction rate. Smaller sample size allows faster mass transfer from the sample mass to the solvent. Even though for individual ginsenosides like Re and Rb1, the trend is not so consistent with the ideal situation, for the total amount of ginsenosides, it is consistent as shown in Fig. 4.6.

Table 4.3 DUNCAN analysis results for the different levels in the various factors investigated for different ginsenosides, the different letters in each column means they are significantly different.

Factors	Type of components	Levels			
		1	2	3	4
A Extraction method	Re	a	a	a	b
	mRb1	b	a	b	a
	Rb1	c	a	b	ab
	Total	c	a	b	ab
B Solvent	Re	a	a	b	b
	mRb1	b	b	a	a
	Rb1	a	b	b	b
	Total	a	b	b	b
C Sample/solvent ratio	Re	b	ab	ab	a
	mRb1	c	b	bc	a
	Rb1	d	b	c	a
	Total	d	b	c	a
D Extraction time	Re	d	a	c	b
	mRb1	c	a	b	b
	Rb1	b	a	a	a
	Total	c	a	b	b
Particle size	Re	a	b	c	c
	mRb1	a	b	c	d
	Rb1	a	a	a	b
	Total	a	b	c	d

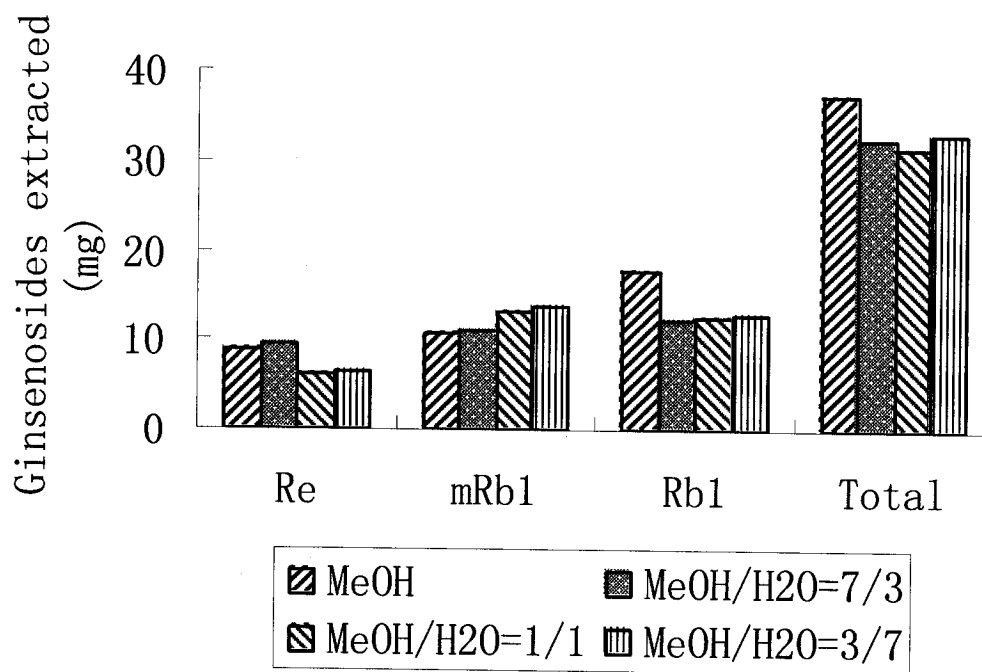


Fig. 4.3 Influence of solvents on the amount of ginsenosides extracted

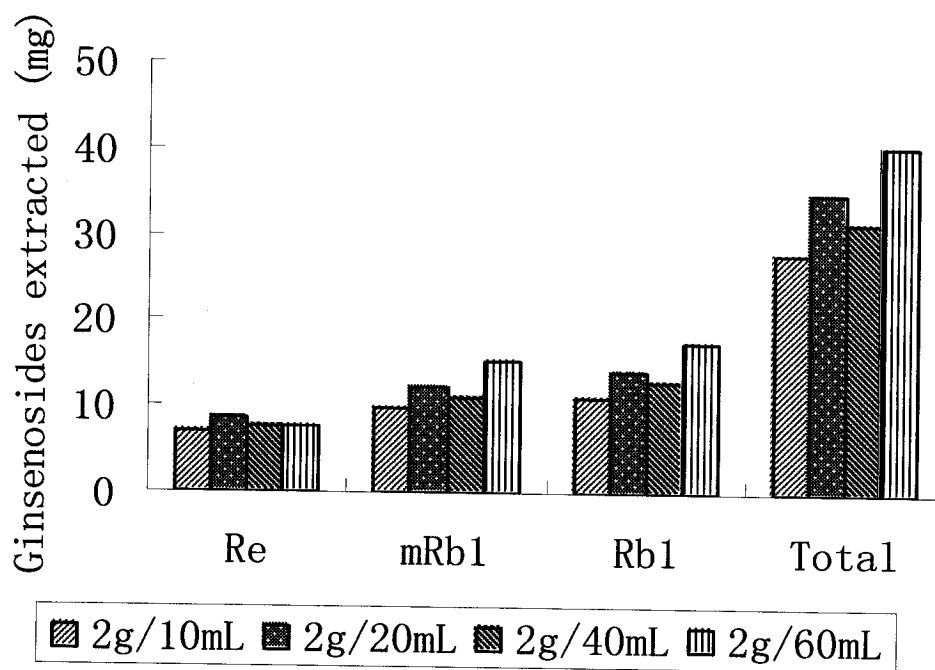


Fig. 4.4 Influence of sample/solvent ratio on the amount of ginsenosides extracted

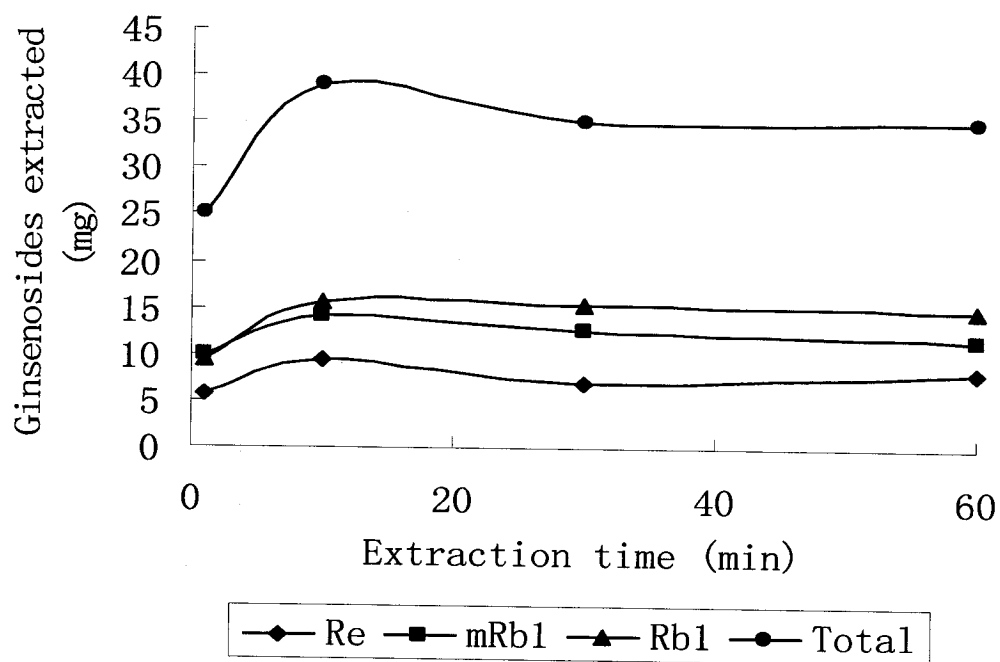


Fig. 4.5 Influence of extraction time on the amount of ginsenosides extracted

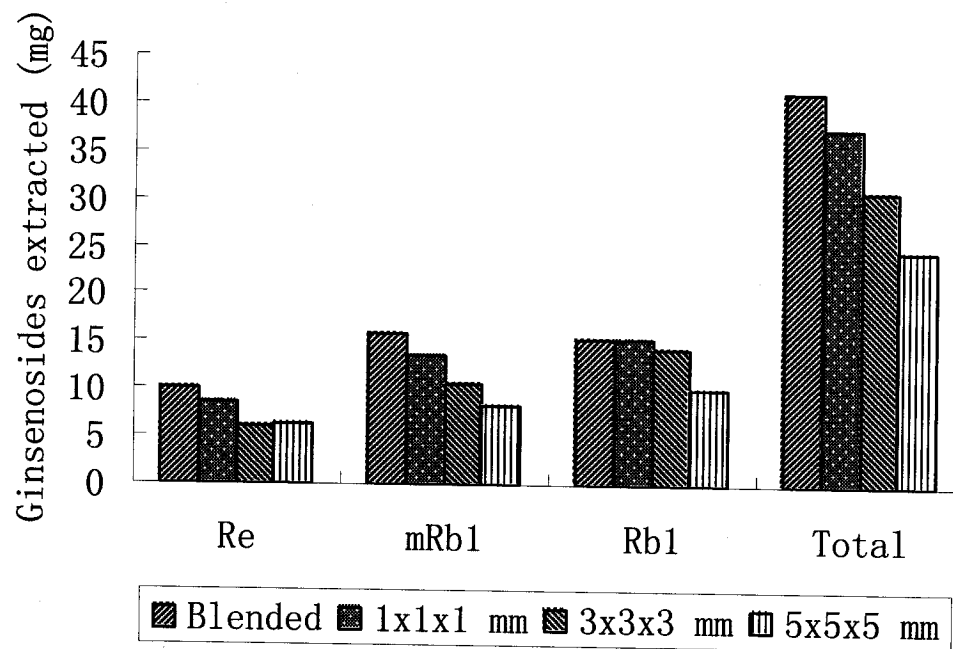


Fig. 4.6 Influence of the size of sample particles on the amount of ginsenosides extracted

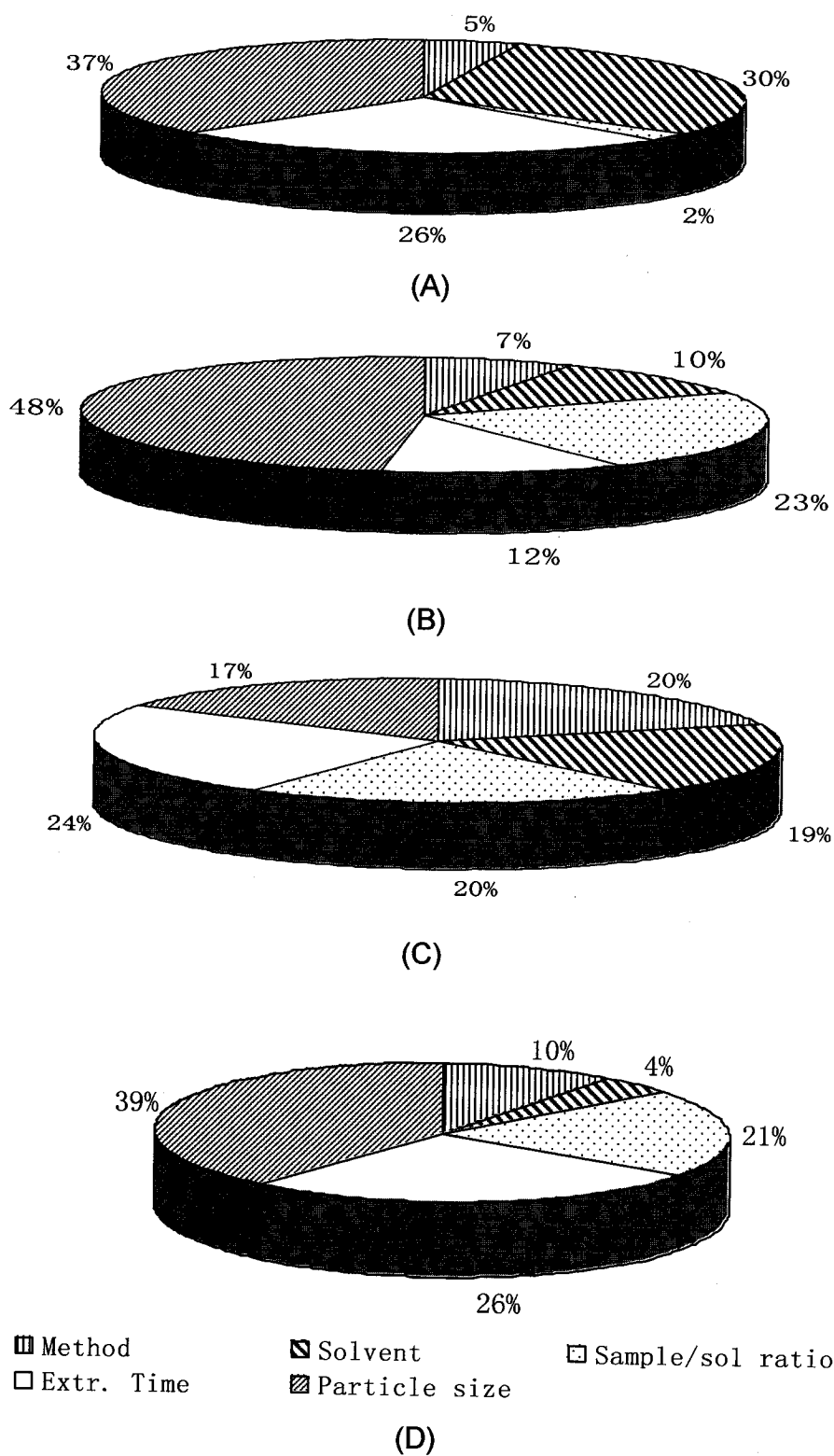


Fig. 4.7 Contribution of different factors on the extraction. A - Re; B - mRb1; C - Rb1; D - Total ginsenosides



ANOVA result showed all but sample/solvent factor for Re to have significant effect at 95% confidence level on the extraction of either individual ginsenosides or total ginsenosides. The contribution of each individual factor on the total effect is plotted in Fig. 4.7. For Re, solvent, extraction time and sample size are major influencing factors, while for mRb1, sample size is the main influencing factor followed by the sample to solvent ratio. For Rb1, almost all factors have equal influence while for the total ginsenosides the effects follows the order sample size > extraction time > sample to solvent ratio > method > solvent.

#### **4.5 Conclusion**

All the factors studied significantly influence the extraction of ginsenosides. Microwave-assisted extraction was not observed to have advantages over conventional extraction methods except for heating effect over the room temperature extraction.

#### **4.6 Acknowledgement**

The authors acknowledge the financial support from Canadian International Development Agency (CIDA), Natural Science and Engineering Research Council (NSERC), FQRNT and Amy Wong Scholarship for this research. The authors also thank Agriculture Canada in Ontario for providing the ginseng samples.

#### **4.6 References**

- Dai, J.; Yaylayan, V.A.; Raghavan, G. S. V.; and Pare, J. R. **1999**. Extraction and colorimetric determination of azadirachtin related limonoids in the neem seed kernel. *J. Agric. Food Chem.* 47, 3738-3742
- Ganzler, K.; Salgo, A.; and Valko, K. **1986**. Microwave extraction: a novel sample preparation method for chromatography." *Journal of Chromatography* 371: 299-306.

- Li, T.S.C., Mazza, G., Cottrell, A.C. and Gao, L. **1996**. Ginsenosides in roots and leaves of American ginseng. *J. Agric. Food Chem.* 44, 717-720
- Pan, X.; Liu, H.; Jia, G.; and Shu, Y. **2000**. Microwave-assisted extraction of glycyrrhizic acid from licorice root. *Biochem. Eng. J.* 5(3), 173-177.
- Paré, J. R. J.; Bélanger, J. M. R. **1994**. Microwave-Assisted Process (MAP): a new tool for the analytical laboratory. *Trends Anal. Chem.* 13, 176-184.
- Pastor, A.; Vazquez, E.; Ciscar, R.; and de la Guardia, M. **1997**. Efficiency of the microwave-assisted extraction of hydrocarbons and pesticides from sediments. *Anal. Chim. Acta.* 344(3), 241-249.
- Ren, G. and Chen, F. 1999. Degradation of Ginsenosides in American Ginseng (*Panax quinquefolium*) Extracts during Microwave and Conventional Heating *J. Agric. Food Chem.* 47, 1501-1505.
- Ryu, S. K.; Kim, W. S.; Yu, J. H. **1979**. Studies on the extraction of korean ginseng compoment. *Korean J. Food Sci. Technol.* 11, 118-121.
- Sung, H. S.; Yang, J. W. **1986**. Effect of the heating treatment on the stability of saponin in white ginseng. *J. Korean Soc.Food Nutr.* 15,22-26.

### CONNECTING STATEMENT 3

As the continuation of this study, the extraction using microwave-assisted extraction method was compared with room temperature extraction and reflux extraction using hotplate as heat source.

Manuscript has been prepared to be submitted to *journal of Agricultural and food Chemistry*.

**Jianming Dai, G.S.Vijaya Raghavan and M. Ngadi, Extraction of Ginsenosides from American Ginseng (*Panax quinquefolium* L.) Root with Different Extraction Methods and Chromatographic Analysis of the Extracts**  
Department of Bioresource Engineering, McGill University, 21,111 Lakeshore road, Ste-Anne-de-Bellevue, QC, H9X 3V9

Contributions made by different authors are as follows:

The first author, the Ph.D. student did the experimental work and prepared the manuscript; the second author is the supervisor that look who guided the research work; the third author provide the laboratory equipment and provided guidance during the experimental process.

## **CHAPTER V**

### **EXTRACTION OF GINSENOSIDES FROM AMERICAN GINSENG (*PANAX QUINQUEFOLIUM* L.) ROOT WITH DIFFERENT EXTRACTION METHODS AND CHROMATOGRAPHIC ANALYSIS OF THE EXTRACTS**

#### **5.1 Abstract**

Microwave-assisted extraction (MAE) was compared with room temperature extraction (RTE) and reflux temperature extraction (RFX) on the extraction of ginsenosides from fresh American ginseng root. Extraction times of 5, 10, 30 and 60 min was investigated for all extractions. An 86 – 300% increase in extraction rate was observed by raised temperature. The use of microwave energy instead of hotplate heating in the extraction result in a 31 – 96% increase in extraction rate with an exception of ginsenoside Re. Visual analysis of the chromatograms of extracts helps choose conditions for selectively obtaining specific ginsenosides enriched extracts.

**KEYWORDS.** Microwave-assisted extraction; American ginseng; Ginsenosides; Extraction methods; Chromatographic analysis

#### **5.2 Introduction**

American ginseng (*Panax quinquefolium* L.) is one of the most important medicinal herbs in North America. Extracts from American ginseng root were reported to have many biological and pharmaceutical properties e.g. anti-anxiety, antitumor, immune system enhancing, benefit to the central nervous system, preventing aging processes and antioxidant properties (Duda, et al., 2001; Hu and Kitts, 2001; Ni, et al., 2001; Wang, et al., 1999; Yuan, et al., 2001; Zhou and Kitts, 2002). Many of its biological and pharmaceutical properties were believed to be due to the activity of a group of compounds called dammarane saponins, generally referred to as ginsenosides (Ni, et al., 2001; Yuan, et al., 2001; Zhou and Kitts, 2002; Dou, et al., 2001; Li, et al., 1996; Liu, et al., 2001). Major

ginsenosides include Rb1, Rb2, Rc, Rd, Re, Rg1, mRb1, mRb2, mRc and mRd (Wang, et al., 1999; Ren and Chen, 1999). Among the ginsenosides Rb1 and Re contribute 70 – 80% to the total ginsenosides for the ginseng from British Columbia, Canada (Li, et al., 1996). HPLC chromatograms of extracts of ginseng root from Jilin, P.R. China indicate that ginsenosides Re, mRb1 and Rb1 contribute to more than 90% of total ginsenosides (Ren and Chen, 1999).

The majority of American ginseng is consumed in East Asia in the form of dried whole root; a portion is processed into extracts. Due to its many biological and pharmaceutical properties, the American ginseng root extract is processed into medicine or nutraceutical products by itself or in combination with extracts from other herbs. Some extracts are also used in cosmetic, food and drinks (Berg, 2002; Zou, et al., 2001; Meybeck, et al., 1999). Extraction is a process used to produce extracts from solid matrices. In an extraction process, solid matrices are immersed in a proper solvent, into which the constituents of interest are diffused; subsequently the latter is evaporated to obtain the extracts. Many factors can influence the rate; among all the factors, increasing temperature is a common method to achieve higher extraction rate. For ginseng roots, reports showed that even at increased temperature, the extraction process was still a slow one (Ryu, et al., 1979; Sung and Yang, 1986). Microwave-assisted extraction (MAE), an extraction method using microwave energy as heating source, was reported to greatly enhance the extraction rate and increase the extraction yield (Hao, et al., 2002; Pan, et al., 2003; Pan, et al., 2002; Paré and Bélanger, 1994). In this study, whether MAE method is more efficient than conventional methods in extracting various ginsenosides from fresh ginseng roots is investigated.

## **5.3 Material and Methods**

### **5.3.1 Fresh American Ginseng Roots**

Roots of four year old American ginseng (*P. quinquefolium* L.) were provided by Agriculture Canada (ON, Canada). The fresh ginseng roots were

stored in cold room at 4 °C. Before extraction, samples were washed, carefully peeled off and cut into approx. 3mm cubes.

### 5.3.2 Ginsenosides Content of the American Ginseng Root

The above mentioned fresh ginseng root 5 g was homogenized with a small coffee bean blender. 2 g of the paste was transferred into a conical flask followed by the addition of 20 mL methanol. The extraction was carried out under magnetic stirring for 2 hrs. After removing the supernatant from the flask, the residue was further extracted with 20 mL methanol twice and 2 hrs each. Finally, the residue was washed with 20 mL methanol, the resulting solution together with the three supernatants were transferred into a 100 mL volumetric flask. After making the solution to set volume by adding methanol, the solution was filtered through a 0.22 µm syringe filter (Cameo brand, Fisher Scientific, Montreal, Canada) before injecting into the HPLC for ginsenosides analysis. The extraction was repeated to get three replicates.

### 5.3.3 Extraction Procedures for Comparing Different Extraction Methods

(a) Room Temperature Extraction (RTE). 2 g of the above mentioned ginseng was placed in a 100 mL conical flask, followed by the addition of 40 mL of methanol. The extraction was carried out at room temperature under magnetic stirring for 5, 10, 30 and 60 min. After the extraction, the supernatant was filtered through the 0.22 µm syringe filter and injected into the HPLC for analysis. (b) Reflux Extraction (RFX). The procedure was almost the same as that of RTE, except that it was carried out under reflux condition using a hotplate for heating. No stirring was necessary because the system was kept at a boiling state. (c) Microwave-assisted Extraction (MAE). 2 g of sample was placed in the quartz extraction vessel of the Prolabo Synthewave 402 (focused microwave-assisted extraction/synthesis equipment at atmospheric pressure, Fontenay-Sous-Bois, Cesex, France) followed by the addition of 40 mL of methanol. The extraction was carried out using 90 W fixed power continuously for the period of 5, 10, 30, 60 min.

#### 5.3.4 HPLC Analysis

Varian ProStar liquid chromatograph (Walnut Creek, CA, USA) was equipped with a ProStar 410 autosampler, a ProStar 220 pumping system and ProStar 330 photodiode array/UV detector. Separation method was modified from Ren and Chen (10). Separations were carried out using a reverse phase MicroSorb-MV™ 5 µm C<sub>18</sub> column (25 x 4.6 mm). Mobile phases were: (A) deionized water, (B) phosphate buffer at PH 5.82, and (C) acetonitrile (HPLC grade, Fisher Scientific, Montreal Canada) using the following gradient: 0-6 min, 0%A, 73-66% B, 27-34% C; 6-9 min, 0%A, 66% B, 34% C; 9-12 min, 0% A, 66-60% B, 34-40% C; 12-17 min, 0% A, 60-40% B, 40-60% C; 17-21 min, 0% A, 40-15% B, 60-85% C; 21-28 min, 0% A, 15% B, 85% C. The flow rate was 1.0 ml/min until 17 min and 1.3 ml/min until 28 min. The chromatographs were obtained at 203 nm.

#### 5.3.5 Calibration with Standards

Standard ginsenosides Re and Rb1 were purchased from Sigma Chemical Co. (St. Louis, MO, USA). Both ginsenosides Re and Rb1 were made into one mixed stock solution containing 1 mg/mL of each ginsenosides in it. The stock solution was further diluted into 0.5, 0.2, 0.1, 0.05, 0.02 mg/mL. Calibration curves in the concentration range of 0.02 – 0.5 mg/mL were obtained for Re and Rb1 based on triplicate injection of each solution. The location of mRb1 peak was found by comparing with Ren and Chen (10) and the amount of mRb1 was calculated based on the calibration result for Rb1.

#### 5.3.6 Statistical Analysis

Single-factor ANOVA was carried out using Microsoft Excel for each pair of methods under the same extraction time. Linear regression for  $\ln A - t$  relationship shown in the results and discussion section was obtained using Microsoft Excel.

## 5.4 Results and Discussion

### 5.4.1 Extraction of ginsenosides with three extraction methods

The results of extracting ginsenoside Re, mRb1 and Rb1 using three extraction methods MAE, RTE and RFX are presented in Figures 5.1 to 5.3. As far as the individual extraction time is concerned, MAE is observed to be generally more effective than RTE especially at longer extraction times. However, at 5 min, MAE is only more effective than RTE for the extraction of Re. As far as MAE and RFX are concerned, no significant increase is observed for all three ginsenosides at most extraction times except for 10 min for Re, 30 min for mRb1 and 30 min for Rb1.

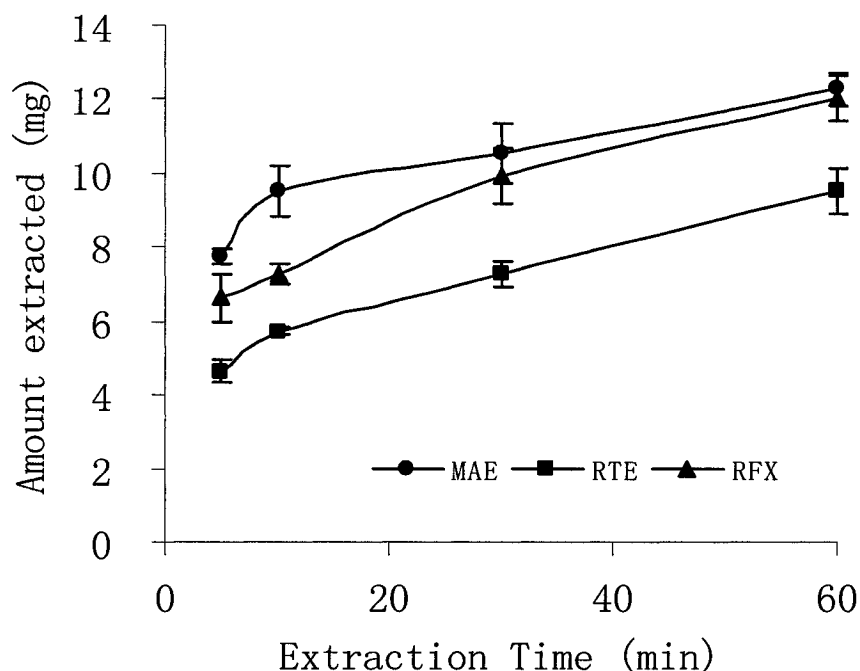


Figure 5.1 Extraction of ginsenoside Re by three extraction methods.



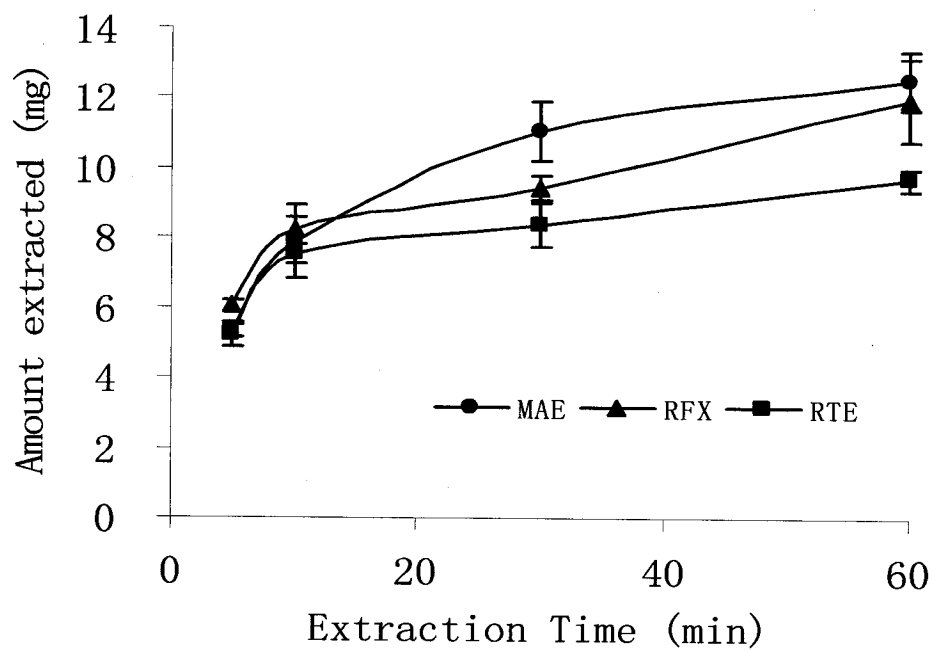


Figure 5.2 Extraction of ginsenoside mRb1 by three extraction methods.

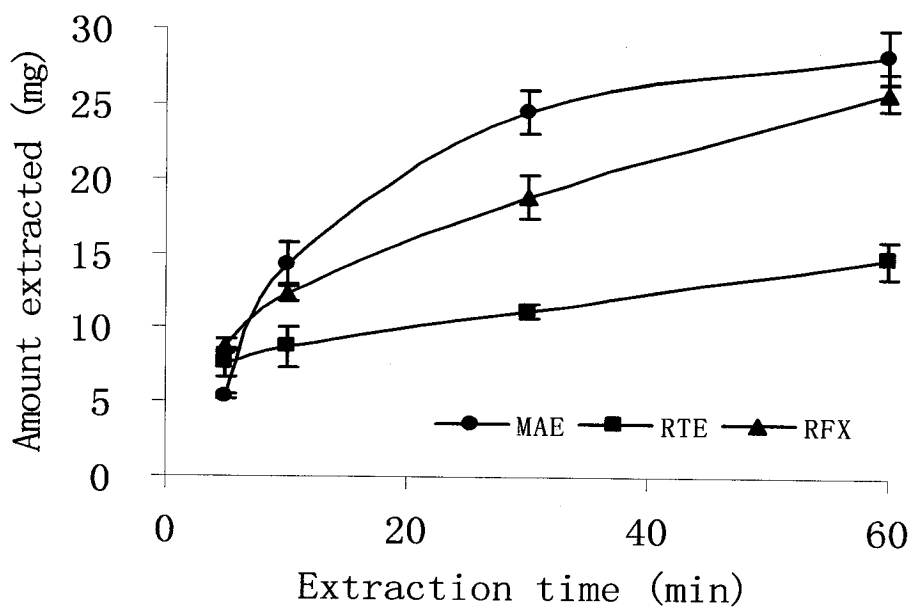


Figure 5.3 Extraction of ginsenoside Rb1 by three extraction methods.

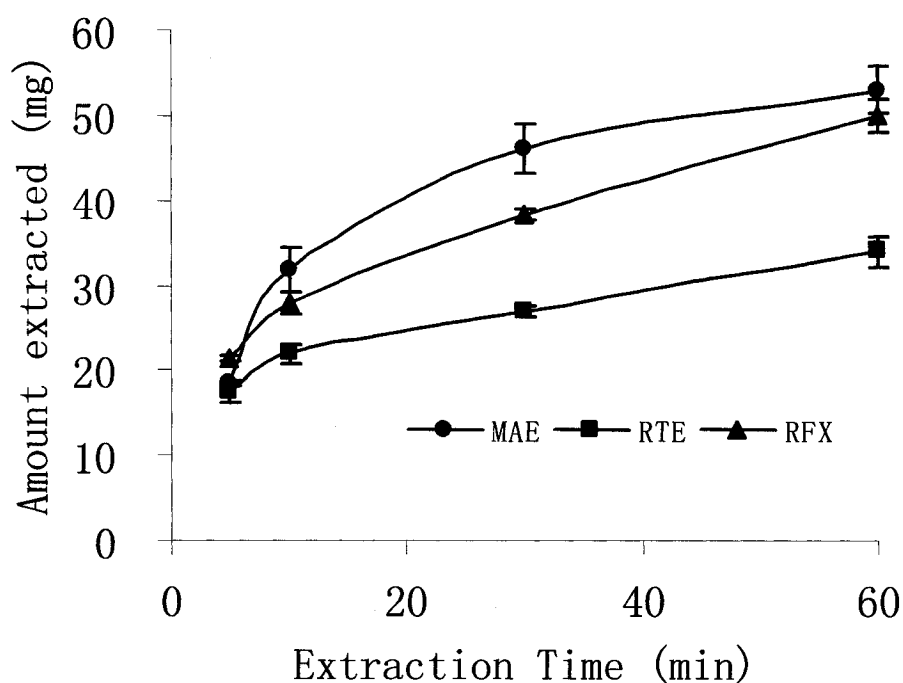


Figure 5.4 Extraction of total ginsenosides represented the Re, mRb1 and Rb1 by three extraction methods

The three ginsenosides Re, mRb1 and Rb1 were reported to contribute to more than 90 percent of the total ginsenosides (Li, et al., 1996). The chromatographs of one-hour RFX or MAE extracts agree with this report (See Figure 5.9). Therefore the sum of three major ginsenosides is used here to represent the total ginsenosides. The extraction of total ginsenosides by the three methods is presented in Figure 5.4. Similar to the three individual ginsenosides, MAE is more effective than RTE at longer extraction time but significant increase in the extract amount is only observed at 30 min extraction when compared with RFX for extracting total ginsenosides.

#### 5.4.2 Comparison of the extraction rates

The predominant mechanism in an extraction process is diffusion, through which constituents of interest are diffused into the solvents. The driving force of

the diffusion process is the concentration gradient between the sample particles and the solution. The extraction rate can be described as:

$$dA / dt = k' \Delta c \quad (5.1)$$

Where: A is the amount of principles of interest, t is extraction time,  $k'$  is constant, and  $\Delta c$  is the concentration gradient.

$$\Delta c = c_s - c_{sol} \quad (5.2)$$

Where  $c_s$  is the concentration in the sample particles, and  $c_{sol}$  is the concentration in the solution.

$$c_s = A / V_{sample} \quad (5.3)$$

$$c_{sol} = (A_o - A) / V_{sol} \quad (5.4)$$

Where:  $V_{sample}$  is the volume of solvent that enters the free space of sample,  $V_{sol}$  is the volume of solution,  $A_o$  is the original amount of principles in the sample. When plenty of solvent is used in an extraction, the volume that enters the sample is much smaller than that in the solution. Therefore  $c_{sol}$  is negligible. Equation 5.1 can be written as:

$$\begin{aligned} dA / dt &= k' (A / V_{sample}) \\ &= kA \end{aligned} \quad (5.5)$$

Where  $k = k' / V_{sample}$  is a constant. Integration of equation 5 results:

$$\ln A = kt + c \quad (5.6)$$

A is the amount of principles that is left in the sample. It can be calculated from the original amount and the amount already extracted:

$$A = A_o - A_{extr} \quad (5.7)$$

In this study, the original amounts of ginsenosides Re, Rb1 and mRb1 are obtained through a procedure "Ginsenosides Content of the Ginseng Root" to be: 14.15 +/- 1.08, 13.40 +/- 0.85, 31.29 +/- 1.84 respectively. The amount of ginsenosides extracted at different extraction times is presented in Fig. 5.1 through 5.3. Therefore, the amount residing in the sample can be obtained. The  $\ln A$  – extraction time (t) relationship for ginsenosides Re, Rb1, mRb1 and the total ginsenosides vs. time are presented in Figs. 5.5 – 5.8. The linear regression results are shown in Table 5.1. Very good linearity was observed as indicated by their R squares.

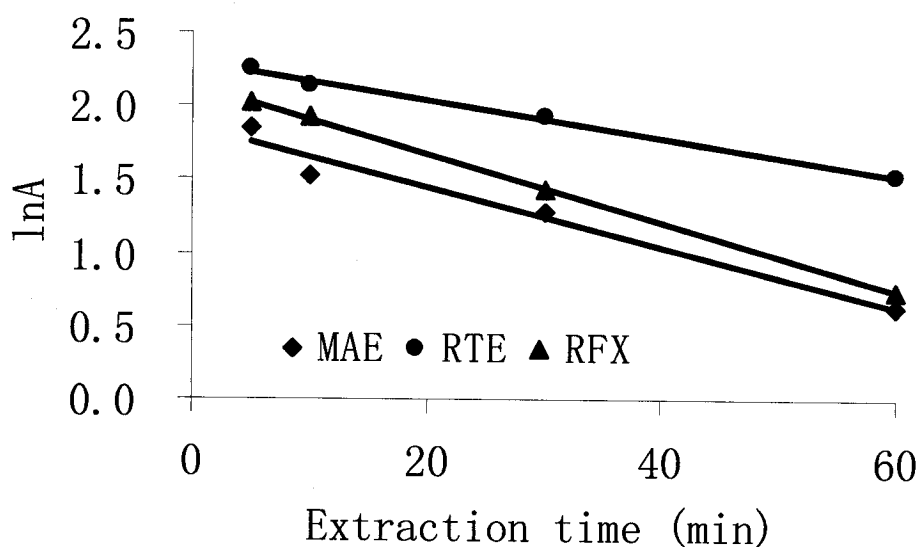


Fig. 5.5 Linear regression of the natural log of residue amount of ginsenoside Re in the sample vs. extraction time for MAE, RTE and RFX extraction methods

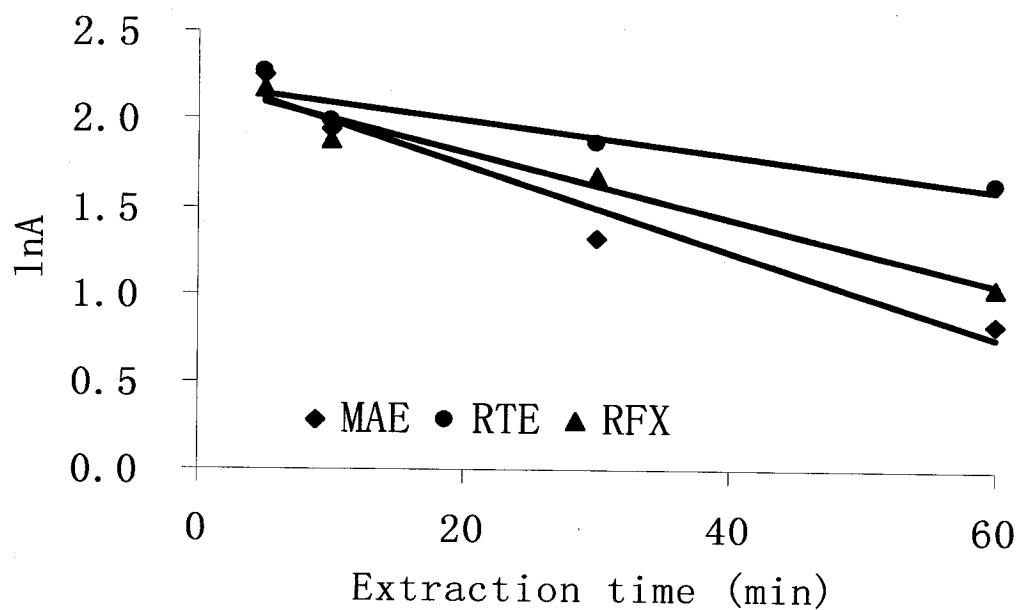


Fig. 5.6 Linear regression of  $\ln A$  vs. extraction time for ginsenoside mRb1 using the three extraction methods.

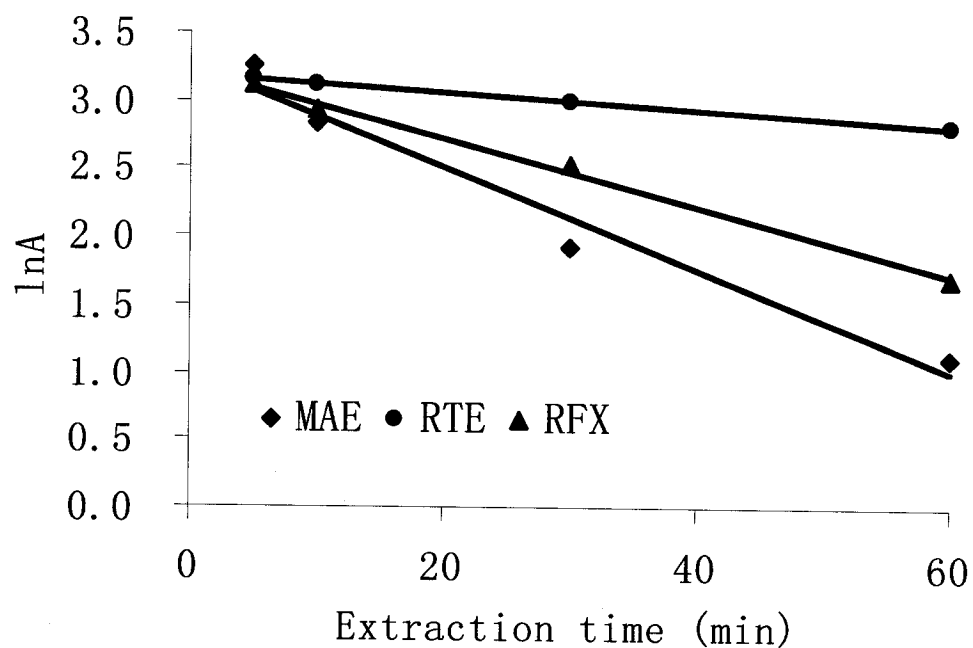


Fig. 5.7 Linear regression of  $\ln A$  vs. extraction time for ginsenoside Rb1 using the three extraction methods.

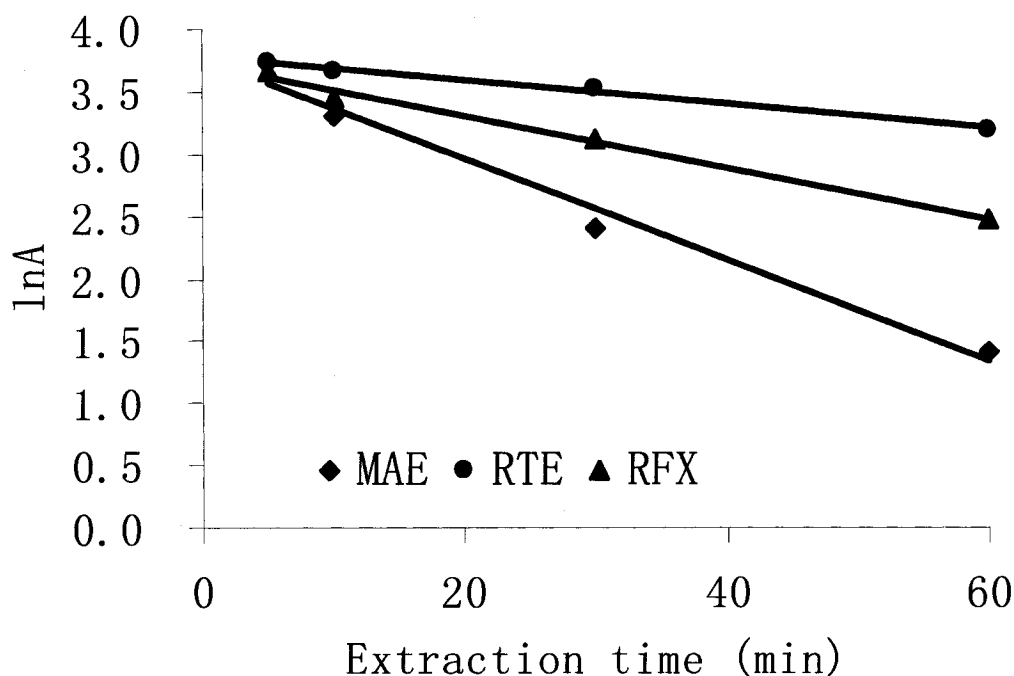


Fig. 5.8 Linear regression of  $\ln A$  vs. extraction time for total ginsenosides using the three extraction methods.

Equation 5.5 shows that the extraction rate is proportional to the residue amount of ginsenosides in the sample and proportionality constant is  $k$ . Therefore, when the amount of ginsenosides left in the sample is the same, the larger the absolute value of the  $k$ , the higher the extraction rate. The linear regression results (Table 5.1) shows that RFX and MAE has generally higher extraction rate than RTE suggesting that extraction rate can be increased by raising temperature. For a diffusion-based extraction process, increased temperature causes a faster diffusion rate between concentration gradients.

Both MAE and RFX work at a temperature of the reflux temperature of the solvent, in this case, methanol. The difference between them is the source of heating with MAE using microwave energy and RFX using conventional hotplate. However the comparison of MAE and RFX shows that MAE has generally larger  $k$  value than RFX except for ginsenoside Re. As discussed earlier, for the sample having the same amount of ginsenosides content, the extraction rate is

proportional to the  $k$  value. The ratio of the  $k$  values for different extraction methods, therefore, represents the acceleration ratio between methods. Table 5.2 shows that increased temperature using hotplate leads to a 86 – 300% increase in extraction rate. However, both at raised temperature, 31 – 96% increase was observed for MAE as compared to RFX with the only exception of Re. Especially for total ginsenosides, the acceleration rate of MAE/RFX is comparable with that of RFX/RTE. This indicates that the acceleration in extraction rate for the extraction process using microwave energy is beyond a temperature factor.

Table 5.1 Linear regression results of  $\ln A - t$  relationships

		C	k	R <sup>2</sup>
Re	MAE	1.86	0.0205	0.9685
	RTE	2.29	0.0126	0.9932
	RFX	2.15	0.0234	0.9994
Rb1	MAE	3.27	0.0375	0.9642
	RTE	3.19	0.0063	0.9986
	RFX	3.23	0.0252	0.9964
mRb1	MAE	2.24	0.0248	0.9541
	RTE	2.19	0.0097	0.8612
	RFX	2.20	0.0189	0.9675
Total ginsenosides	MAE	3.78	0.0408	0.9921
	RTE	3.78	0.01	0.9943
	RFX	3.71	0.0208	0.9908

MAE method is a solvent extraction method using microwave energy as heating source. Microwave energy differs from the conventional hotplate heating in its heating mechanism and heating behavior. Microwave heating comes from the interaction of polar molecules with the alternating electromagnetic field. This heating mechanism leads to the selectivity and volumetric behaviors of

microwave heating. The special microwave-molecule interaction may have caused the acceleration in extraction rate of MAE over RFX, both having similar temperature. The microwave energy has double roles; to increase the temperature thus increasing the diffusion rate and to create localized super heating effect causing an additional increase in extraction rate. The latter reason was suggested by Paré and Bélanger (1994) to be the dominant mechanism when extracting peppermint using nonpolar solvents causing a dramatic increase in extraction rate.

Table 5.2 The extraction rate enhancement factor RFX vs. RTE and MAE vs. RFX.

	Re	Rb1	mRb1	Total
RFX vs. RTE	86%	300%	95%	106%
MAE vs. RFX	-13%	49%	31%	96%

Note: the enhancement factor for RFX vs. RTE =  $(k_{\text{RFX}} - k_{\text{RTE}}) / k_{\text{RFX}} * 100\%$ ; and MAE vs. RFX =  $(k_{\text{MAE}} - k_{\text{RFX}}) / k_{\text{MAE}} * 100\%$ ;  $k_{\text{MAE}}$ ,  $k_{\text{RTE}}$ , and  $k_{\text{RFX}}$  are extraction constants for MAE, RTE, and RFX respectively;

#### 5.4.3 Chromatographic Analysis

Chromatographs of extracts obtained with different extraction methods at different extraction times provide a method to visualize the progress of the extraction process and how different components are extracted (see Fig. 5.9). Chromatographs presented here are not using the same scales; the purpose is to show the relative content of different components in the extracts as indicated by the size of the peaks. On the chromatograph, the small peaks other than the three major ginsenosides are believed to be other ginsenosides as compared with the chromatographs provided by Ren and Chen (1999). The areas of peaks on the chromatograph correspond to the quantity of this ginsenoside in the extract. The relative size of the peak to that of Rb1 corresponds to the relative



content of each individual ginsenoside to that of Rb1. After 5 min of extraction, the chromatographs showed that the various minor ginsenosides have fair content in the extracts, especially for RFX and MAE. With the increase of extraction time, the relative contents of the minor ginsenosides decrease rapidly. At 60 min of extraction, the minor peaks on the chromatographs are negligible as compared with Rb1.

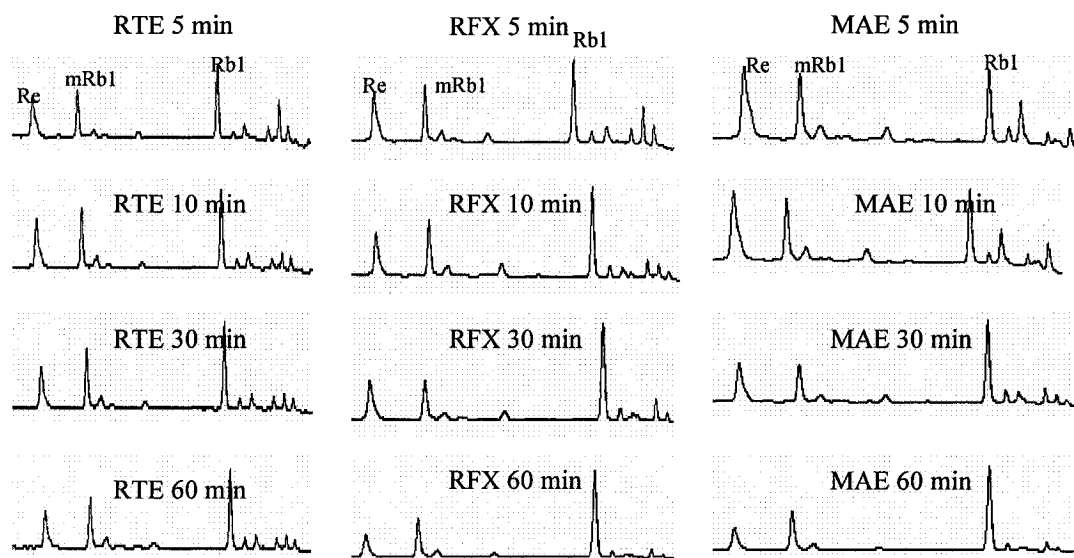


Fig. 5.9 Chromatographs of ginseng root extracts obtained using different extraction methods and extraction times

In the early stage of the extraction process, all components are diffused into the solvent. With the progress of the extraction process, due to the relatively lower amount of the minor ginsenosides, the diffusion process ends within five to ten minutes with the establishment of an equilibrium. While for the major ginsenosides, this equilibrium stage takes longer time resulting in the drop of the relative content of minor ginsenosides in the extracts with the progress of extraction. Similar trend was also observed within the three major ginsenosides. Relative contents of Re and mRb1 also drop with the progress of the extraction process. Comparison of RTE with RFX and MAE indicates that at room

temperature the equilibrium stage comes much later than at the raised temperature.

The visual analysis of the chromatographs provides a method for obtaining specific ginsenosides enriched extracts. At raised temperature and short extraction times, the extract obtained contains relatively higher content of minor ginsenosides. The residue can then be further extracted to obtain extracts containing mainly three major ginsenosides.

## **5.5 Conclusion**

MAE was compared with two conventional extraction methods RTE and RFX on the extraction of ginsenosides from fresh American ginseng root. MAE and RFX have higher extraction rate than RTE suggesting that extraction rate can be accelerated by increasing temperature. MAE has higher extraction rate than RFX due to a factor beyond temperature. Specific ginsenosides enriched extract can be obtained by controlling the extraction time.

## **5.6 Acknowledgement**

The authors acknowledge the financial support from Canadian International Development Agency (CIDA), Natural Science and Engineering Research Council (NSERC), FQRNT and Amy Wong Scholarship for this research. The authors also thank Agriculture Canada in Ontario for providing the ginseng samples.

## **5.7 References**

- Berg, E.E. Cosmetic creams containing ginseng extract. Ger. *Gebrauchsmusterschrift*. DE 20201550, 2002; 8 pp.
- Dou, D.Q.; Zhang, Y.W.; Zhang, L.; Chen, Y.J.; Yao, X.S. The inhibitory effects of ginsenosides on protein tyrosine kinase activated by

- hypoxia/reoxygenation in cultured human umbilical vein endothelial cells. *Planta Medica*. 2001, 67, 19-23.
- Duda, R.B.; Kang, S.S.; Archer, S.Y.; Meng, S.; Hodin, R.A. American ginseng transcriptionally activates p21 mRNA in breast cancer cell lines. *Journal of Korean Medical Science* 2001, 16(Suppl) S54-60.
- Hao, J.Y.; Han, W.; Huang, S.; Xue, B.Y.; Deng, X. Microwave-assisted extraction of artemisinin from *Artemisia annua* L. *Separation and Purification Technology*. 2002, 28, 191-196.
- Hu, C.; Kitts, D.D. Free radical scavenging capacity as related to antioxidant activity and ginsenoside composition of Asian and North American ginseng extracts. *Journal of the American Oil Chemists' Society*. 2001, 78, 249-255.
- Li, T.S.C., Mazza, G., Cottrell, A.C.; Gao, L. Ginsenosides in roots and leaves of American ginseng. *J. Agric. Food Chem.* 1996, 44, 717-720.
- Liu, D.; Li, B.; Liu, Y.; Attele, A. S.; Kyle, J. W.; Yuan, C.S. Voltage-dependent inhibition of brain Na<sup>+</sup> channels by American ginseng. *European Journal of Pharmacology*. 2001, 413, 47-54.
- Meybeck, A.; Dumas, M.; Chaudagne, C.; Bonte, F. Cosmetic and pharmaceutical preparations containing Rb1 ginsenosides for stimulating elastin synthesis. *PCT Int. Appl. WO* 9907338, 1999; 29 pp.
- Ni, X.; Bai, J.; Sun, X.; Chen, C.; Sha, X.; Yu, D. Studies on anti-anxiety effects of saponin extracted from root or stem and leaf of panax ginseng in elevated cross-maze. *Zhongcaoyao (in Chinese)*. 201, 32, 238-241.
- Pan, X.; Niu, G. and Liu, H. Microwave-assisted extraction of tea polyphenols and tea caffeine from green tea leaves. *Chemical Engineering and Processing*. 2003, 42, 129-133.
- Pan, X.; Niu, G. and Liu, H. Comparison of microwave-assisted extraction and conventional extraction techniques for the extraction of tanshinones from *Salvia miltiorrhiza bunge*. *Biochemical Engineering Journal*. 2002, 12, 71-77.

- Paré, J. R. J. and Bélanger, J. M. R. Microwave-Assisted Process (MAP): a new tool for the analytical laboratory. *Trends Anal. Chem.* 1994, 13, 176-184.
- Wang, X.; Sakuma, T.; Asafu-Adjaye, E. and Shiu, G.K. Determination of ginsenosides in plant extracts from *Panax ginseng* and *Panax quinquefolius* L. by LC/MS/MS. *Anal. Chem.* 1999, 71, 1579 – 1584.
- Ren, G.; Chen, F. Degradation of ginsenosides in American ginseng (*Panax quinquefolium*) extracts during microwave and conventional Heating. *J. Agric. Food Chem.* 1999, 47, 1501-1505.
- Ryu, S. K.; Kim, W. S. and Yu, J. H. Studies on the extraction of korean ginseng compoment. *Korean J. Food Sci. Technol.* 1979, 11, 118-121.
- Sung, H. S.; Yang, J. W. Effect of the heating treatment on the stability of saponin in white ginseng. *J. Korean Soc. Food Nutr.* 1986, 15, 22-26.
- Yuan, C.S.; Wang, X.; Wu, J. A.; Attele, A. S.; Xie, J.T.; Gu, M. Effects of panax quinquefolius L. on brainstem neuronal activities: Comparison between Wisconsin-cultivated and Illinois-cultivated roots. *Phytomedicine.* 2001, 8, 178-183.
- Zhou, D.L.; Kitts, D.D. Peripheral blood mononuclear cell production of TNF- $\alpha$  in response o North American ginseng stimulation. *Canadian Journal of Physiology and Pharmacology.* 2002, 80, 1030-1033.
- Zuo, X.; Ma, S.; Hou, Z. Study on processing of American ginseng-pumpkin health beverage containing Bifidobacteria promoting factor. *Shipin Gongye Keji* (in Chinese). 2001, 22, 70-71.

## CONNECTING STATEMENT 4

So far microwave-assisted extraction of peppermint and American ginseng has been studied. Starting from this chapter, microwave assisted synthesis will be investigated.

Manuscript has been published at the proceeding of the 39th Annual Symposium of International Microwave Power Institute, 2005

**Jianming Dai and G.S.Vijaya Raghavan, Microwave-assisted synthesis of n-butylparaben using  $\text{ZnCl}_2$  as catalyst. In proceedings of the 39th Annual Symposium of International Microwave Power Institute, 2005, Seattle, Washington, USA**

Department of Bioresource Engineering, McGill University, 21,111 Lakeshore road, Ste-Anne-de-Bellevue, QC, H9X 3V9

Contributions made by different authors are as follows:

The first author, the Ph.D. student did the experimental work and prepared the manuscript under the supervision and guidance of the second author during the research work

## CHAPTER VI

### MICROWAVE-ASSISTED SYNTHESIS OF N-BUTYLPARABEN USING $\text{ZnCl}_2$ AS CATALYST

#### 6.1 Abstract

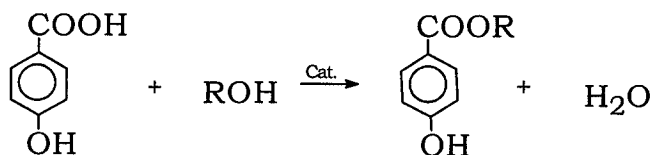
$\text{ZnCl}_2$  was investigated for catalyzing the synthesis of n-butyleparaben under microwave-assisted synthesis (MAS) and conventional heating methods. The catalyzing effect was compared with that of *p*-toluene sulfonic acid (PTSA). Influencing factors like, microwave power, catalyst to reactant ratio, and reaction time are studied for the MAS of n-butyleparaben. The mechanisms of the acceleration effect under microwave irradiation were explained.

Keywords: n-butyleparaben, Microwave-assisted synthesis, PTSA,  $\text{ZnCl}_2$ , transition state, athermal

#### 6.2 Introduction

*p*-Hydroxybenzoic acid esters (parabens) are widely used as antimicrobial preservative agents in food, pharmaceutical, and cosmetics due to their broad antimicrobial spectrum (Soni, et al., 2001). Among weak acid compounds viz., propionates and sorbates, parabens have a wide PH range that makes them as very versatile food preservatives. The antimicrobial activity of parabens is directly dependent on the chain length (Robach, 1980; Dziezak, 1986). For example, the ability of *n*-butylparaben to inhibit bacteria is 4 times that of ethylparaben (Zhang, et al., 1998). The synthesis of parabens from *p*-hydroxybenzoic acid and alcohol normally need a catalyst such as concentrated sulfuric acid or PTSA as indicated in Scheme 6.1. In most cases, large excess of either acid or alcohol is used in the condensation to give a higher yield of the desirable esters. However, these methods have limitations of general applicability owing to low yields, extensive by-product formation and harsh reaction conditions. The use of large amounts of condensing reagents and activators should be avoided in order to promote green and efficient food systems. Microwaves have been reported to increase the

reaction rates (Liao, et al., 2002; Loupy, et al., 2001), improve yield (Liao, et al., 2002; Loupy, et al., 2001), increase the selectivity (Oussaid, et al., 1997). The direct condensation of acids with alcohols using a small amount of catalyst under microwave irradiation may provide a good alternative to the traditional synthesis methods.



Scheme 6.1. The synthesis of parabens (cat.=catalyst such as PTSA, H<sub>2</sub>SO<sub>4</sub>).

## 6.3 Fundamentals of microwave-assisted synthesis

### 6.3.1 Microwaves

Microwaves are located in between the radio frequency and infrared (IR) on the electromagnetic spectrum, having frequencies in the range of 300 MHz to 30 GHz. Microwaves are widely used in RADAR and telecommunications and in order to prevent interferences certain frequencies have been allocated for industry, scientific and medical (ISM) applications. Among these frequencies, the most commonly used ones are 2450 and 915 MHz. Especially, the 2450 MHz is used in domestic microwave oven and in most commercial microwave-assisted chemistry equipment.

### 6.3.2 Microwave-matter interaction

Two major mechanisms are involved in the microwave-matter interaction: dipolar rotation and ionic conduction. By ionic conduction, ions are accelerated by electric fields causing them to move towards the direction opposite to their own polarity. The movement of ions provokes collisions with the molecules of the material such as water molecules and collisions, in consequence reducing to generate heat. For non-ionic materials, dipolar rotation is the dominant mechanism. The energy level of microwaves corresponds to the rotational energy level of polar molecules. Therefore the interaction of microwave energy with

matter is through the dielectric rotation of the molecules. For example, polar molecules subjected to microwave irradiation at 2450 MHz will rotate  $2.45 \times 10^9$  times in a second. The friction between the fast rotating molecules generates heat. In either ionic conduction or dipolar rotation, the heating is volumetric, which means the heat is generated through out the commodity instead of transferring from the surface to the inner part as it is the case in conventional heating method.

The physical parameters that measure microwave-matter interaction include ionic conductivity ( $\sigma$ ), dielectric constant ( $\epsilon'$ ) and the loss factor ( $\epsilon''$ ). The ionic conductivity measures the performance of heating by ionic conduction mechanism. It is important in the drying processes where plenty of water and electrolytes exist, but it is less important in most organic chemistry processes where only organic compounds are involved. The dielectric constant describes the capability of molecules to be polarized by electric field and the loss factor measures the efficiency of molecules to convert microwave energy into heat (Chen, et al., 1993). The following equation is used to calculate the energy absorption:

$$P_v = 2\pi f \epsilon_o \epsilon'' |E|^2 \quad (6.1)$$

Where:  $P_v$  is the energy developed per unit volume ( $\text{W/m}^3$ )

$f$  is the frequency (Hz)

$\epsilon_o$  is the absolute permittivity in vacuum ( $\text{F/m}$ )

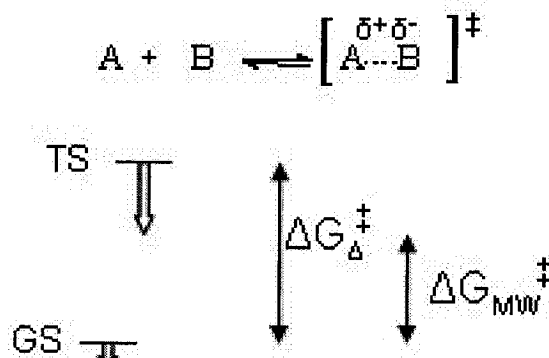
$|E|$  is the electric field strength inside the load ( $\text{V/m}$ ).

### 6.3.3 Mechanism of Microwave-assisted synthesis

Since the pioneer work on the organic synthesis using microwaves was reported by Gedye et al. (1986), many different types of reactions have been investigated. Concerning the athermal effect, there is still not a general acceptable mechanism. One of the most popular explanations on the possible



special microwave acceleration effect is the involvement of microwaves in the dipolar transition state (TS) of a reaction as illustrated in Scheme 6.2.



Scheme 6.2 Appearance of a dipolar transition state during the reaction; the presence of dipolar transition state causes the lower activation energy by microwaves than conventional heating (Loupy, 2004).

During the reaction, the appearance of a dipolar transition state makes it easier to couple with microwaves; as a result the free activation energy is reduced leading to a faster reaction. A few factors determine whether there will be athermal effect of microwaves. a). Polarity of the transition state: If the polarity of the transition state is higher than that of the ground level, then there is a strong possibility of athermal effect. b). Magnitude of the activation energy: fast reactions under conventional heating methods has a relatively small magnitude of the free energy; when microwaves are used, the space for magnitude reduction is limited, as a result the athermal effect will be limited if there will be any. c). Rate determining step: if the formation of the dipolar transition state is the rate determining step, and if it meets other conditions, then athermal effect is likely to appear.

## 6.4 Material and methods

### 6.4.1 Materials

*n*-butanol, methylparaben, *n*butylparaben, *p*-hydroxybenzoic acid, PTSA and ZnCl<sub>2</sub> were purchased from Sigma-Aldrich, Canada (Ontario). All reagents and catalysts were used without further treatment.

### 6.4.2 Experimental procedure

Reactions were carried out using a Synthewave 402 (focused MAP system at atmospheric pressure) obtained from Prolabo (Fontenay-Sous-Bois, Cedex, France). It operates with an emission frequency of 2450 MHz and a 300 W full power. It is equipped with an IR temperature sensor, a tubular quartz reactor (250 ml), and a Graham type condenser.

#### 6.4.3 Microwave-assisted synthesis

A mixture of 8 ml of butanol, 0.18 g ZnCl<sub>2</sub> and 1.72 g *p*-hydroxybenzoic acid was introduced together in the quartz reactor of the synthewave 402 apparatus. The irradiation was carried out in the following sequence at 70% power (300 W× 70%): 15 s off, 30 s on; 15 s off, 30 s on; 15 s off, 30 s on; 30 s off, 30 s on; 15 s off, 30 s on. After heating and cooling, the mixture was diluted by ethanol and analyzed by GC. Methylparaben was used as internal standard to calibrate the yield of reaction.

#### 6.4.4 Conventional heating method

A mixture of 3.46 g of *p*-hydroxybenzoic acid and 0.35 g ZnCl<sub>2</sub> was introduced to 250 ml reaction flask and then 16 ml of butanol was added. The mixture was refluxed on a hotplate for 45 min. After heating and cooling, the product was analyzed as above.

#### 6.4.5 GC analysis

The GC was operated with an injector temperature of 250°C and a helium carrier gas flow rate of 24 ml/min. The GC column was a nonpolar general-purpose capillary column [30 m×0.25 mm i.d., 0.25 µm thickness, Phase DB5 (J&W Scientific Co.). The detector (FID) was operated at 250°C and oven temperature was programmed as: 1) initial temperature was 100°C; 2) Level 1, 5.0°C/min, 100°C, keep 2 min; 3) Level 2, 10°C/min, 160°C, keep 5 min; 4) Level 3, 10°C/min, 250°C, keep 5 min. The products were identified by comparison of

their GC retention time with those of authentic samples. The yields were calculated from the theoretical standard calibration line.

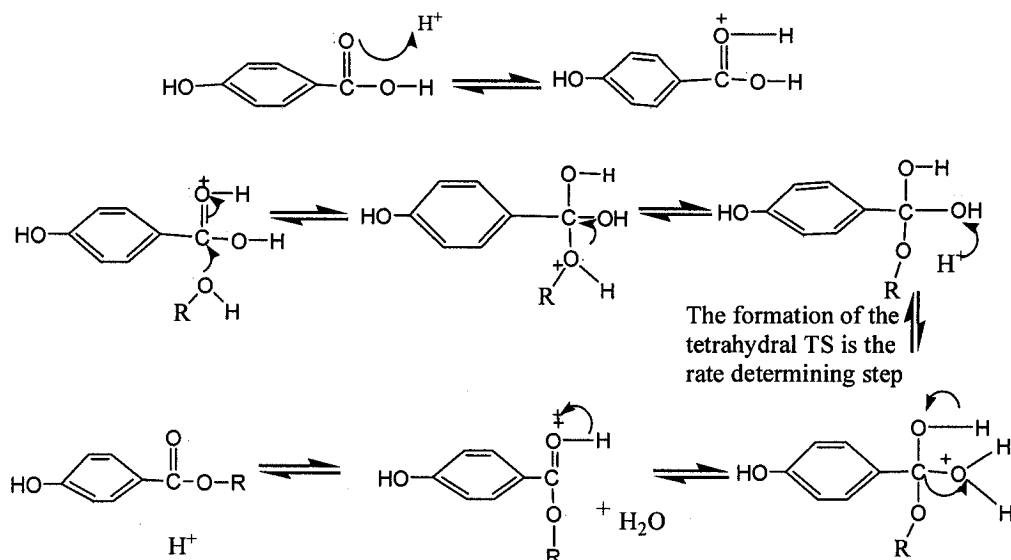
## 6.5 Results and Discussion

Classical esterification reaction using carboxylic acid and alcohols uses a strong acid like concentrated sulfuric acid or PTSA as catalyst. Lewis acid is generally not used in this type of esterification. The yields obtained under both MAS and conventional method with no catalyst and different catalysts are presented in Table 6.1. As expected, no reaction occurs when there is no catalyst added. When PTSA is used, a higher yield was obtained using conventional heating for 45 min than 2 min of MAS. However when  $\text{ZnCl}_2$  was used as catalyst, 2 min of MAS gave a 43% while 45 min of conventional heating generated only 3.5% of the products. A dramatic rate enhancement was observed.

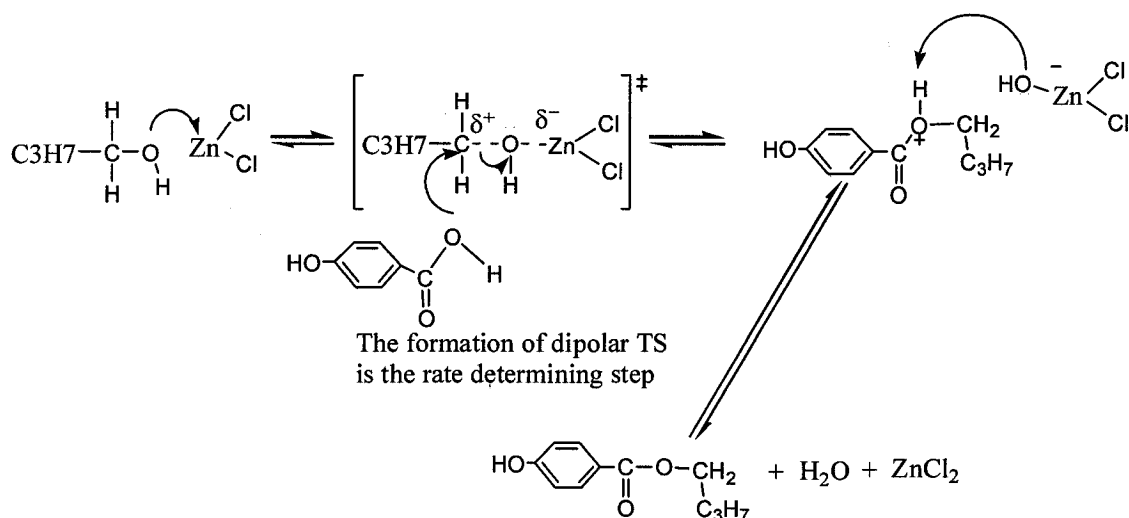
Table 1. Interaction of microwaves and catalyst

Catalyst	Method	Time (min)	Yield (%)
/	MAS	2	0
PTSA	MAS	2	41
$\text{ZnCl}_2$	MAS	2	43
/	Conventional	45	0
PTSA	Conventional	45	76
$\text{ZnCl}_2$	Conventional	45	3.5

In the acid catalyzing process, the formation of the tetrahedral TS is the rate determining process. During the formation of TS (Scheme 6.3), no dipolar structure is formed; therefore no athermal effect is expected when the reaction is through this mechanism. However, in the zinc chloride catalyzed reaction, the formation of a dipolar TS is the rate determining step (Scheme 6.4). Compared with GS, the TS has higher polarity; this will benefit the coupling with microwaves causing the rate enhancement during the reaction. This reaction is difficult under conventional heating conditions because the alcohol is a primary one which will be extremely hard to form the TS state during normal conditions. This explains the low yield obtained under conventional conditions using  $\text{ZnCl}_2$  as catalyst. When there is no catalyst, the reaction is not likely to happen through the analysis of the different catalyzing mechanism, which is experimentally proved.



Scheme 6.3 Mechanism of acid catalyzed esterification reaction



Scheme 6.4  $\text{ZnCl}_2$  catalyzed esterification reaction

## 6.6 Conclusions

Microwaves can be used in the synthesis of butyleparabens through the esterification of *p*-Hydroxybenzoic acid and butanol using different catalysts. When  $\text{ZnCl}_2$  is used, the formation of a dipolar TS determines the rate of the reaction and can be accelerated through the coupling with microwaves. When the classic acid catalyst was used, the advantage of using microwaves is less significant due to the lack of a dipolar TS.

## 6.7 Acknowledgement

The authors wish to acknowledge the Natural Science and Engineering Research Council of Canada (NSERC), FQRNT and Canadian International Development Agency (CIDA) for their financial support.

## 6.8 References

- Chen, X.; Hong, P.; Dai, S. **1993**. Synthesis of nipagin esters with microwave irradiation. *Huaxue Tongbao*. **1993**, 38–39.
- Dziezak, J. D. **1986**. Preservatives: antimicrobial agents. *Food Technol.* **40**, 104–111.
- Gedye, R.; Smith, F.; Westaway, K.; Ali, H.; Baldisera, L.; Laberge, L.; and J. Rousell. **1986**. The use of microwave ovens for rapid organic synthesis. *Tetrahedron Lett.* **27**(3): 279-82.
- Liao, X.; Raghavan, G.S.V.; and Yaylayan, V.A. **2002**. A novel way to prepare n-butylparaben under microwave irradiation. *Tetrahedron Letters*, **43**, 45–48.
- Loupy, A. **2004**. Solvent-free microwave organic synthesis as an efficient procedure for green chemistry. *Comptes Rendus Chimie* **7**(2), 103-112.
- Loupy, A.; Perreux, A.; and Petit, A. **2001**. Solvent-free microwave assisted organic synthesis. *Ceramic trans.* **111**, 163 -172.
- Oussaid, A.; Thach,Le, N.; and Loupy, A. **1997**. Selective dealkylation of alkyl aryl ethers in heterogeneous basic media under microwave irradiation. *Tetrahedron Letters*, **38**, 2451 – 2454.
- Robach, M. C. **1980**. Use of preservatives to control micoroorganisms in food. *Food Technol.* **34**, 81–84.
- Soni, M. G., Burdock, G. A., Taylor, S. L., and Greenberg, N. A. **2001**. Safety assessment of propyl paraben: a review of the published literature. *Food and Chemical Toxicology*, **39**(6), 513-532.
- Zhang, Z.; Zhang, M.; Zhan, D.; Wang, A. **1998**. New method for synthesis of p-hydroxybenzoic acid esters. *Huagong Shikan*. **12**, 24–25.

## CONNECTING STATEMENT 5

Chapter VI demonstrated that using  $\text{ZnCl}_2$  as catalyst, microwave-assisted synthesis of n-butyl paraben showed great rate enhancement over the classic synthesis method. A transition state theory is proposed to explain this rate enhancement phenomenon. It is therefore interesting to study the synthesis of paraben with different alcohol so that we will have a better idea about the transition state theory.

Manuscript was prepared to be submitted to *Tetrahedron*.

**Jianming Dai and G.S.Vijaya Raghavan,  $\text{ZnCl}_2$  Catalyzed Synthesis of Various Parabens under Microwave Irradiation. Prepared to be submitted to *Tetrahedron*.**

Department of Bioresource Engineering, McGill University, 21,111 Lakeshore road, Ste-Anne-de-Bellevue, QC, H9X 3V9

Contributions made by different authors are as follows:

The first author, the Ph.D. student did the experimental work and prepared the manuscript under the supervision and guidance of the second author during the research work

## CHAPTER VII

### **ZnCl<sub>2</sub> CATALYZED SYNTHESIS OF VARIOUS PARABENS UNDER MICROWAVE IRRADIATION**

#### **7.1 Abstract**

The synthesis of various parabens using ZnCl<sub>2</sub> as catalyst under microwave irradiation was studied. More than 97% of conversion can be achieved on the synthesis of n-butyl paraben within 2 minutes under microwaves. During the synthesis of ethyl and n-butyl paraben, a transition curve was observed on the temperature profile. During this period, temperature increases slower than normal. On the synthesis of sec-butyl paraben, ZnCl<sub>2</sub> showed greater advantage over concentrated H<sub>2</sub>SO<sub>4</sub> as catalyst. When ZnCl<sub>2</sub> was applied on the reaction of p-hydroxybenzoic acid with 1-octanol, no paraben was obtained, but the existence of di-n-octyl ether and 2-octene were detected.

Keywords: n-butyleparaben, Microwave-assisted synthesis, ZnCl<sub>2</sub>, transition state, athermal, octyl-ether

#### **7.2 Introduction**

p-Hydroxybenzoic acid esters (parabens) are widely used as antimicrobial preservative agents in food, pharmaceutical, and cosmetics due to their broad antimicrobial spectrum (Soni, et al., 2001). Among weak acid compounds e.g., propionates and sorbates, parabens have a wide PH range that makes them as very versatile food preservatives. The antimicrobial activity of parabens is directly dependent on the chain length (Robach, 1980; Dziezak, 1986). For example, the ability of n-butylparaben to inhibit bacteria is 4 times that of ethylparaben. We have reported earlier the synthesis of n-butyl-paraben using ZnCl<sub>2</sub> as catalyst under microwave irradiation (Liao, et al., 2001; Dai and Raghavan, 2005). Great acceleration was observed compared to conventional heating method. While the difference between microwave heating and conventional heating when using

PTSA as catalyst is negligible (Liao, et al., 2001); based on our observation, we noted that the use of  $\text{ZnCl}_2$  as catalyst may have gone through a different mechanism from the PTSA or concentrated  $\text{H}_2\text{SO}_4$  (Dai and Raghavan, 2005). Using  $\text{ZnCl}_2$  as catalyst, the reaction goes through a dipolar transition state which is the rate determining step in the reaction, and this transition state can couple with the microwaves resulting in the acceleration in reaction rate. This is very common microwave enhancing mechanism as proposed by Loup (2004). In this paper, the  $\text{ZnCl}_2$  catalyzed parabens synthesis is further studied.

### 7.3 Material and methods

#### 7.3.1 Materials

*n*-butanol, sec-butanol, methylparaben, *n*-butylparaben, *p*-hydroxybenzoic acid,  $\text{ZnCl}_2$  were purchased from Sigma-Aldrich, ON, Canada. Ethanol was obtained from our lab stock.

#### 7.3.2 Experimental procedure

Reactions were carried out using a STAR system (Open vessel system) obtained from CEM (Matthews, NC, USA). It operates with an emission frequency of 2450 MHz and a 600 W full power. It is equipped with an IR temperature sensor, a tubular quartz reactor (250 ml), and a Graham type condenser. By default, the equipment works on temperature control. In order to obtain the power control program at certain power level, the temperature was set at a temperature much higher than it is possible to achieve for example 300 °C while the maximum temperature possible to be 200 °C. By this way, the equipment will work at the set power level.

#### 7.3.3 Temperature profile

A mixture of 1.38 g of *p*-hydroxybenzoic acid, 0.93 mL of butanol or 0.6 mL of ethanol, with and without 0.069g of  $\text{ZnCl}_2$  was introduced to the quartz



reactor of the STAR apparatus. The irradiation was carried out at 50% power (600 W× 50%). Temperature profile was recorded during the heating. After heating and cooling, the mixture was diluted using acetone and analyzed by GC/MS. Temperature profiles for only *p*-hydroxybenzoic acid with ZnCl<sub>2</sub> and only n-butanol with ZnCl<sub>2</sub> were also recorded and after heating the mixture analyzed with GC/MS.

#### 7.3.4 Synthesis of n-butyl paraben under controlled temperature

A mixture of 1.38 g of *p*-hydroxybenzoic acid, 0.93 mL of butanol and 0.069g of ZnCl<sub>2</sub> was introduced to the quartz reactor of the STAR apparatus. The temperature was controlled at 120 °C and 100 °C, respectively for 2 minutes and the maximum power was set at 50% of full power. After reaction, the mixture was analyzed with GC/MS.

#### 7.3.5 Reaction of *p*-hydroxybenzoic acid with different alcohols

1.38 g of *p*-hydroxybenzoic acid was reacted with 0.93 mL of sec-butanol, tert-butanol, 2-methyl-1-propanol or 1.29 g of 1-octanol. 0.069 g of ZnCl<sub>2</sub> was used. 0.01mL of H<sub>2</sub>SO<sub>4</sub> was also studied to catalyze sec-butyl paraben. The reaction is carried out at 120 °C for reaction with sec-butanol, tert-butanol, 2-and methyl-1-propanol, no temperature limit was set for the reaction with 1-octanol. After reaction, GC/MS was used to analyze the mixture.

#### 7.3.6 Interaction of ZnCl<sub>2</sub> with microwaves

2 g of ZnCl<sub>2</sub> was added to the reaction vessel and a drop of water is added. 50% power was applied for 30 s. No temperature control was used during the heating.

### 7.3.7 GC/MS analysis

#### 7.3.7.1 GC/MS conditions

The GC (Agilent 6890N) was equipped with an 7683 series auto sampler. The injector temperature was set to be 220°C and oven temperature 200 °C during the analysis. Helium carrier gas has a constant flow rate of 1 ml/min. The GC column is a nonpolar general-purpose capillary column [30 m×0.25 mm i.d., 0.25 µm thickness, Phase DB5 (J&W Scientific Co.). MS (5973 MS) tune parameter is as follows: EI source (EMV: 1200V); Source temperature: 230 °C; Quadrapole temperature: 150 °C; Emission: 34.6 µA; electronic energy: 69.9 eV.

#### 7.3.7.2 Calibration

Standard p-hydroxybenzoic acid and n-butyl paraben with concentrations of 0.02, 0.20, 2.00, and 20.00 mg/mL were used to obtain the calibration curve as shown in Figures 7.1 and 7.2, respectively. These calibration curves were used in the reactions to determine the quantities of both components, therefore to estimate the conversion rate of the reactant into target product.

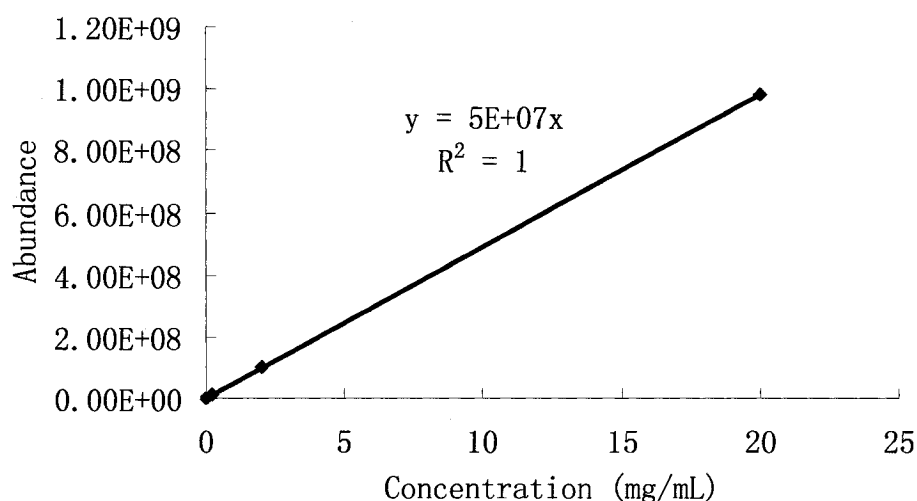


Fig. 7.1 Calibration curve for n-butyl paraben from 0.02mg/mL to 20 mg/mL

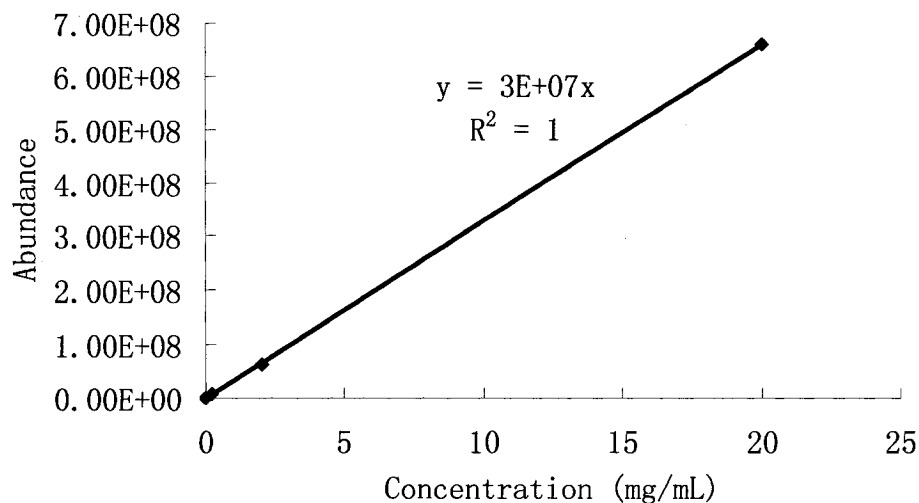


Fig. 7.2 Calibration curve for *p*-hydroxybenzoic acid from 0.02mg/mL to 20 mg/mL

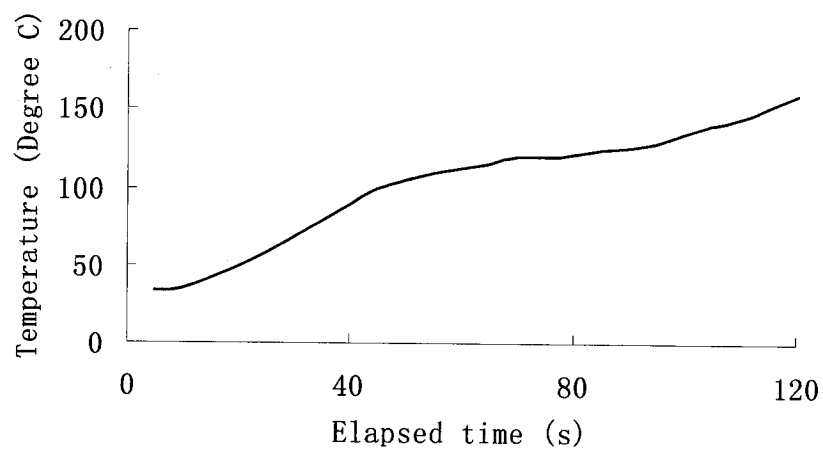
#### 7.4 Results and Discussion

Previous studies suggested that  $\text{ZnCl}_2$  as catalyst can greatly accelerate the synthesis of *n*-butyl paraben under microwave irradiation (Dai and Raghavan, 2005; Liao, et al., 2002). Based on the phenomena, we have proposed that the use of  $\text{ZnCl}_2$  goes through a different mechanism than the concentrated sulfuric acid catalyzed paraben synthesis. More investigation was carried out to study the use of  $\text{ZnCl}_2$  as catalyst for the synthesis of various parabens and to confirm the proof of the proposed mechanism.

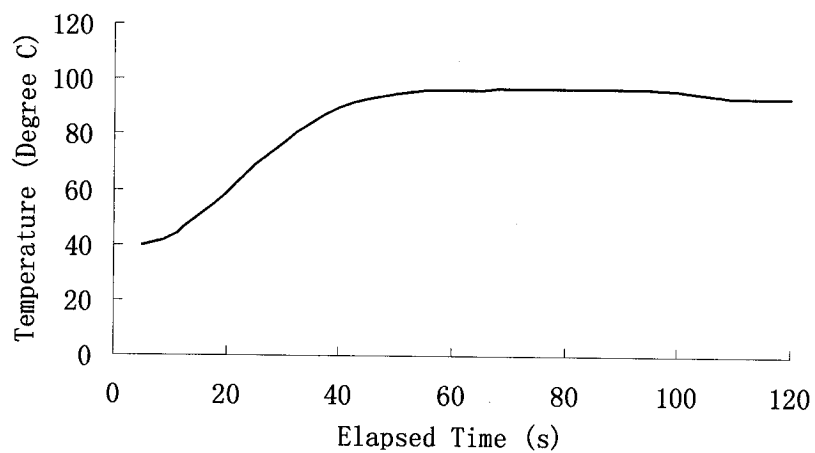
Temperature profiles were recorded during the  $\text{ZnCl}_2$  catalyzed synthesis of *n*-butyl parabens under microwave irradiation. For comparison purpose, the microwave-assisted heating of the corresponding mixture of the two reactants without catalyst, each individual reactant with catalyst were also recorded (See Figures 7.3 – 7.5). Figures 7.3 shows that without the addition of catalyst, the temperature of the mixture increases to a certain level regulated by the boiling point of the alcohol. During the heating, the *p*-hydroxybenzoic acid remains solid. With the addition of the  $\text{ZnCl}_2$  both processes goes through a transition stage where temperature increase slower than normal. During this stage, *p*-

hydroxybenzoic acid and the  $\text{ZnCl}_2$  start to dissolve into the alcohol. This stage starts at about 100 °C and terminate at about 130 °C when the temperature starts to rise rapidly again. After the termination of the transition stage, all the solids were dissolved into the liquid. With further increase of temperature, the liquid starts to change to light brownish color. Smoke was observed when the temperature exceeds 150 °C. GC/MS indicated that *p*-hydroxybenzoic acid was decomposed into phenol (Fig. 7.6). Figure 7.4 showed that when only *n*-butanol was mixed with the  $\text{ZnCl}_2$  temperature increase stops at its boiling point. No reaction was observed during the heating. However when only *p*-hydroxybenzoic acid is mixed with  $\text{ZnCl}_2$ , temperature increase to the level when the acid started to decompose to phenol as indicated by the GC/MS analysis (Fig. 7.7). Phenyl-4-hydroxybenzoate was also detected during the reaction.

Heating profile of pure *n*-butanol and pure *p*-hydroxybenzoic acid without the addition of  $\text{ZnCl}_2$  are shown in Figs. 7.8 and 7.9, respectively. The heating of pure *n*-butanol and *n*-butanol with the addition of  $\text{ZnCl}_2$  does not show much difference in the heating profile. However, when only *p*-hydroxybenzoic acid is heated using microwaves, temperature did not increase during the entire process. While with the addition of  $\text{ZnCl}_2$  the temperature increases to the point that causes *p*-hydroxybenzoic acid to decompose. Heating of only  $\text{ZnCl}_2$  revealed that the  $\text{ZnCl}_2$  is the component that leads to the temperature increase in the mixture of *p*-hydroxybenzoic acid and  $\text{ZnCl}_2$  (Fig. 7.10). In the mixture of *n*-butanol and  $\text{ZnCl}_2$ , the temperature is mainly regulated by the boiling point of the alcohol. During the reaction of *p*-hydroxybenzoic acid with the existence of  $\text{ZnCl}_2$  as catalyst, the temperature increases beyond the boiling point of *n*-butanol which is mainly due to the  $\text{ZnCl}_2$ .



(a)



(b)

Fig. 7.3 Temperature profile of the synthesis of n-butyl paraben: a) with  $\text{ZnCl}_2$  as catalyst; b) without catalyst. Microwave power level: 50% (Full power 600W).

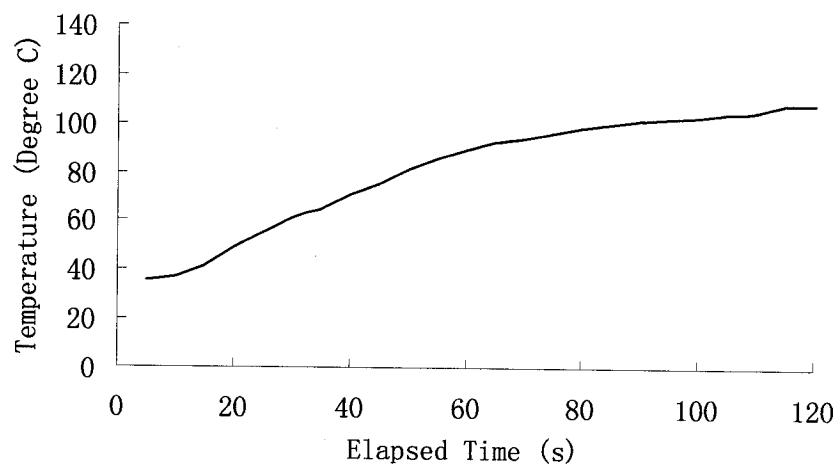


**Fig. 7.4** Temperature profile of 2 mL of n-butanol with the addition of 0.1g of ZnCl<sub>2</sub> under microwaves of 300W

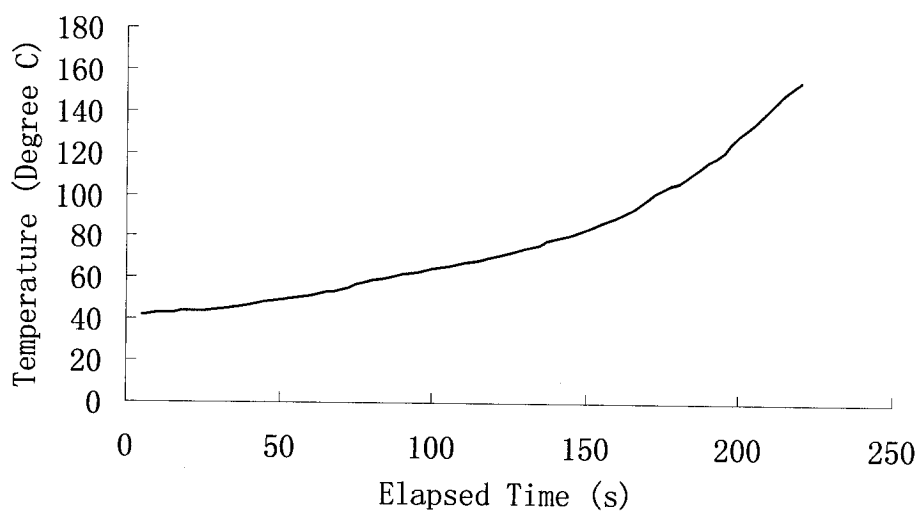


**Fig. 7.5** Temperature profile of 1.38g of *p*-hydroxybenzoic acid with the addition of 0.07g of ZnCl<sub>2</sub> under microwaves of 300W

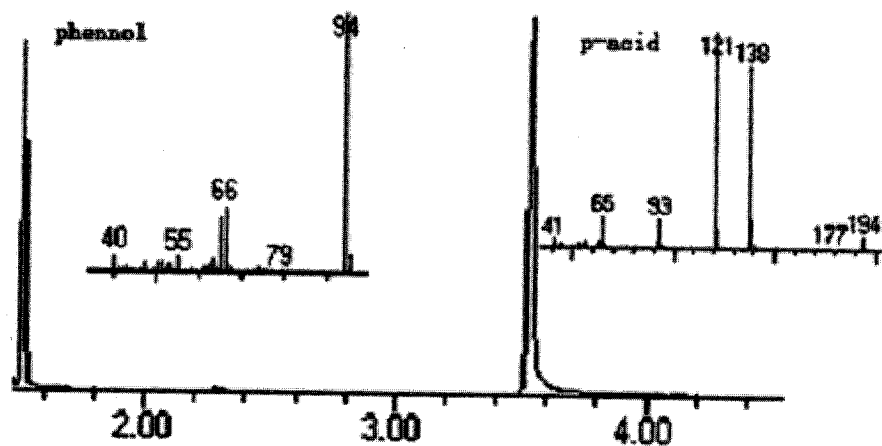


Fig. 7.6 Decomposition of *p*-hydroxybenzoic acid during the  $\text{ZnCl}_2$  catalyzed synthesis of *n*-butyl-paraben when temperature reaches over  $150^\circ\text{C}$ . Phenol was the product of decomposition of *p*-hydroxybenzoic acid; *n*-butyl paraben was also obtained.

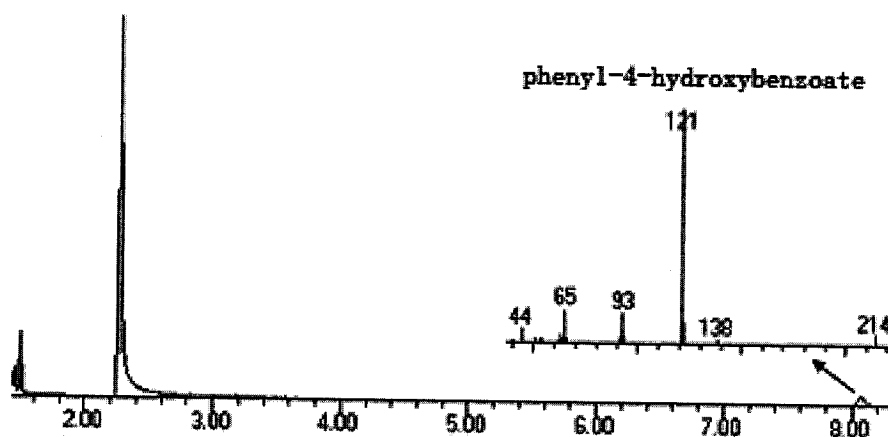


Fig. 7.7 Microwave-assisted heating of *p*-hydroxylbenoic acid with the addition of  $\text{ZnCl}_2$ , phenyl-4-hydroxybenzoate was obtained during the heating.

During the synthesis of n-butyl paraben, temperature controlled program of the microwave irradiation was carried out at 100 °C and 120 °C. At 100 °C, the solid is not dissolved, while at 120 °C, solids were completely dissolved into the liquid. GC/MS analysis showed that at 100 °C, part of the acid is converted into the paraben (Fig. 7.11) while at 120 °C, after about 2 minutes, more than 97% of the acid is converted into paraben (Fig. 7.12). Investigation of reaction of *p*-hydroxybenzoic acid with other alcohols like 1-propanol, ethanol, 2-methyl-1-propanol also showed that there is a transition state, but appears at different temperature. However, for most of the reactions, the solids start to dissolve into the liquid at about 120 °C. Therefore a temperature control run at 120 °C was used to synthesize these parabens (Figs 7.13 - 7.15).

When concentrated H<sub>2</sub>SO<sub>4</sub> was used to catalyze the synthesis of sec-butyl paraben, at temperatures over 100 °C, the mixture was carbonized with the addition of only 0.01 mL of H<sub>2</sub>SO<sub>4</sub>. GC/MS analysis showed that only a very small amount of ester was obtained (Fig. 7.17). However, this reaction can be realized using ZnCl<sub>2</sub> as catalyst as shown in Fig. 7.16 after 2 minutes of microwave irradiation at 120 °C. Tert-butyl paraben can not be obtained using either concentrated H<sub>2</sub>SO<sub>4</sub> or ZnCl<sub>2</sub>.

Comparison of the reactions of *p*-hydroxybenzoic acid with various isomers of butanol showed that the reaction with n-butanol has the highest yield followed by 2-methyl-1-propanol. The reaction with iso-butanol is relatively more difficult with only about 20% yield. No reaction happened with tert-butanol. Spatial structure and the location of the hydroxyl group determined this sequence. This suggests that even with microwave-assisted synthesis, the sequence did not change.

Comparison of the reaction with ethanol, 1-propynol, and n-butanol showed a sequence of n-butanol > 1-propynol > ethanol. This seems to be decided by the boiling point. 1-butanol has a boiling point about 118 °C. At this temperature *p*-hydroxybenzoic acid starts to dissolve into the liquid while browning (decomposition of the acid) is not in the horizon yet. With further



increase of the length of carbon chain, for example 1-octanol, no paraben was obtained.

During the reaction of *p*-hydroxybenzoic acid with n-octanol using  $\text{ZnCl}_2$  as catalyst, no paraben is obtained as shown in Fig. 7.18. However di-octyl ether and 2-octene were detected. By heating n-octanol with  $\text{ZnCl}_2$  without the existence of *p*-hydroxybenzoic acid, n-octyl ether was formed (Fig. 7.19). The difference is that no 2-octene was detected. This suggests that the proposed mechanism (Dai and Raghavan, 2005) is very likely to be the mechanism  $\text{ZnCl}_2$  catalyzed esterification goes through (scheme 7.1). During the heating of n-butanol, no ether was detected indicating that temperature played an important role during the formation of ether. In the case of 1-octanol, the temperature during the heating is about 194 °C regulated by the boiling point of 1-octanol however, the temperature is only 117°C for n-butanol.

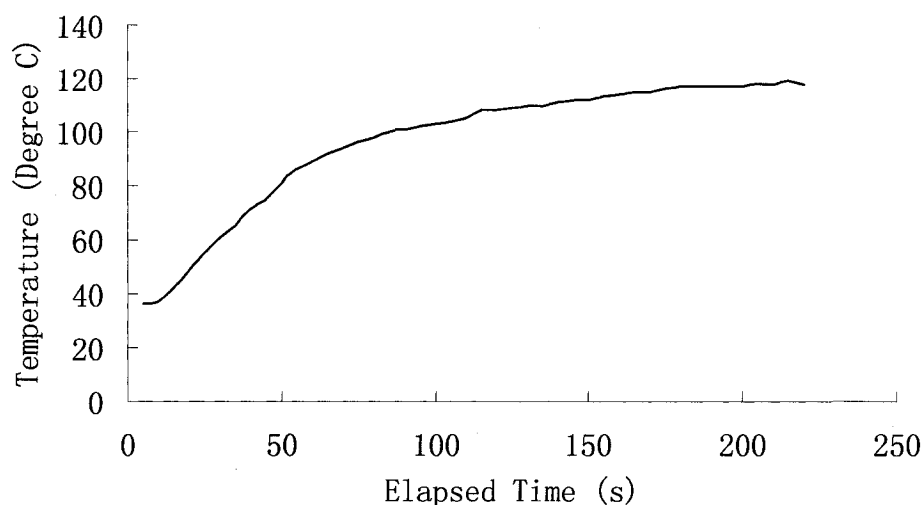


Fig. 7.8 Temperature profile of 5 mL of n-butanol under microwaves of 300W without the addition of  $\text{ZnCl}_2$ .

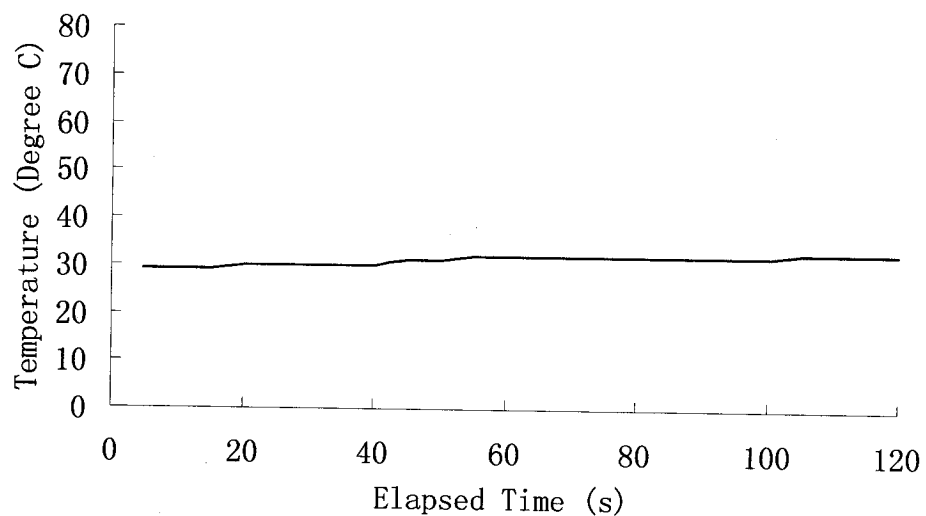


Fig. 7.9 Temperature profile of 5g of *p*-hydroxybenzoic acid under microwaves of 300W without the addition of  $\text{ZnCl}_2$ .

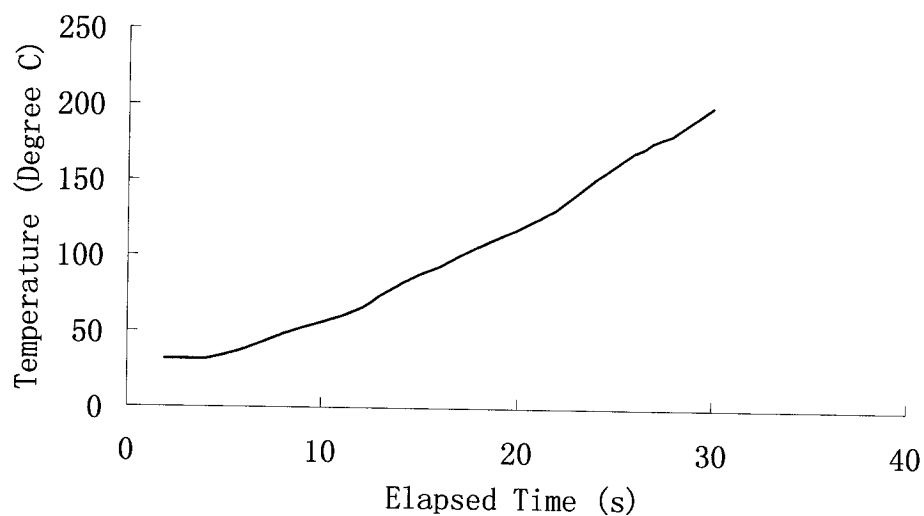


Fig. 7.10 Temperature profile of 5g of  $\text{ZnCl}_2$  under microwaves of 300W

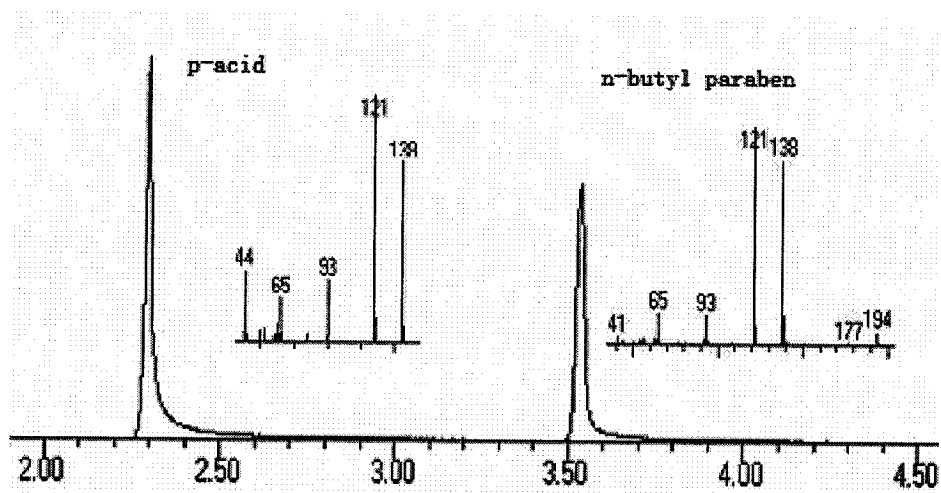


Fig. 7.11 Synthesis of n-butyl-paraben with temperature controlled at 100 °C for 2 min, microwave power level was set at 50% (300W) during the temperature control.

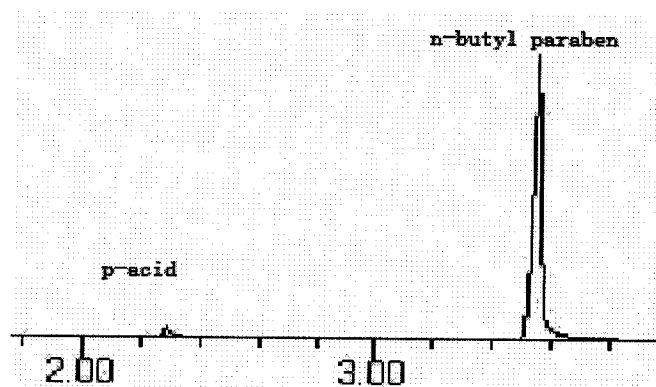


Fig. 7.12 Synthesis of n-butyl-paraben with temperature controlled at 120 °C for 2 min, microwave power level was set at 50% (300W) during the temperature control.

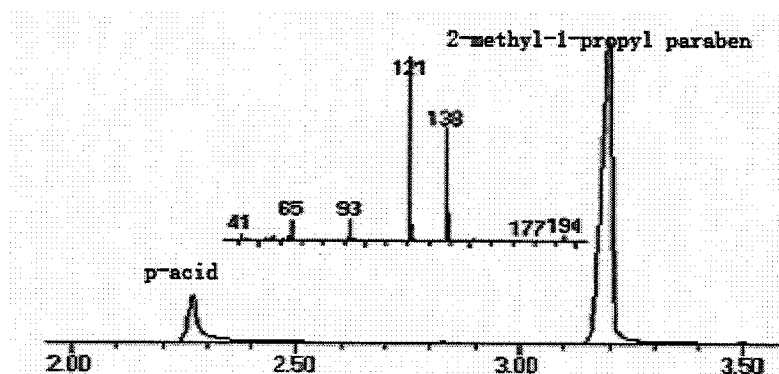


Fig. 7.13 Synthesis of 2-methyl-1-propyl-paraben with temperature controlled at 120 °C for 2 minutes. Microwave power level was set at 50% (300W) during the temperature control.

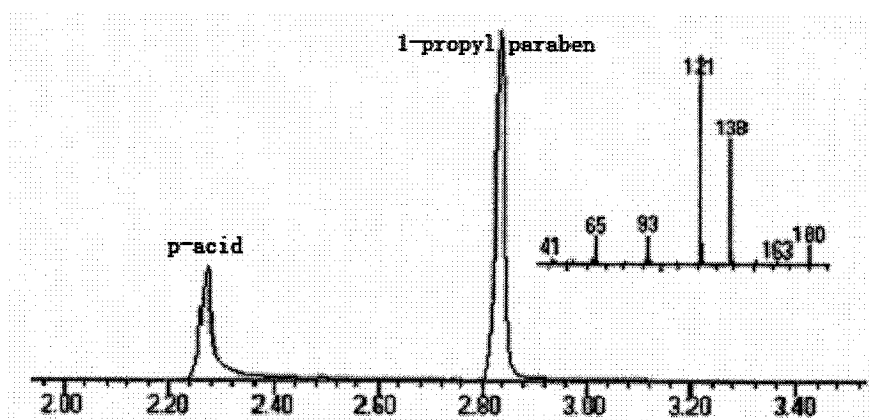


Fig. 7.14 Synthesis of 1-propyl-paraben with temperature controlled at 120 °C for 2 minutes. Microwave power level was set at 50% (300W) during the temperature control.

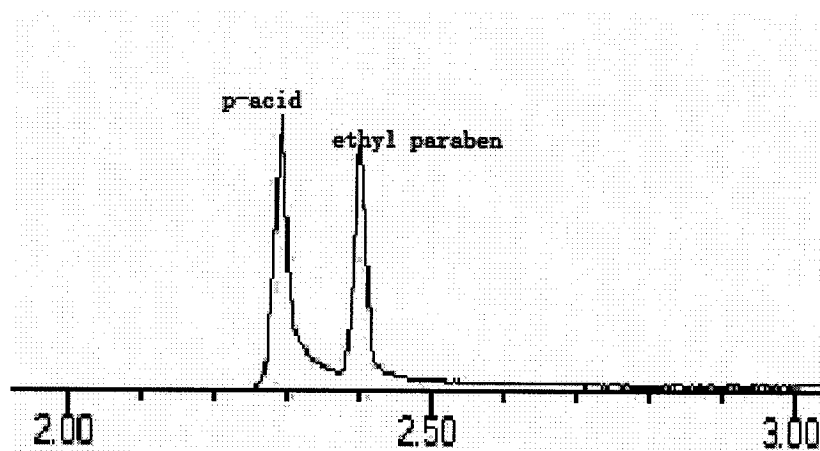


Fig.7.15 Synthesis of ethyl paraben with temperature controlled at 120 °C for 2 min. Microwave power level was set at 50% (300W) during the temperature control.

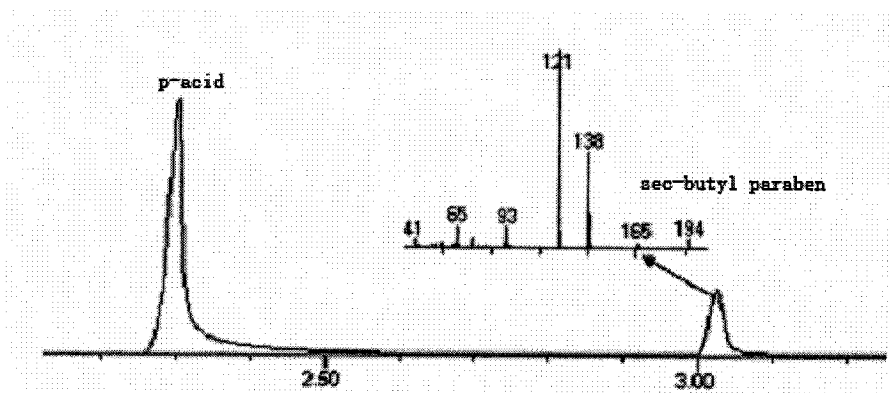


Fig. 7.16 Synthesis of sec-butanol paraben with  $\text{ZnCl}_2$  as catalyst under microwave irradiation (300W, 2 minutes)

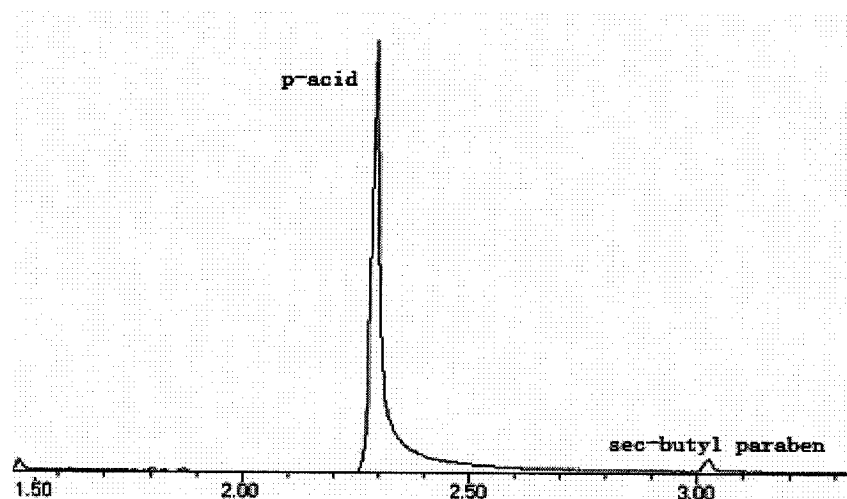


Fig. 7.17 Synthesis of sec-butanol paraben using conc.  $\text{H}_2\text{SO}_4$  (0.01 mL) as catalyst under microwave irradiation (300W, 2 minutes).

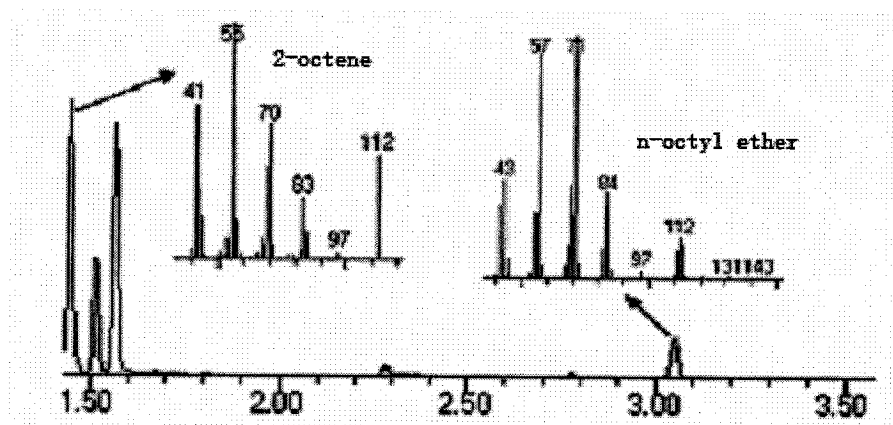


Fig. 7.18 Synthesis of 1-octyl paraben with  $\text{ZnCl}_2$  as catalyst under microwave irradiation (300W, 2 minutes). 2-octene and n-octyl ether were detected.

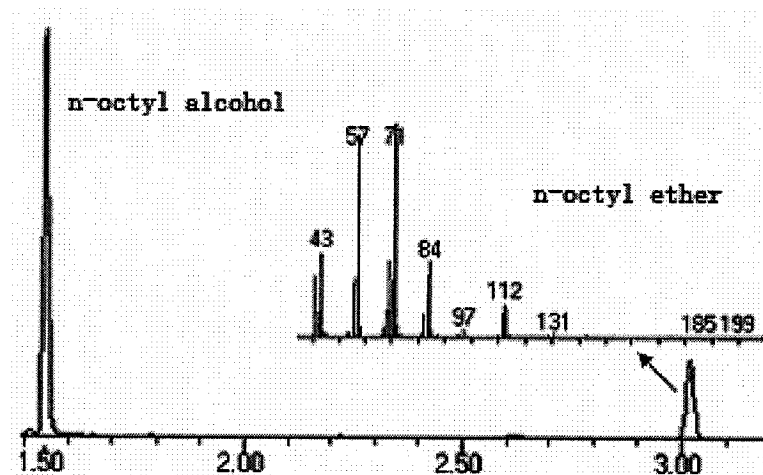
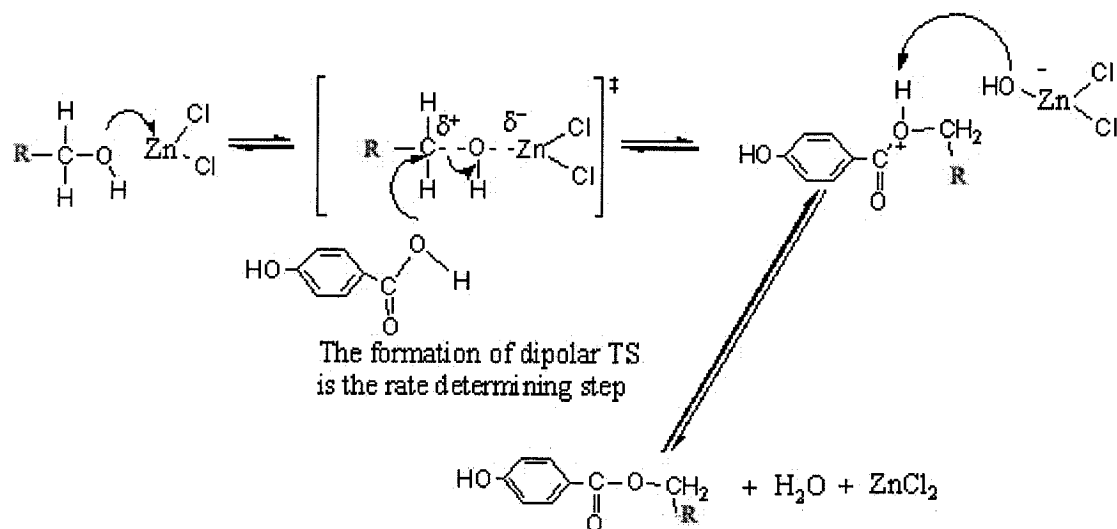


Fig. 7.19 Microwave-assisted heating of n-octanol with the addition of  $\text{ZnCl}_2$  under microwave power of 300W for 2 min.



Scheme 7.1 Mechanism of  $\text{ZnCl}_2$  catalyzed synthesis of parabens.

## 7.5 Conclusions

ZnCl<sub>2</sub> can be used as catalyst in the synthesis of many different parabens under microwave irradiation. Depending on the alcohol used during the synthesis, the yield of parabens is different. It follows a similar rule as conventional heating with a strong acid as catalyst. ZnCl<sub>2</sub> does show advantage over concentrated H<sub>2</sub>SO<sub>4</sub> on the synthesis of sec-butyl-paraben. The appearance of 2-octene and di-octyl ether during the the reaction of p-hydroxybenzoic acid with 1-octanol using ZnCl<sub>2</sub> under microwaves prove the proposed mechanism by Dai and Raghavan (2005).

## 7.6 Acknowledgement

The authors wish to acknowledge the Natural Science and Engineering Research Council of Canada (NSERC), FQRNT and Canadian International Development Agency (CIDA) for their financial support.

## 7.7 References

- Dai, J. and G.S.Vijaya Raghavan, Microwave-assisted synthesis of n-butylparaben using ZnCl<sub>2</sub> as catalyst. In proceeding of 39th Annual Symposium of International Microwave Power Institute, **2005**, Seattle, Washington, USA
- Dziezak, J. D. **1986**. Preservatives: antimicrobial agents. *Food Technol.* 40, 104–111.
- Liao, X.; Raghavan, G.S.V.; and Yaylayan, V.A. **2002**. A novel way to prepare n-butylparaben under microwave irradiation. *Tetrahedron Letters*, 43, 45–48.
- Loupy, A. **2004**. Solvent-free microwave organic synthesis as an efficient procedure for green chemistry. *Comptes Rendus Chimie* 7(2), 103-112.
- Robach, M. C. **1980**. Use of preservatives to control micoroorganisms in food. *Food Technol.* 34, 81–84.
- Soni, M. G., Burdock, G. A., Taylor, S. L., and Greenberg, N. A. **2001**. Safety assessment of propyl paraben: a review of the published literature. *Food and Chemical Toxicology*, 39(6), 513-532.



## CONNECTING STATEMENT 6

Chapter VII demonstrated using  $\text{ZnCl}_2$  as catalyst, many different type of parabens can be obtained using microwave-assisted synthesis method. Among the parabens studied, sec-butyl paraben can be synthesized using  $\text{ZnCl}_2$  as catalyst but can not be obtained using conc.  $\text{H}_2\text{SO}_4$ . With longer chain alcohol, the paraben can not be easily obtained even using microwave-assisted synthesis method. N-butyl paraben is a very good preservative with very active antimicrobial activities. Since microwave-assisted synthesis method was demonstrated to be an efficient method to produce this chemical, it is therefore important to know what are the factors that influence the synthesis.

Manuscript was prepared to be submitted to *Tetrahedron*.

**Jianming Dai and G.S.Vijaya Raghavan, Influence of various factors on the synthesis of n-butyl-paraben using  $\text{ZnCl}_2$  as catalyst under microwave irradiation. Prepared to be submitted to *Tetrahedron*.**

Department of Bioresource Engineering, McGill University, 21,111 Lakeshore road, Ste-Anne-de-Bellevue, QC, H9X 3V9

Contributions made by different authors are as follows:

The first author, the Ph.D. student did the experimental work and prepared the manuscript under the supervision and guidance of the second author during the research work

## CHAPTER VIII

### INFLUENCE OF VARIOUS FACTORS ON THE SYNTHESIS OF N-BUTYL-PARABEN USING $\text{ZnCl}_2$ AS CATALYST UNDER MICROWAVE IRRADIATION

#### 8.1 Abstract

The influence of various factors, viz. synthesis time, microwave power, reactant ratio and amount of catalyst on the synthesis of n-butyl paraben was investigated. Two-step orthogonal experimental design was used to carry out the study. Preliminary study using a  $L_8(2^7)$  design suggested that time and power are significant at 99% of confidence and catalyst amount significantly affects the yield at 90% confidence level. Extended study showed that all factors affect the yield at 99% confidence level when the level of the factors are extended.

Keywords: n-butyleparaben, Microwave-assisted synthesis,  $\text{ZnCl}_2$ , orthogonal experimental design

#### 8.2 Introduction

p-Hydroxybenzoic acid esters (parabens) are widely used as antimicrobial preservative agents in food, pharmaceutical, and cosmetics due to their broad antimicrobial spectrum (Soni, et al., 2001). Among weak acid compounds e.g., propionates and sorbates, parabens have a wide PH range that makes them as very versatile food preservatives. The antimicrobial activity of parabens is directly dependent on the chain length (Robach, 1980; Dziezak, 1986). For example, the ability of n-butylparaben to inhibit bacteria is 4 times that of ethylparaben. We have reported earlier the synthesis of n-butyl-paraben using  $\text{ZnCl}_2$  as catalyst under microwave irradiation (Liao, et al., 2001; Dai and Raghavan, 2005). Great acceleration was observed compared to conventional heating method. While the difference between microwave heating and conventional heating when using PTSA as catalyst is negligible (Liao, et al., 2001); based on our observation, we propose that the use of  $\text{ZnCl}_2$  as catalyst might have gone through a different mechanism from the PTSA or concentrated  $\text{H}_2\text{SO}_4$  (Dai and raghavan, 2005).

Using  $\text{ZnCl}_2$  as catalyst, the reaction goes through a dipolar transition state which is the rate determining step in the reaction, and this transition state can couple with the microwaves resulting in the acceleration in reaction rate. This is very common microwave enhancing mechanism as proposed by Loup (2004). In this paper, the  $\text{ZnCl}_2$  catalyzed parabens synthesis is further studied.

### 8.3 Material and methods

#### 8.3.1 Materials

*n*-butanol, *n*-butylparaben, *p*-hydroxybenzoic acid, and  $\text{ZnCl}_2$  were purchased from Sigma-Aldrich, Canada (Ontario, Canada). Acetone was obtained from Fisher Scientific International Inc. (Ontario, Canada)

#### 8.3.2 Experimental procedure

Reactions were carried out using a CEM STAR open vessel microwave system (Matthews, NC, USA). It operates with an emission frequency of 2450 MHz and a 600 W full power. It is equipped with an IR temperature sensor, a tubular quartz reactor (250 ml), and a Graham type condenser. By default, the equipment works on temperature control. In order to obtain the power control program at certain power level, the temperature was set at a temperature much higher than it is possible to achieve; for example 300 °C while the maximum temperature possible to be 200 °C. By this way, the equipment will work at the set power level.

#### 8.3.3 A two-level study using an $L_8(2^7)$ orthogonal array

The influence of factors, viz. reaction time, catalyst amount, acid/alcohol ratio and microwave power was investigated. The factors and levels are shown in Table 8.1. An orthogonal array  $L_8(2^7)$  (Table 8.2) was chosen for the preliminary study to determine the range of the reactions. The interaction between the reaction time and the amount of catalyst was arranged in the array. After each reaction, the mixture was completely dissolved into 10 mL of acetone; 0.4mL of the acetone solution was transferred to a 2 mL vial followed by the addition of

0.6mL of acetone to make it 1mL. GC/MS was used to estimate the amount of n-butyl paraben produced. The percentage yield of n-butyl paraben was calculated based on this value. Each run is repeated to obtain two replicates.

#### 8.3.4 A four-level study using an $L_{16}(4^5)$ orthogonal array

The influence of the same four factors was further studied by increasing the range of levels. Factors and levels are shown in Table 8.3 and the  $L_{16}(4^5)$  array is shown in Table 8.4. The GC/MS analysis was the same as the two level studies. Two replicates were also obtained for each combination.

#### 8.3.5 GC/MS analysis

##### 8.3.5.1 GC/MS conditions

The GC (Agilent 6890N) was equipped with a 7683 series auto sampler. The injector temperature was set to be 220°C and oven temperature 200 °C during the analysis. Helium carrier gas has a constant flow rate of 1 ml/min. The GC column was a nonpolar general-purpose capillary column [30 m×0.25 mm i.d., 0.25 µm thickness, Phase DB5 (J&W Scientific Co.)]. MS (5973 MS) tune parameter is: EI source (EMV: 1200V); Source temperature: 230 °C; Quadrapole temperature: 150 °C; Emission: 34.6 µA; electronic energy: 69.9 eV.

##### 8.3.5.2 Calibration

Standard p-hydroxybenzoic acid and n-butyl paraben with concentrations of 0.02, 0.20, 2.00, and 20.00 mg/mL were used to obtain the calibration curve as shown in Figures 8.1 and 8.2, respectively. These calibration curves were used in the reactions to determine the quantities of both components, which helps in estimating the conversion rate of the reactant into target product.

##### 8.3.5.3 Determination of the conversion percentage

Based on the calibration curves, the percentage of conversion was calculated using the flowing equation:

$$\text{Conversion}\% = \frac{250 \times \text{PeakArea} / (5 \times 10^7)}{3.86} \times 100 \quad (8.1)$$

#### 8.3.5.4 Statistical Analysis

Analysis of Variance Procedure (ANOVA) was performed using SAS software. Duncan's Multiple Range Test was performed to investigate the significance between the levels of each factor. The percentage contribution to total influencing effect is calculated as:

$$\text{Contribution}\% = \frac{F_i}{\sum_{i=1}^N F_i} \quad (8.2)$$

Where:  $F_i$  is the F value of the  $i^{\text{th}}$  factor, and  $\sum_{i=1}^N F_i$  is the sum of all the F values.

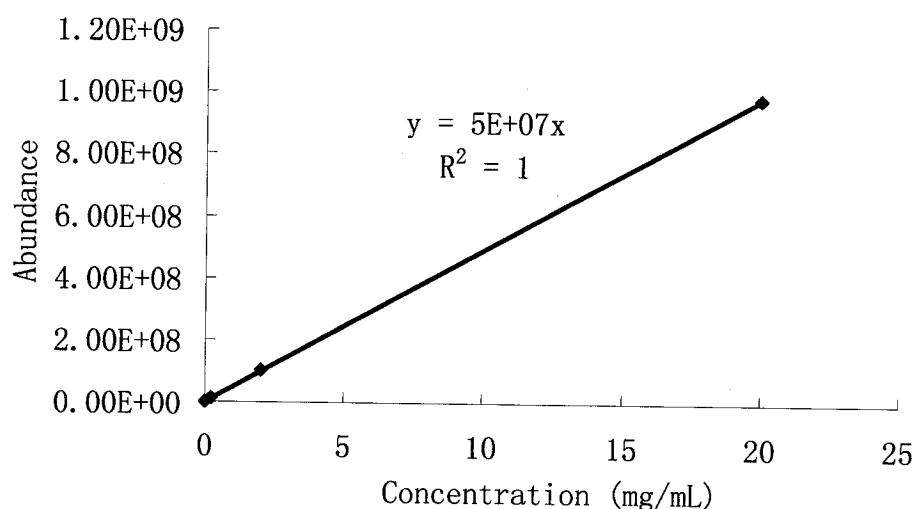


Fig. 8.1. Calibration curve for n-butyl paraben from 0.02mg/mL to 20 mg/mL

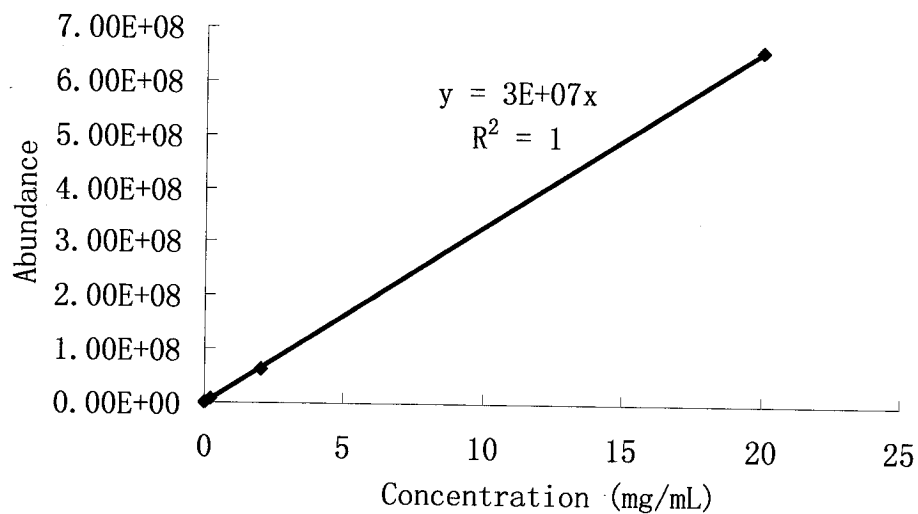


Fig. 8.2 Calibration curve for p-hydroxybenzoic acid from 0.02mg/mL to 20 mg/mL

Table 8.1. Factors and levels used in the investigation.

Levels	Factors			
	A1 Time	B1 Catalyst amount (%)*	C1 Power (%)**	D1 Acid/ Alcohol mol. ratio***
1	1 min	2%	50	1/1
2	2 min	5%	75	1/1.2

\* Based on the weight of p-hydroxybenzoic acid (2.76g)

\*\* Full power of the microwave equipment is 600W

\*\*\* The alcohol used here is n-butanol

Table 8.2.  $L_8(2^7)$  array of experimental design

Run	Treatments						
	A1	B1	A1xB1*	C1	E1**	E2***	D1
1	1	1	1	1	1	1	1
2	1	1	1	2	2	2	2
3	1	2	2	1	1	2	2
4	1	2	2	2	2	1	1
5	2	1	2	1	2	2	2
6	2	1	2	2	1	1	1
7	2	2	1	1	2	1	1
8	2	2	1	2	1	2	2

\* Interaction between Factors A1 and B1

\*\* Error column 1

\*\*\* Error column 2

Table 8.3. Factors and levels in the four-level study

Levels	Factors			
	A2	B2	C2	D2
	Time	Power (%)*	Acid/ alcohol mol ratio**	Catalyst amount (%)***
1	1 min	25	1.5/1	2
2	2 min	50	1/1	5
3	3 min	75	1/1.5	10
4	4 min	100	1/3	20

\* Full power of the microwave equipment is 600W

\*\* The alcohol used here is n-butanol

\*\*\* Based on the weight of p-hydroxybenzoic acid (2.76g)

Table 8.4.  $L_{16}(4^5)$  orthogonal array experimental design

	A2	B2	C2	D2	Error
Run	Time	Power	Acid/alcohol mol ratio	Catalyst amount	
1	1	1	1	1	1
2	1	2	2	2	2
3	1	3	3	3	3
4	1	4	4	4	4
5	2	1	2	3	4
6	2	2	1	4	3
7	2	3	4	1	2
8	2	4	3	2	1
9	3	1	3	4	2
10	3	2	4	3	1
11	3	3	1	2	4
12	3	4	2	1	3
13	4	1	4	2	3
14	4	2	3	1	4
15	4	3	2	4	1
16	4	4	1	3	2

#### 8.4 Results and Discussion

The percentage recovery of the two-level study is presented in Table 8.5. It was shown that the conversion percentage varies greatly with the change in combination of different factors. The lowest is less than 2% and the highest is almost 70% of conversion. Statistical analysis result is presented in Table 8.6. At 99% of confidence, reaction time and microwave power have significant influence on the percentage conversion. The amount of catalyst is only significant at a confidence level of about 92%. Acid to alcohol mol ratio did not show significant



influence on the conversion percentage at the current two levels. It is also shown that there is no interaction between the reaction time and amount of catalyst.

Based on the above two-level study, the same four factors were further studied by increasing the number of levels to four. A wider range was investigated. The percentage conversion rate is shown in Table 8.7. The value varies from 0 to 60%. Temperature was also recorded for each reaction and is also presented Table 8.7. Study in the previous chapters (Fig. 8.3) showed that during the reaction under microwave irradiation, temperature will first increase to a certain level at a relatively fast rate; After reaching about 120°C, the increase rate is much slower than normal which was suggested to be the transition state (Dai and Raghavan, 2005). After the transition state, temperature kept to increase to the level that caused the decomposition of the p-hydroxybenzoic acid. Even though no general correlation between the percentage recovery and temperature was observed, the high temperature of certain runs suggested that decomposition is the reason of low conversion rates such as runs No. 16, and 15 in Table 8.7 (Fig. 8.4). The highest percentage conversion was obtained at No. 8 with the end temperature of 135 °C. Fig. 8.5 indicates that the p-hydroxy benzoic acid starts to decompose to phenol but with a very small portion.

Statistical study result was presented in table 8.8. It was shown that at the four levels, all the factors investigated significantly affect the percentage conversion including the acid/alcohol mol ratio factor. The contribution factor obtained by the percentage of the F values of each individual factor is shown in Fig. 8.6. It suggests that the reaction time has the strongest influence to the percentage conversion followed by microwave power. The acid /alcohol ratio and the amount of catalyst have similar effect. The first two factors agree with the result of the two-level study. While by extending the range of the level studied, the acid to alcohol mol ratio starts to affect the conversion. The percentage conversion was plotted vs. different levels of each factor (Figures 8.7 - 8.10). The DUNCAN's multiple range test results are also shown in Figs. 8.7 - 8.10.

Fig. 8.7 showed the influence of reaction time on the conversion. At 2 min and 3 min, the conversions were significantly higher than that at 1 and 4 min.

While there were no significant difference between 2 and 3 min and 1 and 4 min. The low conversion at 4 min was mainly due to the decomposition of p-hydroxybenzoic acid caused by the long time, high power and large amount of catalyst (No. 15 and 16 of Table 8.7).

Fig. 8.8 showed the influence of microwave power on the paraben yield. As can be seen, with the increase of microwave power, the yields significantly increase with 100% power much higher than all the other power levels. As suggested by (Dai and Raghvan, 2005) that a transition state exists during the synthesis of n-butyl paraben and the reaction rate will be very rapid when reaching the transition state temperature. When higher power level is used, time needed to reach the transition state temperature will be shortened. Therefore the reaction rate will be greatly accelerated.

Fig. 8.9 showed the influence of acid/alcohol ratio on the yield of paraben. It can be seen that the yield increases with the increase of alcohol ratio up to alcohol is 1.5 times mol number of acid. But with further increase in the alcohol amount to 3 times, the yield decrease greatly. Since esterification reaction is a reversible reaction, in order to achieve high yield, excess amount of either acid or alcohol is necessary. However, in this reaction, either excess amount of acid or alcohol does not lead to high yield. When higher ratio of acid is used, when temperature reaches above the boiling temperature of n-butanol, the alcohol will be evaporated and the amount of alcohol available to react with the solid acid is even less. Therefore low yield can be expected in this case. However, when large excess amount of n-butanol is used, the temperature of the mixture is mainly determined by the boiling temperature which is equal or lower to the transition state temperature. As we can see from previous discussions, the lower temperature is the reason that the presence of large excess amount of alcohol will lead to the lower reaction rate. The best acid/alcohol ratio is determined so far to be 1/1.5.

Fig. 8.10 shows the influence of catalyst amount on the yield of paraben. It can be seen that at 5% optimum yield is obtained. Either too low or too high will

result in lower yield. At low percentage, the reaction is very slow but at higher percentage, the reaction is hard to control and lead to decomposition of acid.

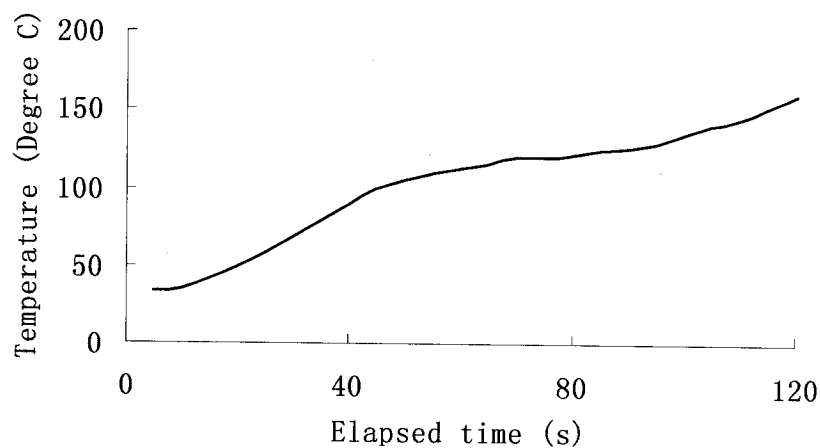


Fig. 8.3 Temperature profile during the synthesis of n-butylparaben under microwave irradiation using  $\text{ZnCl}_2$  as catalyst.

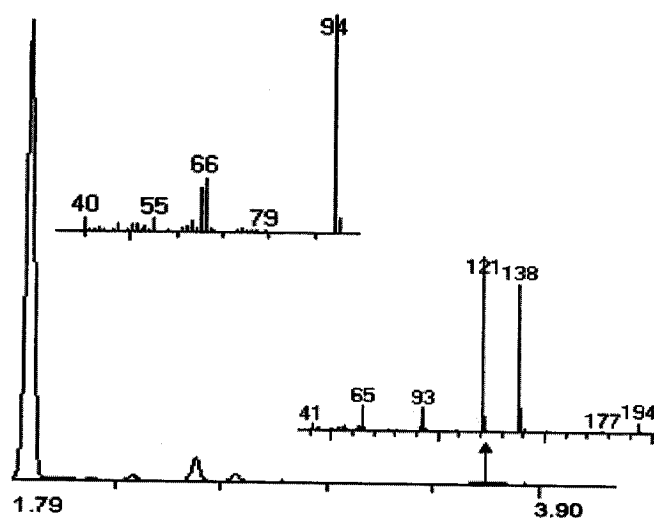


Fig. 8.4 GC chromatograph and MS spectroscopy result of run No. 15 of Table 8.7 indicating the majority of p-hydroxybenzoic acid was decomposed into phenol.

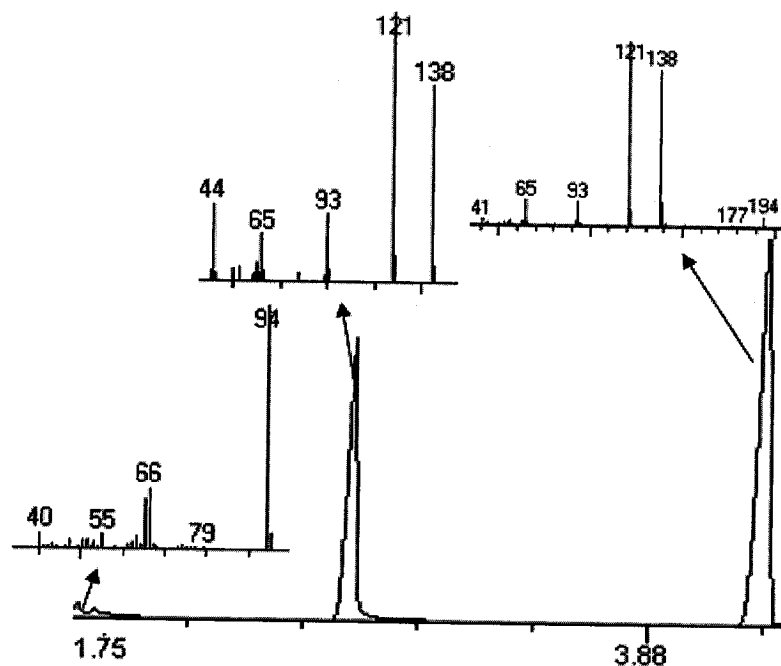


Fig. 8.5. GC chromatograph and MS spectroscopy result of run No. 8 of Table 8.7. Relatively high conversion rate was obtained and at this temperature the acid starts to decompose to phenol.

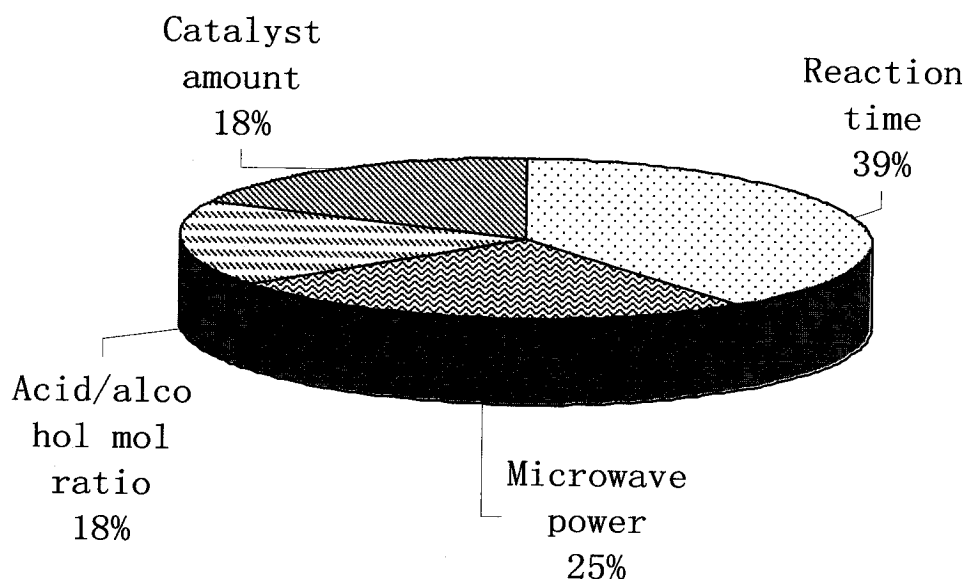


Fig. 8.6. Contribution of different factors on the percentage conversion rate of the n-butyl paraben

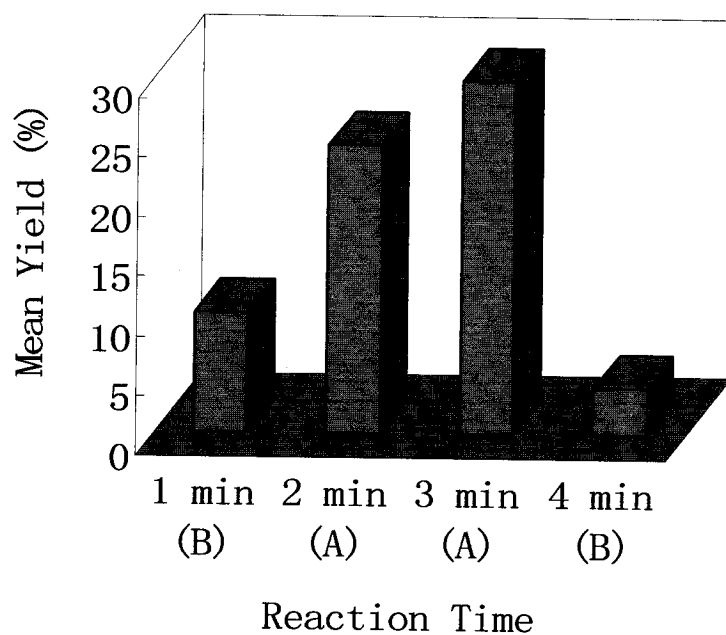


Fig. 8.7. Influence of reaction time on paraben yield. The letters in the bracket under each category is the Duncan grouping symbols at ( $\alpha=0.10$ ); Means with the same letter are not significantly different.

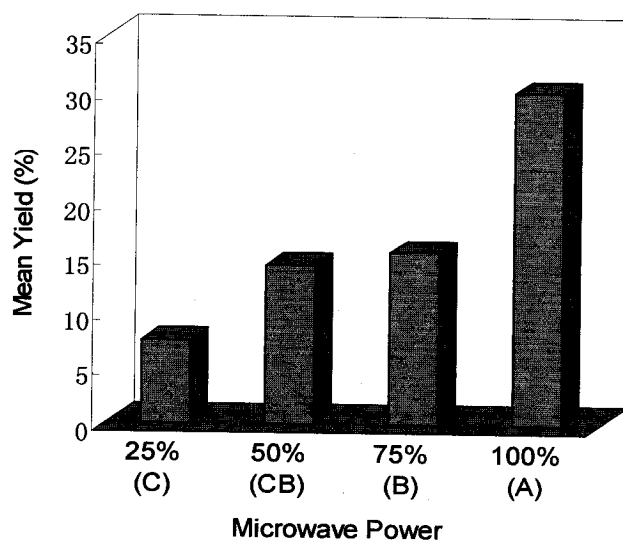


Fig. 8.8. Influence of Microwave Power on paraben yield. The letters in the bracket under each category is the Duncan grouping symbols at ( $\alpha=0.10$ ); Means with the same letter are not significantly different.

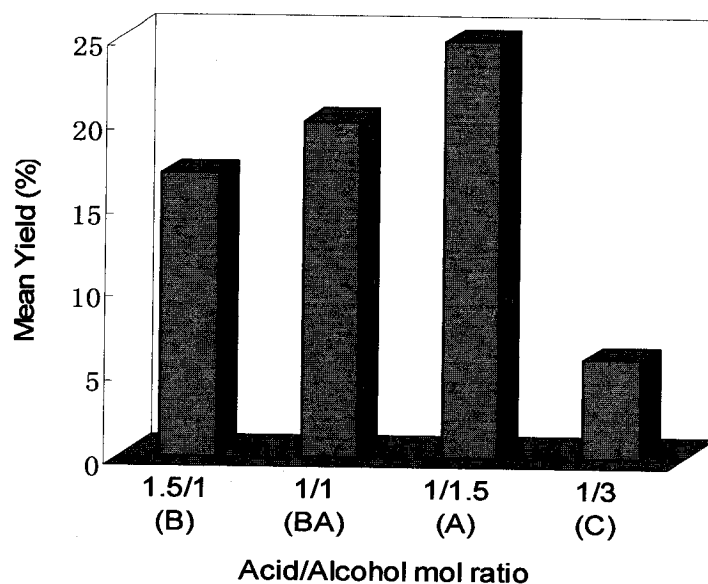


Fig. 8.9. Influence of acid/alcohol mol ratio on paraben yield. The letters in the bracket under each category is the Duncan grouping symbols at ( $\alpha=0.10$ ); Means with the same letter are not significantly different.

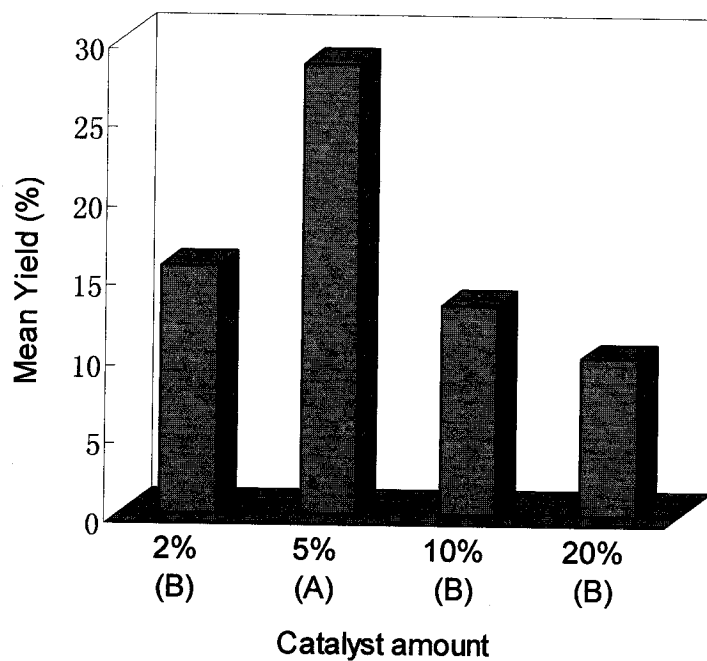


Fig. 8.10. Influence of the amount of catalyst on paraben yield. The letters in the bracket under each category is the Duncan grouping symbols at ( $\alpha=0.05$ ); Means with the same letter are not significantly different.

Table 8.5 Percentage conversion results of the two-level study

Runs	Treatments							Conversion%	
	A1	B1	A1xB1	C1	E1	E2	D1	Rep 1	Rep 2
1	1	1	1	1	1	1	1	1.65	1.72
2	1	1	1	2	2	2	2	4.59	4.48
3	1	2	2	1	1	2	2	5.06	5.21
4	1	2	2	2	2	1	1	17.70	18.10
5	2	1	2	1	2	2	2	3.13	3.20
6	2	1	2	2	1	1	1	47.30	48.83
7	2	2	1	1	2	1	1	17.12	16.85
8	2	2	1	2	1	2	2	68.60	68.72

Table 8.6 ANOVA procedure results of the two-level study

Source	DF	ANOVA SS	Mean Square	F Value	Pr > F
A1	1	2895.52	2895.52	16.94	0.0021
B1	1	656.13	656.13	3.84	0.0786
A1xB1	1	77.44	77.44	0.45	0.5162
C1	1	3146.65	3146.65	18.41	0.0016
D1	1	2.46	2.46	0.01	0.9068

Table 8.7 Percentage conversion of the four-level study

Runs	Treatments					Conversion%		Temperature (°C)
	A2	B2	C2	D2	Error	Rep 1	Rep 2	
1	1	1	1	1	1	0.14	0.18	110
2	1	2	2	2	2	11.2	12.8	122
3	1	3	3	3	3	15.6	17.5	125
4	1	4	4	4	4	10.9	11.5	120
5	2	1	2	3	4	13.0	13.9	128
6	2	2	1	4	3	24.3	25.5	198
7	2	3	4	1	2	0.43	0.56	113
8	2	4	3	2	1	56.4	58.9	135
9	3	1	3	4	2	15.0	13.5	118
10	3	2	4	3	1	9.0	11.2	111
11	3	3	1	2	4	42.1	42.8	130
12	3	4	2	1	3	50.5	52.6	158
13	4	1	4	2	3	1.8	2.1	111
14	4	2	3	1	4	10.2	11.1	127
15	4	3	2	4	1	2.9	3.1	198
16	4	4	1	3	2	0.0	0.0	211

Table 8.8 ANOVA procedure results of the four level study

Source	DF	ANOVA SS	Mean Square	F Value	Pr > F
A2	3	3439.83	1146.61	17.02	0.0001
B2	3	2170.09	723.36	10.74	0.0002
C2	3	1534.26	511.42	7.59	0.0016
D2	3	1570.11	523.37	7.77	0.0014



### 8.5 Conclusions

All the factors studied have some influence on the yield of n-butyl paraben during the microwave-assisted synthesis using  $\text{ZnCl}_2$  as catalyst. The yield will increase with the reaction time to a certain extent and will drop after. This is mainly due to the decomposition at the extended synthesis period. Temperature also affects the synthesis in two ways. When the temperature is not reaching a certain level, the reaction will not happen. But under the catalyzed condition when the temperature loses control, the obtained product will be decomposed and phenol will be the final product. The optimum amount of catalyst was determined to be 5% of the p-hydroxybenzoic acid amount. The alcohol/acid ratio should not be too high because that will limit the temperature of the reactant. And the reaction obtained at 100% power gives the best result.

### 8.6 Acknowledgement

The authors wish to acknowledge the Natural Science and Engineering Research Council of Canada (NSERC), FQRNT and Canadian International Development Agency (CIDA) for their financial support.

### 8.5 References

- Dai, J. and G.S.Vijaya Raghavan, Microwave-assisted synthesis of n-butylparaben using  $\text{ZnCl}_2$  as catalyst. In proceeding of 39th Annual Symposium of International Microwave Power Institute, **2005**, Seattle, Washington, USA
- Dziezak, J. D. **1986**. Preservatives: antimicrobial agents. *Food Technol.* 40, 104–111.
- Liao, X.; Raghavan, G.S.V.; and Yaylayan, V.A. **2002**. A novel way to prepare n-butylparaben under microwave irradiation. *Tetrahedron Letters*, 43, 45–48.
- Loupy, A. **2004**. Solvent-free microwave organic synthesis as an efficient procedure for green chemistry. *Comptes Rendus Chimie* 7(2), 103-112.

Robach, M. C. **1980**. Use of preservatives to control micoroorganisms in food. *Food Technol.* 34, 81–84.

Soni, M. G., Burdock, G. A., Taylor, S. L., and Greenberg, N. A. **2001**. Safety assessment of propyl paraben: a review of the published literature. *Food and Chemical Toxicology*, 39(6), 513-532.

## CONNECTING STATEMENT 7

Chapters III-V showed the microwave-assisted extraction processes and Chapters VI - VIII showed the microwave-assisted synthesis process. As an always important factor, the power distribution of microwave need to be studied. In this chapter, an experimental method will be presented to determine the microwave power distribution in a domestic microwave oven.

Manuscript was prepared to be submitted to *Journal of Microwave Power and Electrical Energy*.

**Jianming Dai and G.S.Vijaya Raghavan. Visualization of Microwave Energy Distribution in a Multimode Microwave Cavity Using  $\text{CoCl}_2$  on Gypsum Plates. Prepared to be submitted to *Journal of Microwave Power and Electrical Energy*.**

Department of Bioresource Engineering, McGill University, 21,111 Lakeshore road, Ste-Anne-de-Bellevue, QC, H9X 3V9

Contributions made by different authors are as follows:

The first author, the Ph.D. student did the experimental work and prepared the manuscript under the supervision and guidance of the second author during the research work

## CHAPTER IX

### VISUALIZATION OF MICROWAVE ENERGY DISTRIBUTION IN A MULTIMODE MICROWAVE CAVITY USING $\text{CoCl}_2$ ON GYPSUM PLATES

#### 9.1. Abstract.

This chapter provides a facile method to map the microwave field distribution in a multimode microwave cavity. Anhydrous calcium sulfate powder was used to make the gypsum plate as the carrying medium. Cobalt chloride hexahydrate, whose color changes when losing part or all of its crystal waters, is selected as an indicator of the energy absorption. The cobalt chloride aqueous solution at a concentration of 1.6% was absorbed by the dried gypsum plate. After introducing the plate into a microwave field, those areas that receive more microwave energy will be heated resulting in the release of the moisture and consequently the loss of crystal water from cobalt chloride hexahydrate. The color change on the plate will form a color map indicating the microwave field distribution. This method was used in this study to investigate the energy distribution of a microwave oven by placing single or multiple plates in horizontal or vertical positions at different location.

**Keywords.** Microwave distribution, gypsum, calcium sulfate, cobalt chloride, visualization, mapping, power distribution, multimode cavity

#### 9.2. Introduction

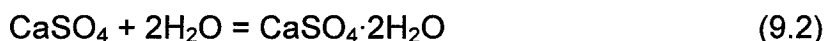
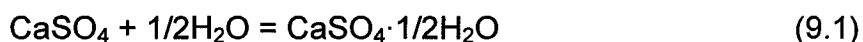
Despite the popularity and the intense attention microwave energy has been receiving from various fields, the non-uniformity of the energy distribution remains a problem in most applications. When dealing with food, the uneven energy distribution is believed to be responsible for the rubbery and soggy texture in the end product, unacceptable flavor development, insufficient microbiological destruction, and even safety hazard due to the overheating of the

center of infant formula bottles (Zhou et al., 1995; Ma et al., 1995). The localized overheating in the drying processes leads to the burning of the commodity. Therefore it is wise to know how microwave energy is distributed within the applicator and the commodity before the process is carried out.

Different methods could be used to visualize the energy distribution within an applicator. Thermal imaging is one of the most versatile tools to visualize the heating profile of a surface or a newly cut surface from a solid sample (Thompson et al., 1978; De Leo et al., 1991; van Remmen et al., 1996; Ryyne, 2002). But considering the price of the equipment, many other methods are also used. Iskander (1993) reported the use of a liquid crystal sheet in a multimode cavity to map the field distribution patterns of a multimode cavity. The price is still an important issue in using the liquid crystal. Thermal paper was also suggested by some researchers to be used to map the microwave distribution. However the thermal paper itself does not absorb microwave energy to produce a mark, an energy-absorbing plate must be used. Problems arise while selecting for an energy absorbing plate that makes good contact with the thermal paper while also transferring heat energy to that thermal paper in the exact distribution that the microwave energy was absorbed. In this paper a facile method was developed to map the field distribution in a commercial microwave oven.

### 9.3. Principle of the Method

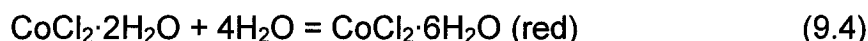
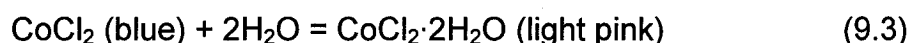
Anhydrous calcium sulfate is also called anhydrite, plaster of Paris, or drierite. It is used as a drying reagent or to make plaster cast, plaster model, some cement, and wallboard. Powder anhydrous sulfate, when in contact with water, undergoes two possible reactions depending on the amount of water available and temperature.



Dihydrate will be obtained if enough water is provided. Given enough water to make slurry from the powder and left it in a mold with a flat bottom, after

drying a porous plate of calcium sulfate dehydrates (gypsum) is formed. This porous gypsum plate has a hardness of about 2 and also has a strong ability to absorb water. The water absorbed can be released when subject to heat.

Cobalt chloride is used in silica gel drying reagents as a water indicator. The anhydrous cobalt chloride has a blue color. In the presence of water, two possible reactions happen depending on the amount of water:



These two reactions are reversible when subjected to heat, which means the red hexahydrate can lose four crystal waters to become the light pink dihydrate or further lose two crystal waters to form the blue anhydrate. This property is used in this study. The moisturized gypsum plate has a red color when cobalt chloride hexahydrate is added. When the plate is introduced into the microwave applicator, the parts that absorb microwave energy will increase in temperature. The two consequences of this rise in temperature are the loss of water from the gypsum plate and loss of crystal water from the cobalt sulfate hexahydrate to become either light pink dihydrate or blue anhydrate. The color map on the gypsum plate in return indicates the power distribution inside the cavity.

## **9.4. Material and Methods**

### **9.4.1. Gypsum plate preparation.**

Gypsum plates were prepared in two sizes i.e. 25 cm x 41 cm and 41cm square for the vertical and horizontal studies, respectively. Duck<sup>®</sup> tape (OH, USA) was attached around the glass pieces with the same size as the required gypsum plates to form a container. These containers were used as the mold for the gypsum plate. For the 25 cm x 41 cm plate, 150 g of powder anhydrous calcium sulfate (Fisher Scientific Co. Ltd., ON, Canada) and 125 mL of water

was added. After adequate stirring, the slurry was poured into the mold. The mold was shaken to allow the slurry evenly distributed over the bottom and then was left on a level for 48 hrs to allow the slurry to undergo the reaction and to dry. After being completely dried, the Duck<sup>®</sup> tape was removed from the mold and gypsum plate was easily detached from the glass plate. Cobalt chloride hexahydrate (Fisher Scientific Co. Ltd., ON, Canada) was prepared into an aqueous solution with a  $\text{CoCl}_2$  concentration of 1.6%. The dried porous gypsum plate together with the glass plate was dipped into the cobalt chloride solution to saturate the gypsum plate with the solution. Since the gypsum plate tends to be more fragile when saturated with water, the glass plate was used during the solution saturation process. After taking out the gypsum plate together with the glass plate from the solution, they were left in ambient conditions for 4 hrs to drain and also for part of the absorbed water to evaporate before subjecting it to microwave irradiation. For the 41cm x 41 cm plate, the procedure was the same and the amount of anhydrous calcium chloride was 250 g and water 200 mL. The thickness of both plates were about 1.5 mm.

#### 9.4.2. Experimental setup.

A commercial multimode microwave oven (Panasonic, 1.2 kW, oven dimension 47 cm x 27 cm x 47 cm) was used in this study. The magnetron of the microwave oven is mounted on the center of the right-hand side wall. The turn table was disabled throughout the experiment.

In order to study the microwave distribution at different locations using the gypsum plates, two different stands were designed to hold the plates both vertically and horizontally (Fig. 9.1 a, b). The stand was fabricated from acrylic plates that are almost transparent to microwave energy. In the vertical position, the same stand can be used so that the plates face the magnetron or are parallel to it because the bottom of the oven is a square. With the grooves on the stand, a single plate could be studied at locations from 4 cm to 36 cm (with an increment of 4 cm) to either magnetron or to the back wall of the microwave

oven. In the horizontal orientation, 5 positions are allowed from 5 cm to 25 cm (with an increment of 5 cm) from the bottom.

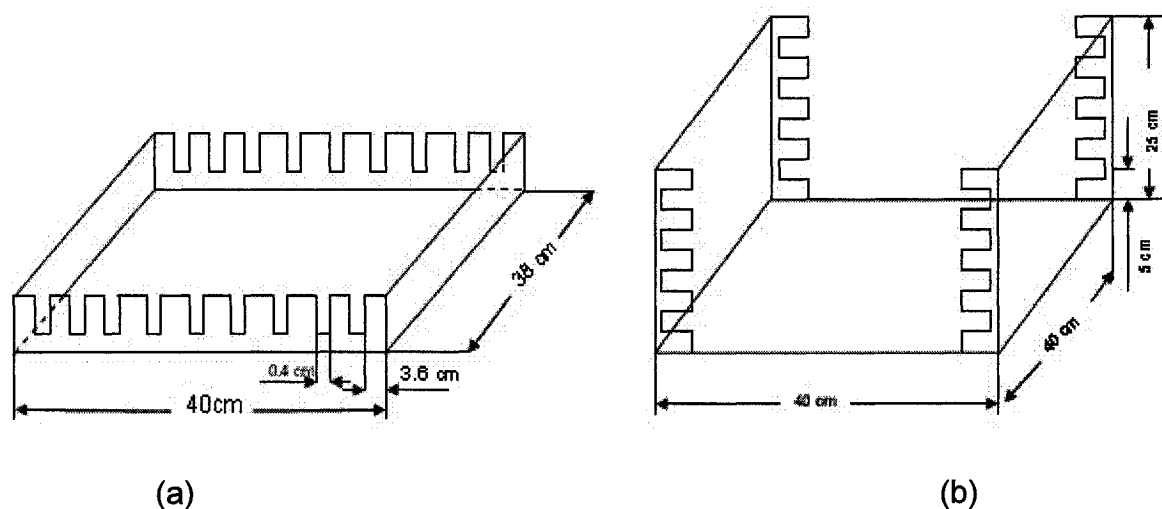


Fig. 9.1. The stands used for holding the plates at both vertical and horizontal positions. The stands were made from acrylic plate.

#### 9.4.3. Experimental procedure.

- 1). Single plate vertical orientation: A single gypsum plate with dimensions 25 cm x 41 cm with cobalt chloride solution absorbed was loaded onto the acrylic stand (Fig. 9.1 a) in one of the nine positions (4 cm to 36 cm with 4 cm increment). The stand was carefully loaded into the microwave cavity facing the magnetron. The microwave oven operated at full cycle for 3 minutes. After microwave irradiation, the plate was carefully taken out from the stand and a photo was taken with a digital camera (Nikon Coolpix 4300, 4.0 M pixels). The plate could then be reused by immersing it into the cobalt chloride solution for 2 hrs.
- 2). Multiple plate vertical orientation: Three plates were placed at positions 1, 5 and 9, which correspond to the distances of 4, 20, and 36 cm from the magnetron. The full cycle of microwave irradiation was applied for 9 minutes. A photo of the individual plate was taken after the treatment and the plates were regenerated.



- 3). Multiple plate vertical orientation: Three vertical size gypsum plates were placed on the stand at location 1, 5 and 9. The stand was loaded into the cavity in a way that the plates were perpendicular to the previous orientation. Full cycle of microwave irradiation was applied for 9 minutes and photos were taken for each individual plate.
- 4). Multiple plate horizontal orientation: 5 plates with size of 41 cm x 41 cm were loaded onto the stand for horizontal orientation (Fig. 9.1 b) at positions 1 to 5 corresponding to the distance of 5 to 25 cm from the bottom with 5 cm increments. The fully loaded stand was carefully placed into the cavity and the full cycle of microwave irradiation for 10 minutes was applied to the plates. After irradiation a photo was taken for each individual plate before they were regenerated.
- 5). A single plate in horizontal orientation at position 1 in comparison with the multiple plate horizontal orientation: A single plate of the horizontal size was placed on the stand at position 1 corresponding to the distance of 5 cm from the bottom of the cavity. After irradiation for 4 minutes, a photo was taken.
- 6). A single horizontally-oriented plate in a reflection free cavity: A reflection-free cavity was created by placing water absorbed cardboard on each of the cavity walls. A single horizontal size plate was placed on the stand at position 1 and then subjected to microwave irradiation at full cycle power and 10 minutes. Photo was taken for each individual plate before it is regenerated. This was repeated with the plate at position 3.

## **9.5. Results and Discussion**

The photos for the nine positions of the single plate vertical orientation are presented in Fig. 9.2. Location 1 corresponds to a distance of about 4 cm from the magnetron. At this distance, with the plate covering almost all of the vertical cross section of the cavity, the power the plate received is almost in the center of the plate corresponding to the position of the magnetron position. A small focus was also observed on the left side-hand side of the plate. Another 4 cm away, the major focus moved slight downward while the left-hand side spot

moved slightly upward but with higher intensity. In addition, two heating spots were located almost symmetrically on both sides of the center and a small spot was observed on the right bottom corner. Compared with position 1, the plate received higher total power from the cavity at this distance, as indicated by the presence of more blue spots and the pink color surrounding the spots. An additional 4 cm away produced a pattern on the plate that seems to be simplified again with three major spots, two on top and one on bottom, oriented symmetrically. This seems to be a bottom-up reversed pattern of location 8 which corresponds to 32 cm from the magnetron. It is interesting to note that location 4 is almost the repeat of location 1 except that location 4 received more power than location 1 as indicated by the pink color surrounding the major center spot. Location 4 corresponds to 16 cm to the magnetron and is 12 cm (1 full wavelength of 2450 MHz Microwaves) from location 1. Due to the complexity in reflection, these two locations are the only two with their patterns repeated among all the pairs having a distance of one wavelength. Location 5 only received a few small spots on the top edge, while the color of plate indicated that it is one of the plates that received the least amount of power. Location 6 showed an interesting pattern with three spots vertically aligned in the middle of the plate. Location 7 showed similar patterns to location 3 except the pattern at location 7 contained an extra intense spot on the top right corner and also consisted of a bottom spot that is much smaller and lighter than the pattern on location 3. Location 9 is the farthest from the magnetron, which is 8 cm from the opposite wall. It showed a symmetrical pattern on the two top corners.

The photos for multiple plates vertical orientated facing the magnetron are shown in Fig. 9. 3. Compared with the result from the single plate at location 1, the multiple plate one showed a similar pattern with microwave energy focused in the center of the plate. The difference between the two is due to the relatively longer irradiation time in the case of the loaded multiple plates. The small spot which is not shown well in the single one showed more clearly with more energy being supplied. The comparison of the location 5 in both single and multiple plates showed similar pattern on the top edge.

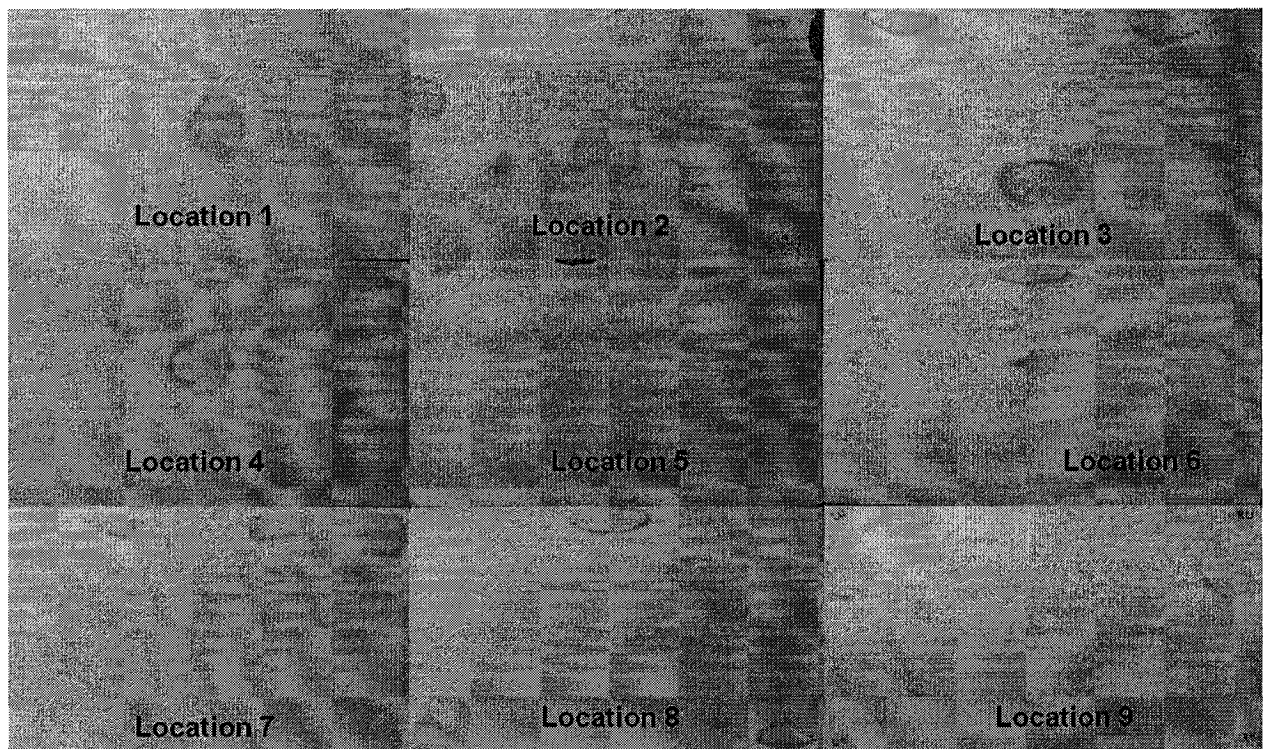


Fig. 9.2. Single plate vertical orientation facing the magnetron. Locations 1 through 9 corresponding to the distance to the magnetron from 4 to 36 cm with 4 cm increment.

Results for the vertically oriented multiple plate perpendicular to the previous orientation are presented in Fig. 9.4. Location 1 is the inner most one receiving energy on a few spots. Part of the formation was believed to be due to the reflection from the inner wall. Location 5 is in the center cross section of the magnetron. It received power only at the location close to the magnetron and two small spots on both top and bottom edge of the plate. Location 9 received more energy than the other locations. The energy comes from both direct energy dissipation and reflection from the door.

The photos for the five positions of the multiple-horizontal orientation are presented in Fig 9.5. Location 1 corresponds to a distance of 5cm from the bottom of the microwave cavity. At this distance, the plate shows six large areas, each of which is approximately 6cm from each other, or half the microwave wavelength at 2450 MHz. Location 2, which corresponds to a distance of 10cm

from the bottom of the microwave cavity, does not show much discoloration at all. However, location 3, which is 15cm from the bottom of the cavity, shows a spot at the upper-left position of the plate. This is probably due to reflections from the side walls of the oven. Location 4, which is 20cm from the bottom of the cavity, shows a spot to the upper right of the plate. This spot is probably due to reflections from the side walls of the oven. Location 5, which is 25cm from the bottom and 2cm from the top of the cavity, shows many spots towards the left side and the right side of the plate. This is likely due to the reflections from the top wall of the oven.

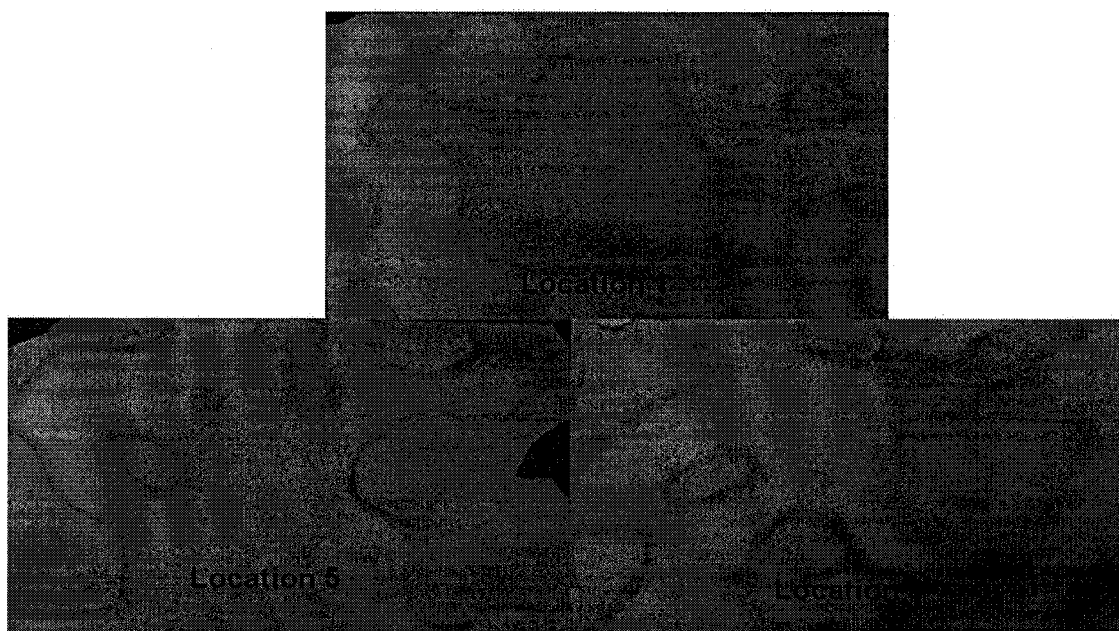


Fig. 9.3. Multiple plates vertically oriented facing the magnetron. Plates were loaded at locations 1, 5 and 9, corresponding to the distance to the magnetron of 4, 20, and 36 cm.

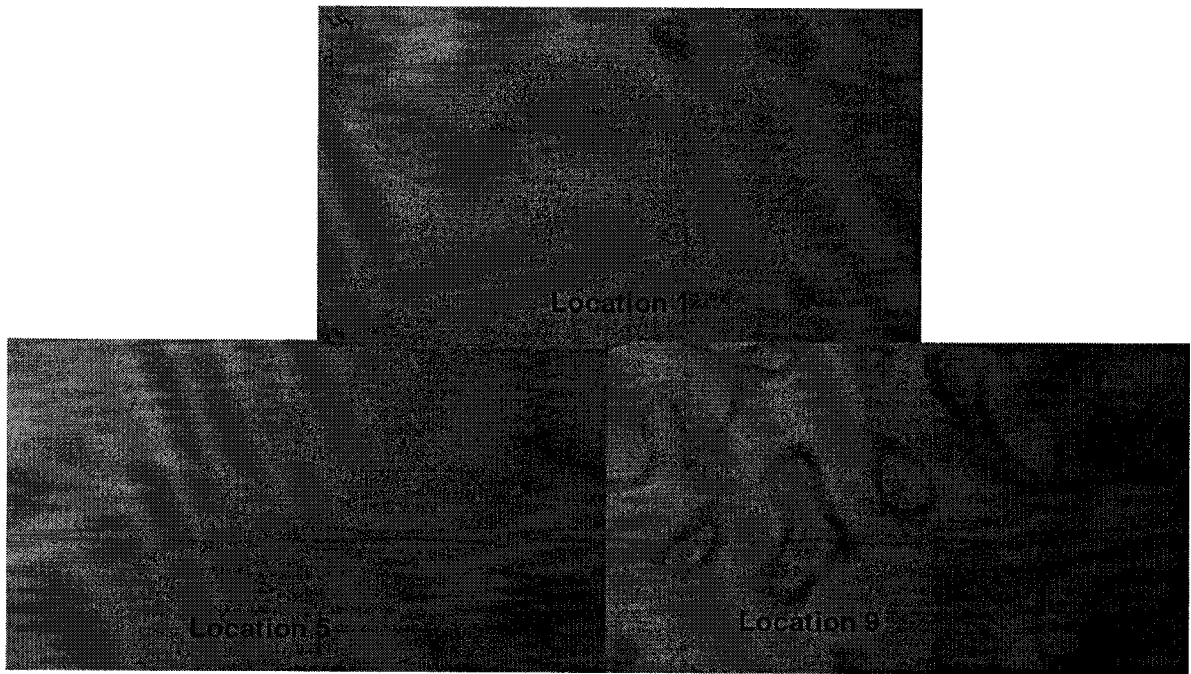


Fig. 9.4. Multiple plates vertically oriented parallel to the magnetron. Plates were loaded at locations 1, 5 and 9, corresponding to the distance to the back wall of 4, 20, and 36 cm.

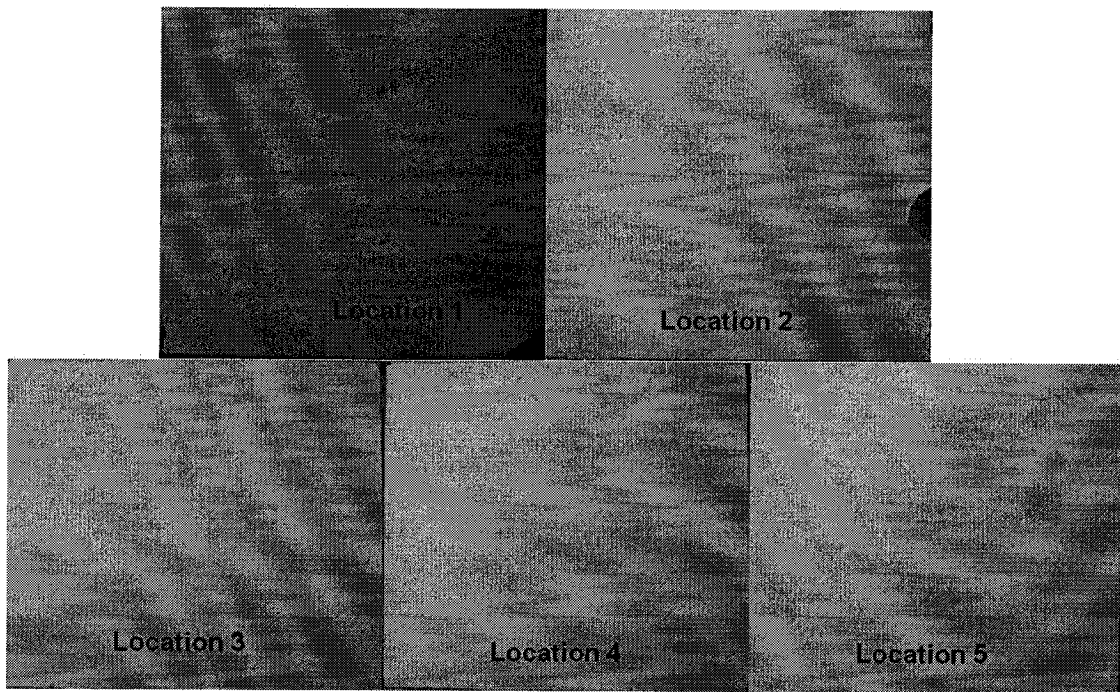


Fig. 9.5. Multiple-horizontal oriented loading. Locations 1 through 5 correspond to the distance to the bottom of the cavity of 5 to 25 cm with 5 cm increment.

In the five-horizontal oriented load, each of the middle plate receives microwave energy mostly from the magnetron directly and maybe a little portion from the side wall. Reflection from the top and bottom wall will be absorbed by the top and bottom plates. Therefore, each of the middle plate is almost equivalent to be subjected to a cavity with perfect absorbing boundaries. To verify if this is the case, a reflection free cavity is created by applying water absorbed cardboards on all the walls of the cavity. Microwaves that travel towards the walls will be absorbed by the cardboard. Even if it can not be absorbed completely, it will still reach the wall and be reflected back. The reflected energy will be absorbed again by the cardboard. After being absorbed twice, the contribution to the gypsum plate can be neglected. Location 1 and 3 are tested for reflection free cavity, and in comparison to the location 1 in the free cavity is also investigated.

The photos for a single plate in horizontal location 1 and for a single plate in horizontal location 1 or 3 enclosed in a reflection-free cavity are presented in Fig.9.6. In the reflection free cavity, the location 1 showed very close pattern as that in the multiple-horizontal oriented loading. The spots of white on the plate which is mixed with the blue coloration is probably due to condensation which resulted when the full cycle of the microwave ended and the door to the oven was opened. However location 1 in the normal cavity (Fig. 9.7) showed a completely different pattern from the same location in either reflection free cavity or multiple-horizontally loaded orientation. This suggests that the pattern on the location 1 in normal cavity is mainly produced by reflection from the cavity walls. On the plate in location 3, two spots were observed, one at the top middle and one at the top right. The one at the top middle was probably due to its closeness to the magnetron, while the one at the top right was probably due to heat given off by parts of the cardboard once it dried during the 10 minute cycle of the microwave. No heating pattern other than these two spots was observed which is in agreement with the one in multiple loaded orientations. This again suggests that the reflection free cavity created in this study could be a useful tool to study the energy distribution in a space without reflection.

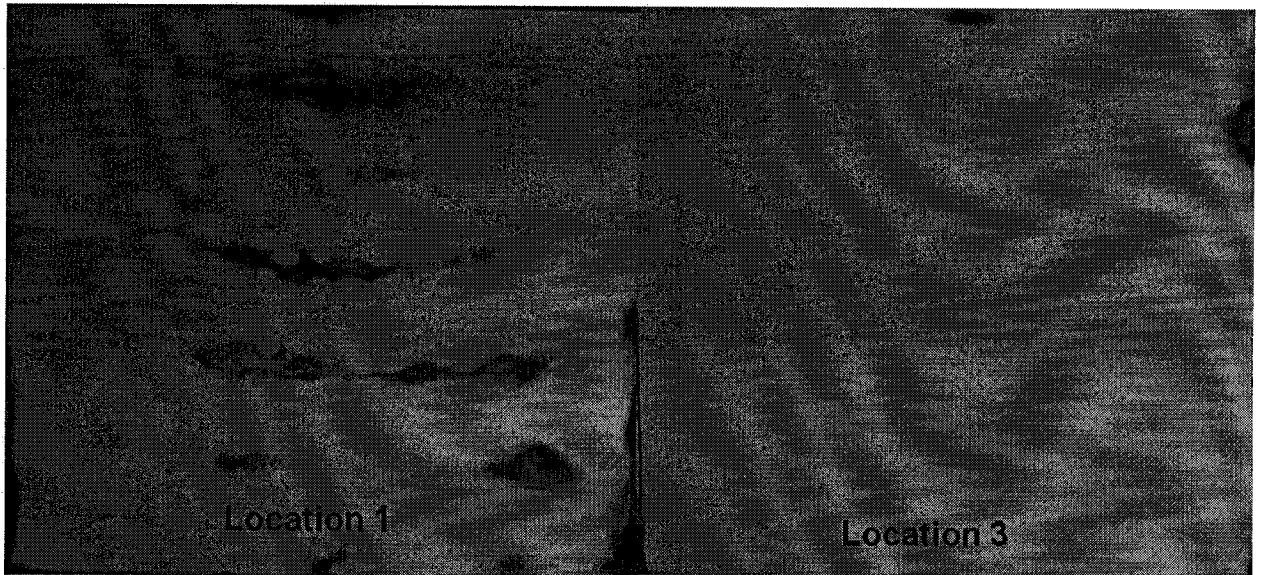


Fig. 9.6. Single plate horizontally oriented in a reflection free cavity. Locations 1 and 3 correspond to the distance of 5 and 15 cm from the bottom.

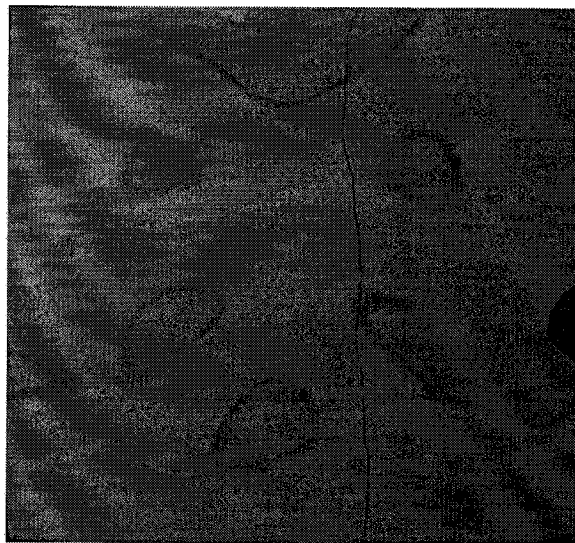


Fig. 9.7. Single plate horizontally oriented at location 1 corresponds to the 5 cm from the bottom of the cavity

### 9.6. Conclusions

Gypsum plate using cobalt chloride as indicator was proven to be able to map the microwave energy distribution in a multimode microwave cavity.



Although energy maps in various locations and different orientation were obtained, due to the complexity in microwave-matter interaction, reflection, and the existence of different modes, very few correlations of the energy distribution from different locations was collected. From this study, it is impossible to generalize the microwave distribution in a 3-D multimode microwave cavity. But the information on certain locations could be useful in arranging studies on food processing or drying in a multimode microwave cavity. The method could also be useful to verify the simulation results using numerical methods.

## **9.6 Acknowledgement**

The authors wish to acknowledge the Natural Science and Engineering Research Council of Canada (NSERC), FQRNT and Canadian International Development Agency (CIDA) for their financial support.

## **9.7. References**

- De Leo, R.; Cerri, G.; and Mariani P, V. 1991. TLM techniques in microwave ovens analysis: numerical and experimental results. *International Conference on computation in Electromagnetics*. Nov. 25-27. In proceeding page: 361 -364.
- Iskander, M.F. 1993. Computer Modeling and Numerical Simulation of Microwave Heating Systems. *MRS bulletin*. 18(11) 30-36.
- Ma L.H.; Paul, D.L.; and Potheary, N. 1995. Experimental validation of combined electromagnetic and thermal FDTD model of a microwave heating process. *IEEE transactions on microwave theory and techniques*. 43 (11) 2563-2572.
- Ryynane, S. 2002. Microwave heating uniformity of multicomponent prepared foods. Academic dissertation, University of Helsinki.
- Thompson, J.E.; Simpson, T.L.; Caulfield, J.B. 1978. Thermographic Tumor Detection Enhancement Using Microwave Heating. *IEEE Transactions on Microwave Theory and Techniques*. 26(8): 573 -580.



- Van Remmen, H. H. J.; Ponne, C.T.; Nijhuis, H.H.; Bartels, P.V.; and Kerkhof, P.J.A.M. 1996. Microwave heating distributions in slabs, sphere and cylinders with relation to food processing. *Journal of food science*. 61(6) 1105 – 1113.
- Zhou L.; Puri, V.M., Anantheswaran, R.C. and Yeh, G. 1995. Finite element modeling of heat and mass transfer in food materials during microwave heating – model development and validation. *Journal of food engineering*. 25, 509-529.

## CONNECTING STATEMENT 8

Chapter IX introduced an experimental method to determine the microwave power distribution in a domestic microwave oven. However, due to many restricting factors, it can not be used to determine the power distribution in a more complex system, especially when considering the scale-up of microwave-assisted extraction and synthesis equipment. A numerical solution will be more flexible in obtaining the power distribution information. More importantly, it could be used to assist in the design of the scaled-up equipments for the microwave-assisted extraction and synthesis processes. In this chapter, a simulation program developed in C programming language will be presented.

Manuscript was prepared to be submitted to *Journal of Microwave Power and Electrical Energy*.

**Jianming Dai and G.S.Vijaya Raghavan, FDTD simulation of microwave DISTRIBUTION and assist in the design of scaled-up Microwave-assisted extraction and synthesis equipment.**

Department of Bioresource Engineering, McGill University, 21,111 Lakeshore road, Ste-Anne-de-Bellevue, QC, H9X 3V9

Contributions made by different authors are as follows:

The first author, the Ph.D. student did the experimental work and prepared the manuscript under the supervision and guidance of the second author during the research work

## CHAPTER X

### FDTD SIMULATION OF MICROWAVE DISTRIBUTION AND ASSIST IN THE DESIGN OF SCALED-UP MICROWAVE-ASSISTED EXTRACTION AND SYNTHESIS EQUIPMENT

#### 10.1. Abstract

A FDTD based program written in C language is used in this chapter to simulate the E field and power dissipation in lossy dielectric media. The E field and power dissipation in a thin lossy dielectric plate placed in different locations of a domestic microwave oven was simulated. Simulation was verified with the experimental results. Good matching was observed for certain locations. But due to the complexity in terms of geometry and power entry port of the domestic microwave oven, not all of the simulated results match the experimental ones. This program is used to assist in the design of microwave-assisted chemical reactor/extractor. A cylindrical reactor with multiple magnetron placed vertically was more practical than the oven type of reactor/extractor. This program is also capable of analyzing the power dissipation in different layers of a chemical reactor/extractor.

#### 10.2. Introduction

Microwaves haven been intensively investigated for their application in various chemical processes including organic synthesis and extraction processes since the 1980s. Many of the laboratory studies have suggested that microwaves have a lot of advantages over conventional methods, including increase in extraction recovery or synthesis yield, greatly shorten process time, reduce energy and solvent usage (Gedye, et al., 1986; Ganzler, et al., 1986; Mattina, et al., 1997; Gao, 1997; Seifert, et al. 2000; Hao, et al. 2000; Pan, et al., 2000; Liu, et al. 2000; Pare and Belanger, 1994, 1997; Huang, et al. 2000; Pan, et al. 2000; Li and Jin, 2000; Lee, et al. 2000 ). However, most of the applications are limited to laboratory. In order to apply the microwaves in the industries, a few problems

have to be considered, like the power distribution and penetration depth of the microwave power.

Two basic types of methods are used for the simulation of energy distribution in a multimode cavity, i.e. using the Lambert's Law and solving the Maxwell equation. Both methods have been successfully applied in their corresponding problem solving situation (van Remmen, et al., 1996; Nykvist and Decareau, 1976; Fu and Metaxas, 1994; Harms, et al. 1996; Meredith, 1994; Zhou, et al. 1995; Ma, et al., 1995; Sullivan, 2000). Lambert's law deals with the one dimensional penetration of microwave power into materials. It is a very simple approach for simulation of the energy distribution. It is applicable only when the sample can be regarded as infinite in thickness, therefore it has very limited applications. In order to get a more accurate simulation for a more complex problem, or to get the energy distribution in a multimode cavity, solving Maxwell's equation provide a better solution. Finite element and Finite Difference Time Domain (FDTD) are two commonly used methods for solving Maxwell's equation to get the energy distribution in a complex object or within a multimode cavity and both methods are capable of simulating power density distribution in 3-D (Fu and Metaxas, 1994; Harms, et al. 1996; Meredith, 1994; Zhou, et al. 1995; Ma, et al., 1995). The finite element method is suitable for arbitrarily shaped inhomogeneous objects and this method requires the solution of a sparse matrix which may be very complicated. While FDTD is a very straight forward method that can readily model inhomogeneous and anisotropic materials as well as arbitrarily shaped geometries; it can also provide both time and frequency domain analyses which are important to microwave heating problems like field distribution, scattering parameters and dissipated power distribution for various materials and geometries (Harms, et al., 1996; Mittra and Harms, 1993).

### **10.3. The Model**

#### **10.3.1. Maxwell's equations**

Time-dependent Maxwell's equations are:

$$\varepsilon_0 \varepsilon' \frac{\partial E}{\partial t} = \nabla \times H - J \quad (10.1)$$

$$\mu_0 \mu' \frac{\partial H}{\partial t} = \nabla \times E \quad (10.2)$$

Where  $E$  and  $H$  are vectors in three dimensions.  $\varepsilon_0$  is the dielectric constant in free space and  $\varepsilon'$  is the relative dielectric constant of dielectric material.  $\mu_0$  is the magnetic permittivity of free space and  $\mu'$  is the relative magnetic permittivity of magnetic material. The study here deals with non-magnetic material and  $\mu'$  is 1.  $J$  is the current density and can be written as:

$$J = \sigma \cdot E \quad (10.3)$$

Where  $\sigma$  is the effective conductivity. For dielectric material without ion conduction, the effective conductivity can be written as:

$$\sigma = \varepsilon'' \varepsilon_0 \omega \quad (10.4)$$

Where  $\varepsilon''$  is the dielectric loss factor of dielectric materials and  $\omega$  is the angular speed of light and:

$$\omega = 2\pi f \quad (10.5)$$

Where  $f$  is the microwave frequency. Equations 10.1 and 10.2 can be rewritten as:

$$\frac{\partial E}{\partial t} = \frac{1}{\varepsilon_0 \varepsilon'} \nabla \times H - \frac{2\pi f \varepsilon''}{\varepsilon'} E \quad (10.6)$$

$$\frac{\partial H}{\partial t} = \frac{1}{\mu_0 \mu'} \nabla \times E \quad (10.7)$$

From equations 10.6 and 10.7, six scalar equations can be written as:

$$\frac{\partial E_x}{\partial t} = \frac{1}{\epsilon_0 \epsilon'} \left( \frac{\partial H_z}{\partial y} - \frac{\partial H_y}{\partial z} \right) - \frac{2\pi f \epsilon''}{\epsilon'} E_x \quad (10.8)$$

$$\frac{\partial E_y}{\partial t} = \frac{1}{\epsilon_0 \epsilon'} \left( \frac{\partial H_x}{\partial z} - \frac{\partial H_z}{\partial x} \right) - \frac{2\pi f \epsilon''}{\epsilon'} E_y \quad (10.9)$$

$$\frac{\partial E_z}{\partial t} = \frac{1}{\epsilon_0 \epsilon'} \left( \frac{\partial H_y}{\partial x} - \frac{\partial H_x}{\partial y} \right) - \frac{2\pi f \epsilon''}{\epsilon'} E_z \quad (10.10)$$

$$\frac{\partial H_x}{\partial t} = \frac{1}{\mu_0} \left( \frac{\partial E_y}{\partial z} - \frac{\partial E_z}{\partial y} \right) \quad (10.11)$$

$$\frac{\partial H_y}{\partial t} = \frac{1}{\mu_0} \left( \frac{\partial E_z}{\partial x} - \frac{\partial E_x}{\partial z} \right) \quad (10.12)$$

$$\frac{\partial H_z}{\partial t} = \frac{1}{\mu_0} \left( \frac{\partial E_x}{\partial y} - \frac{\partial E_y}{\partial x} \right) \quad (10.13)$$

### 10.3.2. The Yee scheme

One of the most popular approaches to approximate the E and H field and the relationship between E and H field were described by the Yee scheme as shown in Fig. 10.1 (Yee, 1996).

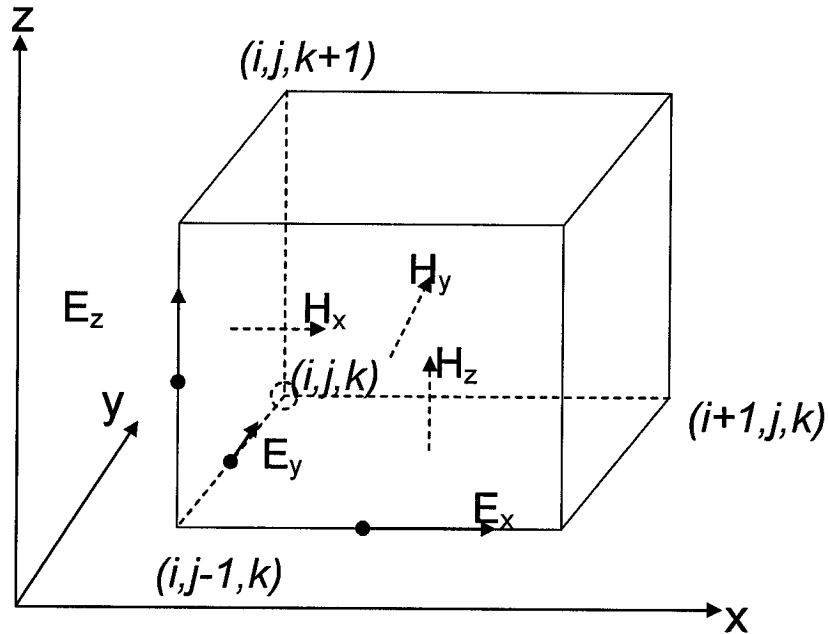


Fig. 10.1. The Yee cell that shows the relative location of E and H field in 3D

### 10.3.3 Finite difference approximation and implementation in C language

The central-difference approximations of the E and H can therefore be written as:

$$\begin{aligned} \frac{E_x^{n+1/2}(i+1/2, j, k) - E_x^{n-1/2}(i+1/2, j, k)}{\Delta t} &= \frac{1}{\epsilon_0 \epsilon'} \left( \frac{H_z^n(i+1/2, j+1/2, k) - H_z^n(i+1/2, j-1/2, k)}{\Delta y} \right. \\ &\quad \left. - \frac{H_y^n(i+1/2, j, k+1/2) - H_y^n(i+1/2, j, k-1/2)}{\Delta z} - \frac{2\pi f \epsilon''}{\epsilon'} \left( \frac{E_x^{n+1/2}(i+1/2, j, k) + E_x^{n-1/2}(i+1/2, j, k)}{2} \right) \right) \end{aligned} \quad (10.14)$$

$$\begin{aligned} \frac{E_y^{n+1/2}(i, j+1/2, k) - E_y^{n-1/2}(i, j+1/2, k)}{\Delta t} &= \frac{1}{\epsilon_0 \epsilon'} \left( \frac{H_x^n(i, j+1/2, k+1/2) - H_x^n(i, j+1/2, k-1/2)}{\Delta z} \right. \\ &\quad \left. - \frac{H_z^n(i+1/2, j+1/2, k) - H_z^n(i-1/2, j+1/2, k)}{\Delta x} - \frac{2\pi f \epsilon''}{\epsilon'} \left( \frac{E_y^{n+1/2}(i, j+1/2, k) + E_y^{n-1/2}(i, j+1/2, k)}{2} \right) \right) \end{aligned} \quad (10.15)$$

$$\begin{aligned} \frac{E_z^{n+1/2}(i, j, k+1/2) - E_z^{n-1/2}(i, j, k+1/2)}{\Delta t} &= \frac{1}{\epsilon_0 \epsilon'} \left( \frac{H_y^n(i+1/2, j, k+1/2) - H_y^n(i-1/2, j, k+1/2)}{\Delta x} \right. \\ &\quad \left. - \frac{H_x^n(i, j+1/2, k+1/2) - H_x^n(i, j-1/2, k+1/2)}{\Delta y} - \frac{2\pi f \epsilon''}{\epsilon'} \left( \frac{E_z^{n+1/2}(i, j, k+1/2) + E_z^{n-1/2}(i, j, k+1/2)}{2} \right) \right) \end{aligned} \quad (10.16)$$

$$\begin{aligned} \frac{H_x^{n+1}(i, j+1/2, k+1/2) - H_x^n(i, j+1/2, k+1/2)}{\Delta t} &= \frac{1}{\mu_0} \left( \frac{E_y^{n+1/2}(i+1/2, j, k+1) - E_y^{n+1/2}(i+1/2, j, k)}{\Delta z} \right. \\ &\quad \left. - \frac{E_z^{n+1/2}(i+1/2, j+1, k) - E_z^{n+1/2}(i+1/2, j, k)}{\Delta y} \right) \end{aligned} \quad (10.17)$$

$$\begin{aligned} \frac{H_y^{n+1}(i+1/2, j, k+1/2) - H_y^n(i+1/2, j, k+1/2)}{\Delta t} &= \frac{1}{\mu_0} \left( \frac{E_z^{n+1/2}(i+1, j+1/2, k) - E_z^{n+1/2}(i, j+1/2, k)}{\Delta x} \right. \\ &\quad \left. - \frac{E_x^{n+1/2}(i, j+1/2, k+1) - E_x^{n+1/2}(i, j+1/2, k)}{\Delta z} \right) \end{aligned} \quad (10.18)$$

$$\frac{H_z^{n+1}(i+1/2, j+1/2, k) - H_z^n(i+1/2, j+1/2, k)}{\Delta t} = \frac{1}{\mu_0} \left( \frac{E_x^{n+1/2}(i, j+1, k+1/2) - E_x^{n+1/2}(i, j, k+1/2)}{\Delta y} - \frac{E_y^{n+1/2}(i+1, j, k+1/2) - E_y^{n+1/2}(i, j, k+1/2)}{\Delta x} \right) \quad (10.19)$$

Where n is the time notation, i, j, k are the x, y, z indices of the Cartesian coordinate,  $\Delta t$  is the time step and  $\Delta x, \Delta y, \Delta z$  are the cell dimension in x, y, z directions.

Rearrangement of Equations 10.14 and 10.17 to obtain:

$$E_x^{n+1/2}(i+1/2, j, k) = \left( \frac{\epsilon' - \eta \epsilon'' \Delta t}{\epsilon' + \eta \epsilon'' \Delta t} \right) E_x^{n-1/2}(i+1/2, j, k) + \frac{\Delta t}{(\epsilon' + \eta \epsilon'' \Delta t) \epsilon_0 \Delta y} (H_z^n(i+1/2, j+1/2, k) - H_z^n(i+1/2, j-1/2, k)) - \frac{\Delta t}{(\epsilon' + \eta \epsilon'' \Delta t) \epsilon_0 \Delta z} (H_y^n(i+1/2, j, k+1/2) - H_y^n(i+1/2, j, k-1/2)) \quad (10.20)$$

$$H_x^{n+1}(i, j+1/2, k+1/2) = H_x^n(i, j+1/2, k+1/2) + \frac{\Delta t}{\mu_0 \Delta z} (E_y^{n+1/2}(i+1/2, j, k+1) - E_y^{n+1/2}(i+1/2, j, k)) - \frac{\Delta t}{\mu_0 \Delta y} (E_z^{n+1/2}(i+1/2, j+1, k) - E_z^{n+1/2}(i+1/2, j, k)) \quad (10.21)$$

The rest of the E and H field can be rearranged in a similar way so that it can be expressed using the C language code. Using the C language programming, equations 10.14 to 10.19 can be expressed as:

$$ex[i][j][k] = ca * ex[i][j][k] + (cb / \Delta y) * (hz[i][j][k] - hz[i][j-1][k]) - (cb / \Delta z) * (hy[i][j][k] - hy[i][j][k-1]) \quad (10.22)$$

$$ey[i][j][k] = ca * ey[i][j][k] + (cb / \Delta z) * (hx[i][j][k] - hx[i][j][k-1]) - (cb / \Delta x) * (hz[i][j][k] - hz[i-1][j][k]) \quad (10.23)$$

$$ez[i][j][k] = ca * ez[i][j][k] + (cb / \Delta x) * (hy[i][j][k] - hy[i-1][j][k]) - (cb / \Delta y) * (hx[i][j][k] - hx[i][j-1][k]) \quad (10.24)$$



$$\begin{aligned} hx[i][j][k] = & hx[i][j][k] + (ch/dz) * (ey[i][j][k+1] - ey[i][j][k]) \\ & + (ch/dy) * (ez[i][j+1][k] - ez[i][j][k]) \end{aligned} \quad (10.25)$$

$$\begin{aligned} hy[i][j][k] = & hy[i][j][k] + (ch/dx) * (ez[i+1][j][k] - ez[i][j][k]) \\ & + (ch/dz) * (ex[i][j][k+1] - ex[i][j][k]) \end{aligned} \quad (10.26)$$

$$\begin{aligned} hz[i][j][k] = & hz[i][j][k] + (ch/dy) * (ex[i][j+1][k] - ex[i][j][k]) \\ & + (ch/dx) * (ey[i+1][j][k] - ey[i][j][k]) \end{aligned} \quad (10.27)$$

Where:

$$ca = \frac{\varepsilon' - \pi f \varepsilon'' \Delta t}{\varepsilon' + \pi f \varepsilon'' \Delta t}$$

$$cb = \frac{\Delta t}{\varepsilon_0 (\varepsilon' + \pi f \varepsilon'' \Delta t)}$$

$$ch = \Delta t / \mu_0$$

#### 10.3.4. The stability Criteria

In order for the simulation to be stable, the time step selection has to meet a certain criteria with respect to the spatial discretization  $x$ ,  $y$  and  $z$ . One of the most commonly used criteria is Courant-Friedrichs-Lewy Stability (CFL) criteria:

$$\Delta t \leq \frac{1}{C_0 \sqrt{\frac{1}{\Delta x^2} + \frac{1}{\Delta y^2} + \frac{1}{\Delta z^2}}} \quad (10.28)$$

Where  $C_0$  is the light speed in free space.

During the simulation,  $\Delta t$  is set to be  $\frac{1}{C_0 \sqrt{\frac{1}{\Delta x^2} + \frac{1}{\Delta y^2} + \frac{1}{\Delta z^2}}}$ .

### 10.3.5. Boundary conditions

For the simulation of a multimode cavity, a perfect electrical conductor (PEC) boundary condition can be used. The PEC boundary condition requires the tangential E field to be zero at the boundary. The implementation of the PEC during this simulation is to set all the E field components to zero on the boundaries:

$$E_x = E_y = E_z = 0 \quad (10.29)$$

### 10.3.6. Dielectric properties of the object simulated

The simulation applies to the whole range of cavity, including the load and the empty part which have different dielectric properties. Therefore the introduction of the dielectric properties, i.e. dielectric constant ( $\epsilon'$ ) and loss factor ( $\epsilon''$ ) can not be through simple initiation unless the space has no load or has uniform load throughout the space simulated. 3-D arrays corresponding to the Cartesian mesh can be used to specify the dielectric properties of each cell. In equations 10.22-10.24, the two constants  $ca$  and  $cb$  are a function of  $\epsilon'$  and  $\epsilon''$  which can be expressed in 3-D array as:

$$ca[i][j][k] = \frac{\epsilon'[i][j][k] - \pi f \Delta t * \epsilon''[i][j][k]}{\epsilon'[i][j][k] + \pi f \Delta t * \epsilon''[i][j][k]} \quad (10.30)$$

$$cb[i][j][k] = \frac{\Delta t}{\epsilon_0 (\epsilon'[i][j][k] + \pi f \Delta t * \epsilon''[i][j][k])} \quad (10.31)$$

Therefore, equations 10.22-10.24 can be rewritten as:

$$\leftarrow \begin{aligned} ex[i][j][k] = & ca[i][j][k] * ex[i][j][k] + (cb[i][j][k] / \Delta y) * (hz[i][j][k] - hz[i][j-1][k]) \\ & - (cb[i][j][k] / \Delta z) * (hy[i][j][k] - hy[i][j][k-1]) \end{aligned} \quad (10.32)$$

$$\begin{aligned} ey[i][j][k] = & ca[i][j][k] * ey[i][j][k] + (cb[i][j][k] / \Delta z) * (hx[i][j][k] - hx[i][j][k-1]) \\ & - (cb[i][j][k] / \Delta x) * (hz[i][j][k] - hz[i-1][j][k]) \end{aligned} \quad (10.33)$$

$$\begin{aligned} ez[i][j][k] = & ca[i][j][k] * ez[i][j][k] + (cb[i][j][k] / \Delta x) * (hy[i][j][k] - hy[i-1][j][k]) \\ & - (cb[i][j][k] / \Delta y) * (hx[i][j][k] - hx[i][j-1][k]) \end{aligned} \quad (10.34)$$

### 10.3.7. Power dissipation

Power absorption by the lossy dielectric material can be calculated by:

$$P_{abs} = 2\pi f \epsilon_0 \epsilon'' |E|^2 V \quad (10.35)$$

In the simulation space, the E field distribution can be obtained through the simulation. Since the E field is not uniform throughout the simulation space of interest and it also changes with time, only one cell at certain simulation steps can be expressed with the equation 10.35 and can be rewritten as:

$$\begin{aligned} P_{abs}[i][j][k] &= 2\pi f \epsilon_0 \epsilon'' |E[i][j][k]|^2 dV \\ &= 2\pi f \epsilon_0 \epsilon'' |E[i][j][k]|^2 \Delta x \Delta y \Delta z \end{aligned} \quad (10.36)$$

Where  $dV$  is the volume of one cell.

Therefore the energy dissipated in a certain cell can be written as:

$$\begin{aligned} Q[i][j][k] &= \sum_{t=0}^{n\Delta t} P_{abs}^t[i][j][k] * \Delta t \\ &= \sum_{t=0}^{n\Delta t} 2\pi f \epsilon_0 \epsilon'' \Delta t |E^t[i][j][k]|^2 \Delta x \Delta y \Delta z \end{aligned} \quad (10.37)$$

To simplify the simulation, we assume that there is no heat exchange between cells. The total energy accumulated in a certain cell is equal to  $Q[i][j][k]$  and similar to the E field, we can obtain the energy accumulation and distribution during the microwave heating.

During the simulation, each timestep is about  $9.3 \times 10^{-12}$  s, therefore even after one run of 3000 iterations, the total simulated time is only  $2.8 \times 10^{-8}$  s. To simplify the presentation, we scale the time to 1 s of heating by multiplying the total dissipated energy by  $3.578 \times 10^7$ . After this manipulation, the obtained power dissipation for each cell has a unit of Joule per second of heating corresponding to a power dissipation rate in W.

### 10.3.8 Power source

In the simulation of multimode cavity, energy is supplied to the cavity through a rectangular waveguide where the TE<sub>10</sub> mode is the dominant mode. A sinusoidal plane wave was proved to be efficient in this type of simulation (Ma, et al., 1995).

$$Stimulus = k * \sin(2\pi f * currentsimulationtime) \quad (10.38)$$

Where:

k is the magnitude of the stimulus to be determined

*currentsimulationtime* is equal to current iteration multiply by the timestep.

The power transmitted to the cavity can be reflected by assigning a proper *k*. However, it is hard to directly connect the E field magnitude with the Power input. One approach to determine the magnitude of the sinusoidal wave is similar to the measurement of microwave power. The procedure is to assign a relatively high loss factor value to the whole space of the microwave cavity. As a result, the power entering the cavity will be absorbed very quickly. First initialize *k* to be 1. By adding up the dissipated power of each individual cell throughout the microwave cavity, the total dissipated power can be obtained ( $P_{simulation1}$ ). Compare the value with the targeted magnetron output power ( $P_{out}$ ):

$$R_1 = P_{out} / P_{simulation1} \quad (10.39)$$

From Equation 10.35 and 10.36, it can be seen that the power dissipation is proportional to the square of E value. Therefore,  $\sqrt{R_1}$  can be assigned to *k* so that:

$$Stimulus = \sqrt{R_1} * \sin(2\pi f * currentsimulationtime) \quad (10.40)$$

Use this updated formula to the simulation again to get a second total dissipated power value ( $P_{simulation2}$ ) and compare with the  $P_{out}$  again to obtain another correction coefficient. After this two step operation, the simulated power can be very close to the target output power.

The stimulus for the domestic microwave oven with power entry port occupying 153 cells after 3000 iterations was determined to be through this operation:

$$Stimulus = 2.92 * \sin(2\pi f * currentsimulationtime) \quad (10.41)$$

#### 10.3.9. Programming using C language

The simulation is programmed using C language and compiled using Microsoft Visual C++ software. The flow chart for the programming is shown in Chart 10.1. Part of the original source code is shown in Appendix 1.

After the simulation, data files for the E field and accumulated energy dissipation at different time steps were obtained. Matlab software is used to visualize the E field distribution and the accumulated energy dissipation throughout the cavity at different locations of X, Y, or Z direction. But before the programming in Matlab, the 2-D data has to be obtained using the 3-D data at certain time steps. This is realized by writing a C code and compiling in Microsoft Visual C++ software. The flow chart is shown in chart 10.2 and part of the C language code is attached at Appendix 2. Part of the code for matlab visualization is shown in Appendix 3.

### 10.4 Simulation of a domestic microwave oven

The Panasonic domestic microwave oven was simulated with the previously described FDTD algorithm programmed in C language. The microwave oven uses inverter technology having 10 real power levels with total power of 1 kW and 10% interval between each level. As shown in Fig. 10.2, the dimension of the microwave oven cavity is: 47cm (L) x 47 cm (W) x 27 cm (H).

Microwave was guided to the oven through a port with dimension: 8.6cm x 4.3 cm located in the center of the right hand side wall. The 3-D meshing in Cartesian system is shown in Fig. 10.3. The whole oven has a grid size of 97x97x56. The power entry is located at the center of right hand xy plane with the grid size of 1x18x9. A continuous sinusoidal wave is applied through the power entry port to the oven cavity.

#### 10.4.1 Power distribution with a lossy dielectric plate inserted in the cavity

A lossy dielectric plate with dielectric constant ( $\epsilon'$ ) of 20 and loss factor ( $\epsilon''$ ) of 5 was placed in the cavity. The dimension of the plate depends on how it is located in the oven. It is defined using the number of cells in each direction. For horizontal placement, the dimension is: 97 x 97 x 1 cell corresponding to approximately 47 x 47 x 0.5 cm; and for vertical placement, the dimension is 97 x 56 x 1 cell corresponding to 47 x 27 x 0.5 cm. The thickness of the plate is one cell. Nine locations as illustrated in Fig. 10.4. were selected: three horizontal, three vertical facing the power entry port and three parallel to the power entry port.

The power dissipation into the lossy dielectric plate is presented Fig. 10.5 (3D view) and Fig. 10.6 (2D view). The scales of the figures represent the power dissipation within one cell over a period of 1 s. This corresponds to the power dissipation rate in the unit of W. The total power dissipated in whole plate can be calculated by adding up the energy absorption of each cell of the plate.

Similar pattern can be observed for two pairs of plates: horizontal locations H-1 and H-3; vertical locations parallel to the power entry port V-P-1 and V-P-3. H-1/H-3 and V-P-1/V-P-3 are in the symmetrical locations with respect to the power entry port and the power entry port is located exactly at the center of the incident wall of the cavity. Therefore locations within the cavity symmetrical to the power entry port should have similar power absorption pattern. Evidence can be found from all the three vertical locations facing power entry port and V-P-2 and H-2. All of them are self symmetrically located with respect to the power entry port.

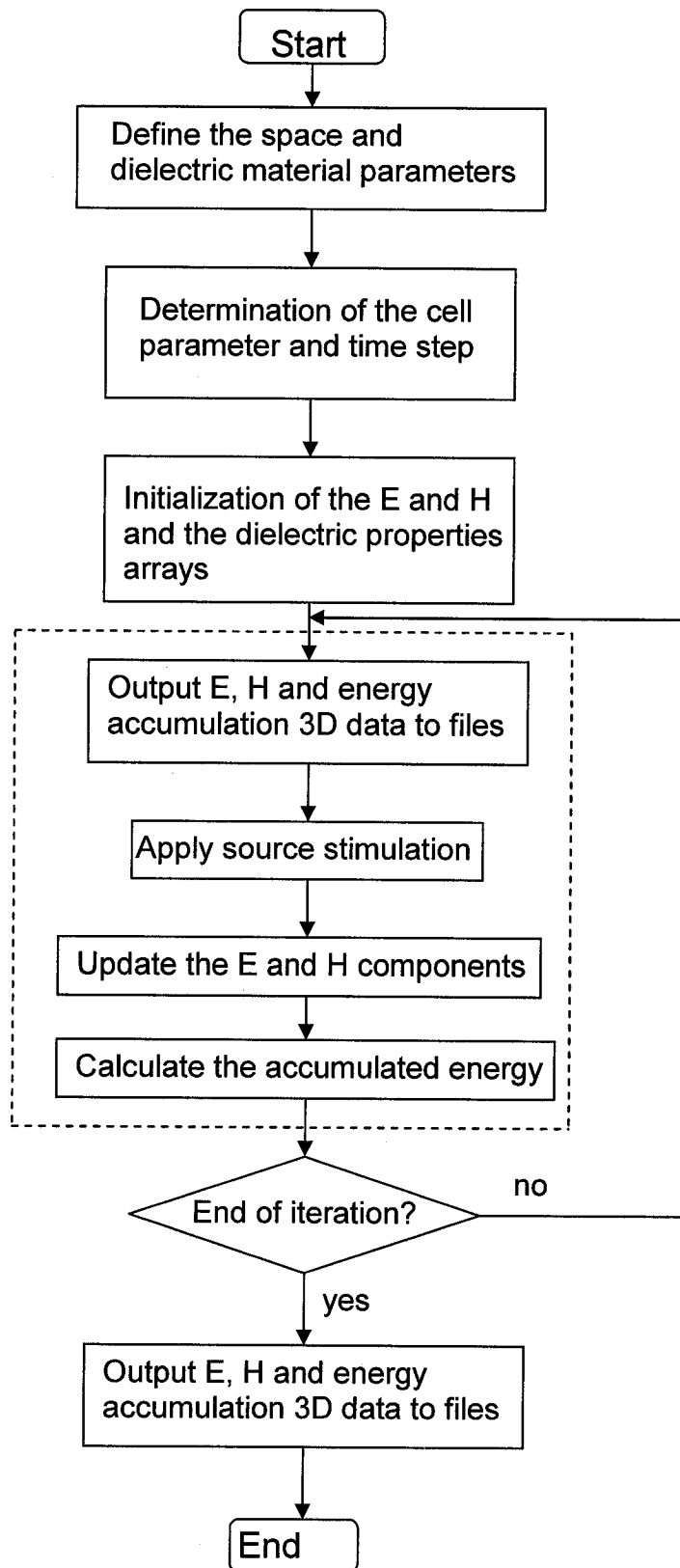


Chart 10.1. Flow chart of the programming in C language

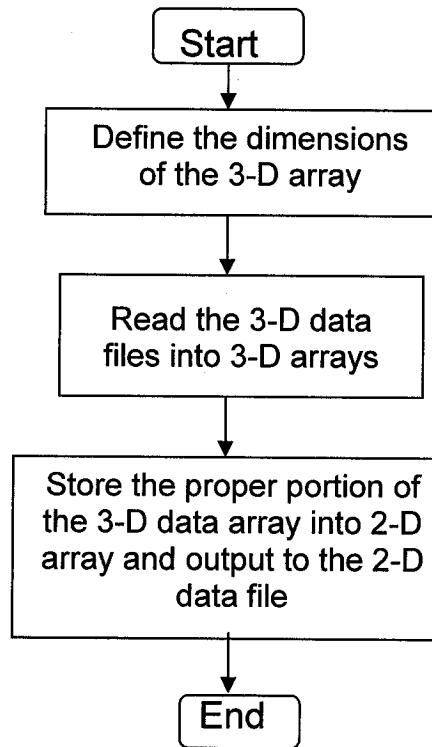


Chart 10.2. Flow chart for the C program in sectioning the 3-D array in X, Y, or Z direction to obtain 2-D arrays.



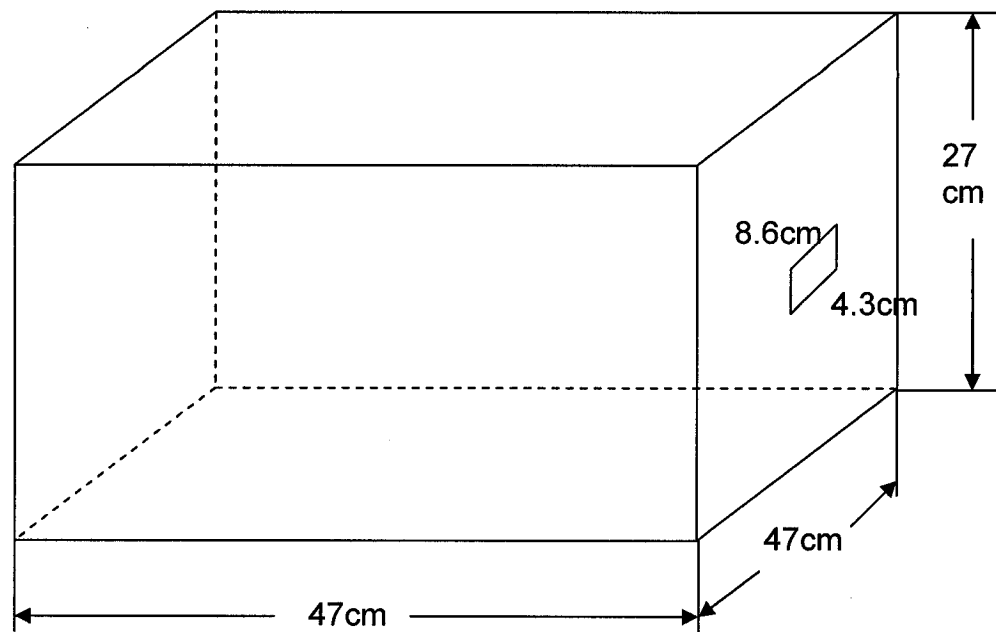


Fig. 10.2. The dimension of the microwave cavity simulated and the location of microwave entry port

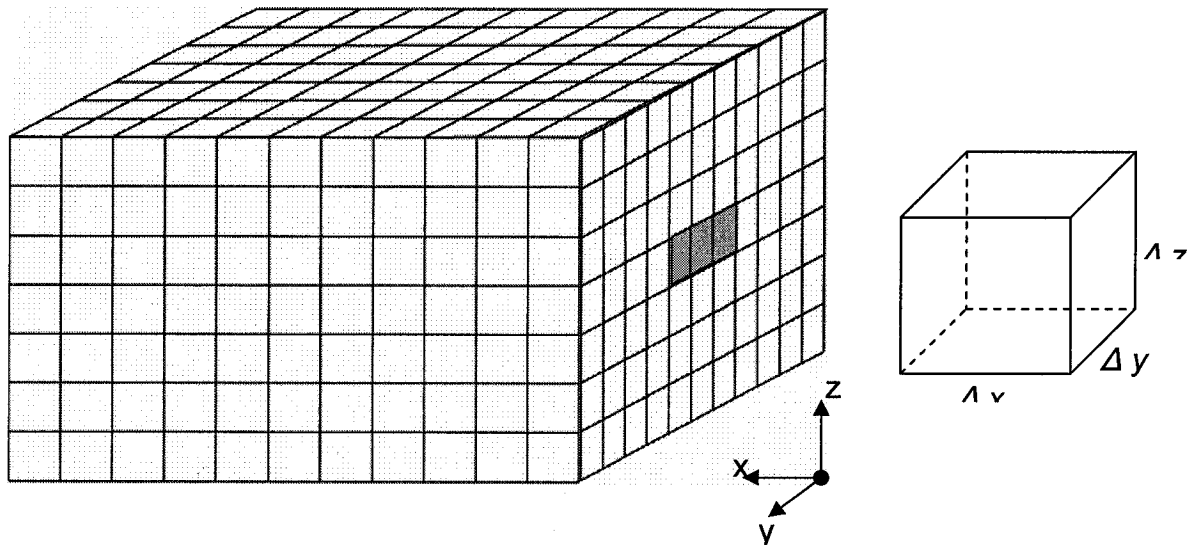


Fig. 10.3. The Cartesian 3-D meshing of the microwave oven. The number of grids is:  $97 \times 97 \times 56$ , the size of the cell is:  $4.845 \times 4.845 \times 4.821$  mm. The power entry is  $1 \times 18 \times 9$ .

The total power dissipation into the lossy dielectric plate at different locations is presented in Table 10.1. It can be seen that for all different locations, only a small portion of the power is dissipated into the lossy dielectric plate. And the total dissipated power into the plate varies from location to location. For the symmetrical locations, even the patterns were similar, the dissipated power varies slightly. Among all the locations, the highest power absorption was observed at V-P-2. Very strong absorption was observed near the power entry port. The dielectric properties also affect the power dissipation into the plate as shown in Table 10.1 in the case of H-3. With very high dielectric constant and loss factor, the power dissipation reduced greatly. However, higher power dissipation was achieved by increasing the loss factor alone while maintaining the same dielectric constant.

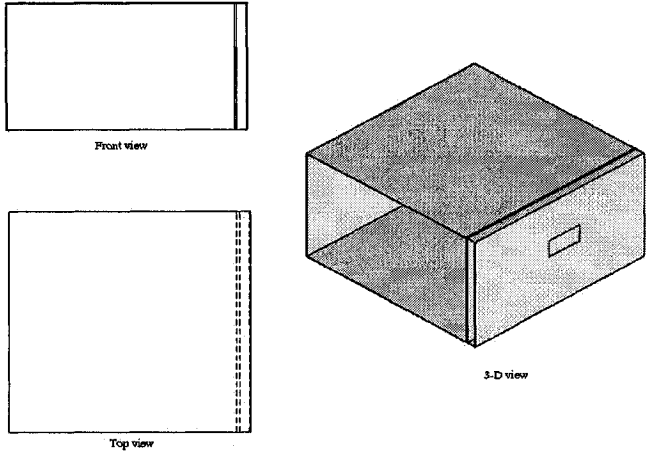
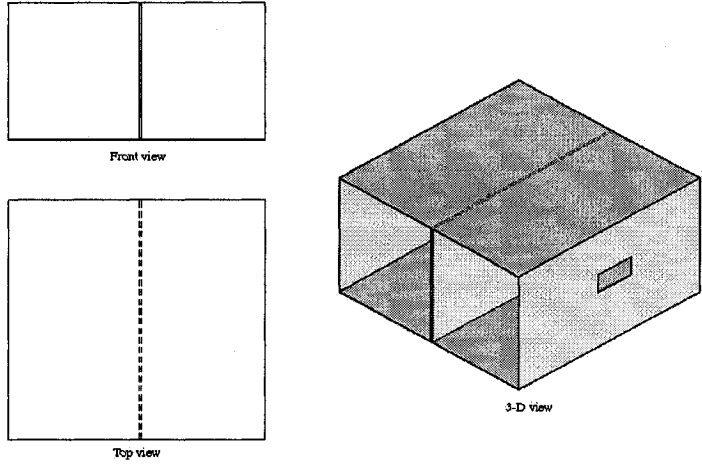
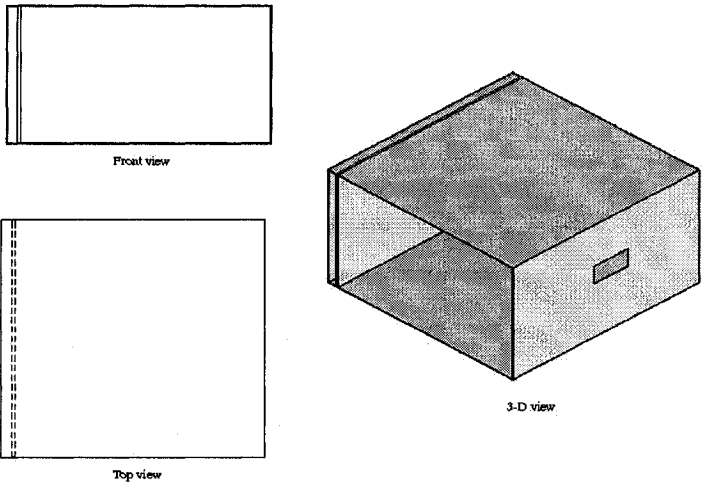
#### 10.4.2 Power dissipation into multiple lossy dielectric plates

When multiple lossy dielectric plates simultaneously exist in the microwave cavity as shown in Fig. 10.7., the power dissipation results are presented in Figures 10.8.

Among the five horizontally placed ones, plates #1, 3 and 5 showed multiple focusing strips along the direction of power entry port. The distances between two focusing strips correspond to the simulated microwave wavelength in free space. In plates # 2 and 3, strong absorptions were observed near the power entry port. Similar patterns were also observed as the other 3 plates but at a lower intensity. The patterns obtained in the case of multiple-plates are completely different from that of single plate at the same location. This is believed to be the result of less reflection received from the top and bottom cavity wall.

The total power dissipated into each plate is shown Table 10.3. Again it can be seen that power is not evenly distributed between the five plates. Similar to the case of single plate, plate #3 received the lowest amount of power. When comparing with the single plate study, much lower amount of energy was dissipated into each individual plate. The total power dissipation into the five plates is slightly higher than location H-1 and H-3 in the single plate situation.

<div data-bbox="337 205 620 375" data-label="Image"> </div> <div data-bbox="443 382 506 404" data-label="Caption"> <p>Front View</p> </div> <div data-bbox="342 465 626 635" data-label="Image"> </div> <div data-bbox="435 639 527 661" data-label="Caption"> <p>Right side view</p> </div> <div data-bbox="678 220 1078 602" data-label="Image"> </div> <div data-bbox="885 602 938 624" data-label="Caption"> <p>3-D view</p> </div>	<p><b>H-1</b> (Fig. 10.4)</p>
<div data-bbox="331 770 620 943" data-label="Image"> </div> <div data-bbox="443 950 506 971" data-label="Caption"> <p>Front View</p> </div> <div data-bbox="334 1013 621 1185" data-label="Image"> </div> <div data-bbox="435 1190 527 1212" data-label="Caption"> <p>Right side view</p> </div> <div data-bbox="706 751 1114 1137" data-label="Image"> </div> <div data-bbox="914 1148 971 1170" data-label="Caption"> <p>3-D View</p> </div>	<p><b>H-2</b> (Fig. 10.4)</p>
<div data-bbox="336 1292 610 1463" data-label="Image"> </div> <div data-bbox="435 1469 500 1491" data-label="Caption"> <p>Front View</p> </div> <div data-bbox="337 1552 612 1723" data-label="Image"> </div> <div data-bbox="435 1727 527 1749" data-label="Caption"> <p>Right side view</p> </div> <div data-bbox="693 1308 1078 1690" data-label="Image"> </div> <div data-bbox="898 1690 948 1712" data-label="Caption"> <p>3-D view</p> </div>	<p><b>H-3</b> (Fig. 10.4)</p>

 <p>Front view</p> <p>Top view</p> <p>3-D view</p>	<p><b>V-F-1</b> (Fig. 10.4)</p>
 <p>Front view</p> <p>Top view</p> <p>3-D view</p>	<p><b>V-F-2</b> (Fig. 10.4)</p>
 <p>Front view</p> <p>Top view</p> <p>3-D view</p>	<p><b>V-F-3</b> (Fig. 10.4)</p>

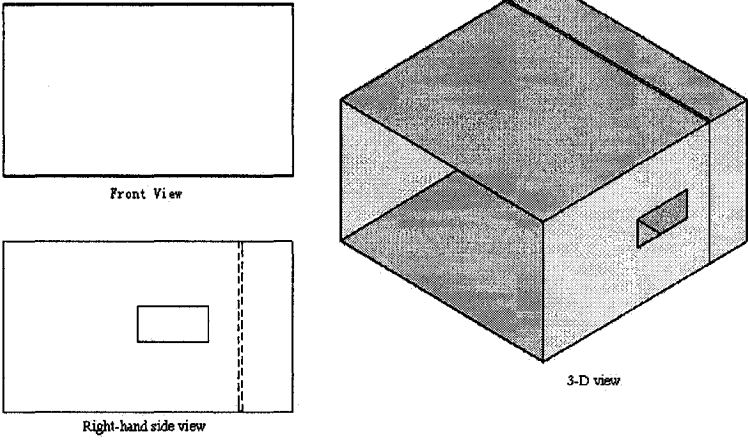
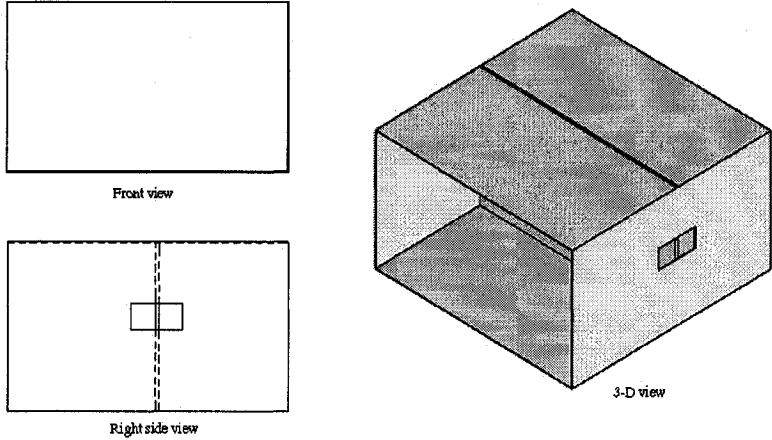
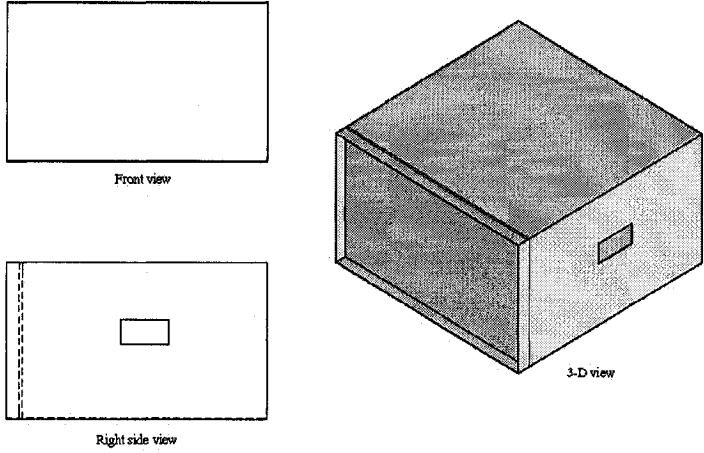
 <p>Front View</p> <p>Right-hand side view</p> <p>3-D view</p>	<p><b>V-P-1</b> (Fig. 10.4)</p>
 <p>Front view</p> <p>Right side view</p> <p>3-D view</p>	<p><b>V-P-2</b> (Fig. 10.4)</p>
 <p>Front view</p> <p>Right side view</p> <p>3-D view</p>	<p><b>V-P-3</b> (Fig. 10.4)</p>

Fig. 10.4. The nine locations of the lossy dielectric plate in the microwave oven.

H-1: Horizontal placement of the plate 9 cell grid above oven bottom,  
corresponding to the location range of 4.5-5 cm above the bottom

H-2: Horizontal placement of the plate 29 cell grid above oven bottom,  
corresponding to 14.5-15cm above the bottom

H-3: Horizontal placement of the plate 47 cell grid above oven bottom  
corresponding to 24.5-25 cm above the bottom

V-F-1: Vertical placement facing the power entrance port, 9 cells from  
the power entrance wall corresponding to a range of 4.5-5 cm

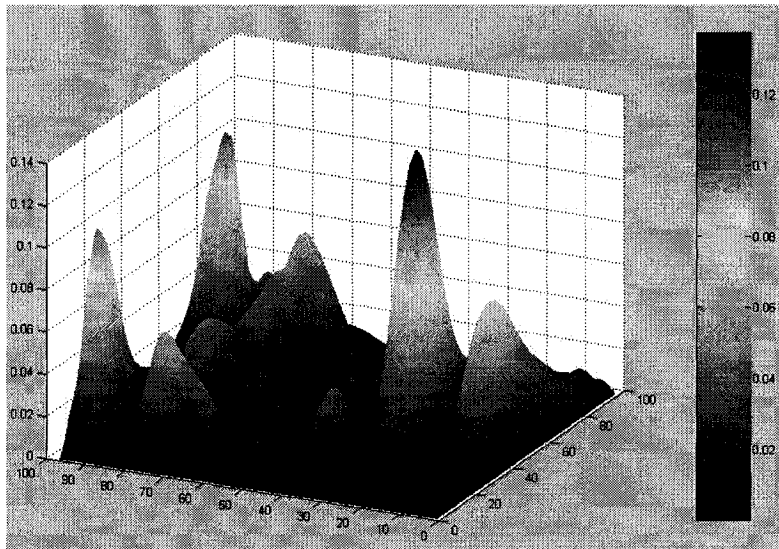
V-F-2: Vertical placement facing the power entrance port, 29 cells from  
the power entrance wall corresponding to a range of 14.5-15 cm

V-F-3: Vertical placement facing the power entrance port, 47 cells from  
the power entrance wall corresponding to a range of 24.5-25 cm

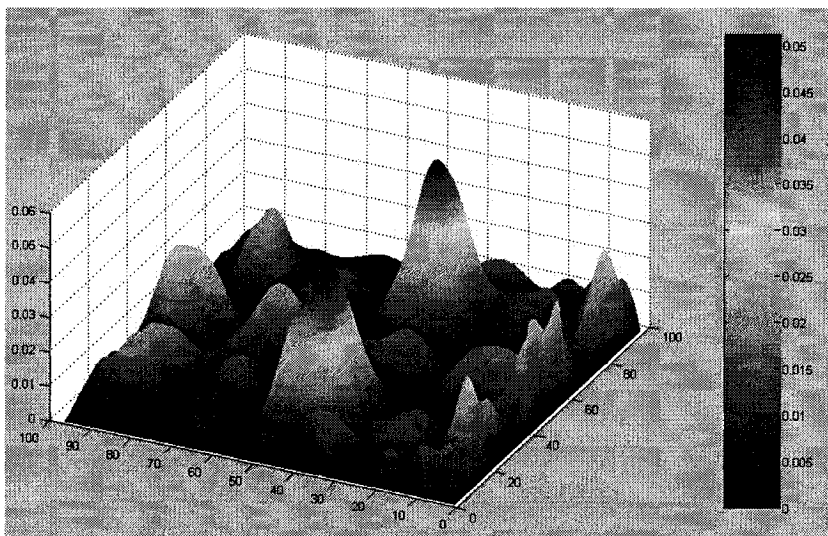
V-P-1: Vertical placement parallel to the power entrance port, 9 cells  
from the back wall corresponding to a range of 4.5-5 cm

V-P-2: Vertical placement facing the power entrance port, 29 cells from  
the back wall corresponding to a range of 14.5-15 cm

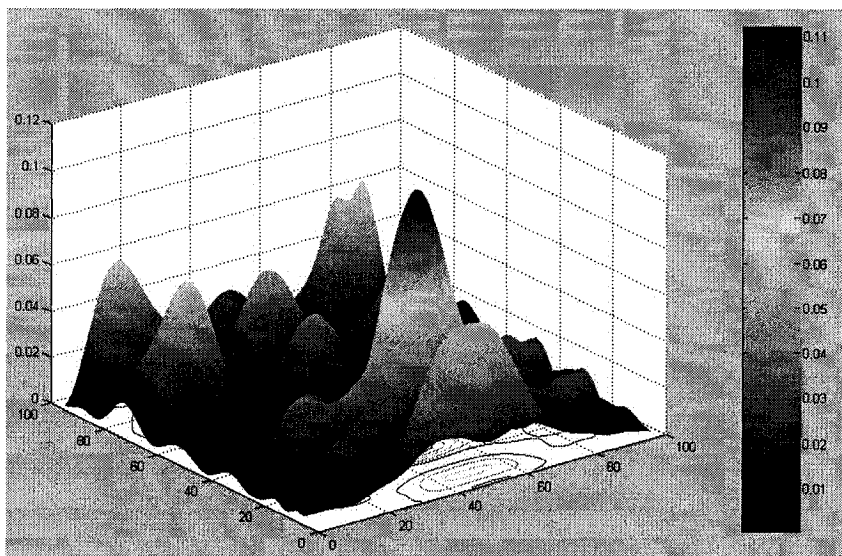
V-P-3: Vertical placement facing the power entrance port, 47 cells from  
the back wall corresponding to a range of 24.5-25 cm



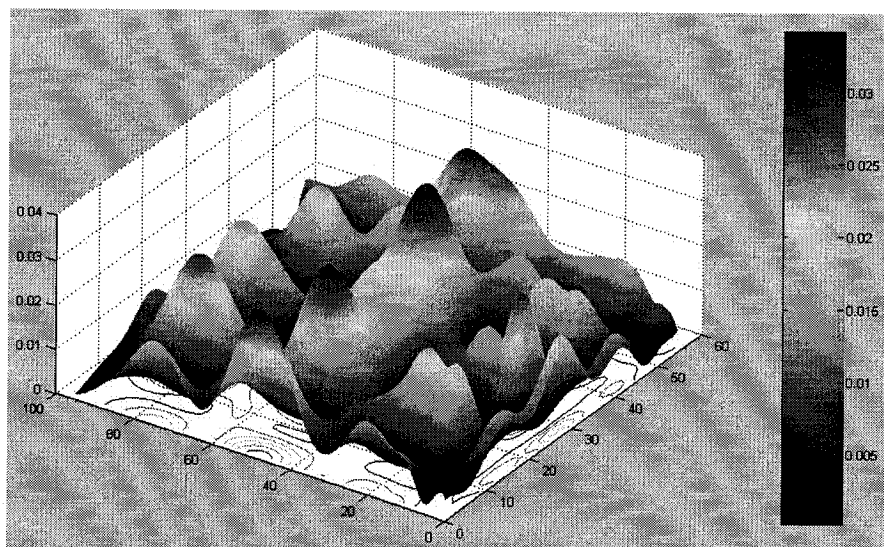
**H-1**  
(Fig. 10.5)



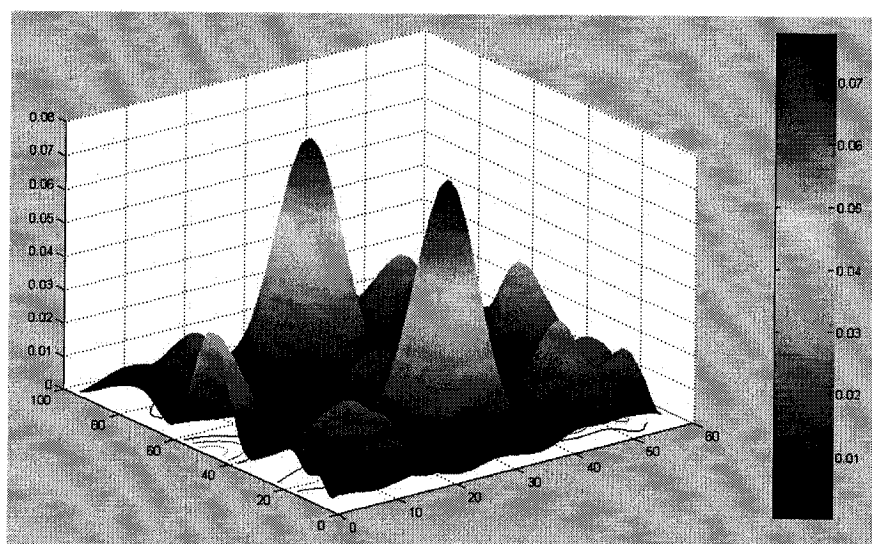
**H-2**  
(Fig. 10.5)



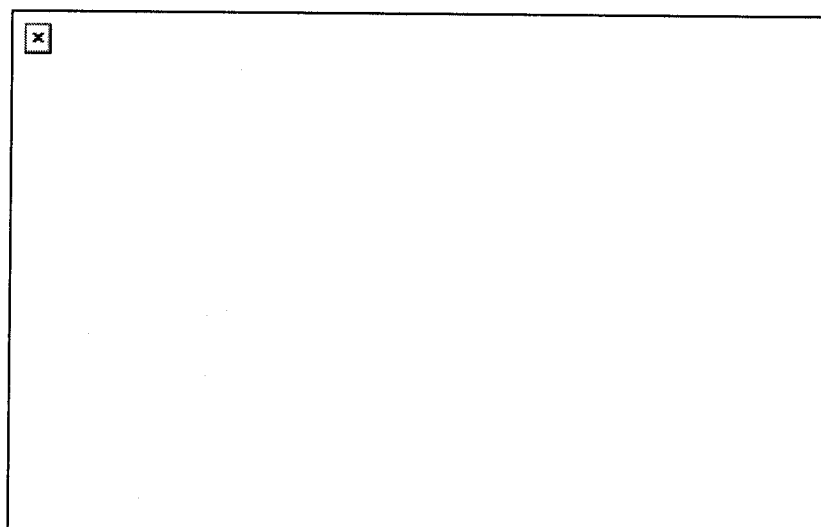
**H-3**  
(Fig. 10.5)



**V-F-1**  
(Fig. 10.5)

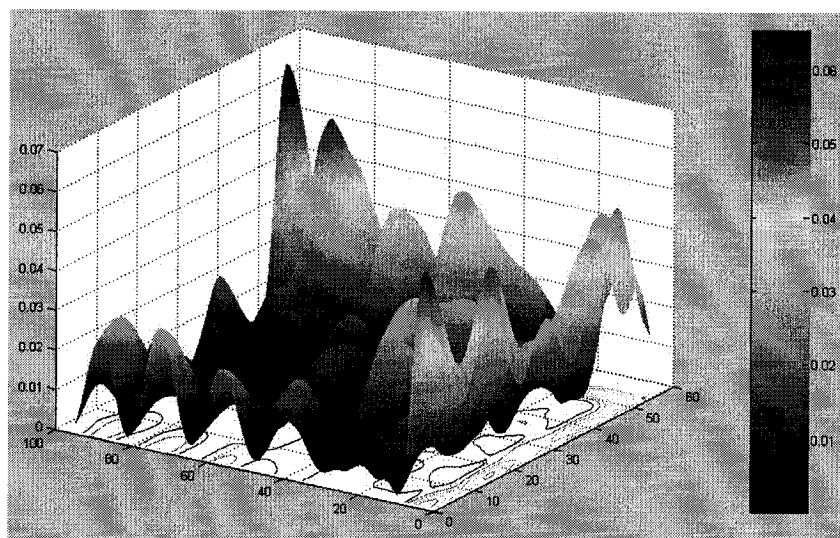


**V-F-2**  
(Fig. 10.5)

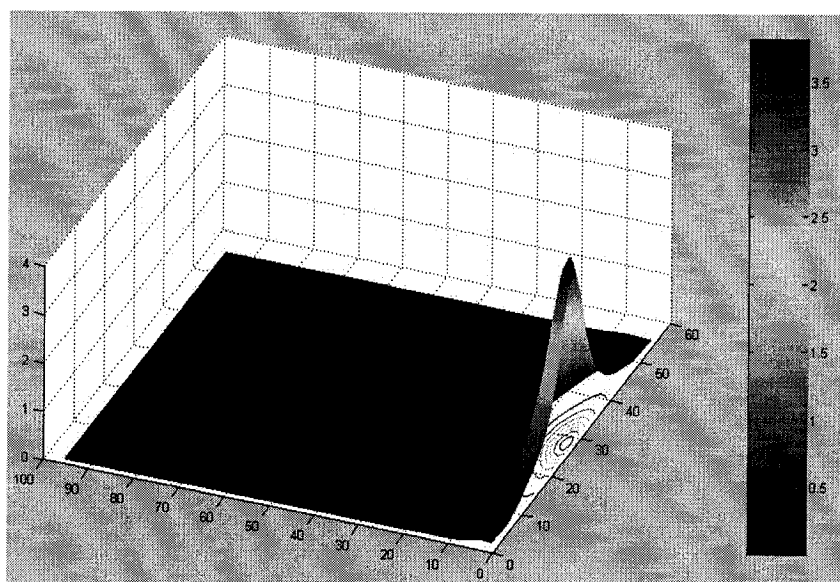


**V-F-3**  
(Fig. 10.5)

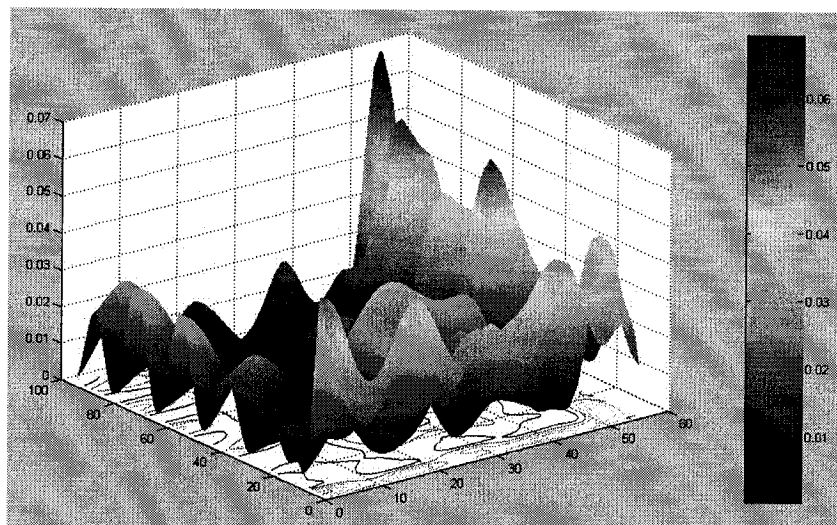




**V-P-1**  
(Fig. 10.5)



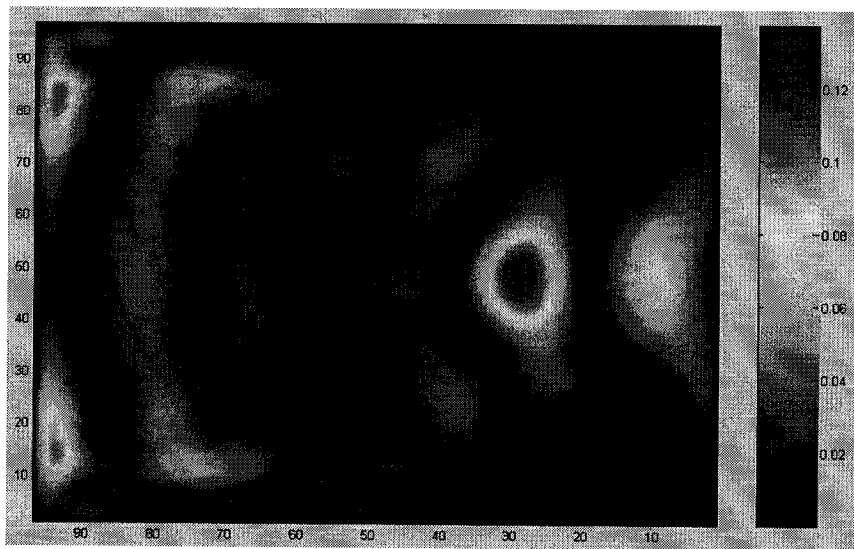
**V-P-2**  
(Fig. 10.5)



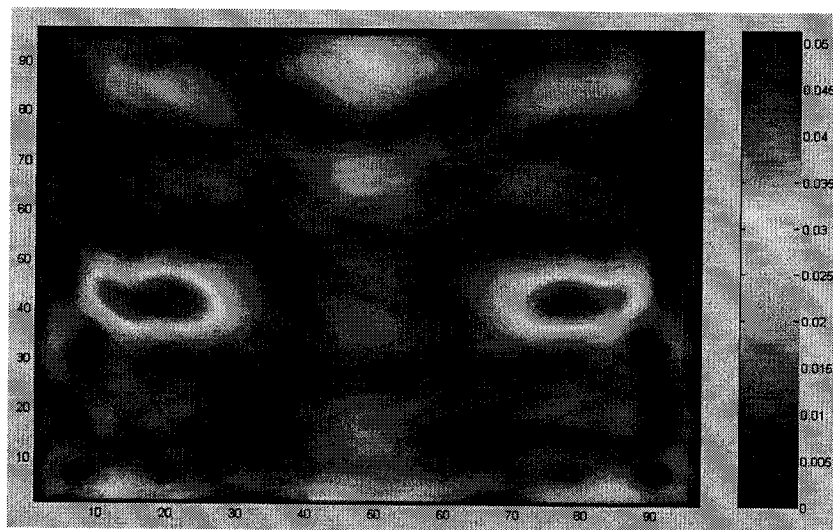
**V-P-3**  
(Fig. 10.5)

Fig. 10.5. The power dissipation on the lossy dielectric plate with dielectric constant:  $\epsilon' = 20$  and dielectric loss factor  $\epsilon'' = 5$ . Simulation was run using an AMD Athlon 3800 dual core personal computer with 1Gb DDR400 PC-3200 computer. Simulation time is 5 min. On the figures, the scale in color map is normalized to 1 s of microwave application at 1KW of incident power. The color map has a unit of joule. Since it is normalized to 1 s, it can also be an energy dissipation rate with the unit of W.

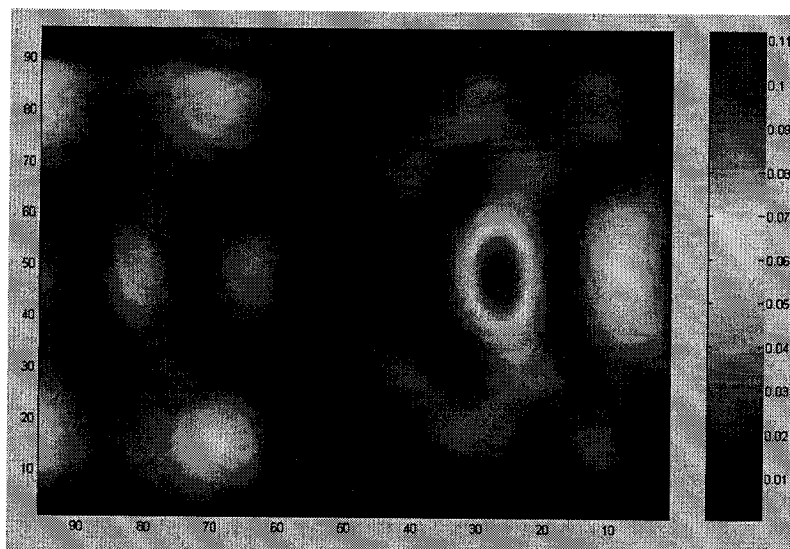
- H-1: Horizontal placement of the plate 9 cell grid above oven bottom, corresponding to the location range of 4.5-5 cm above the bottom
- H-2: Horizontal placement of the plate 29 cell grid above oven bottom, corresponding to 14.5-15cm above the bottom
- H-3: Horizontal placement of the plate 47 cell grid above oven bottom corresponding to 24.5-25 cm above the bottom
- V-F-1: Vertical placement facing the power entrance port, 9 cells from the power entrance wall corresponding to a range of 4.5-5 cm
- V-F-2: Vertical placement facing the power entrance port, 29 cells from the power entrance wall corresponding to a range of 14.5-15 cm
- V-F-3: Vertical placement facing the power entrance port, 47 cells from the power entrance wall corresponding to a range of 24.5-25 cm
- V-P-1: Vertical placement parallel to the power entrance port, 9 cells from the back wall corresponding to a range of 4.5-5 cm
- V-P-2: Vertical placement facing the power entrance port, 29 cells from the back wall corresponding to a range of 14.5-15 cm
- V-P-3: Vertical placement facing the power entrance port, 47 cells from the back wall corresponding to a range of 24.5-25 cm



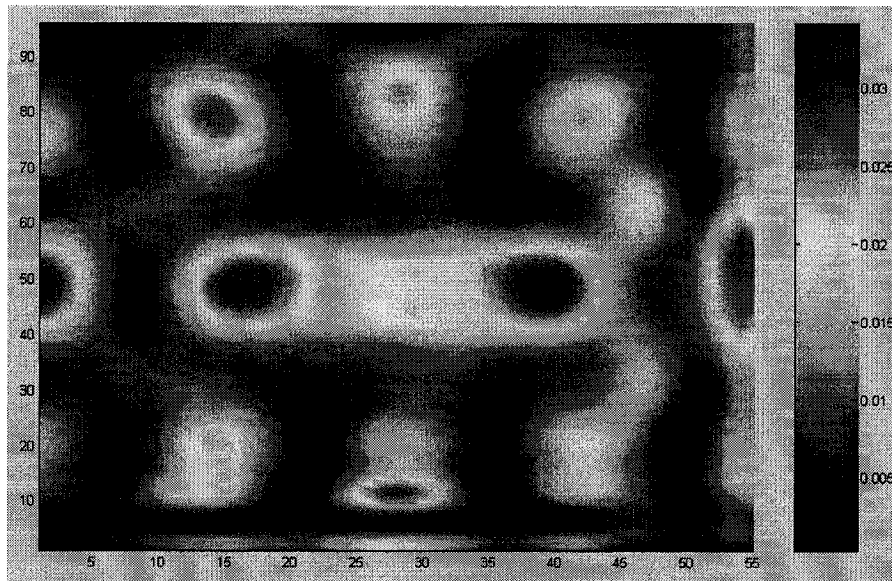
**H-1**  
(Fig. 10.6)



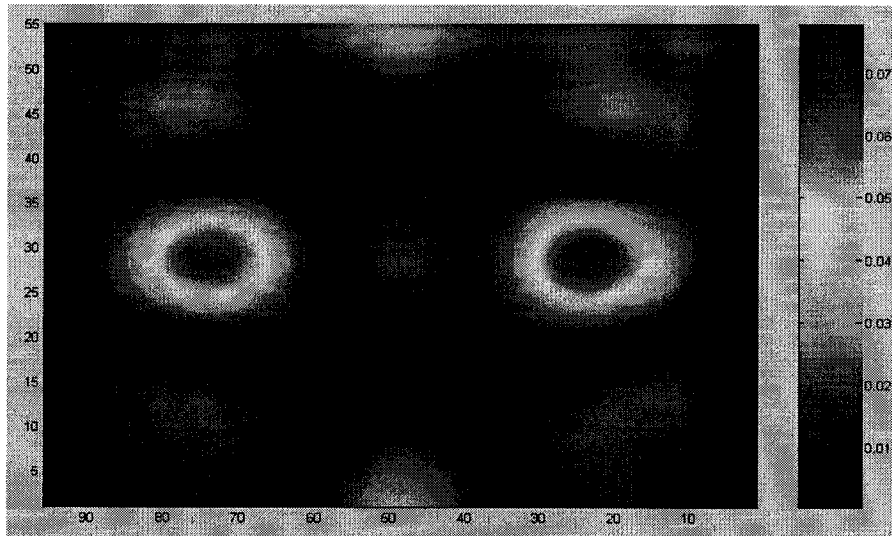
**H-2**  
(Fig. 10.6)



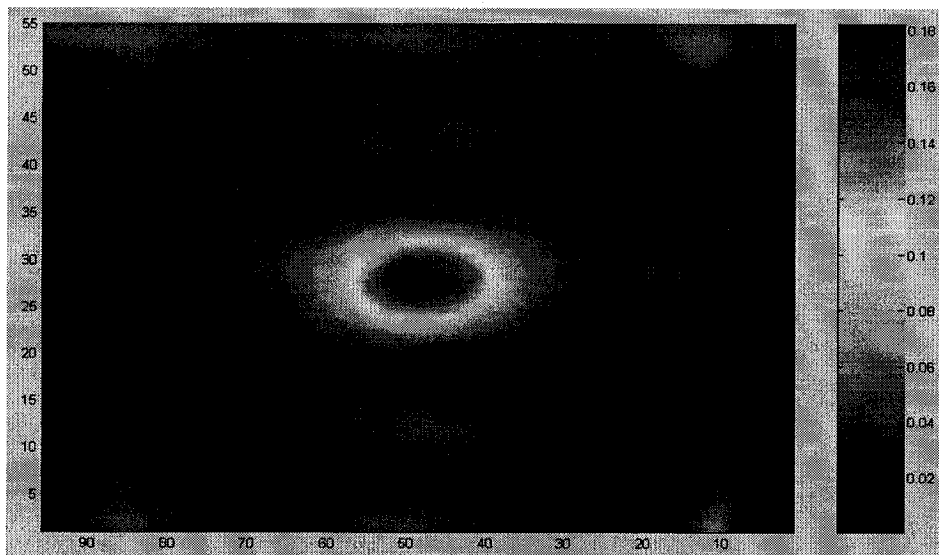
**H-3**  
(Fig. 10.6)



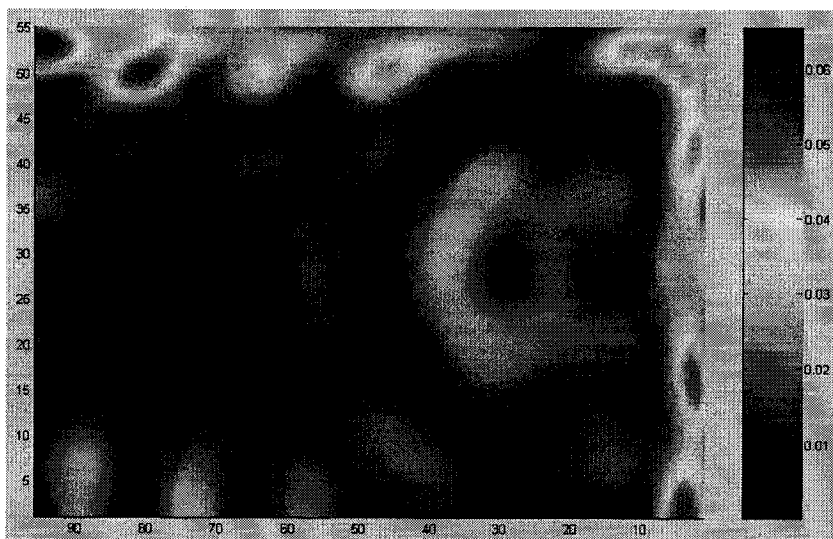
**V-F-1**  
(Fig. 10.6)



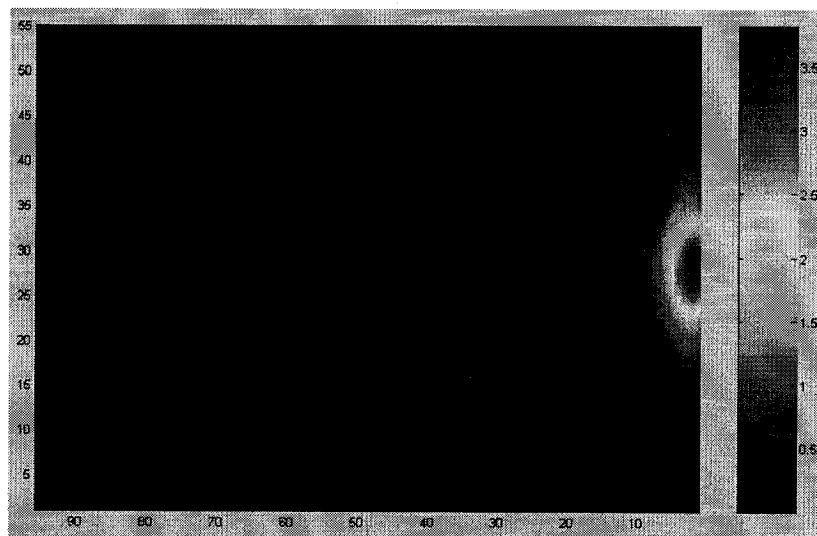
**V-F-2**  
(Fig. 10.6)



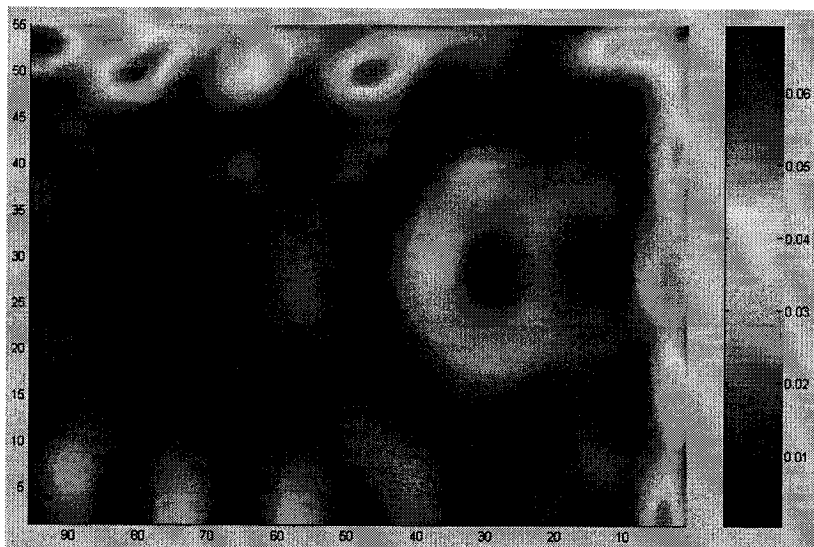
**V-F-3**  
(Fig. 10.6)



**V-P-1**  
(Fig. 10.6)



**V-P-2**  
(Fig. 10.6)



**V-P-3**  
(Fig. 10.6)

Fig. 10.6. The 2D view of Fig. 10.5 to assist in the observation of the pattern and to compare with the experimental results

- H-1: Horizontal placement of the plate 9 cell grid above oven bottom, corresponding to the location range of 4.5-5 cm above the bottom
- H-2: Horizontal placement of the plate 29 cell grid above oven bottom, corresponding to 14.5-15cm above the bottom
- H-3: Horizontal placement of the plate 47 cell grid above oven bottom corresponding to 24.5-25 cm above the bottom
- V-F-1: Vertical placement facing the power entrance port, 9 cells from the power entrance wall corresponding to a range of 4.5-5 cm
- V-F-2: Vertical placement facing the power entrance port, 29 cells from the power entrance wall corresponding to a range of 14.5-15 cm
- V-F-3: Vertical placement facing the power entrance port, 47 cells from the power entrance wall corresponding to a range of 24.5-25 cm
- V-P-1: Vertical placement parallel to the power entrance port, 9 cells from the back wall corresponding to a range of 4.5-5 cm
- V-P-2: Vertical placement facing the power entrance port, 29 cells from the back wall corresponding to a range of 14.5-15 cm
- V-P-3: Vertical placement facing the power entrance port, 47 cells from the back wall corresponding to a range of 24.5-25 cm

Table 10.1 Power dissipation into the lossy dielectric plates at different locations. The dielectric constant is 20 and the loss factor is 5. Results were obtained from the 3000 iteration simulation but normalized to the total energy dissipation within 1 s. The total input power to the cavity is 1kW.

Plate Location	Power dissipated into the plate (W)
H-1	175.45
H-2	96.08
H-3	168.55
	189.62 ( $\epsilon' = 5; \epsilon'' = 20$ )
	50.00 ( $\epsilon' = 80; \epsilon'' = 20$ )
V-F-1	56.78
V-F-2	68.30
V-F-3	113.75
V-P-1	72.15
V-P-2	331.14
V-P-3	78.30

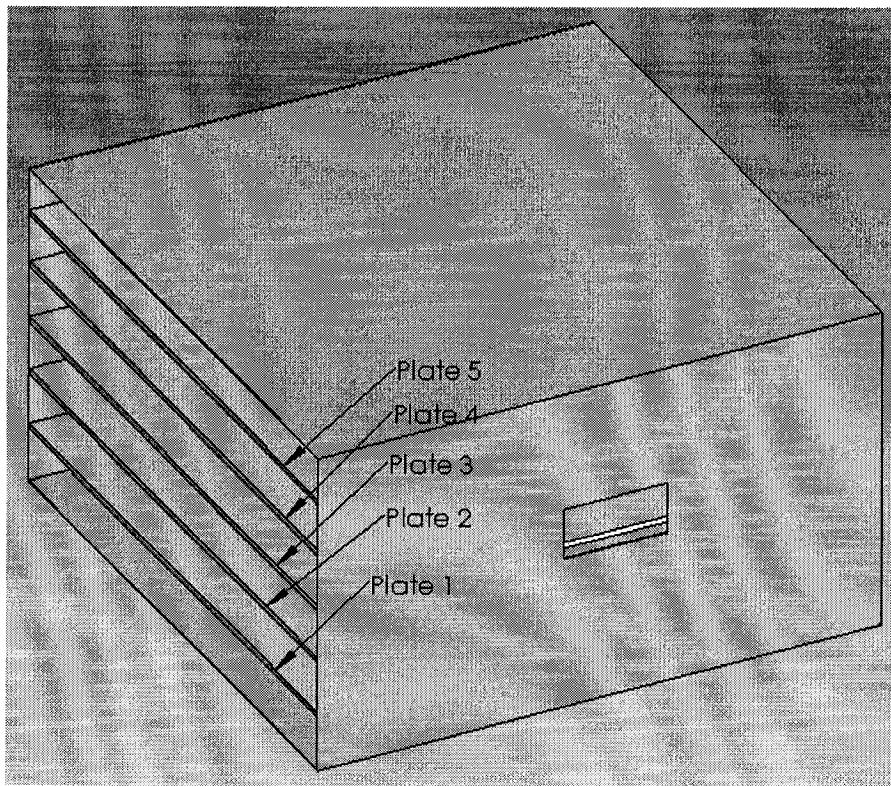


Fig. 10.7. The study of power dissipation when multiple lossy dielectric plates simultaneously exist in a microwave oven.



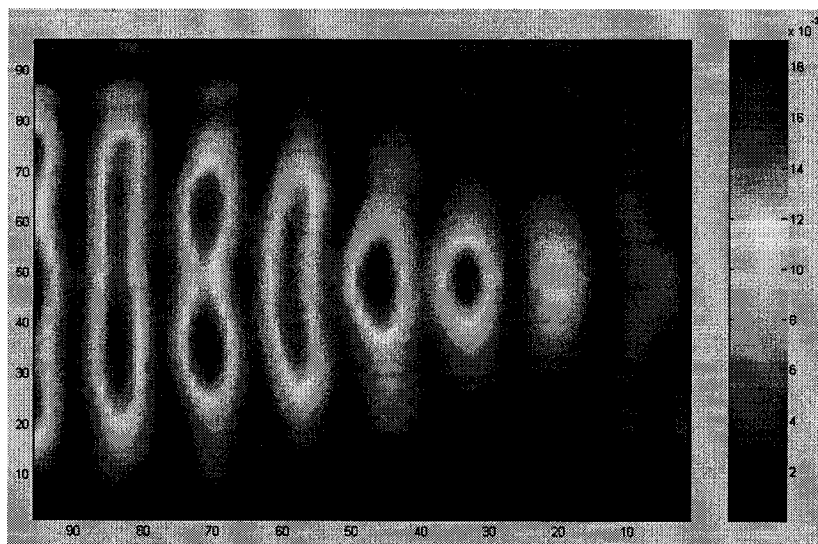


Plate #1  
(Fig. 10.8)

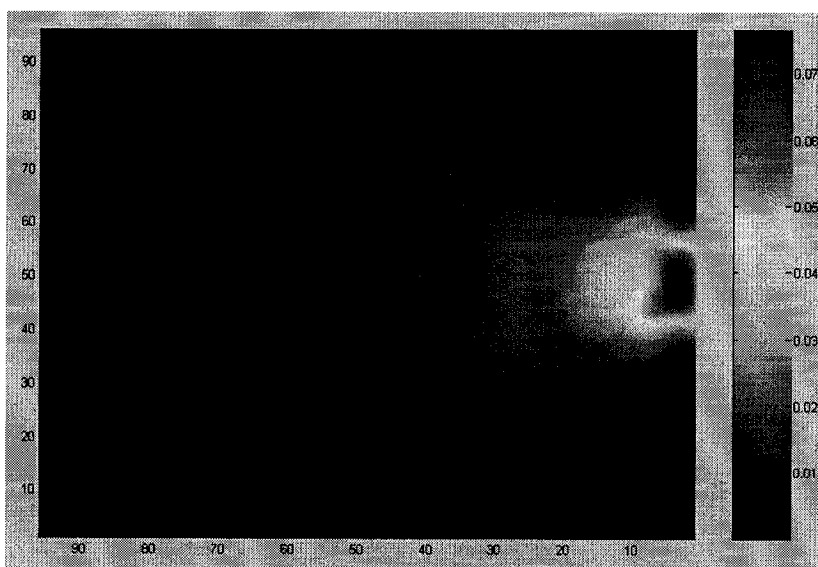


Plate #2  
(Fig. 10.8)

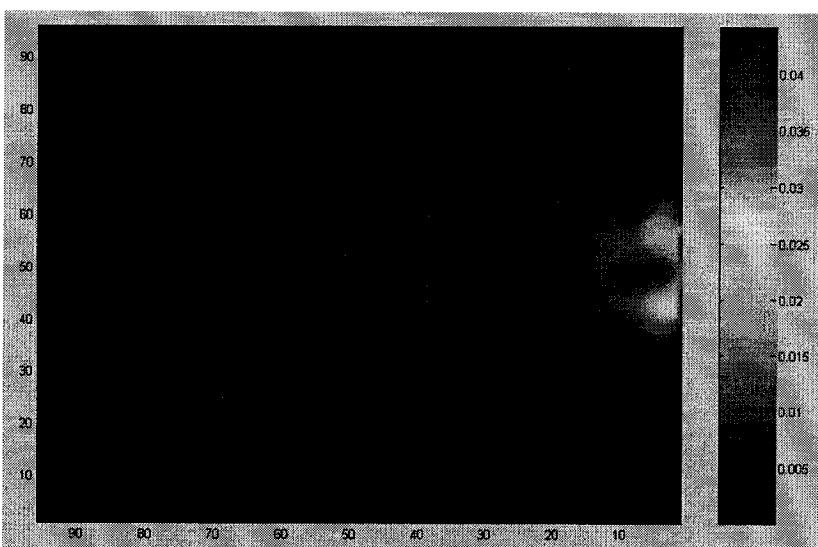


Plate #3  
(Fig. 10.8)

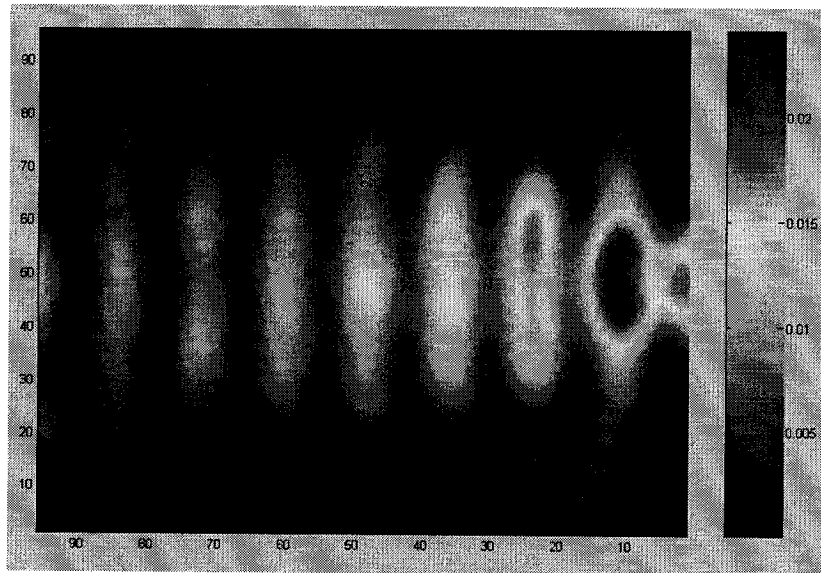


Plate #4  
(Fig. 10.8)

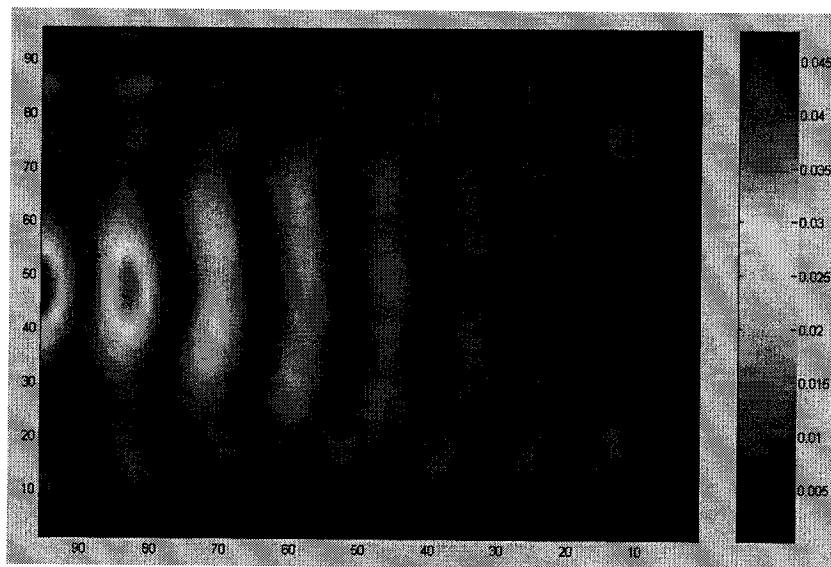


Plate #5  
(Fig. 10.8)

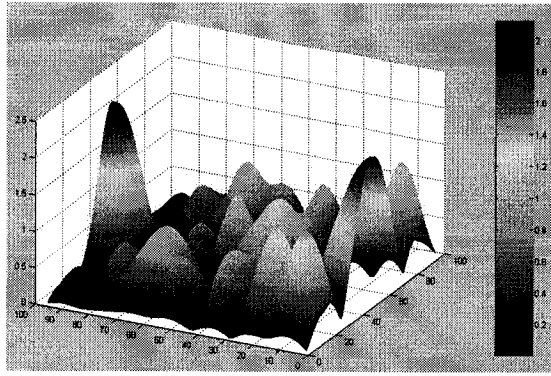
Fig. 10.8. Power dissipation into lossy dielectric plates ( $\epsilon' = 20$  ;  $\epsilon'' = 5$ ) when 5 horizontally placed plates simultaneously exist in the cavity

Table 10.3. Power dissipation into the lossy dielectric plates at different locations in the existence of 5 horizontally placed plates as shown in Fig. 10.7. The dielectric constant of the plates is 20 and the loss factor is 5. Results were obtained from the 3000 iteration simulation normalized to 1 s. The total input power to the cavity is 1KW.

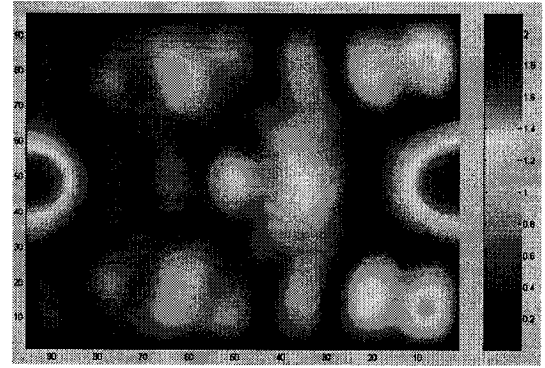
Plate Location	Power dissipated into the plate (W)
Plate #1	44.87
Plate #2	47.83
Plate #3	21.42
Plate #4	39.26
Plate #5	58.30
Total power dissipation within the cavity	211.68

#### 10.4.3. E field distribution and the influence of lossy dielectric materials on the E field distributions

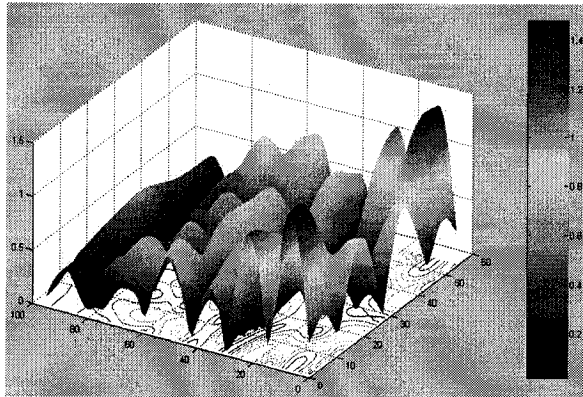
The E field distributions in the empty loaded, single plate and multiple plate loaded cavity are presented in Figs. 10.9 - 10.11. Three planes were studied: the XY plane 5 cm above the bottom; the XZ plane 5 cm from the back wall of the cavity; and the YZ plane 5 cm from the power entry port. The E field distribution may vary with the number of steps. The results presented here is at 3000 timesteps. From the three figures, it can be seen that the introduction of lossy dielectric material completely changed the E field distribution in empty cavity in all three planes. The distribution patterns in the existence of 5 plates are also different from that of one single plate in XY, and XZ planes. Similarity in the YX plane was observed. On the lossy dielectric plate, the E field is much lower than that in other locations. This plane is in the middle and perpendicular to the two of the power entry ports.



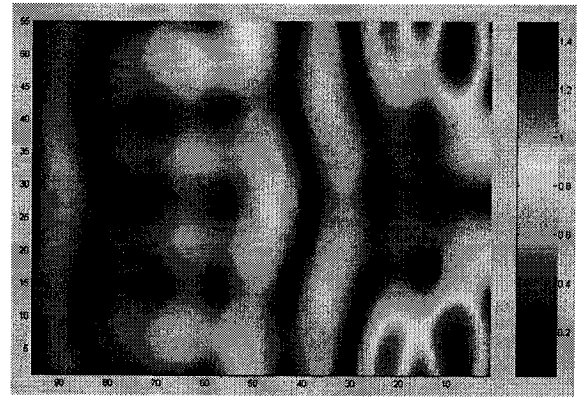
XY plane in 3D view



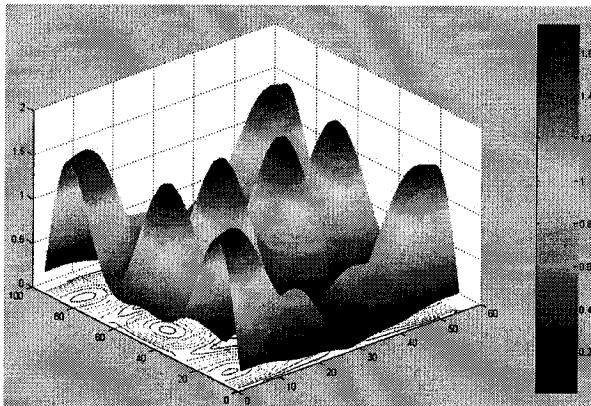
XY plane in 2D view



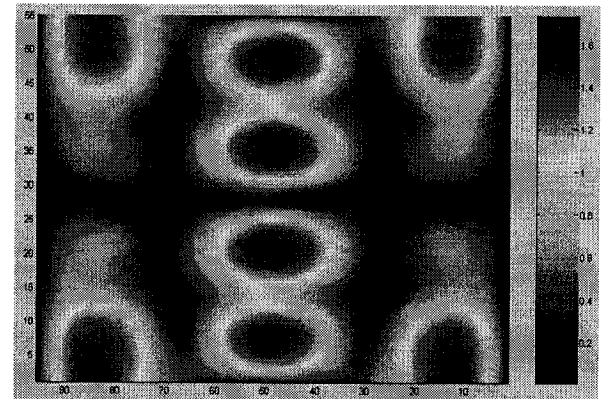
XZ plane in 3D view



XZ plane in 2D view



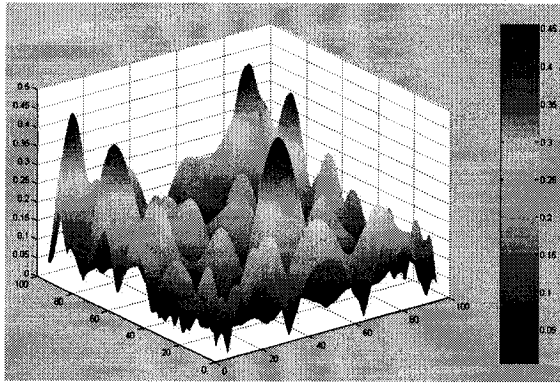
YZ plane in 3D view



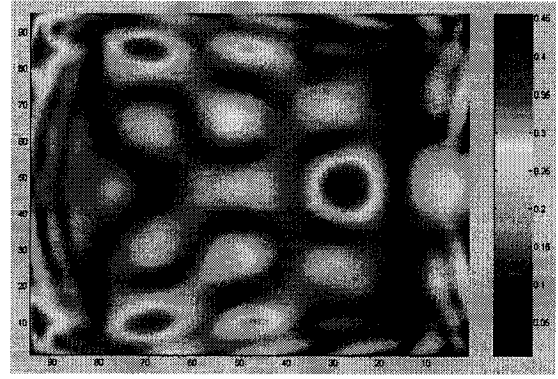
YZ plane in 2D view

Fig. 10.9. E field distribution in the empty cavity after 3000 timesteps ( $2.79 \times 10^{-7}$  s). Total meshing number: 97 x 97 x 56 cells. Simulation was run using an AMD Athlon 3800 dual core personal computer with 1Gb DDR400 PC-3200 memory. Simulation time was 5 min.

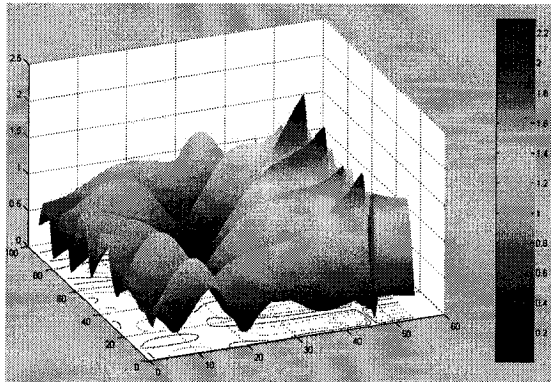
The XY plane is 5 cm from the bottom of the cavity;  
 XY plane is 5 cm from the back wall of the cavity  
 YZ plane is 5 cm from the power entry port wall.



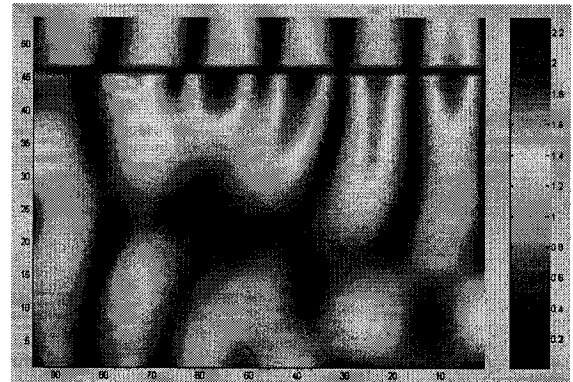
XY plane in 3D view



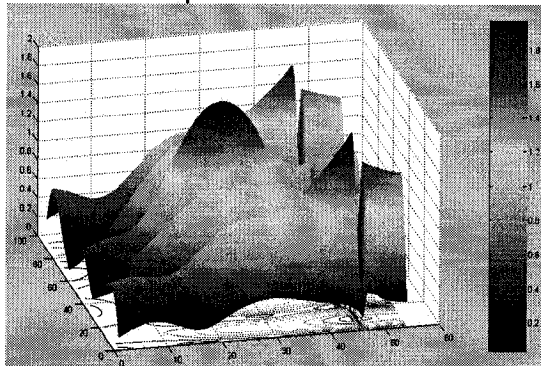
XY plane in 2D view



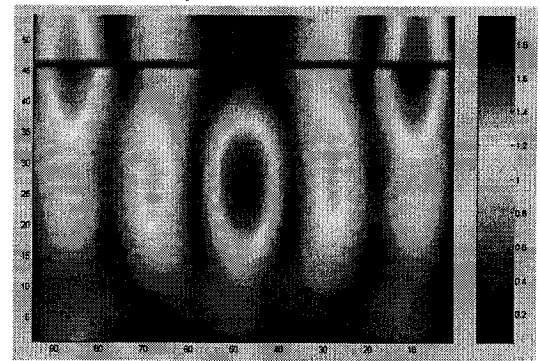
XZ plane in 3D view



XZ plane in 2D view



YZ plane in 3D view



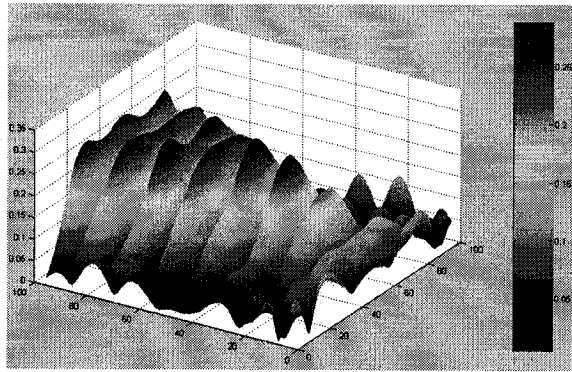
YZ plane in 2D view

Fig. 10.10. E field distribution in the cavity with a single lossy dielectric plate ( $\epsilon' = 20$  ;  $\epsilon'' = 5$ ) horizontally placed 5 cm from the bottom of the cavity. Results were obtained after 3000 timesteps ( $2.79 \times 10^{-7}$  s) of run using an AMD Athlon 3800 dual core personal computer with 1Gb DDR400 PC-3200 memory. Simulation time was 5 min.

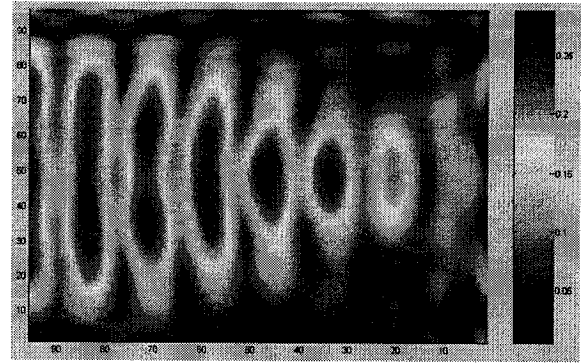
XY plane is 5 cm from the bottom of the cavity

XY plane is 5 cm from the back wall of the cavity

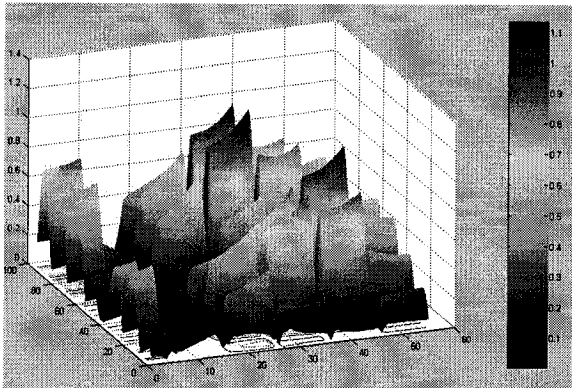
YZ plane is 5 cm from the power entry port wall.



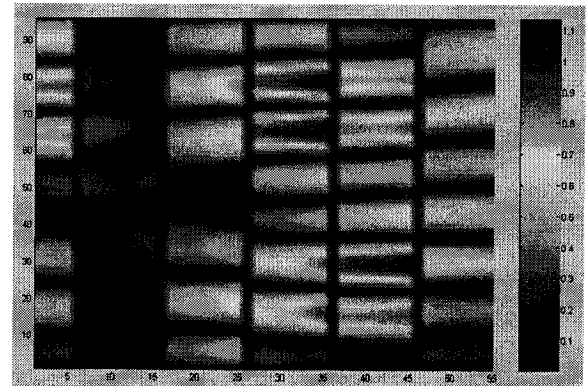
XY plane in 3D view



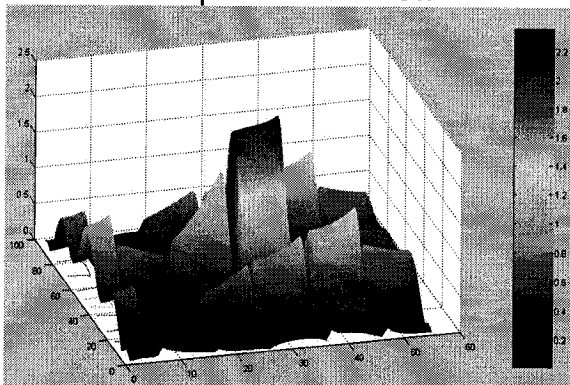
XY plane in 2D view



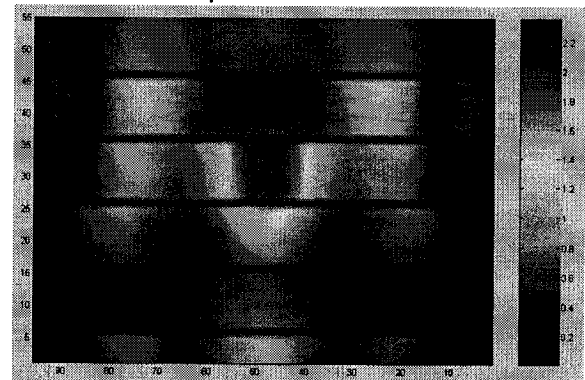
XZ plane in 3D view



XZ plane in 2D view



YZ plane in 3D view



YZ plane in 2D view

Fig. 10.11. E field distribution in the cavity with five lossy dielectric plates ( $\epsilon' = 20$  ;  $\epsilon'' = 5$ ) simultaneously exist. Results were obtained after 3000 timesteps ( $2.79 \times 10^{-7}$  s) of run using an AMD Athlon 3800 dual core personal computer with 1Gb DDR400 PC-3200 memory. Simulation time was 5 min.

XY plane is 5 cm from the bottom of the cavity  
 XY plane is 5 cm from the back wall of the cavity  
 YZ plane is 5 cm from the power entry port wall.



#### 10.4.4. Experimental evaluation of the simulation

Experimental results from the previous chapter were used to evaluate the simulation.

$\text{CaCl}_2$  plates with the addition of  $\text{CoCl}_2$  were used to visualize the power absorption as explained in Chapter 7. The simulation is evaluated using the experimental results. Fig. 10.12 corresponds to the location H-1 in Fig. 10.6. Fig. 10.13 shows the results obtained with multiple plate horizontally placed within the cavity corresponding to the five plates in Fig. 10.8.

As can be seen the single plate horizontal oriented does not match well with the H-1 obtained by the simulation, however very good matching was observed for the same location of plate when multiple plates were present in the cavity. In the Fig. 10.13, all the distributions from plate # 2 to #5 does not show matching pattern with the simulated result. The reasons that the experimental results does not match the simulated ones in many cases lies in the domestic microwave oven cavity geometry and power entry port arrangement. The domestic microwave oven has slightly different geometry from the current simulation. The back wall and the front door are not flat. This may form a focusing effect of the power to the bottom plate because this will favour the everyday heating application in household because whatever food to be heated in the oven will be placed at the bottom of the cavity. Furthermore, the microwave power is not guided into the cavity through a waveguide, instead the magnetron is placed in such a way that the slope of magnetron chamber tends to reflect the power towards the bottom of the cavity so that power will be more focused to the bottom instead of symmetrically distributed in the space. From Fig. 10.13, it is quite clear that the bottom plate absorbed most of the power while leaving all the other plates almost blank. With the present of multiple plates, reflection was from the top and other wall was blocked by other plates, therefore the geometry played a less important role in the power dissipation. As a result, matching patterns were observed in the two bottom plates in the experimental and simulated cavity. Evidence was found when examining the reflection free cavity situations in the experiments as shown in Fig. 10.14. The pattern obtained were

the same as that of the simulated and experimental bottom plate of the 5-plate study.

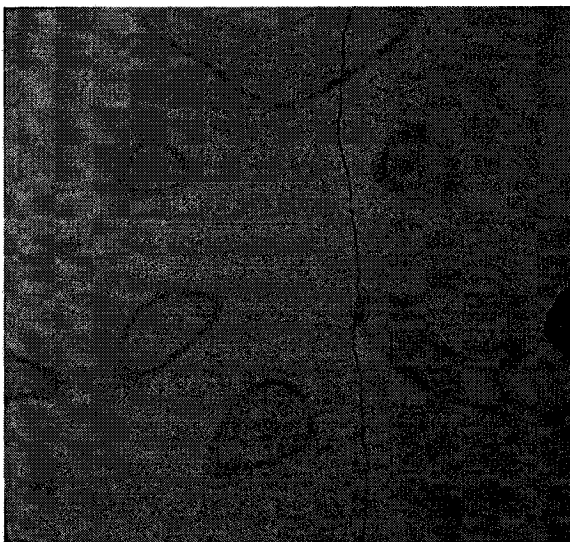


Fig. 10.12. Single plate horizontally oriented at location 1 corresponding 5 cm to the bottom of the cavity. A Panasonic microwave oven 47 x 47 x 27 cm in dimension and 1 KW power output. Pattern obtained after 3 min of heating at full power level.

#### **10.5. Simulation of an oven-type chemical reactor/extractor.**

An oven-type microwave chemical reactor/extractor can be designed as shown in Fig. 10.15. The whole system consists of an oven with three power entry port, a glass (or preferably quartz) container, a stirrer, and a condenser. The dimension of the oven to be simulated here is 80 x 80 x 60 cm. Three power entry ports are located in the center of the left, right and the back wall of the cavity. Each power entry port provides an input power of 1 kW. On top of the cavity, openings are made so that stirrer and condenser can be connected. In practice, a metal tube with proper diameter and corresponding length should be attached to the opening so that microwave will not leak from the cavity. For simplicity, in the simulation, these openings will not be considered. The glass container is chosen to have a diameter of 70 cm and 50 cm high. In the simulation, the reactant will be filled 30 cm giving a volume of 115 liters. The



stirrer is used to make the heating more uniform. But in the simulation, this will not be considered either. Dielectric properties of the reactant are crucial factors to be considered during the microwave-assisted chemical processing. In the simulation, they are categorized into three groups: high loss, medium loss and low loss reactants. Arbitrary dielectric property values were assigned to each of these three categories: high loss:  $\epsilon' = 80$ ,  $\epsilon'' = 15$ ; medium loss:  $\epsilon' = 20$ ,  $\epsilon'' = 5$ ; low loss:  $\epsilon' = 5$ ,  $\epsilon'' = 1$ .

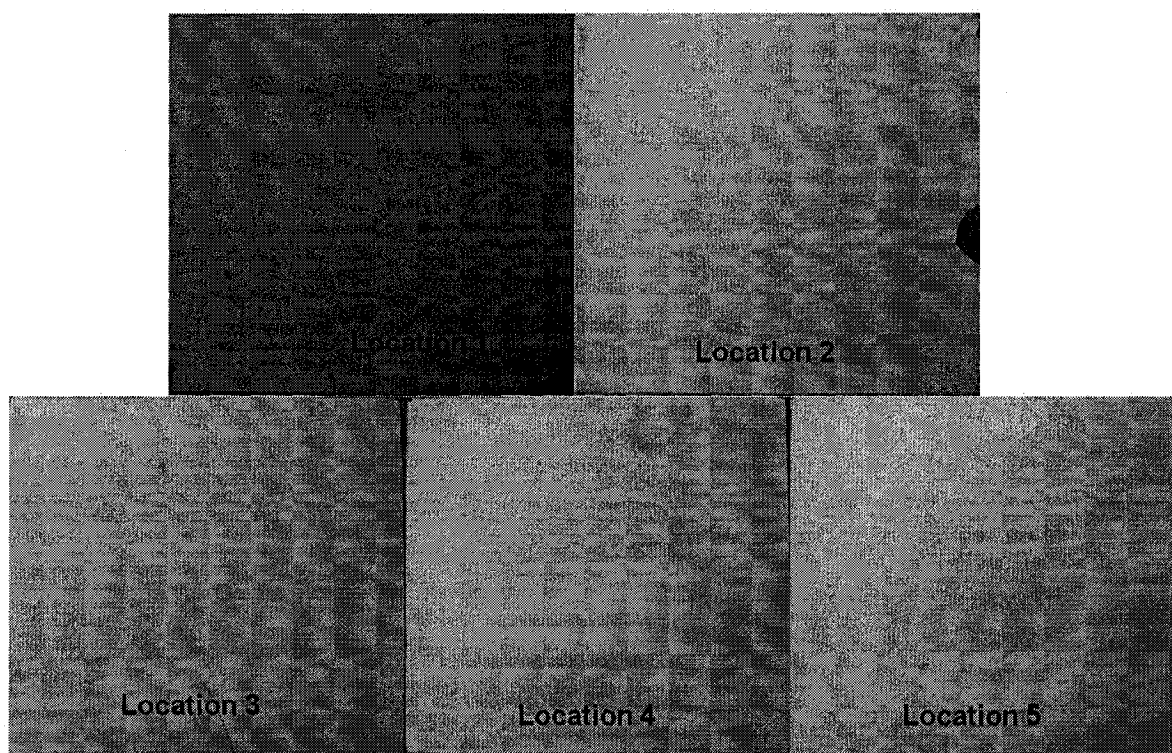


Fig. 10.13. Multiple-horizontal oriented loading. Locations 1 through 5 correspond to the distance to the bottom of the cavity of 5 to 25 cm with 5 cm increment. A Panasonic microwave oven 47 x 47 x 27 cm in dimension and 1 kW power output. Pattern obtained after 9 min of heating at full power level.

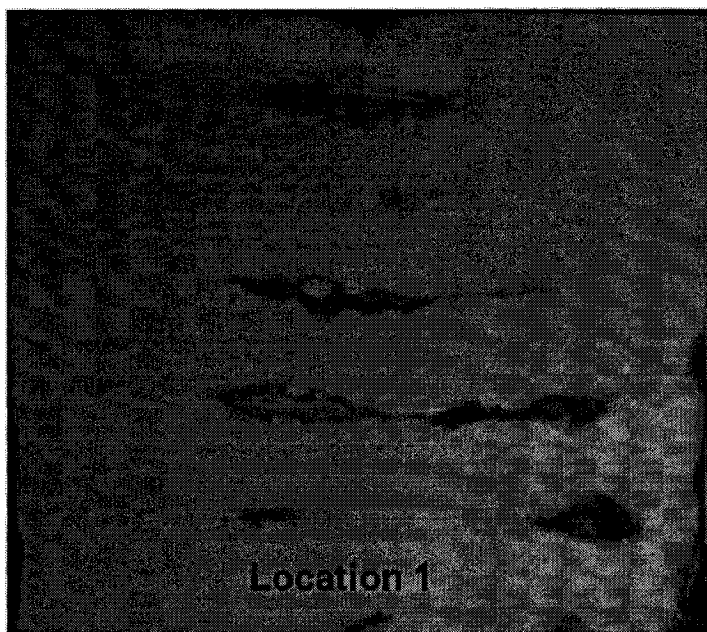


Fig. 10.14. Single plate horizontally oriented at location 1 corresponds to the location 5 cm from the bottom of a reflection free cavity created by adding power absorption materials around the walls. A Panasonic microwave oven 47 x 47 x 27 cm in dimension and 1 kW power output. Pattern obtained after 10 min of heating at full power level.

E field distribution and power dissipation of the horizontal section plane at different depth of the reactor vessel for low loss, medium loss and high loss reactants are presented in Figures 10.16 to 10.18. Figs. 10.16A, 10.17A, and 10.18A are for the top layer. As can be seen, for the low loss and medium loss reactants, three spots have very strong E field distribution. These three spots correspond to the three power entry port. However, for the high loss reactant, the E field is more spread surrounding the cylinder. The power absorption is mainly located in around the three spots of low loss and medium loss reactants. For the high loss one, the spots are very thin focusing mainly on the edge.

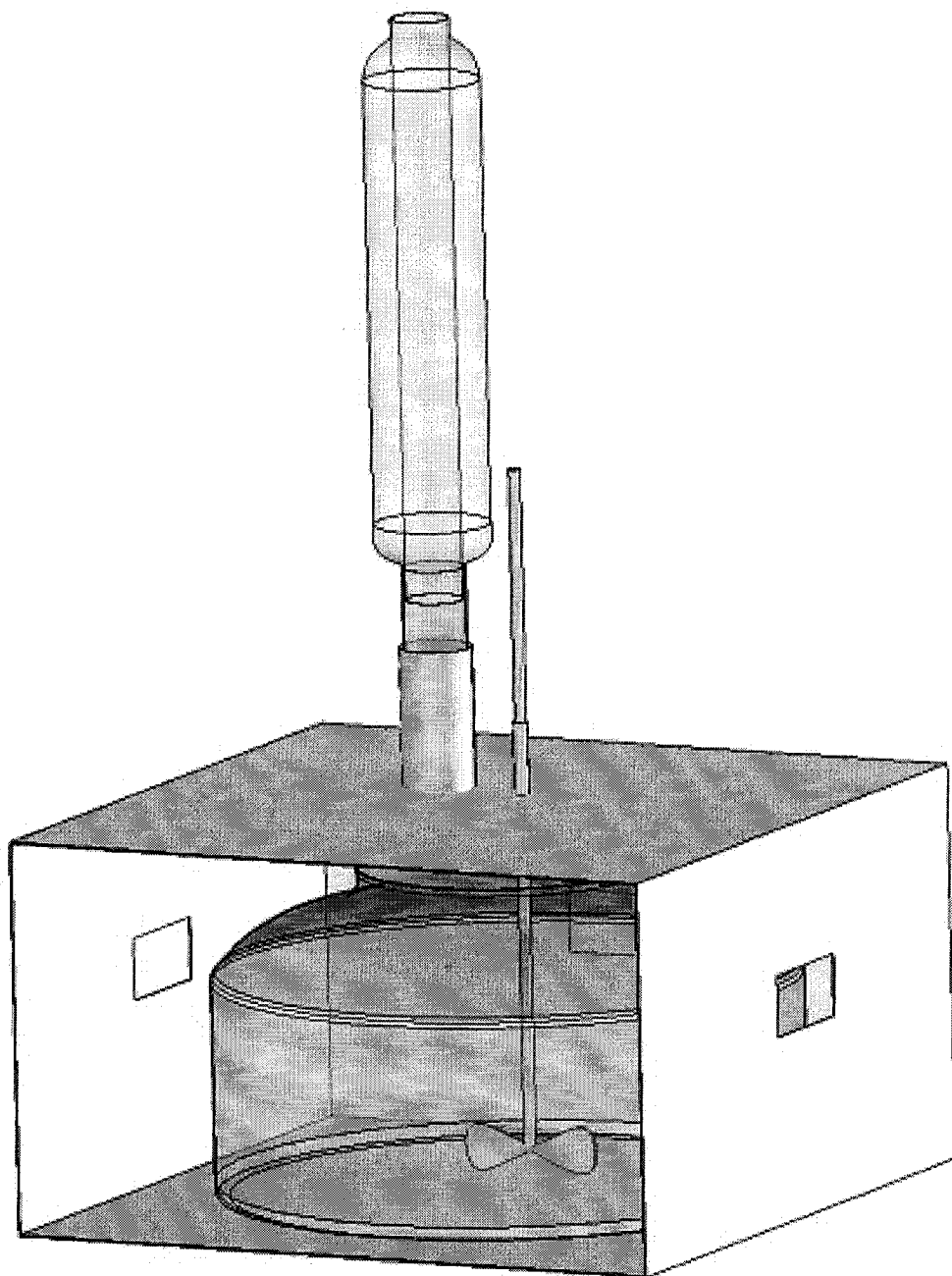
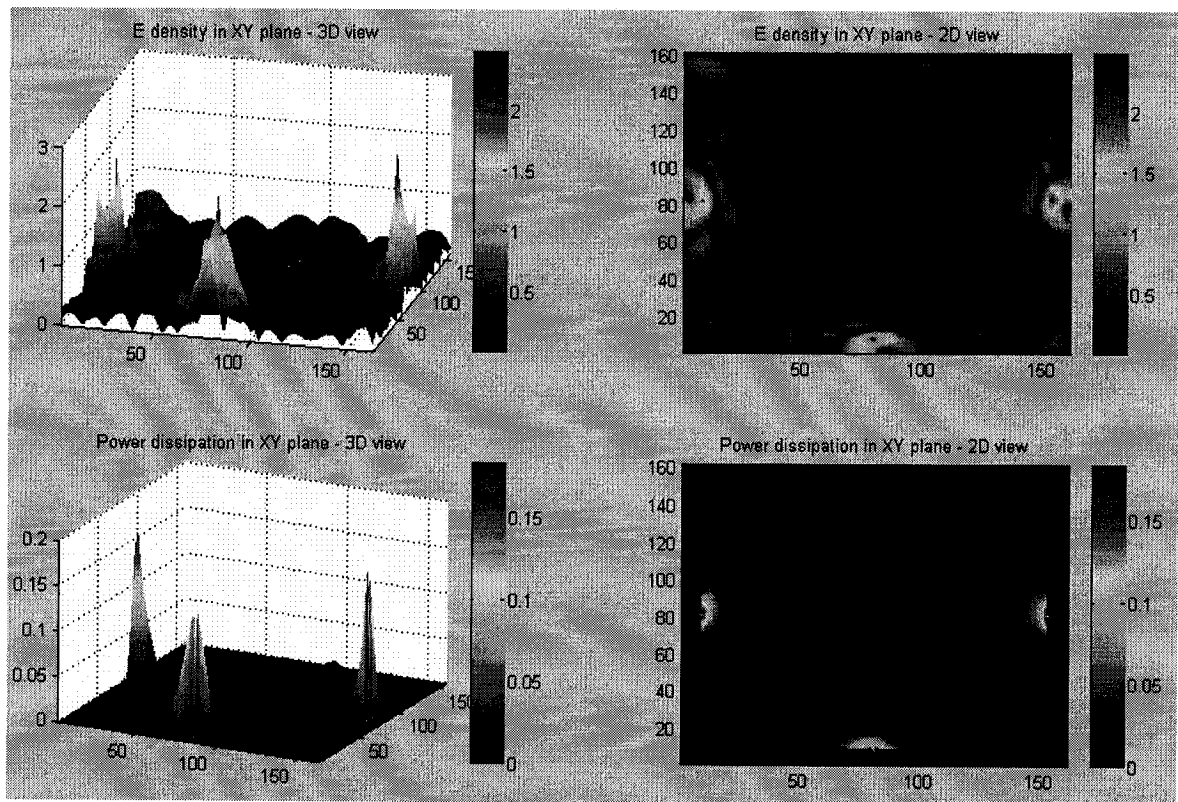


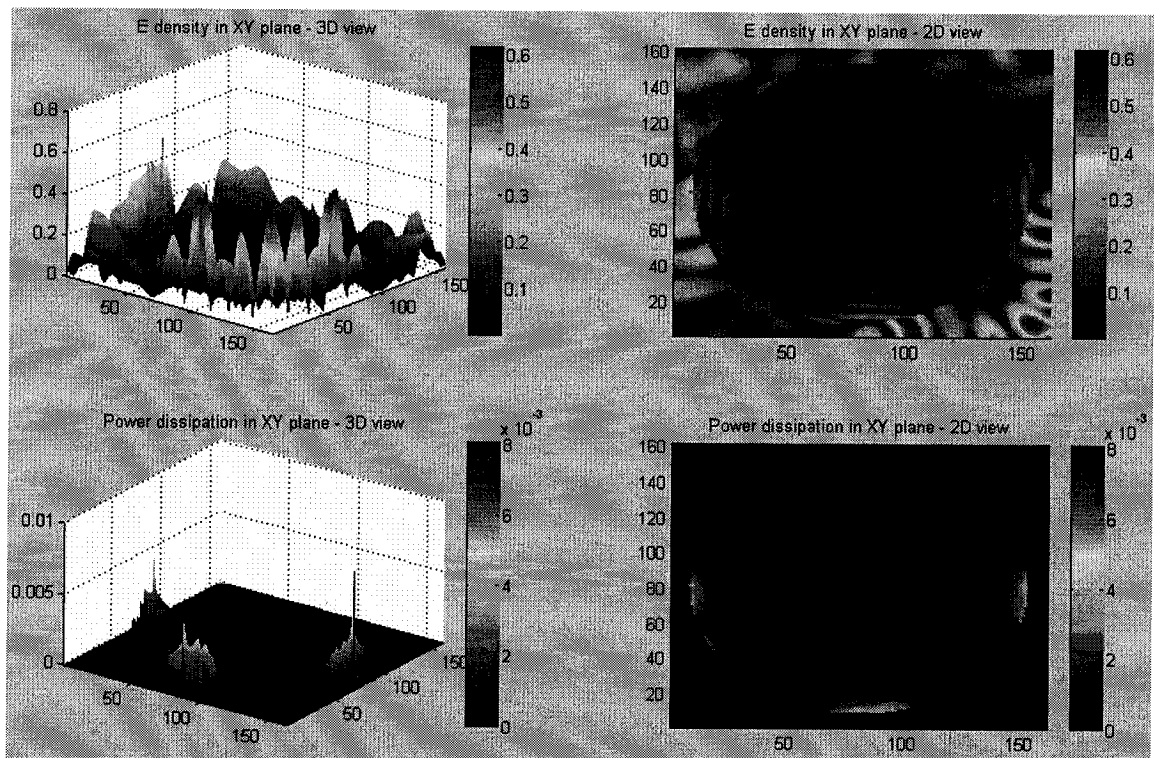
Fig. 10.15. Oven-type chemical reactor. The oven has a dimension of 80 x 80 x 60 cm. Three magnetrons are used and each one delivers a power output of 1 kW. The diameter of the glass container is 70 cm and the height is 50 cm giving a

total volume of 192 liters and the applicable capacity of about 100 liters when half filled.

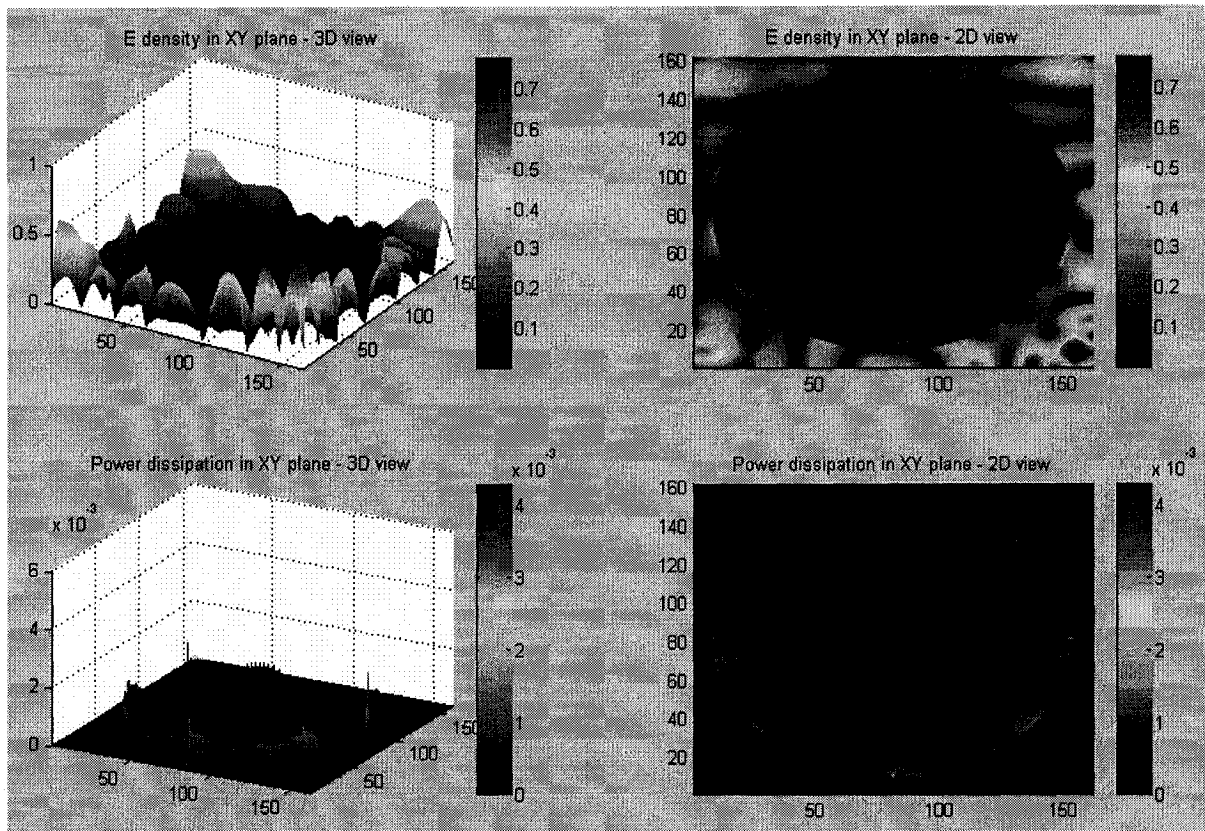
Figs. 10.16B, 10.17B, and 10.18B are the section plane 15 cm from the surface. For the low loss reactant, the container is surrounded by a more spread E field. Throughout the reactant layer, E field has very good uniformity with noticeable scale compared to the surrounding E field in the empty space. Similar pattern was observed at the location 3 cm from the bottom (Fig. 10.16 C). But the E field becomes weaker and weaker towards the center for the latter one. Power absorption is still higher in the locations corresponding to the three power entry port, but generally they are more spread and gets weaker towards the center. The absorption gets more uniform around the edge and taper towards the center. For medium loss, the E field is much weaker in the reactant than the surrounding empty space. Noticeable E field pattern can only be observed near the edge. Power absorption becomes very uniformly spread around the edge starting from 15 cm from the surface and gets even better in uniformity at 3 cm from the bottom. The absorption gets weaker towards the center and it drops much faster than in the low loss reactant. The absorption layer gets much thinner in the high loss reactant for both 15 cm from the surface and 3 cm from the bottom ones.



**A (Fig. 10.16)**



**B (Fig. 10.16)**



**C (Fig. 10.16)**

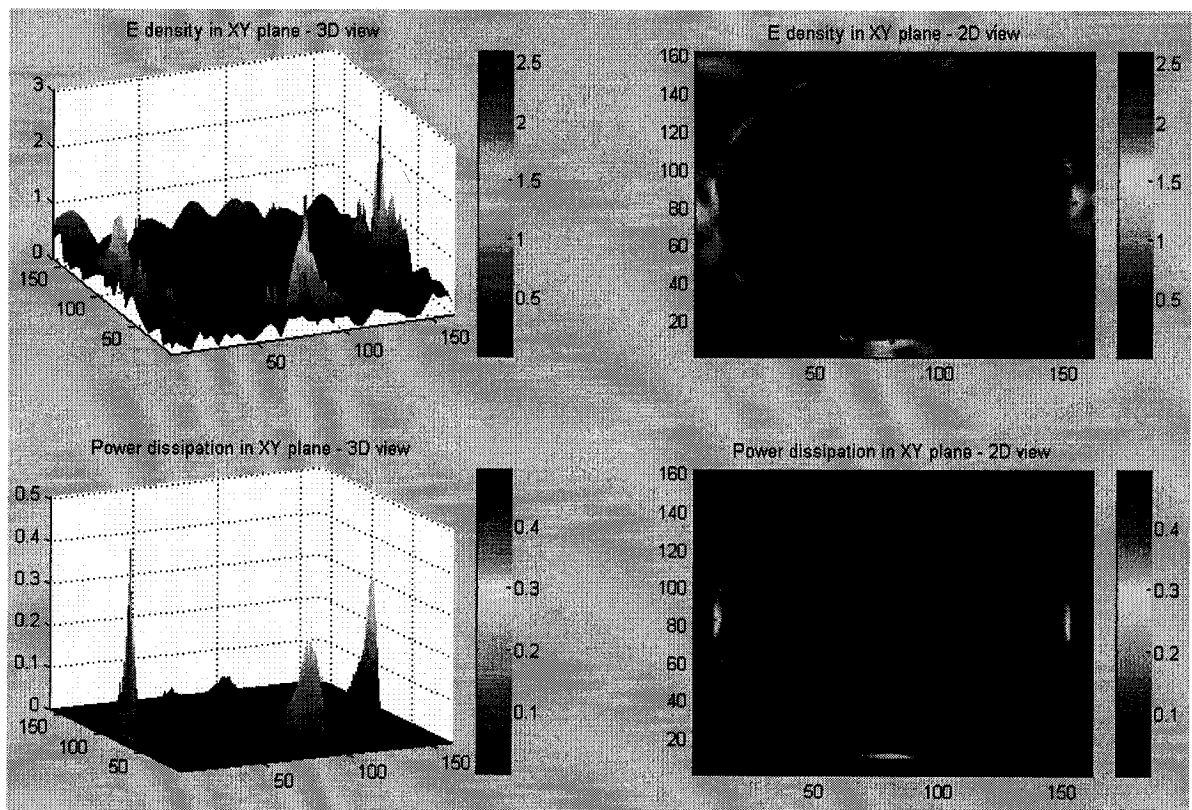
Fig. 10.16. The E field distribution and power dissipation at different depths in the reactor container. The container was filled with 30 cm in depth of low loss dielectric reactant with  $\epsilon' = 5$  and  $\epsilon'' = 1$ . Total meshing number of the whole cavity is:  $164 \times 164 \times 123$  cells. Results obtained after 3000 timesteps ( $2.79 \times 10^{-7}$  s). Simulation was run using an AMD Athlon 3800 dual core personal computer with 1Gb DDR400 PC-3200 memory. Simulation time was 2hr 10 min.

A: the top layer of the reactant corresponds to 30 cm from the bottom of the cavity.

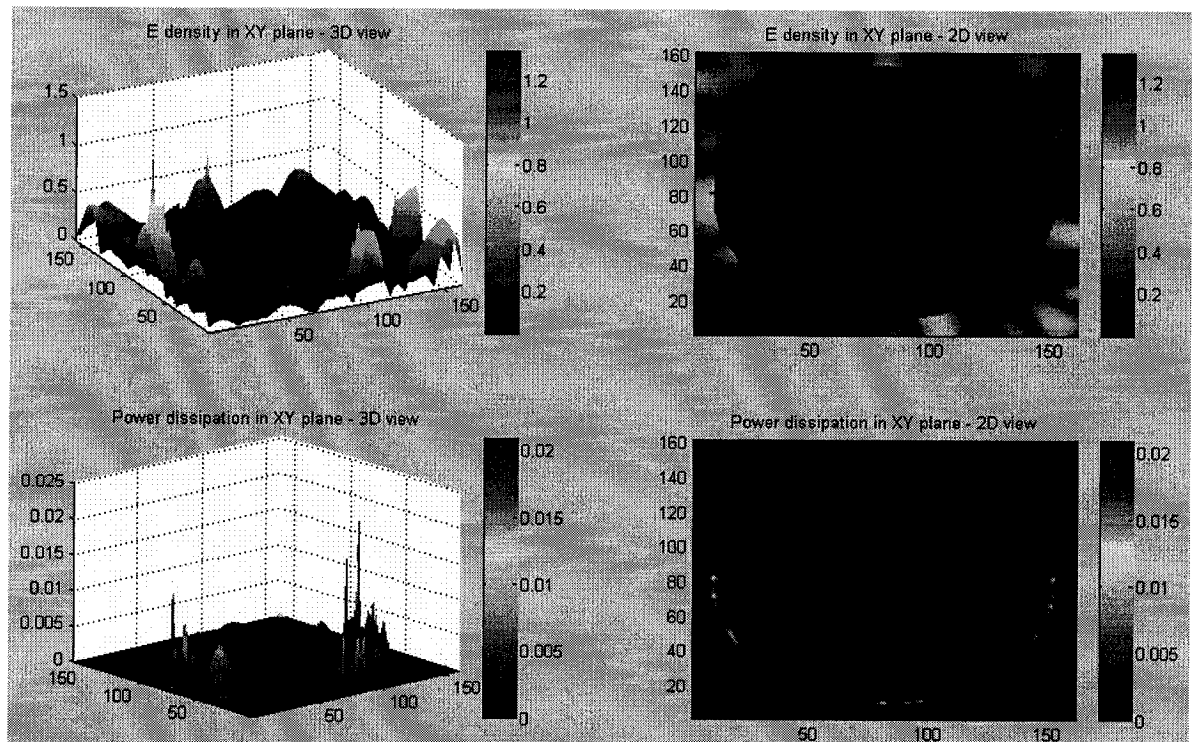
B: 15 cm from the bottom of the cavity.

C: 3 cm from the bottom of the cavity.

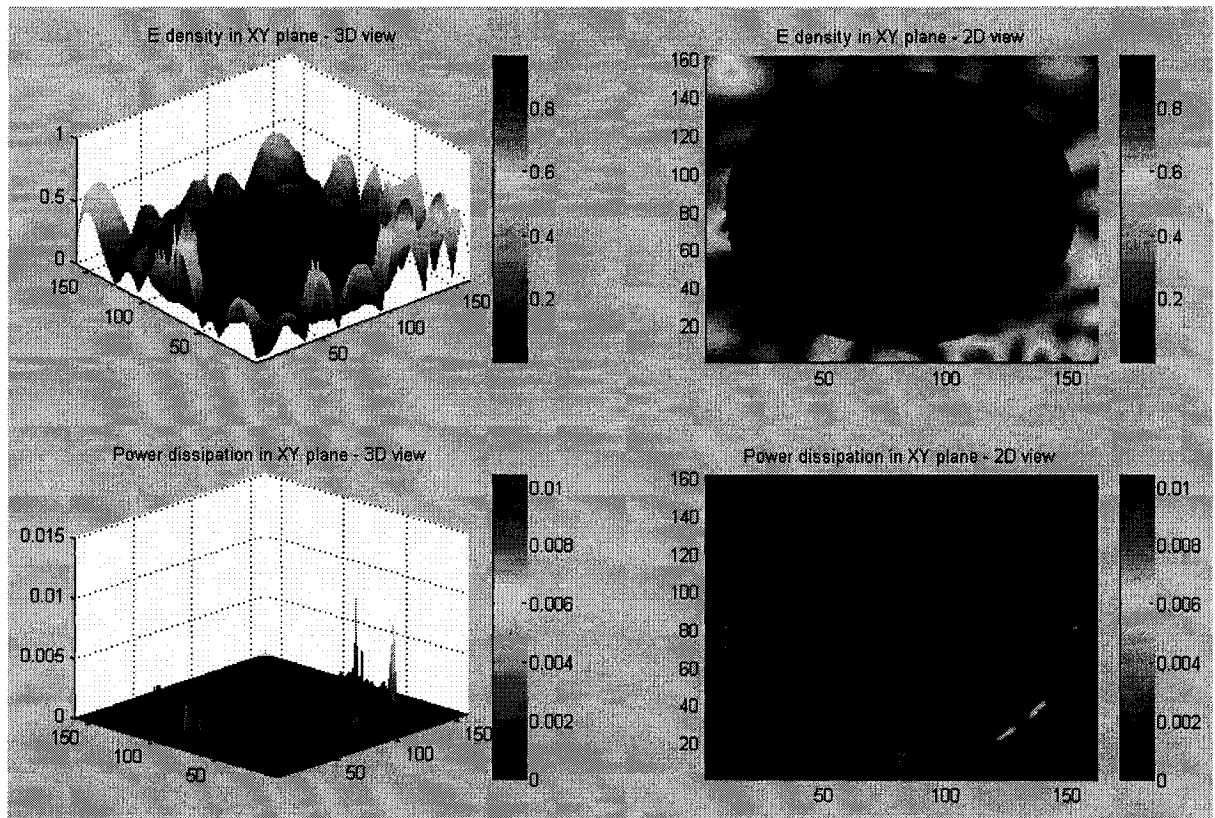




**A (Fig. 10.17)**



**B (Fig. 10.17)**

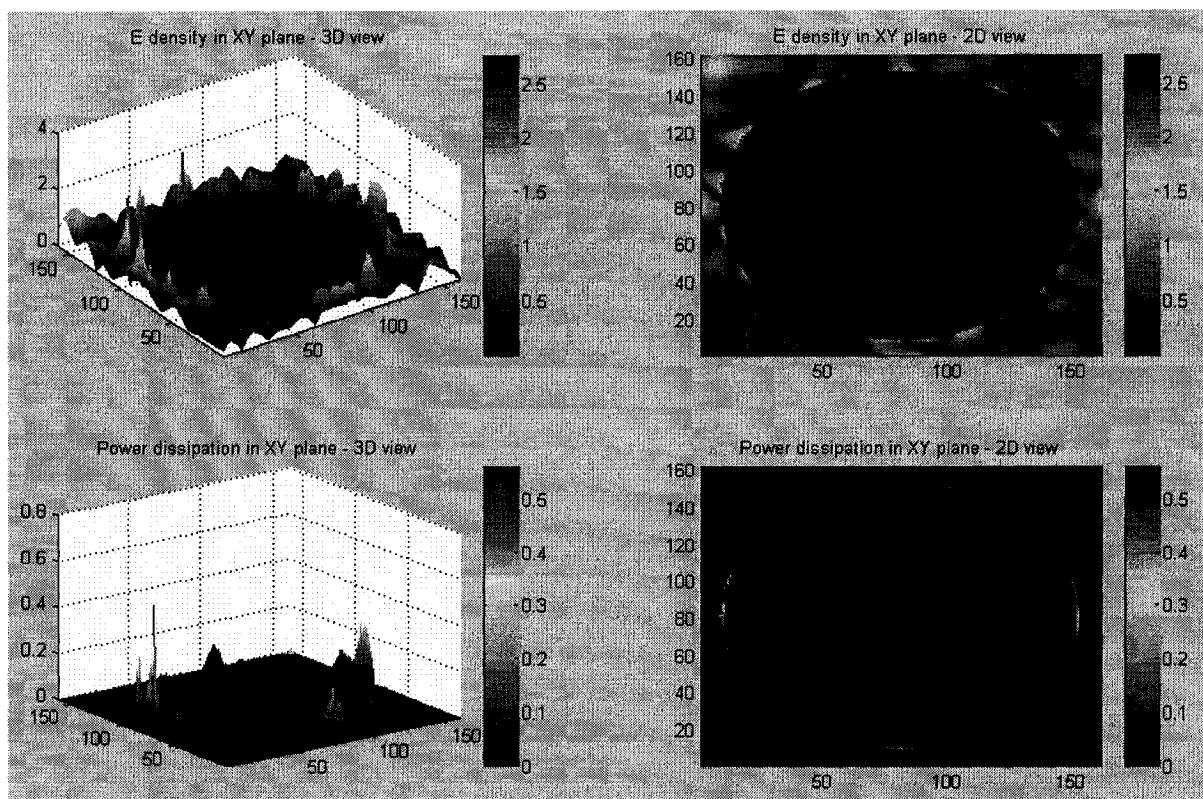


**C (Fig. 10.17)**

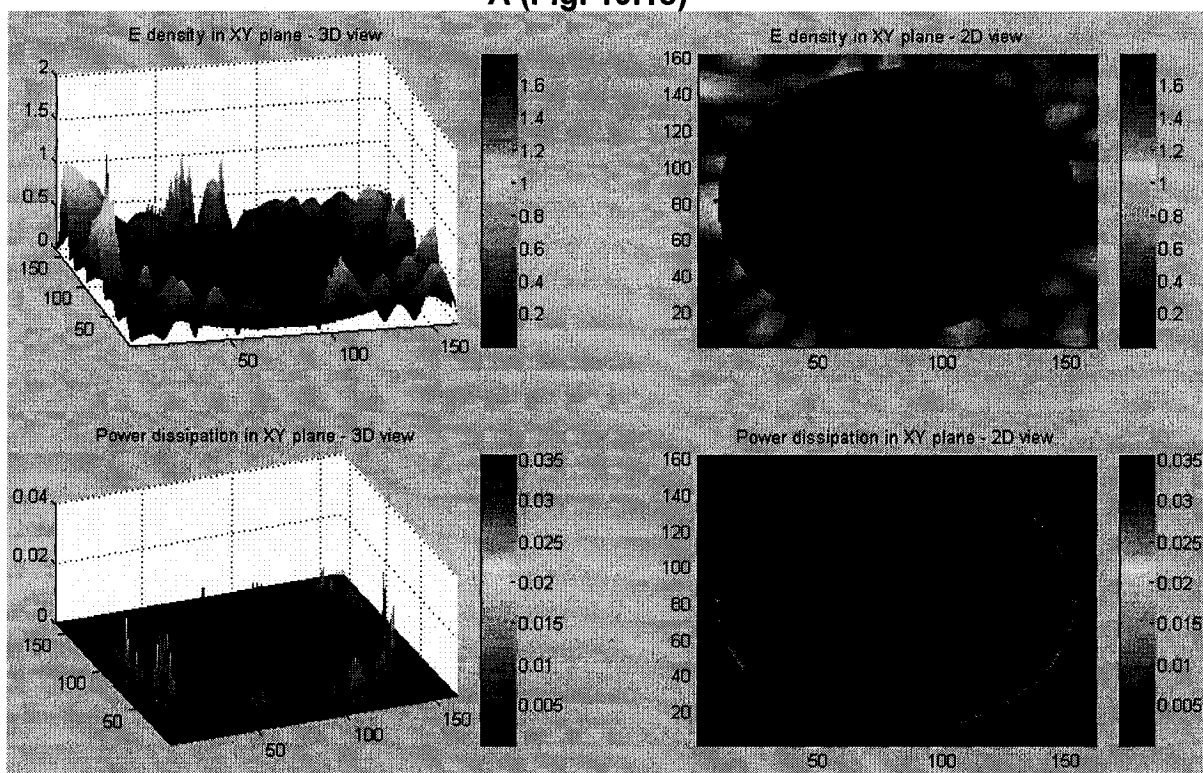
Fig. 10.17. The E field distribution and power dissipation at different depths in the reactor container. The container was filled with 30 cm in depth of medium loss dielectric reactant with  $\epsilon' = 20$  and  $\epsilon'' = 5$ . Total meshing number of the whole cavity is:  $164 \times 164 \times 123$  cells. Results obtained after 3000 timesteps ( $2.79 \times 10^{-7}$  s). Simulation was run using an AMD Athlon 3800 dual core personal computer with 1Gb DDR400 PC-3200 memory. Simulation time was 2hr 10 min.

- A: the top layer of the reactant corresponds to 30 cm from the bottom of the cavity.
- B: 15 cm from the bottom of the cavity.
- C: 3 cm from the bottom of the cavity.

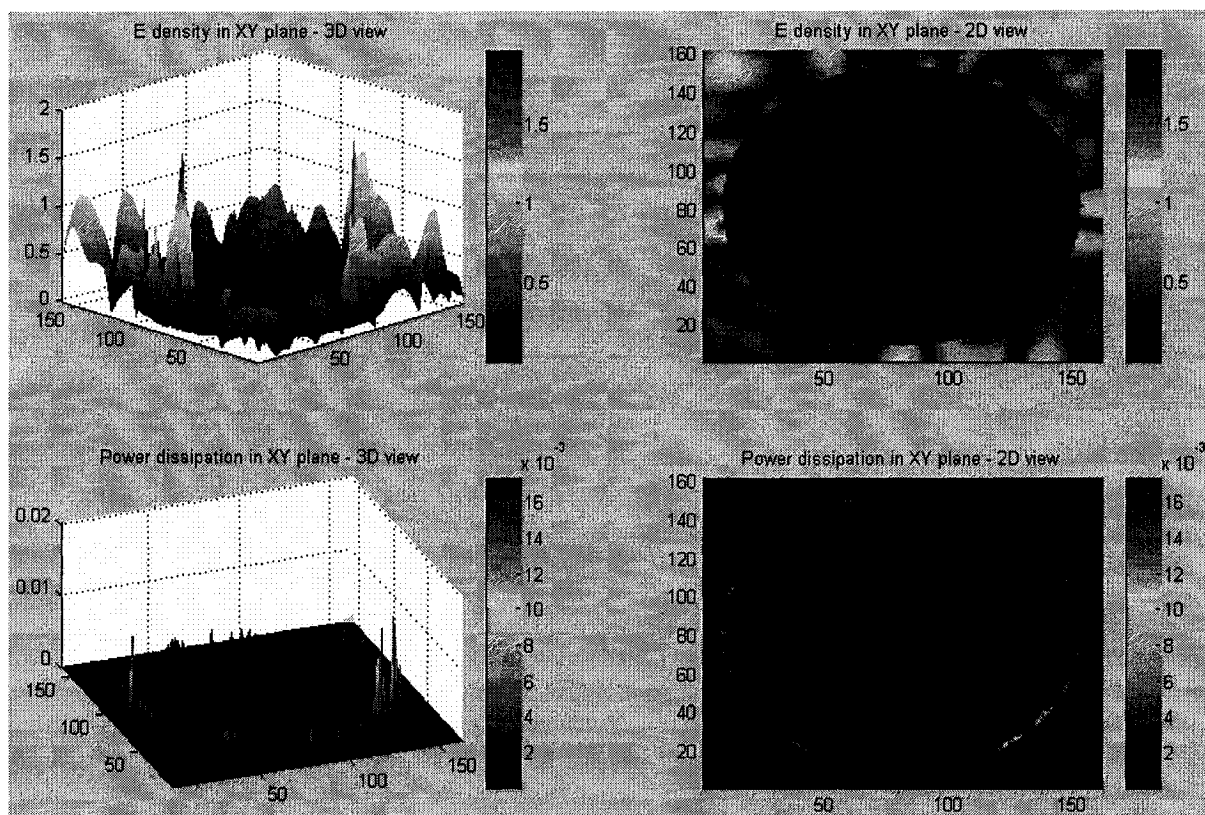




**A (Fig. 10.18)**



**B (Fig. 10.18)**



**C (Fig. 10.18)**

Fig. 10.18. The E field distribution and power dissipation at different depths in the reactor container. The container was filled with 30 cm in depth of High loss dielectric reactant with  $\epsilon' = 80$  and  $\epsilon'' = 15$ . Total meshing number of the whole cavity is:  $164 \times 164 \times 123$  cells. Results obtained after 3000 timesteps ( $2.79 \times 10^{-7}$  s). Simulation was run using an AMD Athlon 3800 dual core personal computer with 1Gb DDR400 PC-3200 memory. Simulation time was 2hr 10 min.

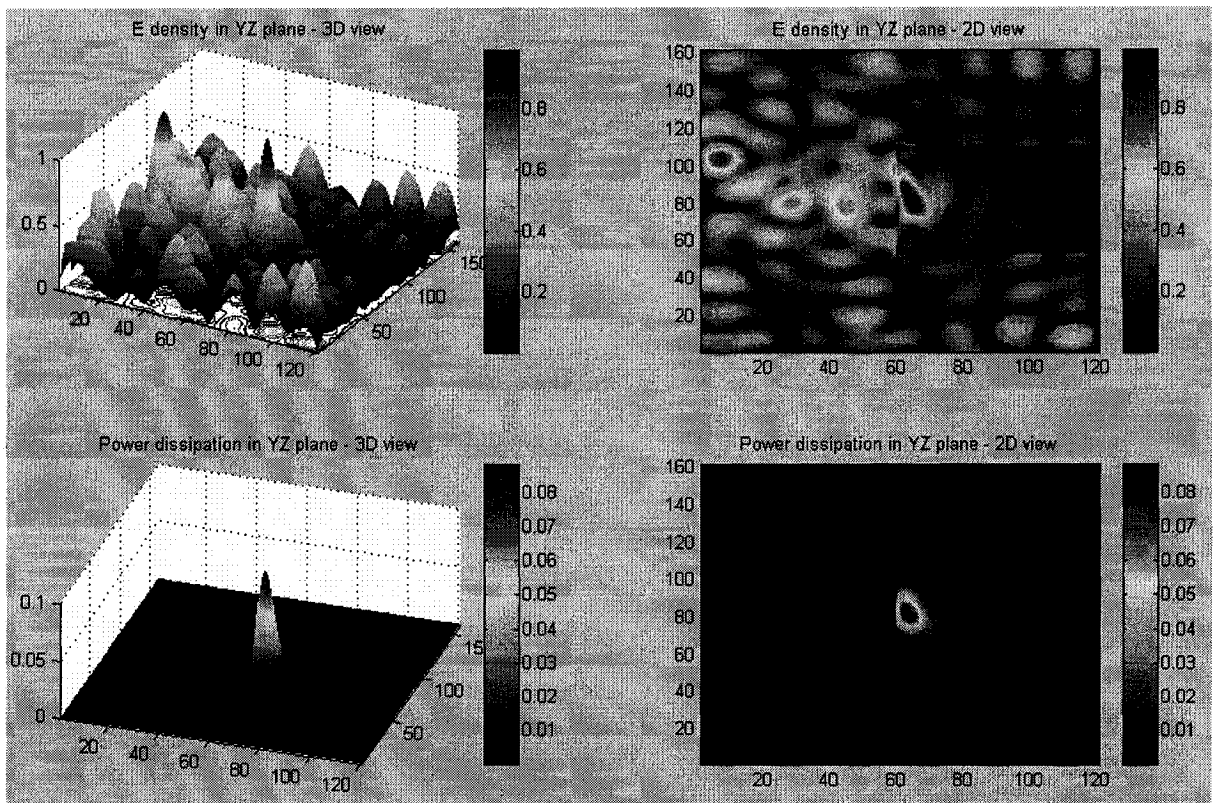
A: the top layer of the reactant corresponds to 30 cm from the bottom of the cavity.

B: 15 cm from the bottom of the cavity.

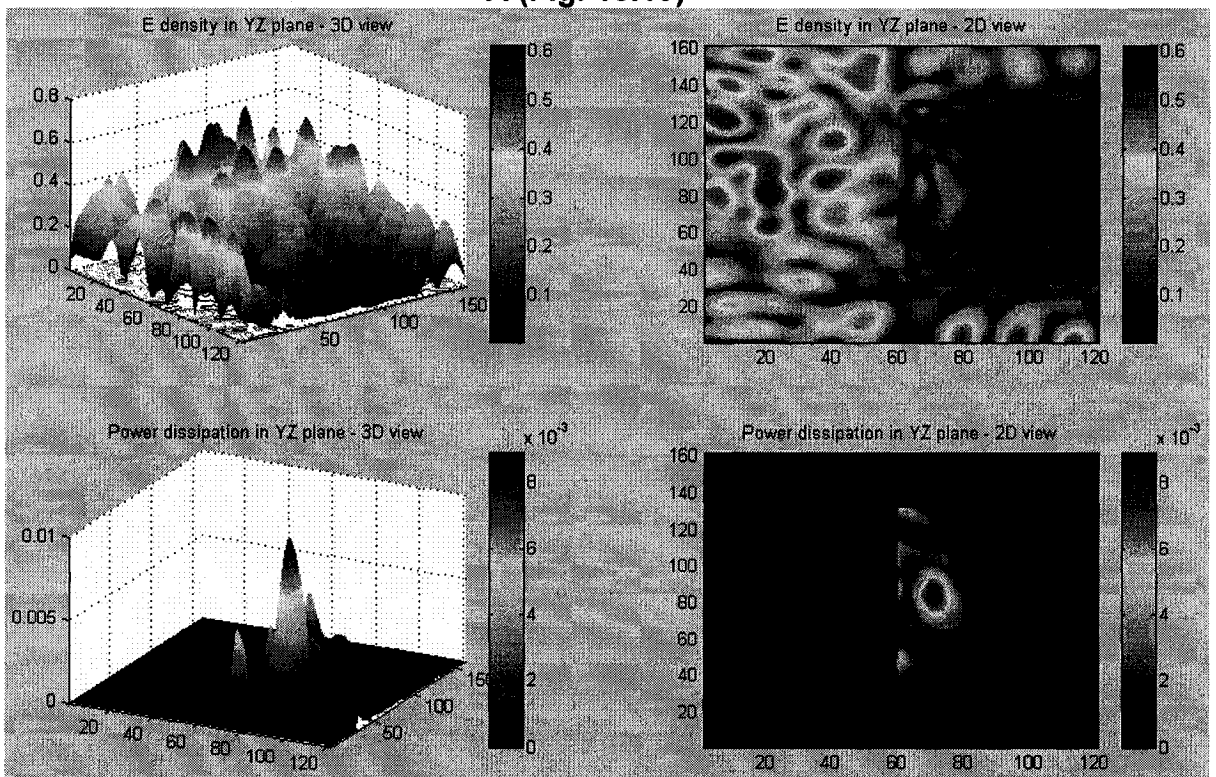
C: 3 cm from the bottom of the cavity.

Figures 10.19 to 10.21 show the XZ section plane with different depths along the Y axis. Fig. 10.19A shows the E field distribution and power absorption on the XZ section plane 5 cm from the container edge in the Y direction for the low loss reactant. The E field has comparable magnitude with the surrounding empty space. A very strong E field spot was observed about 2 cm below the surface. In consequence, very strong power absorption was observed at this location. Another 10cm down the X direction, the E field is still visibly strong with a certain pattern. It gets weaker towards in bottom of the container. A strong absorption spot was observed again at this plane with about 1 cm further down from the surface. The whole top part has relatively strong power absorption and gets weaker towards the bottom of the cavity. Fig. 10.19C shows the XZ section plane in the middle of the X direction. It shows clearly that the E field taper towards the bottom of the container. The power absorption has two strong spots near the power entry port. The absorption gets weaker towards the center and towards the bottom of the container.

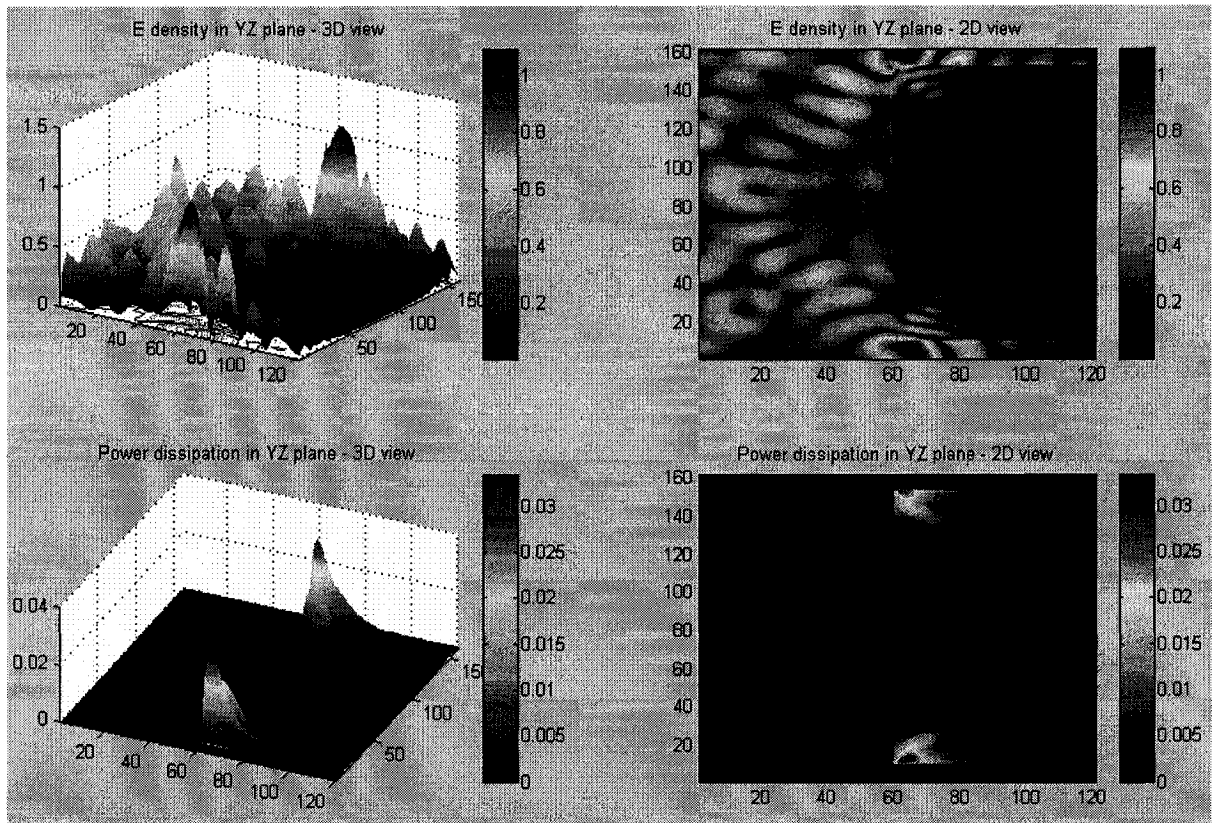
For the medium loss reactant, the XZ section at 5 cm as shown in Fig. 10.20A is very similar to that of the low loss one in both pattern and strong absorption spot in similar location. When it comes to the section plane at 15 cm from the edge, it showed more evidence of limited penetration with the locations 4-5 cm from the surface and from the side very low absorption. The absorption layer gets even thinner at the XZ section in the middle of the Y direction. For high loss reactant, the absorption layers get very thin in all three section planes as shown in Figs. 10.21



**A (Fig. 10.19)**



**B (Fig 10.19)**



**C (Fig. 10.19)**

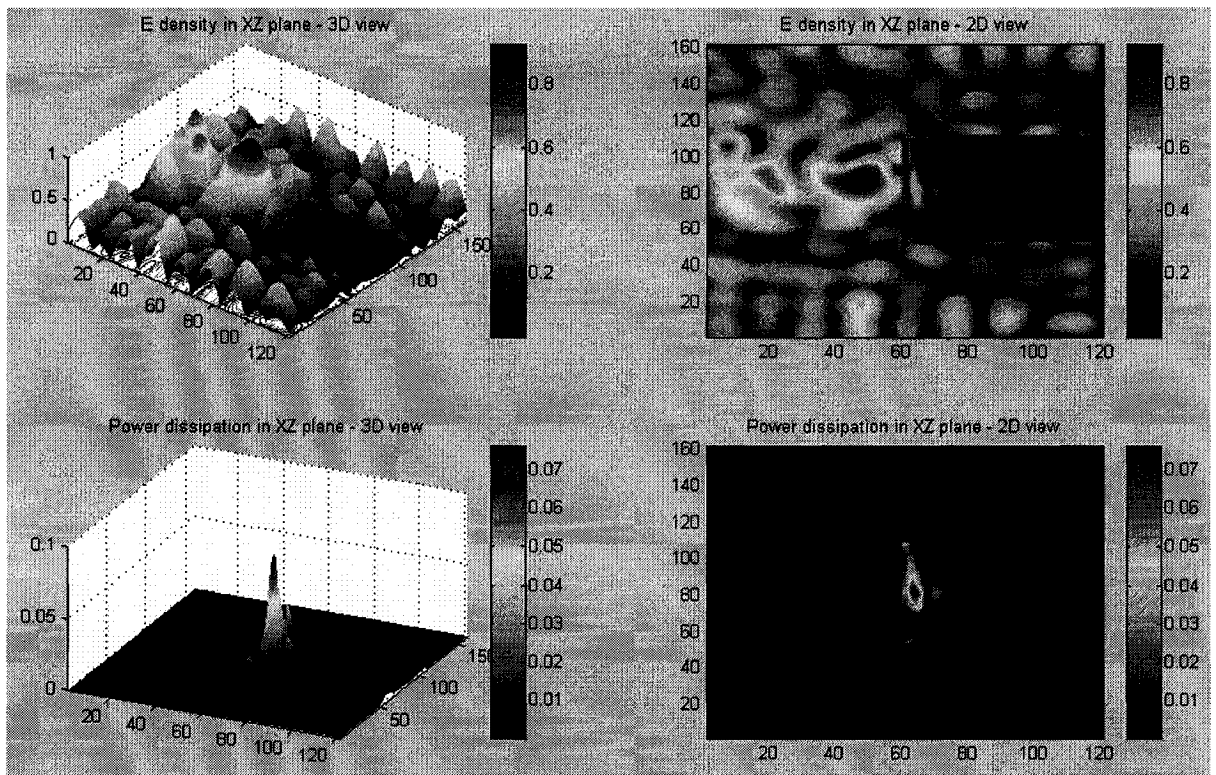
Fig. 10.19. The E field distribution and power dissipation at different distances from the X direction (YZ plane) into the reactor container. The container was filled with 30 cm in depth of low loss dielectric reactant with  $\epsilon' = 5$  and  $\epsilon'' = 1$ . Total meshing number of the whole cavity is:  $164 \times 164 \times 123$  cells. Results obtained after 3000 timesteps ( $2.79 \times 10^{-7}$  s). Simulation was run using an AMD Athlon 3800 dual core personal computer with 1Gb DDR400 PC-3200 memory. Simulation time was 2hr 10 min.

A: YZ plane 5 cm from the container side wall into the container

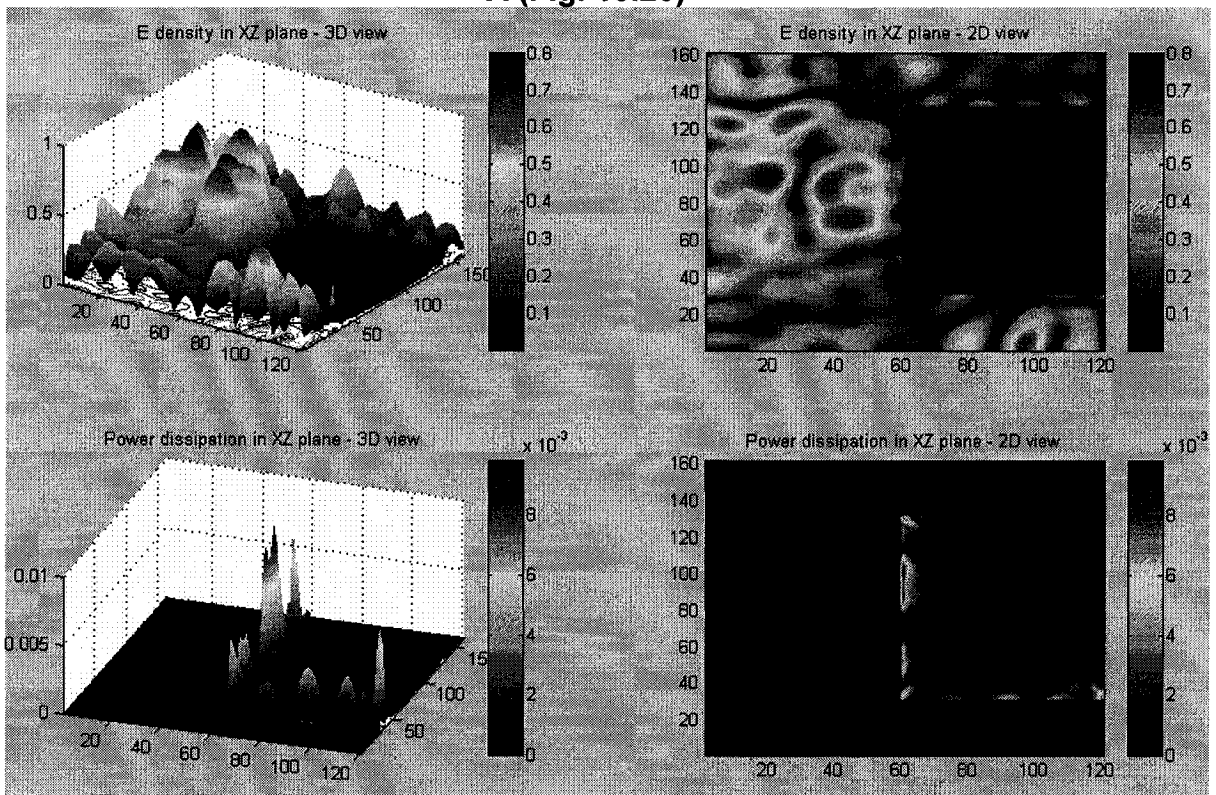
B: YZ plane 10 cm from the container side wall into the container

C: YZ plane in the middle of the container corresponding to 36cm from the container side wall

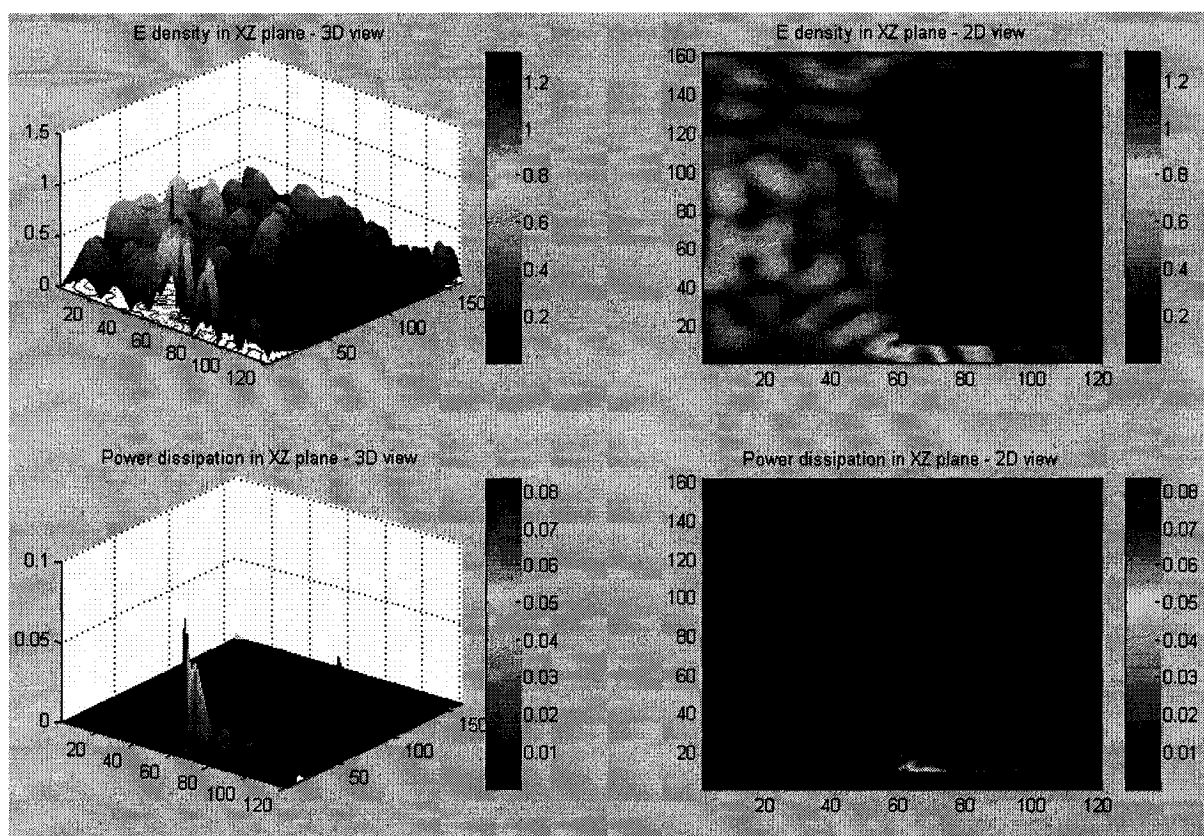




**A (Fig. 10.20)**



**B (Fig. 10.20)**



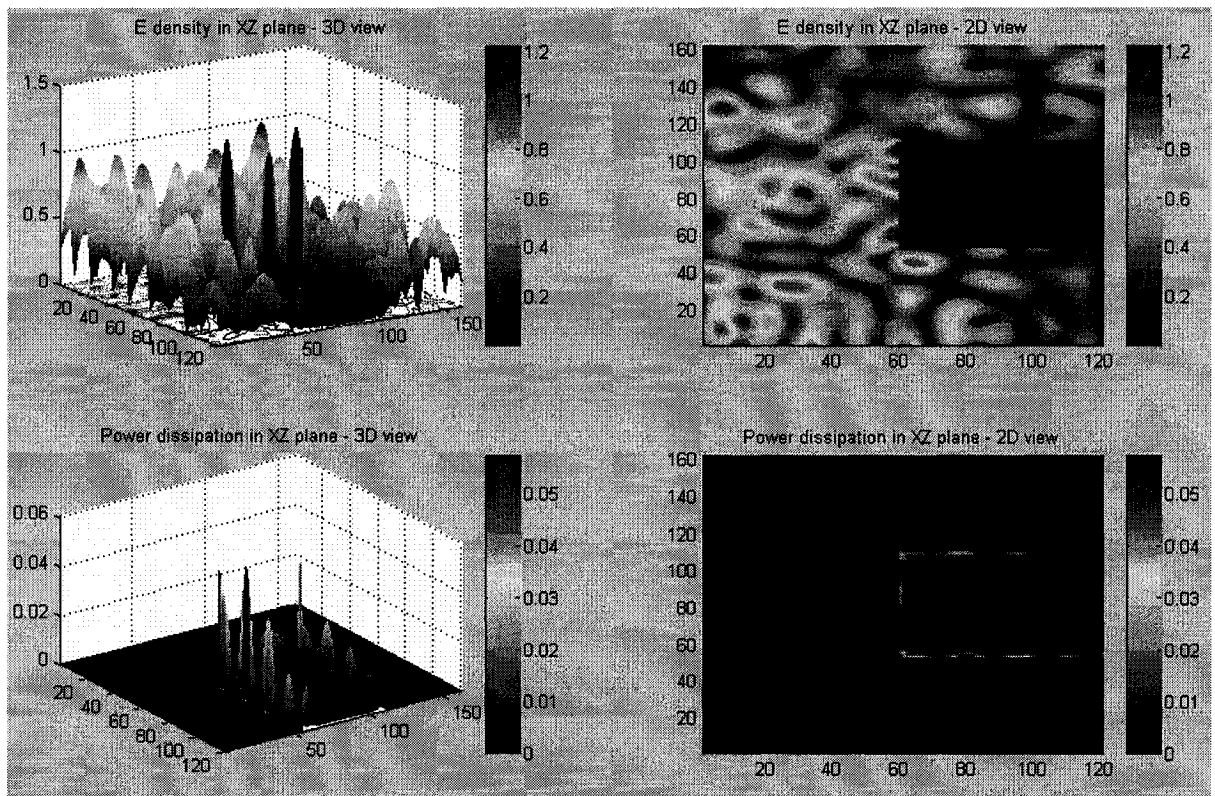
**C (Fig. 10.20)**

Fig. 10.20. The E field distribution and power dissipation at different distances from the X direction (YZ plane) into the reactor container. The container was filled with 30 cm in depth of medium loss dielectric reactant with  $\epsilon' = 20$  and  $\epsilon'' = 5$ . Total meshing number of the whole cavity is:  $164 \times 164 \times 123$  cells. Results obtained after 3000 timesteps ( $2.79 \times 10^{-7}$  s). Simulation was run using an AMD Athlon 3800 dual core personal computer with 1Gb DDR400 PC-3200 memory. Simulation time was 2hr 10 min.

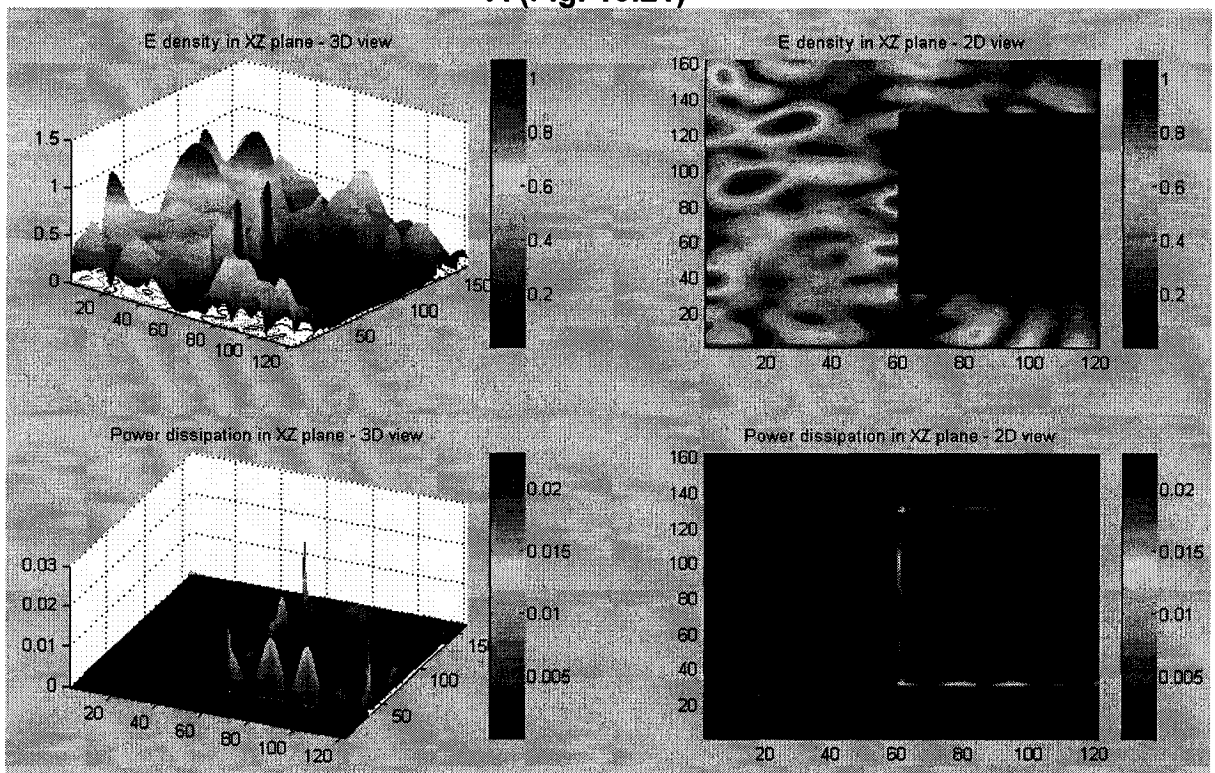
A: YZ plane 5 cm from the container side wall into the container

B: YZ plane 10 cm from the container side wall into the container

C: YZ plane in the middle of the container corresponding to 36cm from the container side wall

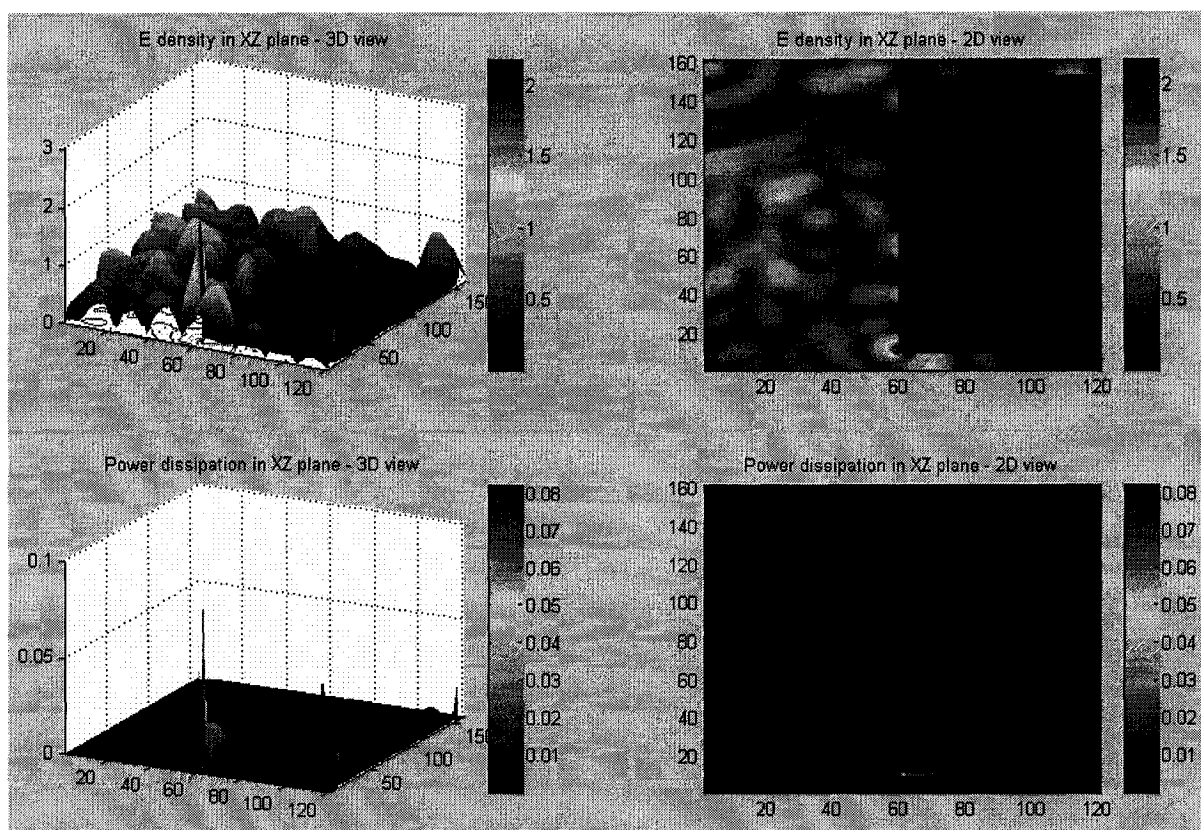


**A (Fig. 10.21)**



**B (Fig. 10.21)**





**C (Fig. 10.21)**

Fig. 10.21. The E field distribution and power dissipation at different distance from the X direction (YZ plane) into the reactor container. The container was filled with 30 cm in depth of high loss dielectric reactant with  $\epsilon' = 80$  and  $\epsilon'' = 15$ . Total meshing number of the whole cavity is:  $164 \times 164 \times 123$  cells. Results obtained after 3000 timesteps ( $2.79 \times 10^{-7}$  s). Simulation was run using an AMD Athlon 3800 dual core personal computer with 1Gb DDR400 PC-3200 memory. Simulation time was 2hr 10 min.

- A: YZ plane 5 cm from the container side wall into the container
- B: YZ plane 10 cm from the container side wall into the container
- C: YZ plane in the middle of the container corresponding to 36cm from the container side wall

The power dissipation in each horizontal layer from the top to the bottom and dissipation in each circular layer in the radius direction was calculated from simulated result using the C language code. Part of the code is shown in Appendix 4. Power dissipations into different horizontal layer for low loss, medium loss and high loss reactants is shown in Fig. 10.22. From the surface down into the reactant, for the low loss one, power first increases then continuously drops up to about 15cm level. After that even there is increase and decrease towards the bottom of the container; the power dissipation was generally low with only about 8% of the top layer. For medium loss and high loss reactants, power continuously drops from the top surface down into the container. At the end, slight increase was observed for the medium loss reactant and very strong increase was found for the high loss one. From the top surface, power dropping rate increases for greater depths into the reactant from low loss to medium loss to high loss reactants. For the low loss reactant, power dissipation drops to the lowest level at about 15 cm, about 8 cm for the medium loss and 2 cm for the high loss reactant.

The power dissipation in circular layer in the radius direction for low loss, medium loss and high loss reactants was shown in Fig. 10.23. For all three type of reactants, total dissipation drops from the outer circular layer as goes towards the center. The power dissipation starts to level off at a radius of 15 cm which is 20 cm into the reactant. It is about 29 cm (6 cm from the outer layer) for medium loss and 33 cm (2 cm from the outer layer) for high loss reactant.

Penetration depth is a frequently used term in microwave power applications. It is defined as the distance that the energy drops to 1/e of its original value. The penetration depth can be written as:

$$D_p = \frac{1}{2\pi f} \sqrt{\frac{2}{\mu_0 \epsilon_0 \epsilon'} \left( \sqrt{1 + \left( \frac{\epsilon''}{\epsilon'} \right)^2} - 1 \right)} \quad (10.41)$$

From this equation, penetration depths for low loss, medium loss and high loss materials are: 8.8cm, 3.5 cm and 2.3 cm. Penetration depths obtained from

simulation are: 7.3 cm, 3 cm, and 1 cm which is very close to what the one calculated from the penetration depth equation. However, the penetration depth works best in one dimensional situation. In the microwave cavity, since power is distributed not uniformly in the cavity, the penetration depth can not be simply applied. Even the power penetration follows the same rule, therefore the power distribution is not uniform at the same depth in the reactant.

From the power dissipation patterns of Figs 10.16-10.21 and power dissipation curves 10.22 and 10.23 it can be seen that power is that for the low loss reactant, power penetration is mainly located about 8 centimeter from the top or the sides, and 3 cm for medium loss and 1 cm for the high loss reactant. Besides, the heating is higher from the top and gets negligibly low at the bottom. Therefore the use of this type of reactor is not practical. With the heating focused on top layers, convection heating becomes difficult making the uniformity of heating difficult. For low loss reactant, agitation through stirrer could partially solve the problem, but for medium loss and high loss reactants this becomes very difficult even with stirrer.

### **10.6 Simulation of a microwave chemical reactor/extractor**

From the previous section it can be seen that with a cavity type chemical reactor/extractor, the performance is restricted by the heating from top part of reactants. A microwave chemical reactor/extractor should be constructed in the way that can at least make convective heating possible if the power dissipation can not be uniform throughout the container. Fig. 10.24 shows a design of a microwave chemical reactor/extractor that can be used to carry out chemical synthesis or extractions. The system consists of a cavity with 8 magnetrons (two on each vertical wall), a condensing system and a stirrer. There are two possible ways to handle the power entry port: by using an inner microwave transparent and chemically inert container like Teflon container placed inside the metal outer cavity; or seal the power entry port with the Teflon material so that reactant will not go into the waveguide. The reactor simulated here has a dimension of 0.6 x

0.6 x 1.8 m. The total volume is 648 liters and the applicable volume is about 400 liters.

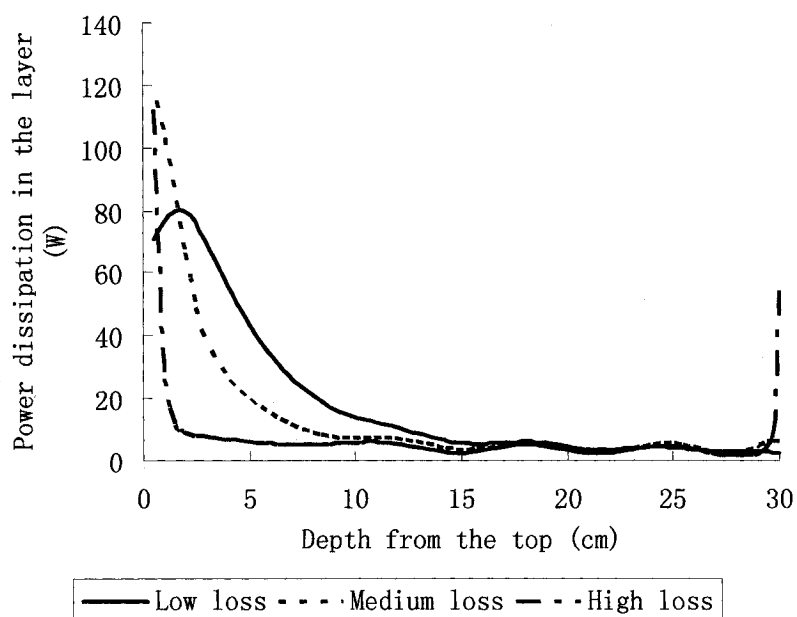


Fig. 10.22. Power dissipations in each horizontal layer from the top to the bottom for low loss, medium loss and high loss reactants.

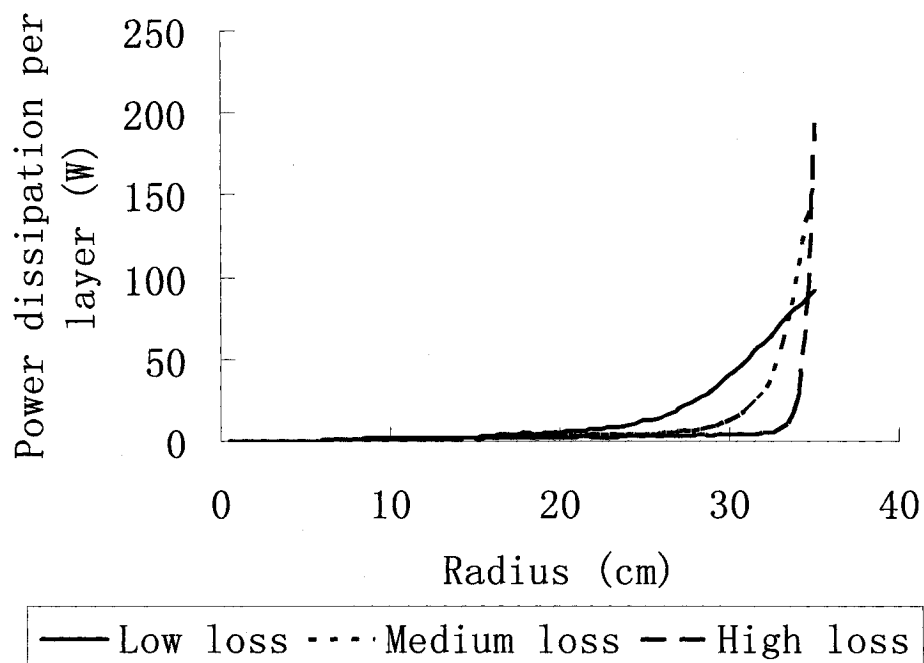


Fig. 10.23. Power dissipations in each circular layer in the radial direction for low loss, medium loss and high loss reactants.

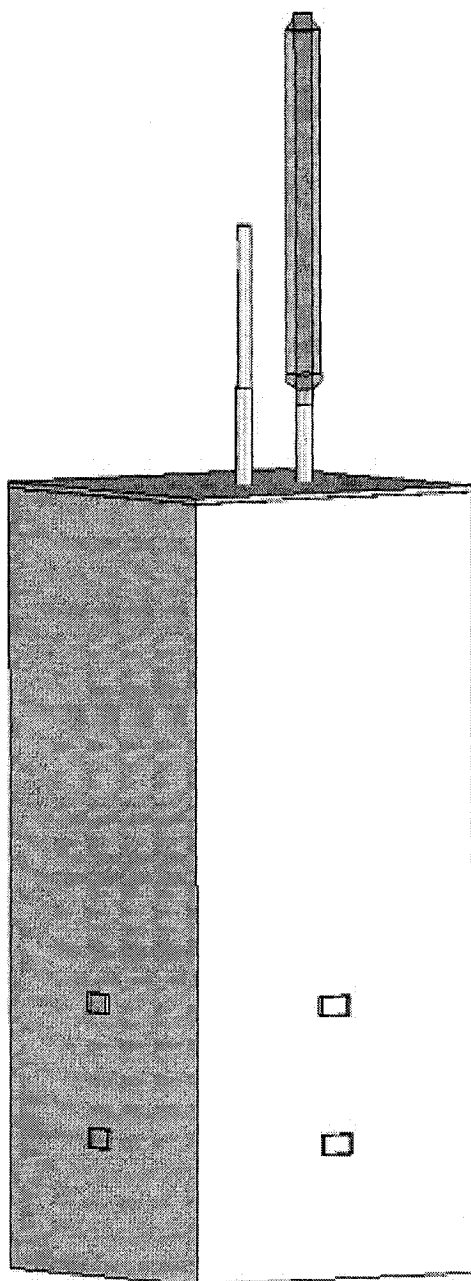


Fig. 10.24. A microwave-assisted chemical reactor/extractor. The dimension is: 0.6 x 0.6 x 1.8 m. Totally 8 magnetrons (1 kW of each) were used with two of them on each vertical wall. The 4 lower power entry ports are located 15-19 cm from the bottom and the 4 upper power entry ports are located 35-39 cm from the bottom.

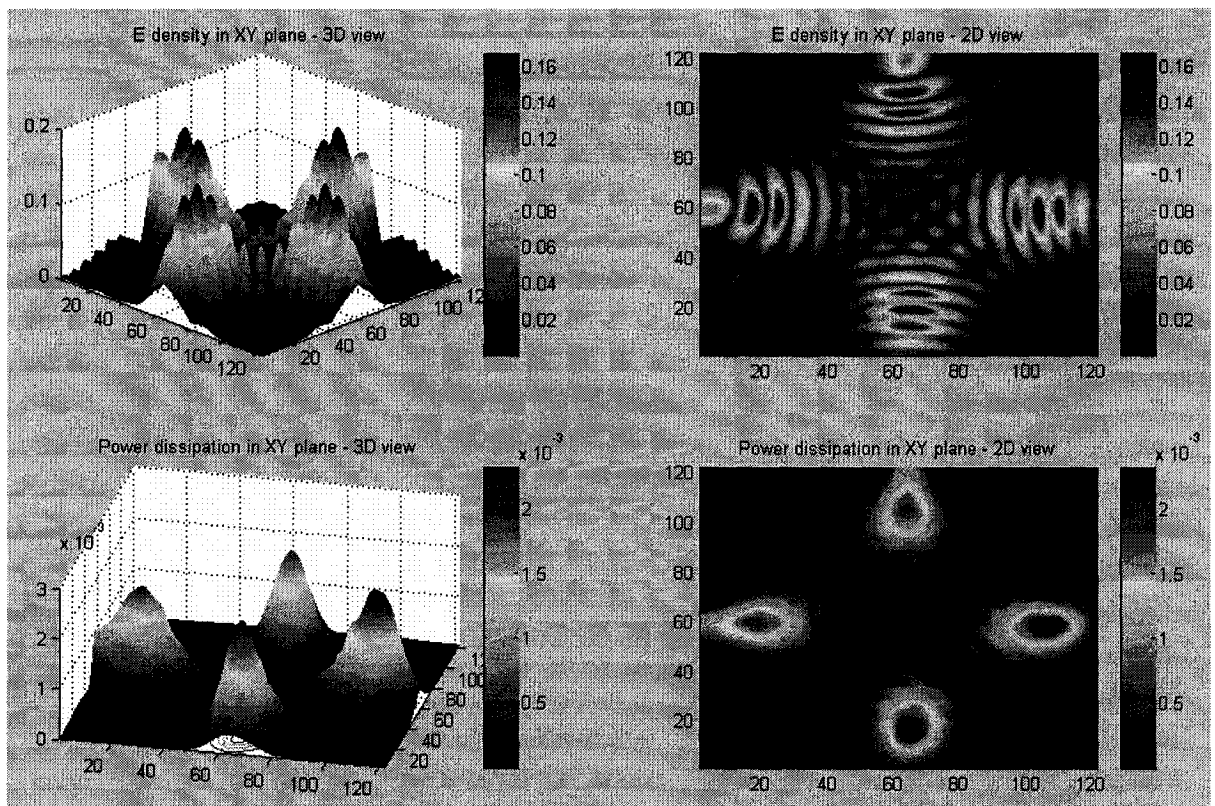
The E field and power dissipation into a horizontal layer at different depth was presented in Fig. 10.25. The location 5 cm from the bottom is 10 cm from the lower power entry port and the location at 45 cm is about 10 cm from the upper power entry port. As a result, their E field distribution and power dissipation patterns are similar as shown in Fig. 10.25 A and C. The E field distribution has four strong zones after each power entry port. The power dissipation reaches the highest about 8 cm from the wall instead of getting highest at the outer layer. Locations at 16 and 36 cm fall in the range of power entry ports. They also have similar power dissipation and E field distribution patterns as shown in Figs. 10.25 B and D. At these two locations, strongest E field distribution and the power dissipation were observed near the power entry port and drop quickly when getting deeper into the container. At 75 cm (40 cm from the upper power entry ports), the E field distribution becomes very weak and the power distribution are negligibly low as shown in Fig. 10.25 E. The E field and power dissipation becomes more uniformly distributed in the center instead of that near the wall.

Fig. 10.26 shows the E field distribution and power dissipation in the XZ plane from at different distances from the wall. At 2.5 cm and 5 cm, the E field and power dissipation are focused on two small locations right after the power entry port. At 15 cm, the E field distribution and power dissipations are more spread and over lapping was observed between the microwaves from the upper and lower ports. At 25 cm and in the middle location (35 cm), the strong E field distribution and power dissipation is mainly due to the 4 power entry locations at the front and back walls.

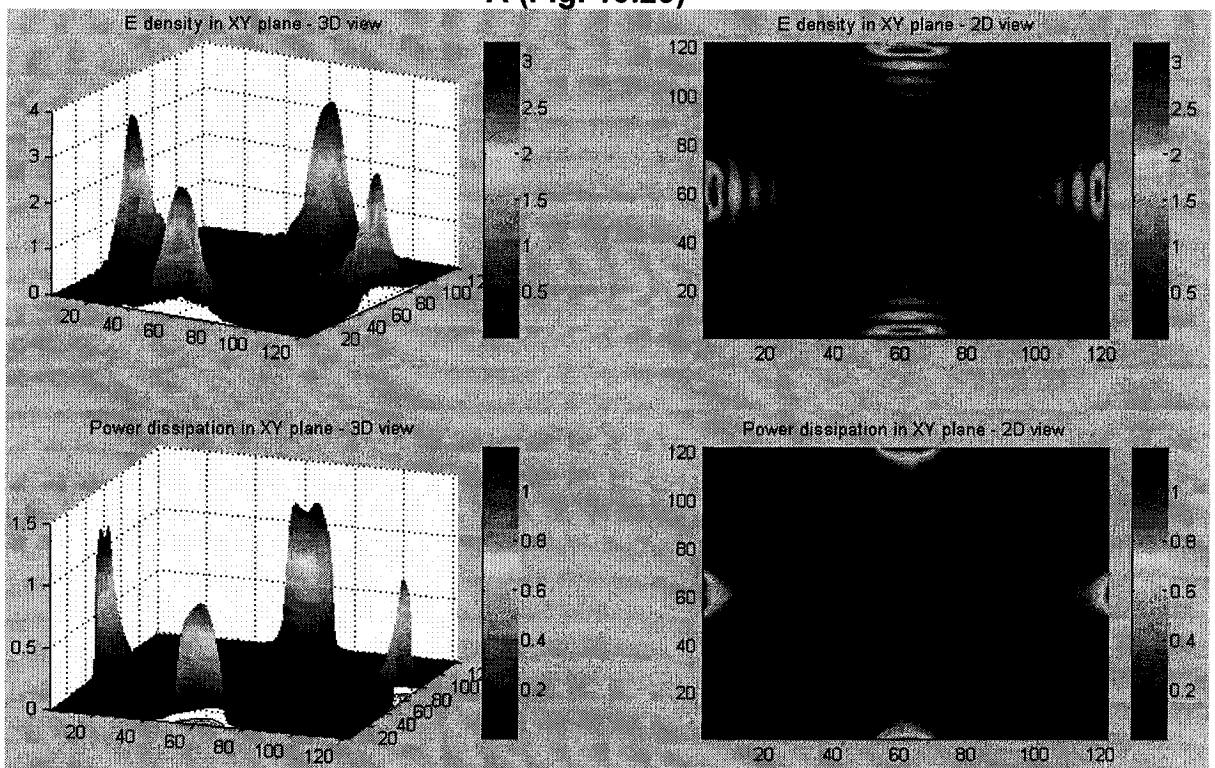
From the E field distribution and power dissipation patterns shown in Figs. 10.25 and 10.26, it can be seen that reflection factors is almost negligible. In Fig. 10.25 B and D, when the E field is strong near the entering ports, it drops very quickly towards the center because it travels in the lossy dielectric medium. By the time it reaches any wall, it already gets so weak that there will be no contribution to the pattern change. When it is a little far from the power entry ports in the upper or lower direction, reflection did happen, but they are so low that they will not contribute much to the general heating profile.

E field distribution and power dissipation for medium loss reactants are presented in Figs. 10.27 and 10.28 for the horizontal layers and the XZ plane layers. For all the horizontal locations, different from the low loss reactants, the strongest E field distribution and power dissipation were observed to be close to the wall. Interaction between the microwaves entering from the ports on different wall is not likely to happen because they become so weak before travelling to the point of interaction. At 75 cm from the bottom, sign of interaction was observed but the E field and power dissipation are negligibly weak. The XZ plane E field distribution and power dissipation at 2.5, 5 cm and the location in the middle (35 cm) are similar to that in the low loss reactant. But for the 15cm one, strong E field distribution and power dissipation were observed near one wall.

Power dissipation in the low loss and medium loss reactants on horizontal layer and on the square layers are presented in Figs. 10.29 and 10.30, respectively. It can be seen from Fig. 10.29 that from the bottom to the top power dissipation are mainly focused at the two narrow zones near the power entry port locations. From Fig. 10.30 it can be seen that for both high loss and low loss reactants, the strongest power absorption occur at about 1 cm from the outer layer. As it moves towards the core, the power absorption of in the medium loss reactant drops faster than in the low loss reactant. The penetration depth of the medium loss one is about 3 cm and about 8 cm for the low loss reactant. This is very close to the ones obtained from the equation 10.41.

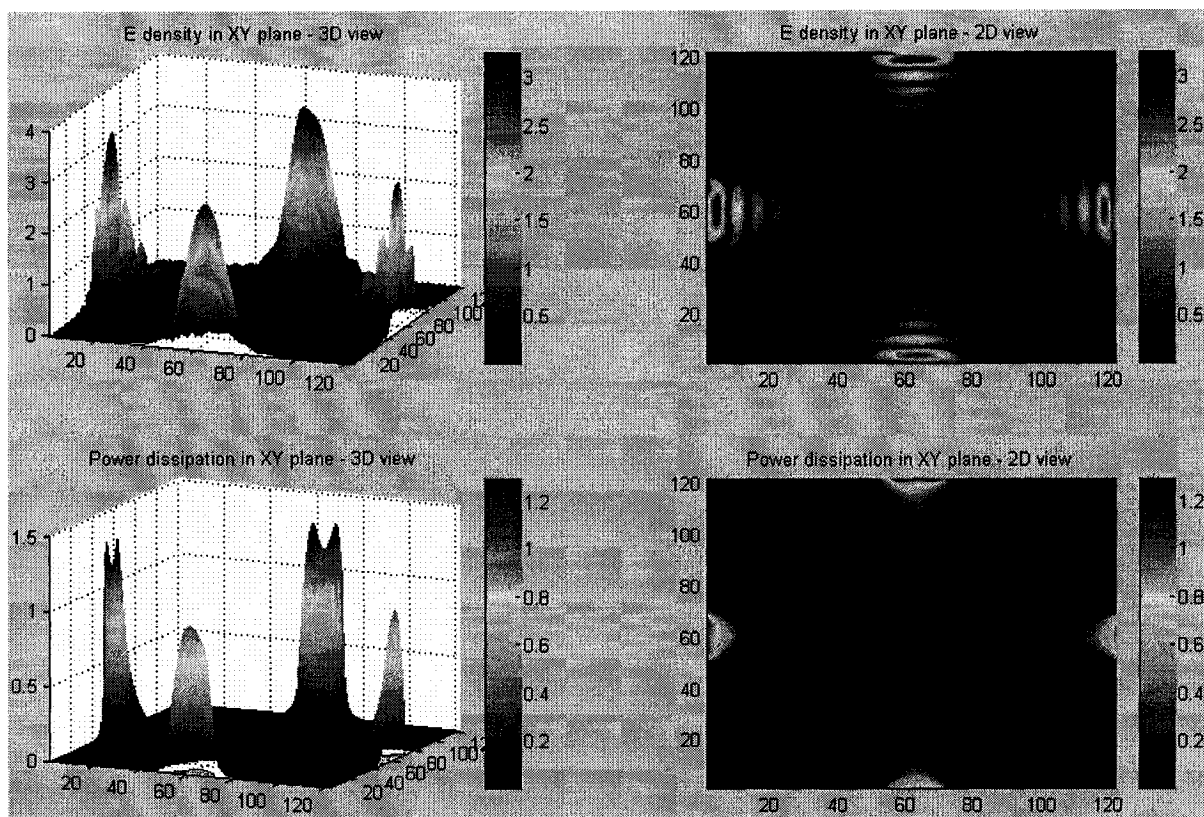


**A (Fig. 10.25)**

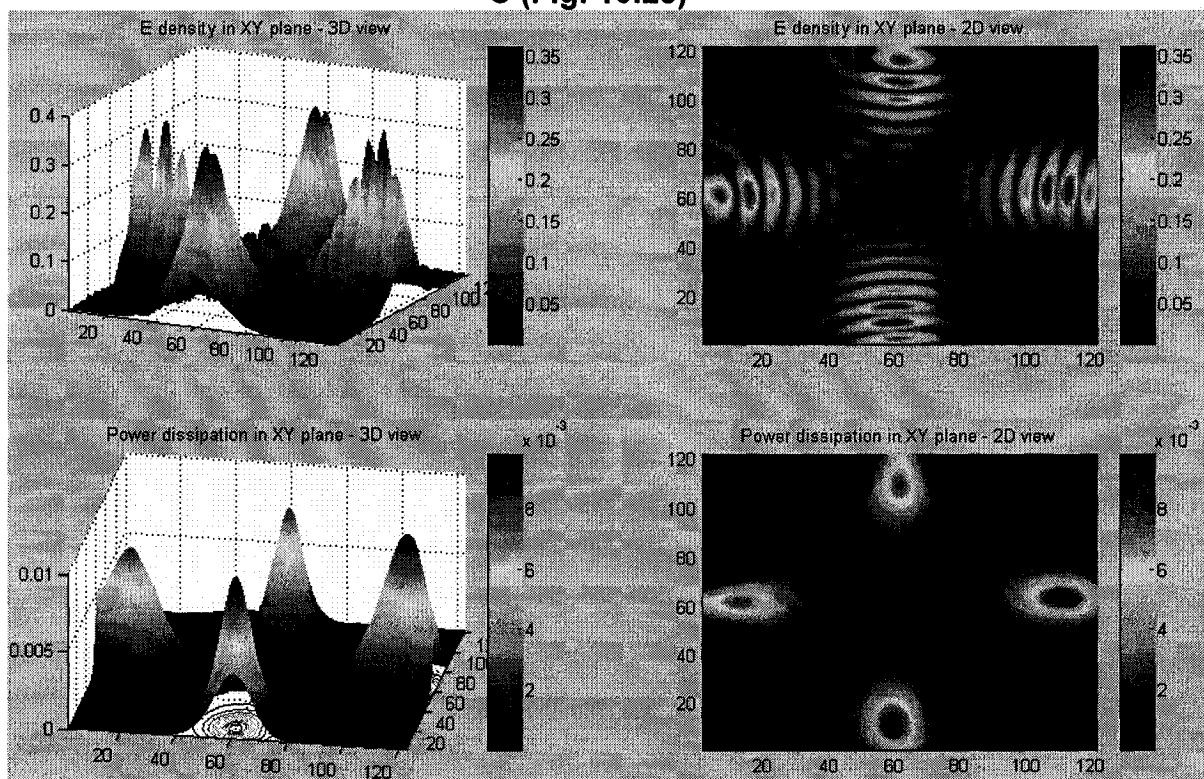


**B (Fig. 10.25)**

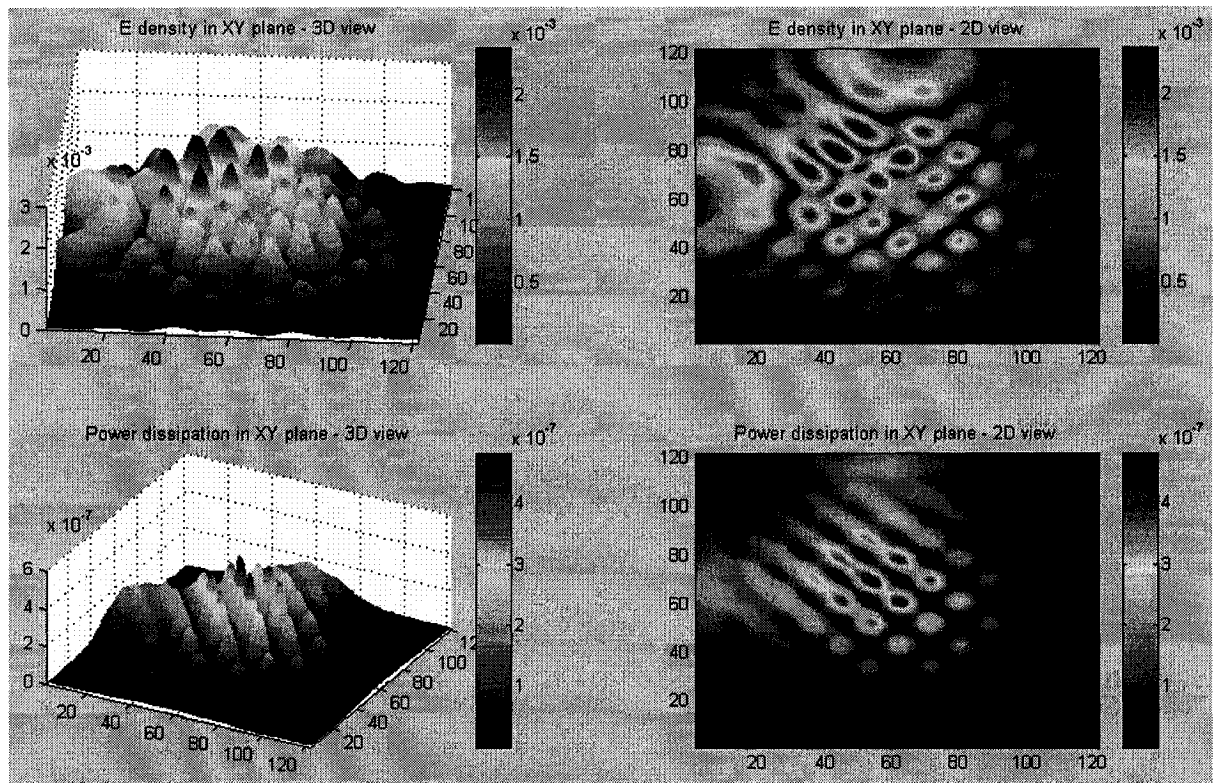




**C (Fig. 10.25)**



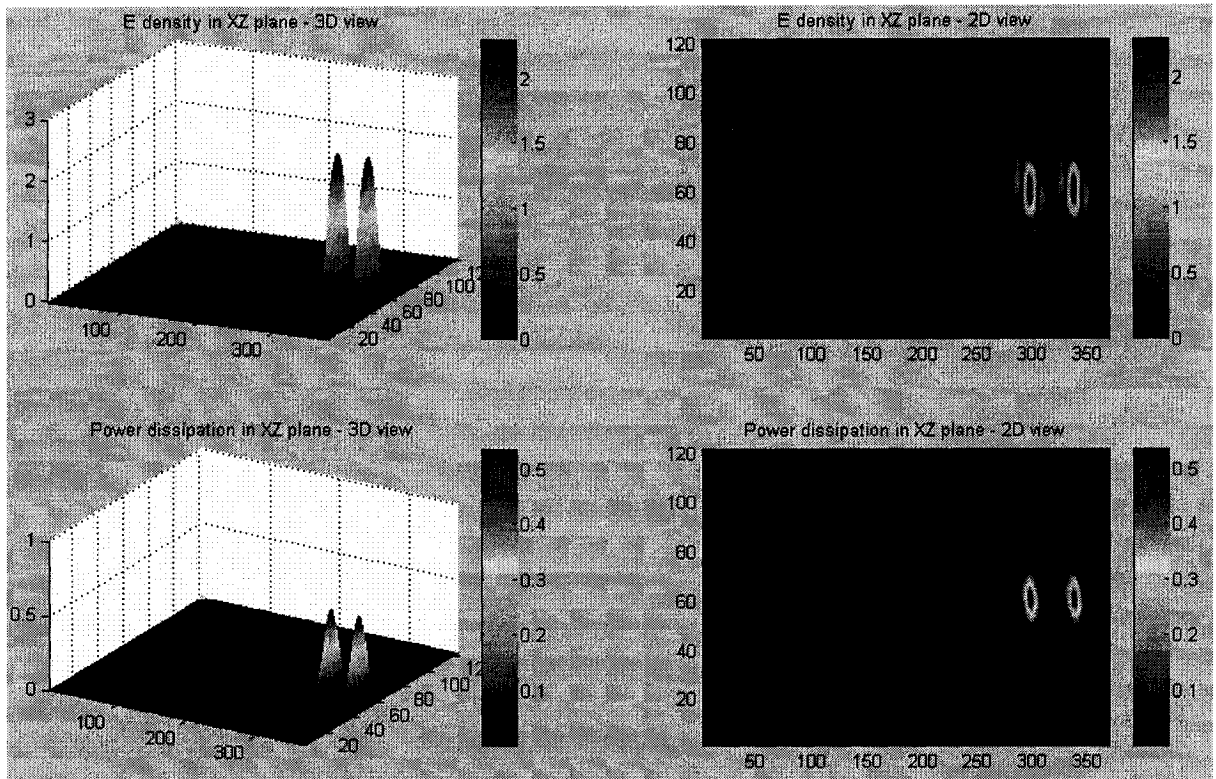
**D (Fig. 10.25)**



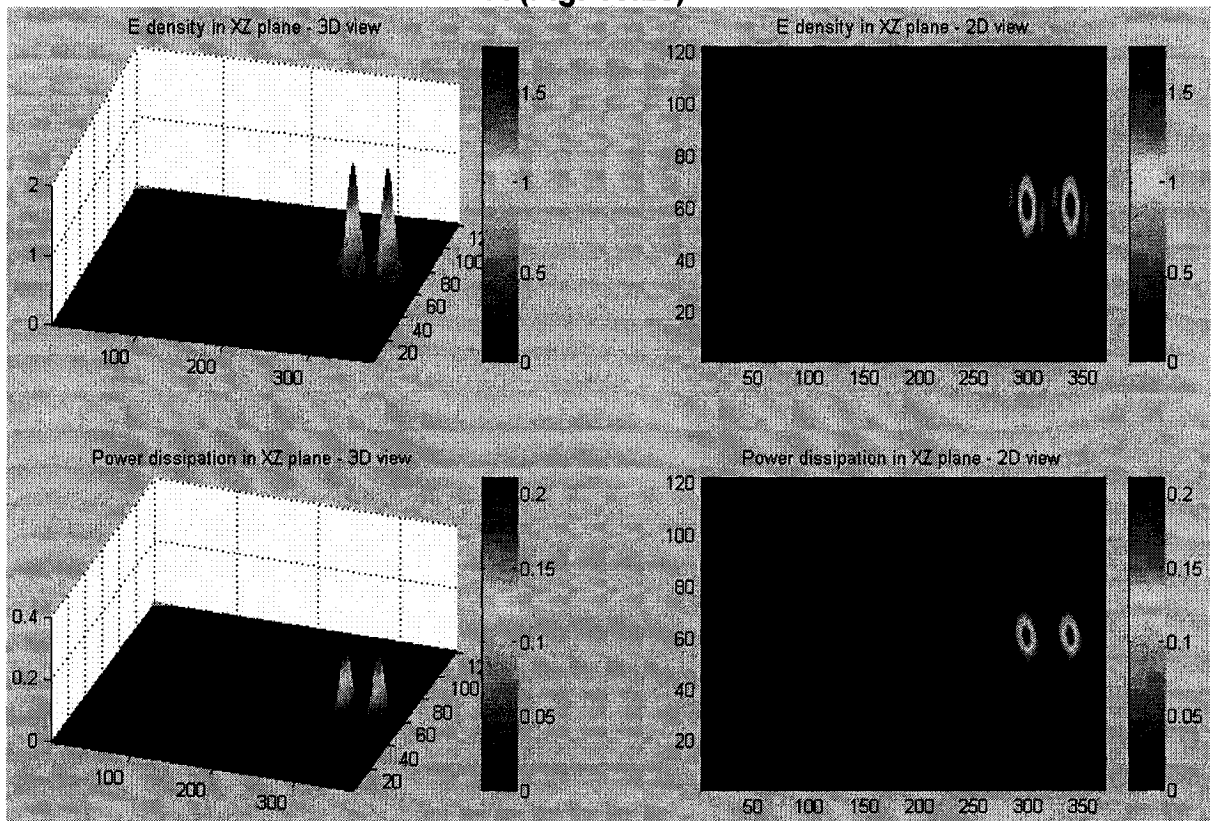
**E (Fig. 10.25)**

Fig. 10.25. E field distribution and power dissipation at different depths of the reactor container. The container was filled with 100 cm in depth of low loss dielectric reactant with  $\epsilon' = 5$  and  $\epsilon'' = 1$ . Total meshing number of the whole cavity is:  $123 \times 123 \times 371$  cells. Results obtained after 3000 timesteps ( $2.79 \times 10^{-7}$  s). Simulation was run using an AMD Athlon 3800 dual core personal computer with 1Gb DDR400 PC-3200 memory. Simulation time was 2hr 50 min.

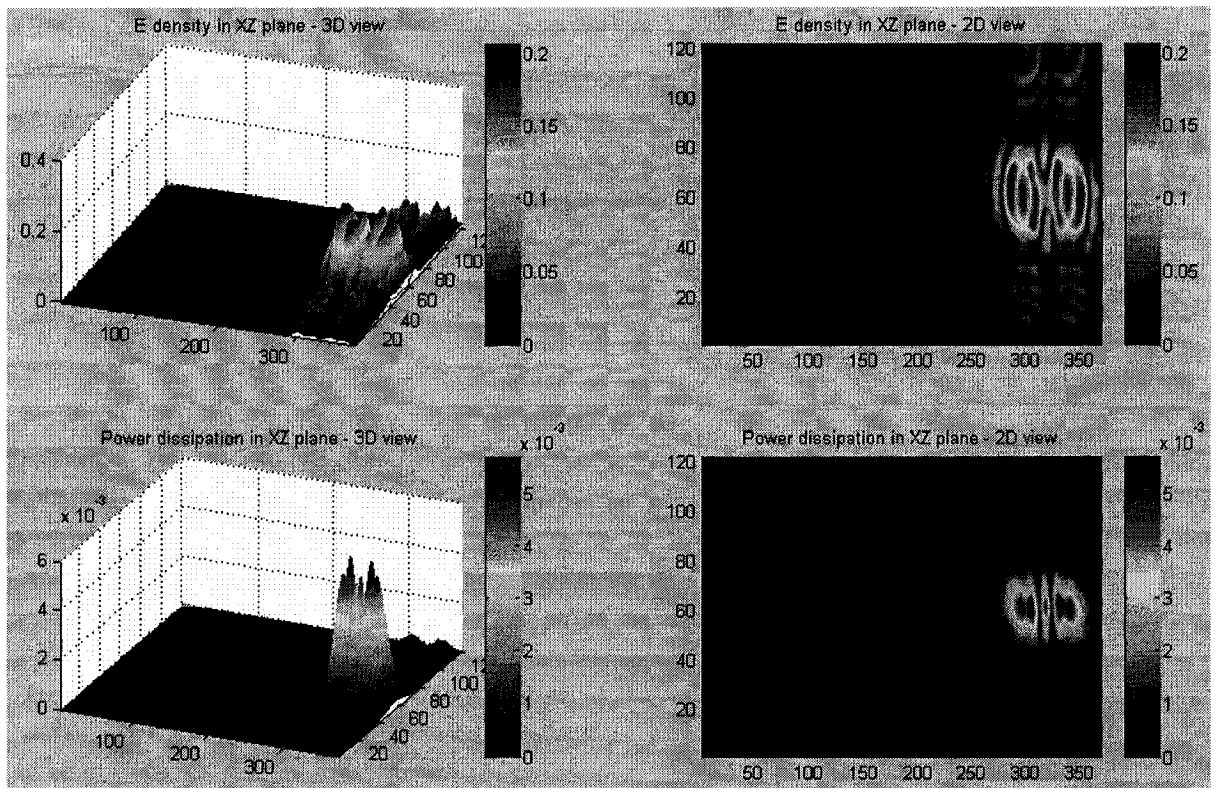
- A: 5 cm from the bottom
- B: 17 cm from the bottom
- C: 35 cm from the bottom
- D: 45 cm from the bottom
- E: 75 cm from the bottom



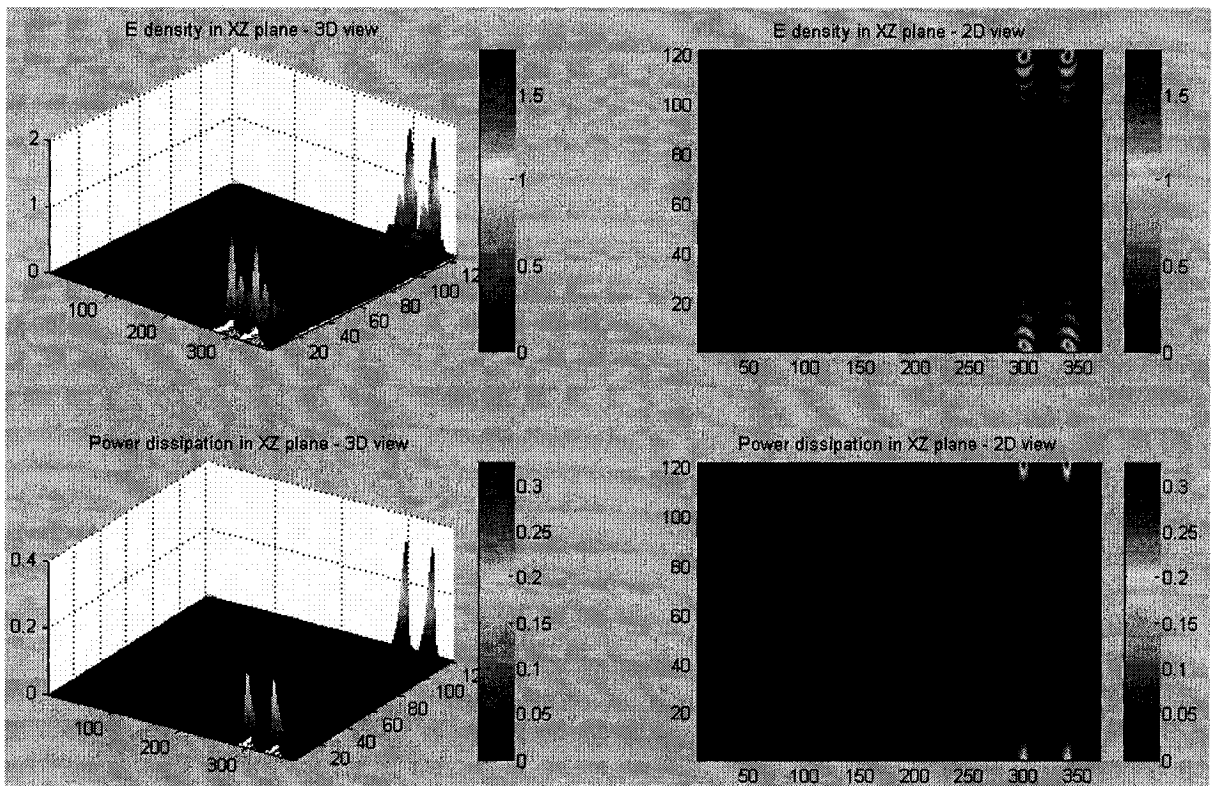
**A (Fig. 10.26)**



**B (Fig. 10.26)**

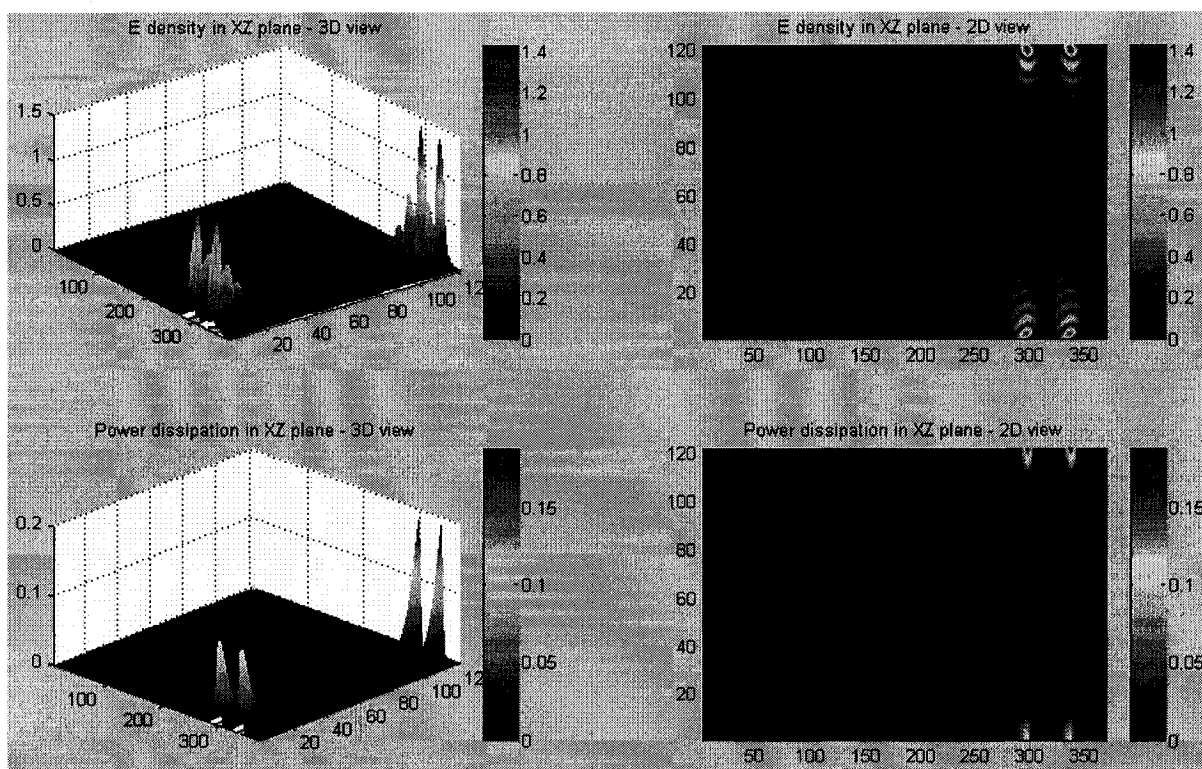


**C (Fig. 10.26)**



**D (Fig. 10.26)**

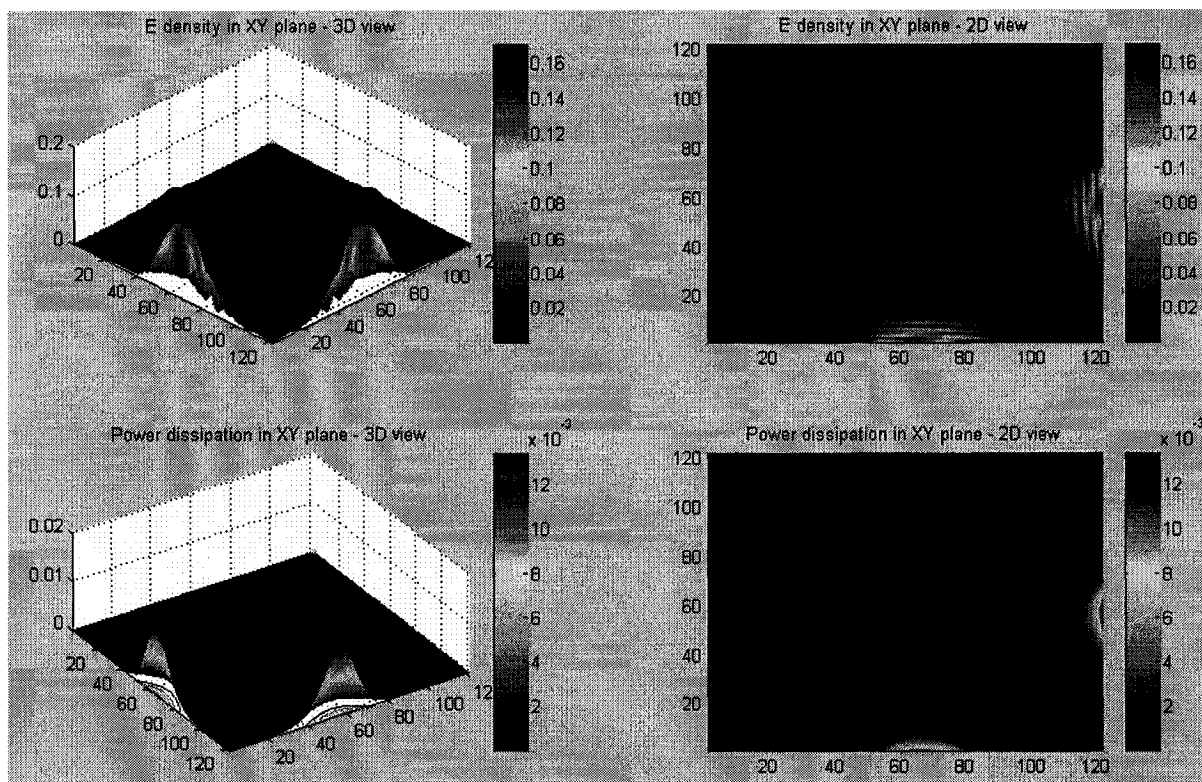




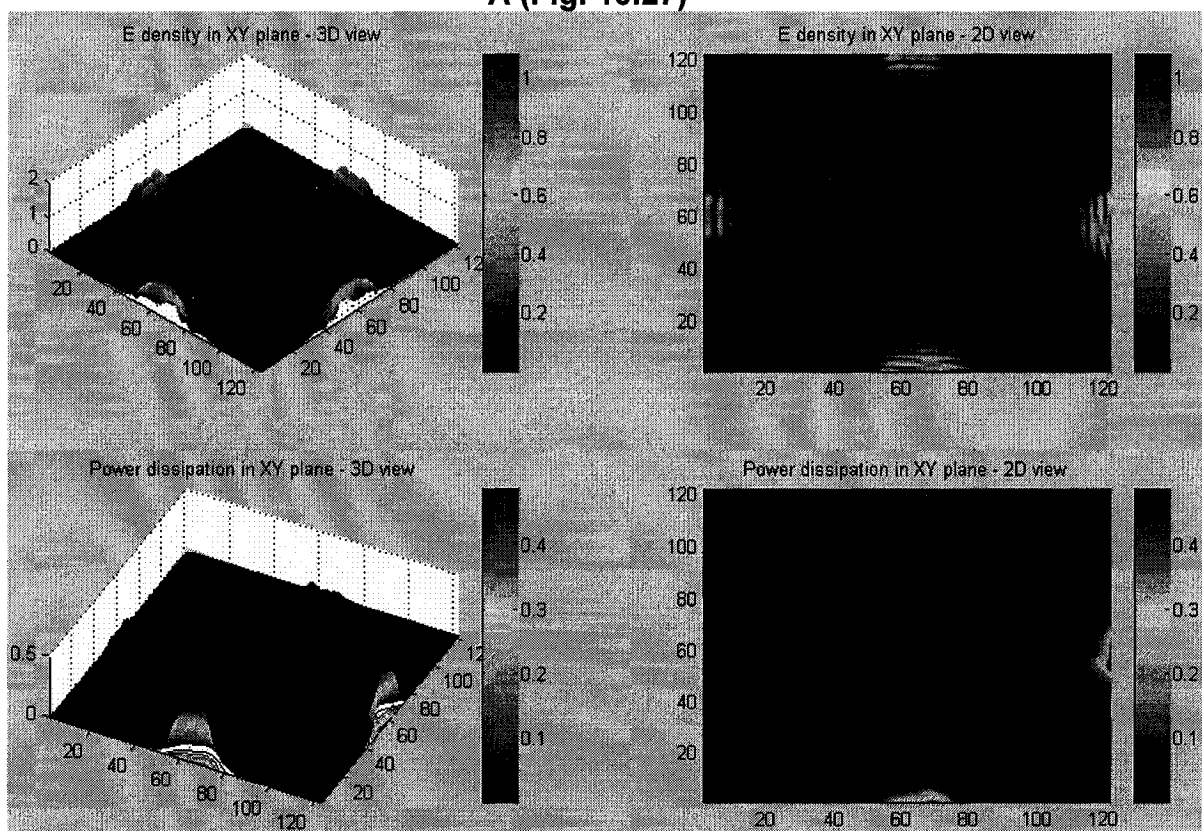
**E (Fig. 10.26)**

Fig. 10.26. The E field distribution and power dissipation at different distances from the Y direction (XZ plane) into the reactor container. The container was filled with 100 cm in depth of low loss dielectric reactant with  $\epsilon' = 5$  and  $\epsilon'' = 1$ . Total meshing number of the whole cavity is: 123 x 123 x 371 cells. Results obtained after 3000 timesteps ( $2.79 \times 10^{-7}$  s). Simulation was run using an AMD Athlon 3800 dual core personal computer with 1Gb DDR400 PC-3200 memory. Simulation time was 2hr 50 min.

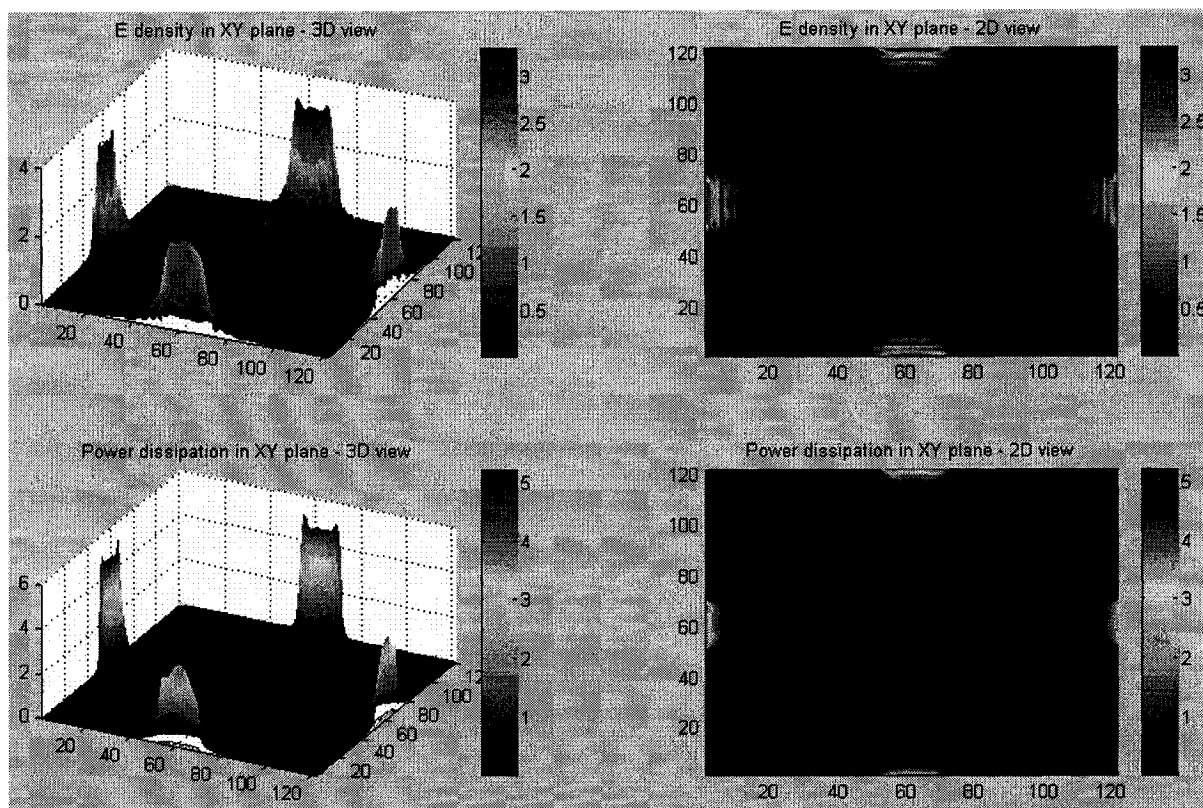
- A: XZ plane 2.5 cm from the container side wall into the container
- B: XZ plane 5 cm from the container side wall into the container
- C: XZ plane 15 cm from the container side wall into the container
- D: XZ plane 25 cm from the container side wall into the container
- E: XZ plane in the middle of the container corresponding to 35cm from the container side wall



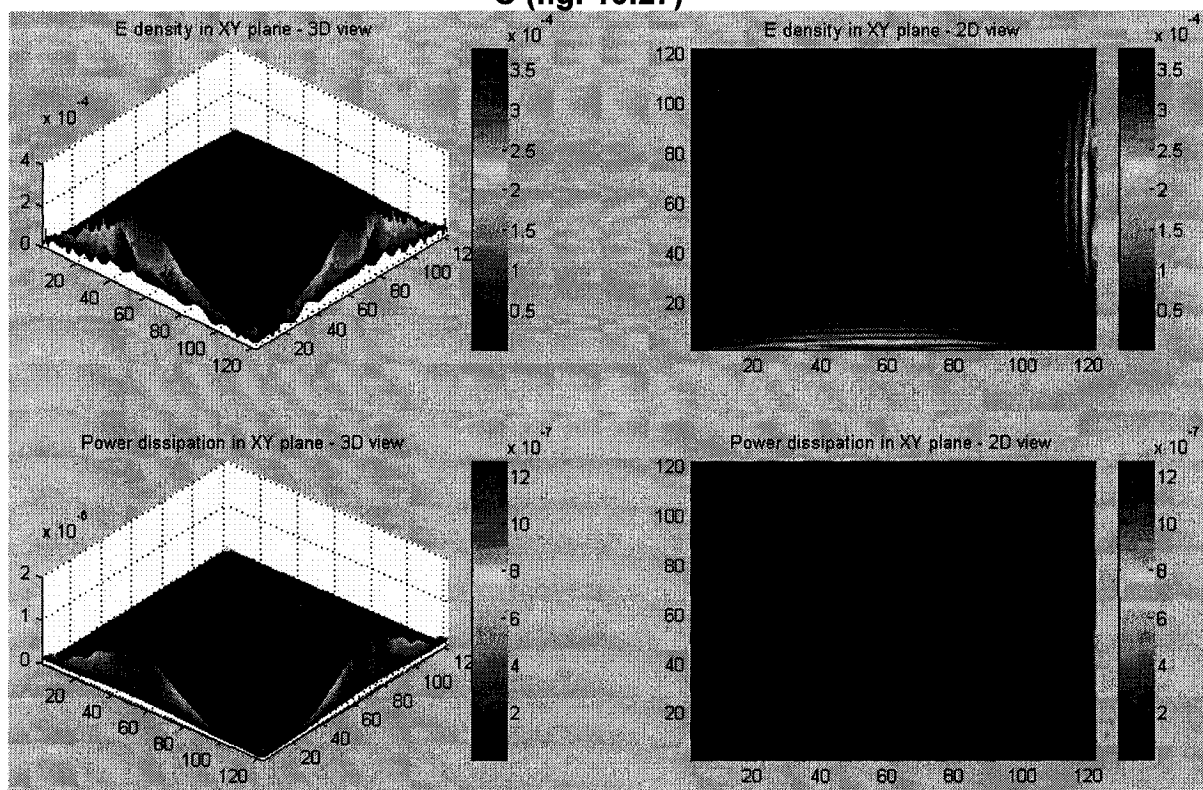
**A (Fig. 10.27)**



**B (Fig. 10.27)**



**C (fig. 10.27)**

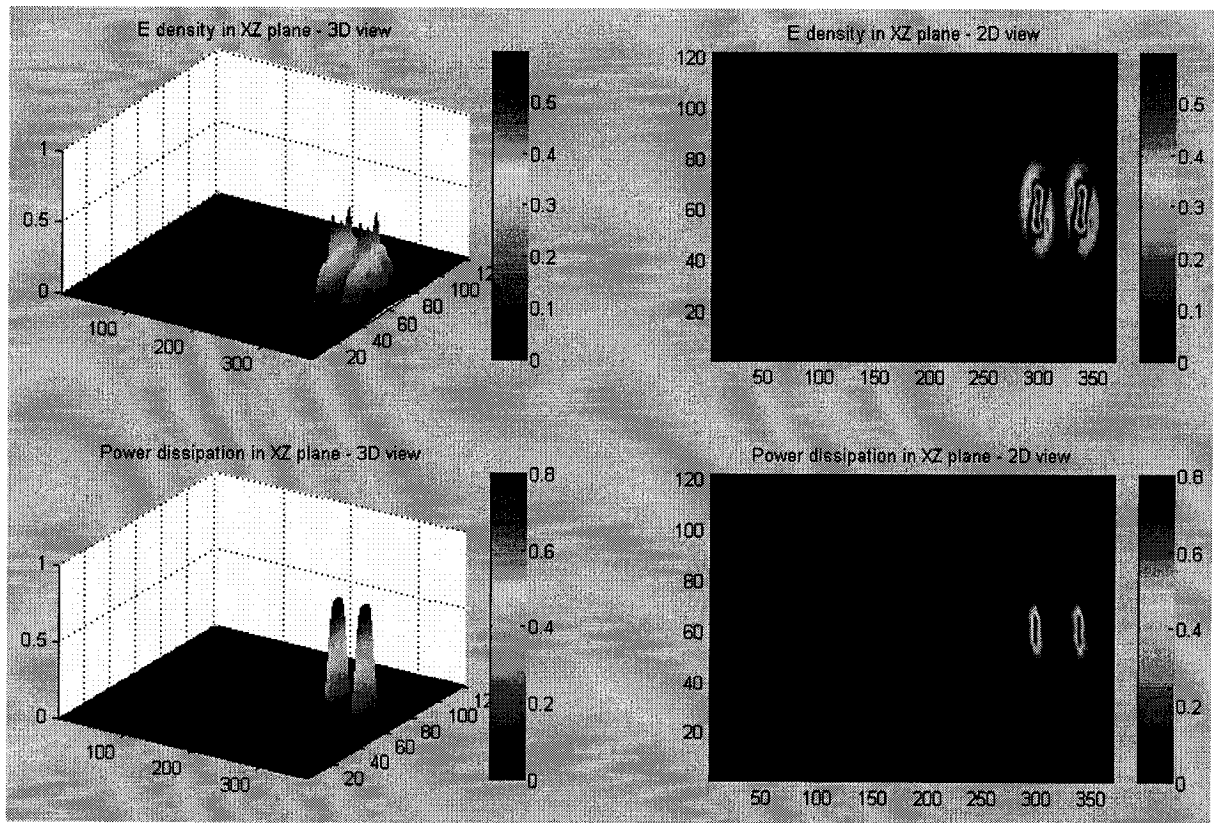


**D (Fig. 10.27)**

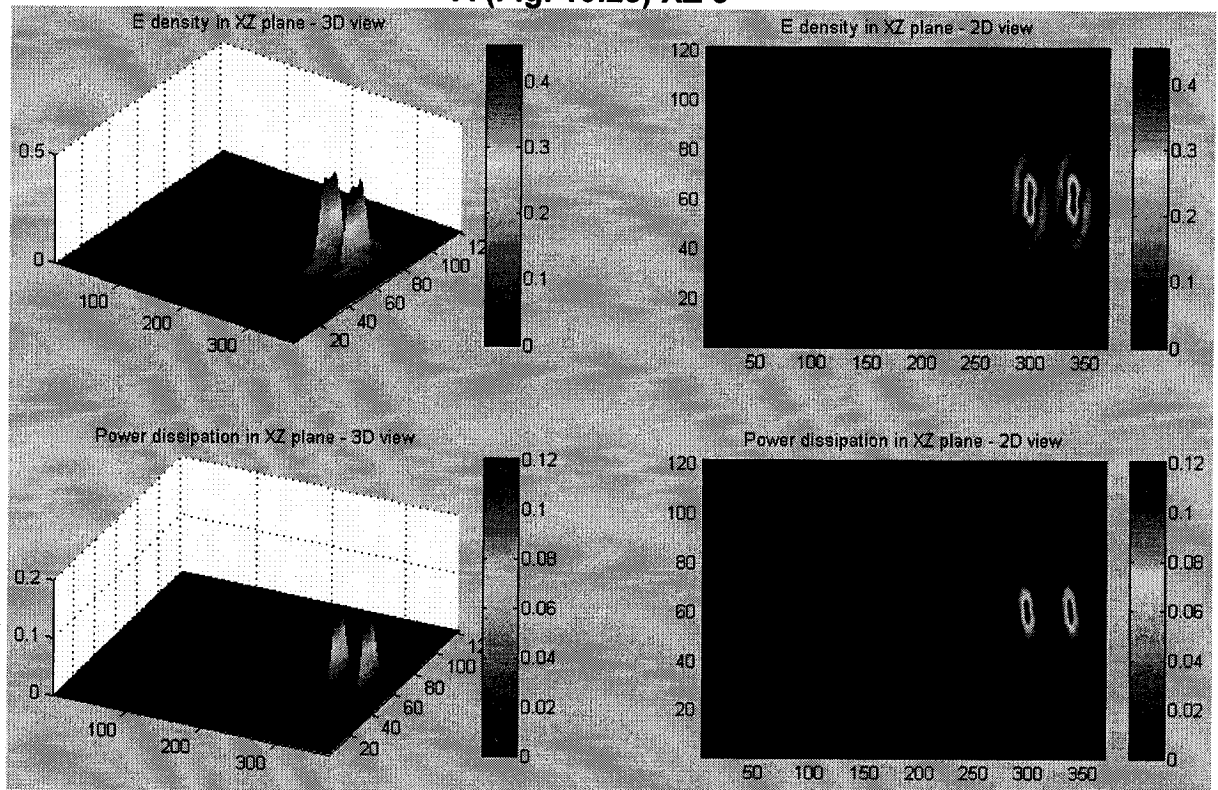
Fig. 10.27. E field distribution and power dissipation at different depths of the reactor container. The container was filled with 100 cm in depth of medium loss dielectric reactant with  $\epsilon' = 20$  and  $\epsilon'' = 5$ . Total meshing number of the whole cavity is: 123 x 123 x 371 cells. Results obtained after 3000 timesteps ( $2.79 \times 10^{-7}$  s). Simulation was run using an AMD Athlon 3800 dual core personal computer with 1Gb DDR400 PC-3200 memory. Simulation time was 2hr 50 min.

- A: 5 cm from the bottom
- B: 12.5 cm from the bottom
- C: 17 cm from the bottom
- D: 35 cm from the bottom
- E: 75 cm from the bottom

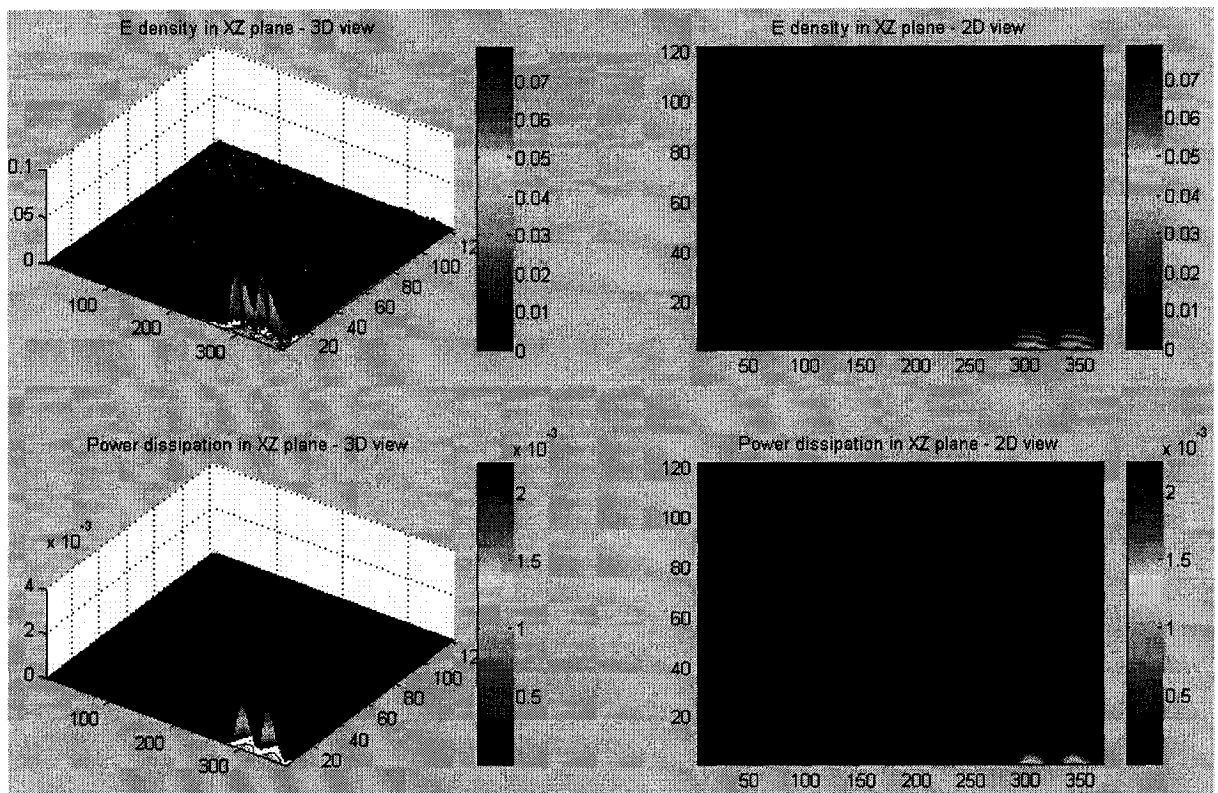




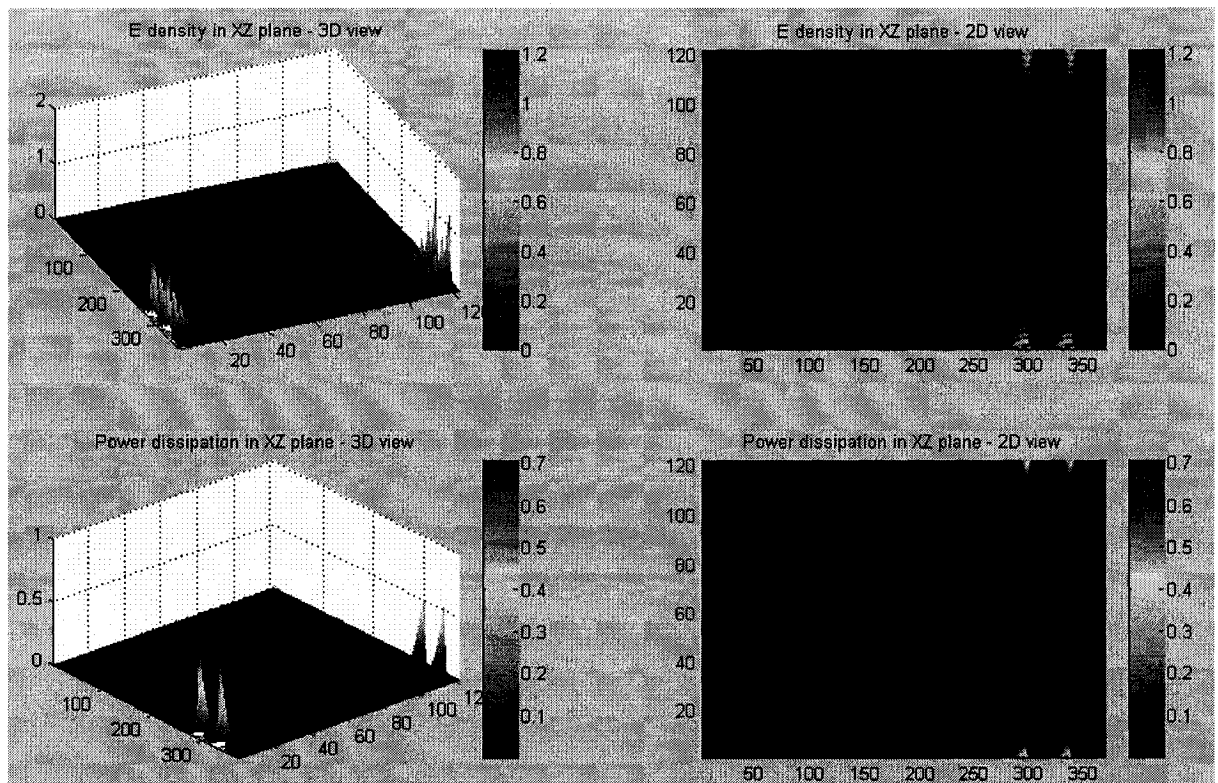
**A (Fig. 10.28) XZ 5**



**B (Fig. 10.28) XZ 10**



**C (Fig. 10.28) XZ 30**



**D (Fig. 10.28) XZ 71**

Fig. 10.28. The E field distribution and power dissipation at different distances from the Y direction (XZ plane) into the reactor container. The container was filled with 100 cm in depth of medium loss dielectric reactant with  $\epsilon' = 20$  and  $\epsilon'' = 5$ . Total meshing number of the whole cavity is: 123 x 123 x 371 cells. Results obtained after 3000 timesteps ( $2.79 \times 10^{-7}$  s). Simulation was run using an AMD Athlon 3800 dual core personal computer with 1Gb DDR400 PC-3200 memory. Simulation time was 2hr 50 min.

- A: XZ plane 2.5 cm from the container side wall into the container
- B: XZ plane 5 cm from the container side wall into the container
- C: XZ plane 15 cm from the container side wall into the container
- D: XZ plane in the middle of the container corresponding to 35cm from the container side wall

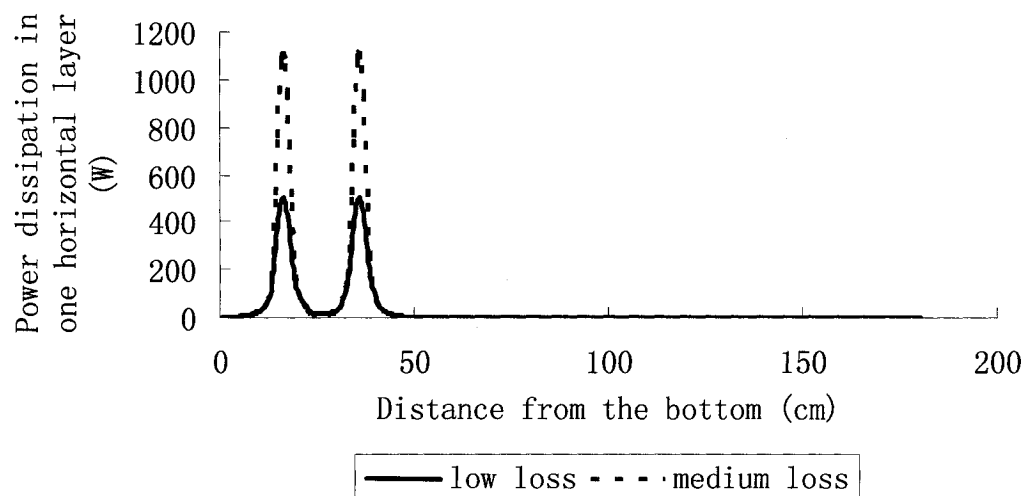


Fig. 10.29. Power dissipations in each horizontal layer for low loss and medium loss reactants.

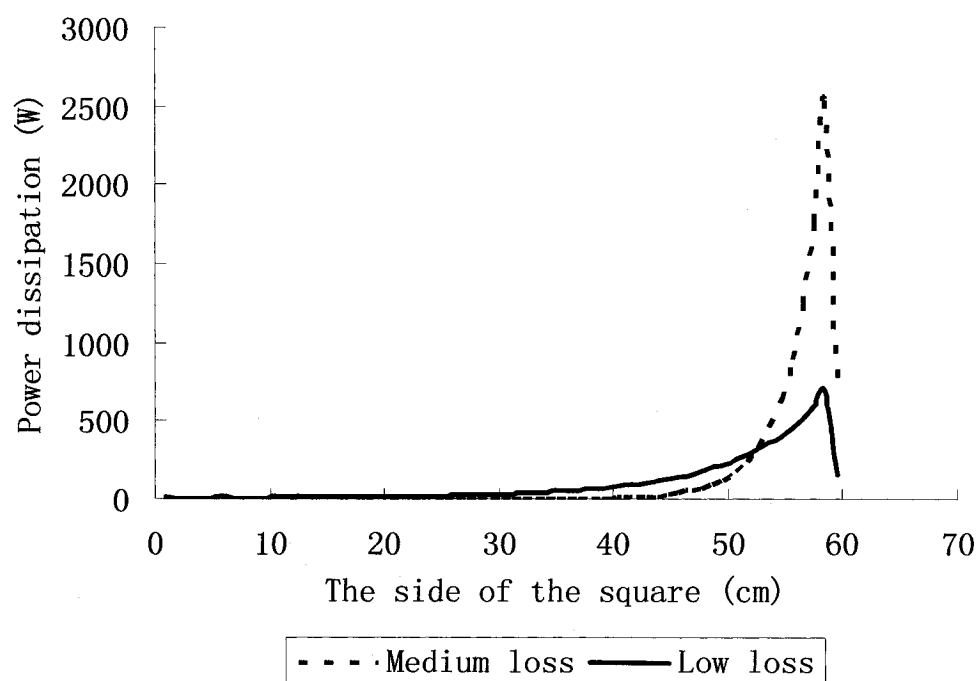


Fig. 10.30. Power dissipation in different layers of squares from inner to outer. The power dissipation value is normalized to the square with a side of 17cm.

A reactor with rectangular solid shape is not very practical in real applications. When the stirrer is used, the each corner will lead to a dead zone where no proper mixing can be achieved. From the E field and power dissipation pattern, the influence from the wall is negligible even for the low loss reactant. Therefore if the square type of reactor is replaced with a cylindrical type of reactor, the shape will not affect the power dissipation but the mixing through stirrer agitation will be greatly improved. Another issue to be considered is the location of the magnetron. Since power is main dissipation in a small zone near the entry port as shown in Fig. 10.29, the lower magnetron need to move farther towards the bottom. Otherwise the lower portion of the reactant can not be heated properly even with agitation. For the low loss reactant, the penetration depth is about 8 cm, but it will still have power dissipation until 20-25 cm down into the center. By this way, near each power entry port there will be a power reception block of about 10 x 20 cm when combining Figs. 10.29 and 10.30. When the stirrer is used, exchange can happen at these power reception blocks. Even with the medium loss reactant, the block is about 10 x 8 cm. In the current design, the eight magnetrons are aligned at two levels, two on each side. Since there is a stirrer to make the reactant pass through the heating block to receive microwave energy, the eight magnetrons can actually be more scattered vertically so that reactant at different depth will be easier to receive power even without very good vertical direction mixing. Such a cylindrical design is shown in Fig. 10.31.

With conventional heating method either using heating coil or heating jacket, the heating will be only from the surface. In comparison, microwave heating will have a greater advantage.

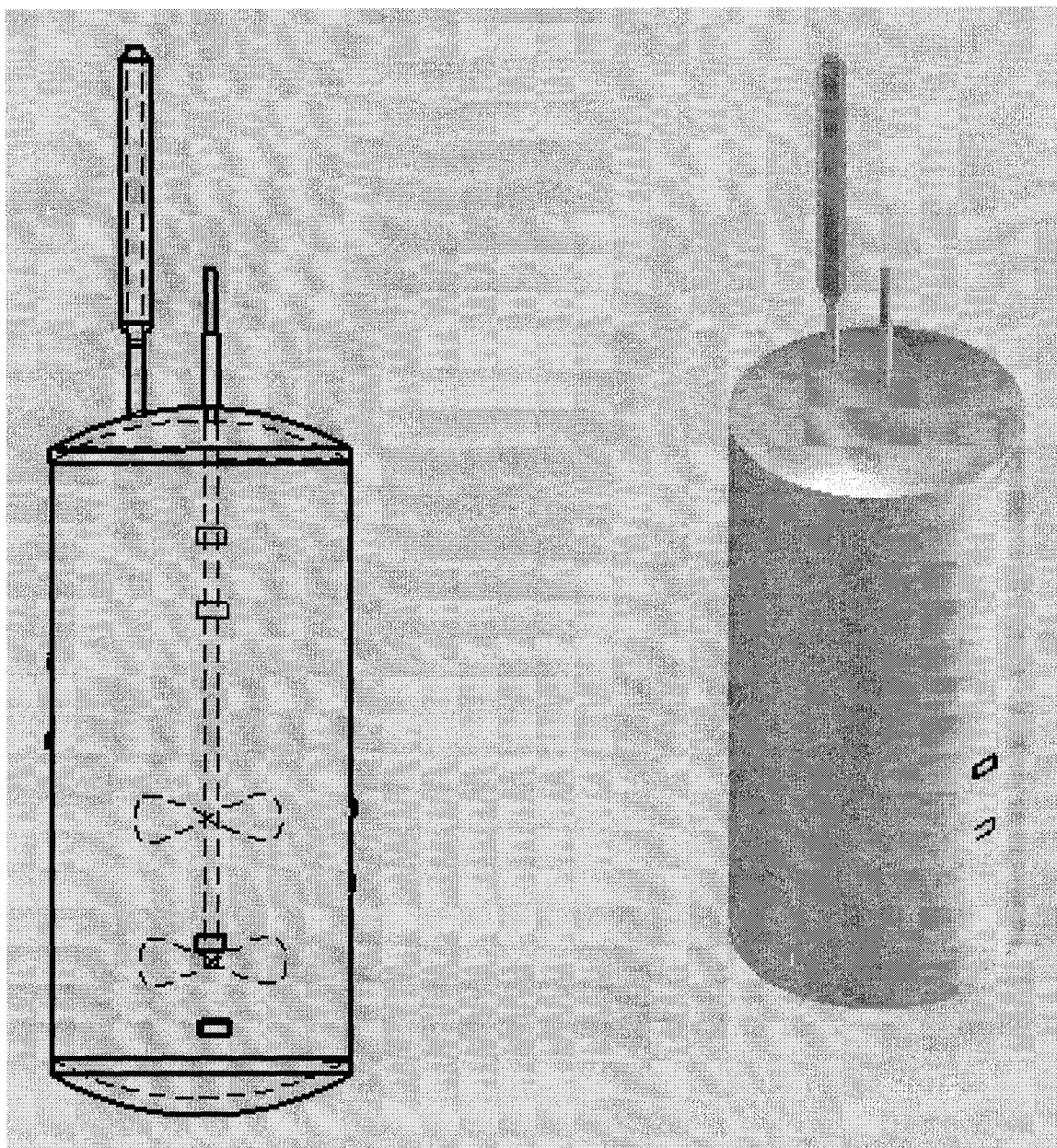


Fig. 10.31. A cylindrical microwave chemical reactor/extractor with 8 magnetrons.

### 10.7 Conclusions

A program written using C language is used to simulate the E field distribution and power dissipation into lossy dielectric materials in a microwave cavity. The program is flexible in simulating cavities with different dimensions and the location of single or multiple power entry ports. This program is used to assist

in the design of different types of microwave-assisted chemical reactors/extractors. Simulation results indicated that the oven type of chemical reactor/extractor is restricted by the heating pattern. A cylindrical reactor with multiple magnetrons installed around the vertical wall and vertically scattered will be practical for industrial use. The diameter of the cylindrical reacting vessel is restricted by the fact that microwaves have limited penetration depth in the high loss dielectric medium. But with proper agitation, it will be more efficient than the conventional reactor heated with steam jacket or coil heating.

### 10.8 Acknowledgement

The authors wish to acknowledge the Natural Science and Engineering Research Council of Canada (NSERC), FQRNT and Canadian International Development Agency (CIDA) for their financial support.

### 10.9 Reference

- Dai, J.; Yaylayan, V.A.; Raghavan, G. S. V.; and Pare, J. R. **1999**. Extraction and colorimetric determination of azadirachtin related limonoids in the neem seed kernel. *J. Agric. Food Chem.* 47, 3738-3742
- Fu, W. and Metaxas, A. **1994**. Numerical prediction of three-dimensional power density distribution in a multimode cavity. *J. Microwave Power and Electromagnetic Energy.* 29(2), 67-75.
- Ganzler, K.; Salgo, A.; and Valko, K. **1986**. Microwave extraction: a novel sample preparation method for chromatography." *Journal of Chromatography.* 371: 299-306.
- Gao, Q. **1997**. Rapid determination of tannic acid in plant samples with microwave extraction. *Fenxi Ceshi Xuebao.* 16(3), 76-710.
- Gedye, R.; Smith, F.; Westaway, K.; Ali, H.; Baldisera, L.; Laberge, L.; and J. Rousell. **1986**. The use of microwave ovens for rapid organic synthesis. *Tetrahedron Lett.* 27(3): 279-82.



- Hao, J; Huang, R.; Wang, P; and Deng, X. **2000**. Study on microwave extraction of orris root. *Xiangliao Xiangjing Huazhuangpin*. 4, 12-17.
- Harms, P.H.; Chen, Y.; Mittra, R.; and Shimony, Y. **1996**. Numerical modeling of microwave heating systems. *J. Microwave Power and Electromagnetic Energy*. 31(2), 114-121.
- Lee, S.; Lee, K. M.; Park, K. A.; and Hong, I. K. **2000**. Microwave assisted solvent extraction (MASE) of rice bran oil. *Kongop Hwahak*. 11(1), 99-104.
- Li, R. and Jin, M. **2000**. Microwave extraction of Ginkgo biloba flavone glycosides. *Shipin Kexue*. 21(2), 39-41.
- Liu, C.; Bai, F.; Feng, P.; Miao, W.; and Su, Z. **2000**. Trehalose extraction from *saccharomyces cerevisiae* after microwave treatment. *Huagong Xuebao (Chin. Ed.)*. 51(6), 810-813.
- Ma, L.; Paul, D.L. and Potheary, N. **1995**. Experimental validation of combined electromagnetic and thermal FDTD model of a microwave heating process. *IEEE transactions on microwave theory and technologies*. 43(11), 2565 – 2572.
- Mattina, M. J. I.; Berger, W. A. I; and Denson, C. L. **1997**. Microwave-Assisted Extraction of Taxanes from *Taxus* Biomass. *J. Agric. Food Chem*. 45(12), 4691-4696.
- Meredith, R.J. **1994**. A three axis model of the mode structure of multimode cavities. *J. Microwave Power and Electromagnetic Energy*. 29(1), 31-44.
- Mittra, R. and Harms, P.H. **1993**. A new finite-difference-time-domain (FDTD) algorithm for efficient field computation in resonator narrow-band structures. *IEEE Microwave Guided Wave lett*. 3, 316-318.
- Nykvist, W.E. and Decareau, R.V. **1976**. Microwave meat roasting. *J. Microwave Power*. 11, 3-24.
- Pan, X.; Liu, H.; Jia, G.; and Shu, Y. **2000**. Microwave-assisted extraction of glycyrrhizic acid from licorice root. *Biochem. Eng. J*. 5(3), 173-177.



- Pare, J. R. J. and Belanger, J. M. R. **1994**. Microwave-Assisted Process (MAP): a new tool for the analytical laboratory. *Trends Anal. Chem.* 13(4), 176-84.
- Pare, J.R.J. and Belanger, J.M.R. **1997**. Microwave-assisted process (MAP): Principles and Applications. In *Instrumental methods in Food Analysis*; Pare, J.R.J., Belanger, J.M.R., Eds.; Elsevier: Amsterdam, 1997, pp 395-420.
- Seifert, P.; Bertram, C.; and Chollet, D. **2000**. Microwave extraction of botanicals. A high tech green approach. *SOFW J.* 126(1/2), 3-4, 6-9.
- Sullivan, M.D. **2000**. Electromagnetic simulation using the FDTD method. IEEE press series on RF and Microwave Technology. New York.
- van Remmen, H.J.H.; Ponne, T.C.; Nijhuis, H.H.; Bartels, V.N.; and Kerkhof, J.A.M. **1996**. Microwave heating distributions in slabs, spheres, and cylinders with relation to food processing. *J. Food sci.* 61(6) 1105-1113.
- Yee, K.S. 1996. Numerical solution of initial boundary value problems involving Maxwell's equations in isotropic media. *IEEE trans. on Antennas and Propagation.* AP-17, 585-589.
- Zhou, L.; Puri, V.M.; Anantheswaran, R.C. and Yeh, G. **1995**. Finite element modeling of heat and mass transfer in food materials during microwave heating – model development and validation. *J. Food Engineering.* 25, 509-529.

## CHAPTER XI

### GENERAL CONCLUSION, CONTRIBUTION TO KNOWLEDGE AND RECOMMENDATIONS FOR FUTURE RESEARCH

#### 11.1 General conclusions

Extraction of peppermint, Microwave-assisted extraction of American ginseng, microwave-assisted synthesis of parabens using  $\text{ZnCl}_2$  as catalyst, and the simulation of microwave distribution using FDTD method were studied throughout the thesis.

On the study of the influence of various factors on the extraction of peppermint, extraction methods was determined to be the most important factors that affect the yield of the extract represented by menthone, menthofuran, and menthol. Using microwave-assisted extraction the yield was significantly higher than that obtained using reflux method with conventional heating method. Since same temperature is used under these two types of extraction methods, the improvement through using microwaves indicated that there could be a special acceleration factor beyond the temperature effect. The extraction time is also an important factor that influences the yield of the extract. The reaction is fast but it is not as fast as suggested in some literature that can finish in less than a minute. At this study we were looking at the time scales of about 20-30 min. Solvent was determined to be a critical factor in the extraction. Best yield was obtained with the mixed solvent of ethanol and hexane in 3 to 7 volumetric ratio. Sample to solvent ratio was observed to be the least important factor due to the relatively small amount of sample used in the study.

Two studies on the extraction of American ginseng were carried out. One is on the investigation of the influence of different factors on the extract efficacy another is focused on the study of microwave-assisted extraction. On the study of the influence of various factors, the sample particle size was determined to be the most influential factor among all the factors investigated. Again extraction time is important with the extraction reaching maximum yield at about 10min. The amount of solvent usage is important for those components that have high

content in the sample and less important for the ones that are very low in percentage in the sample. Extraction method is not an important factor as determined in this study.

In the study of the comparison of microwave-assisted extraction, extraction in reflux condition using hotplate heating, and room temperature extraction methods, microwave-assisted extraction showed greater acceleration over both reflux room temperature extraction and extraction under conventional heating. The extraction rate almost doubled for the one using hotplate heating under reflux condition for the total ginsenosides. Again this can only be explained that there is some effect beyond the temperature in the extraction of ginsenosides when microwaves were introduced into the extraction method. The exact mechanism is not clear yet.

In the study of microwave-assisted synthesis of n-butyl paraben, microwave-assisted synthesis was observed to greatly increase the yield of n-butyl paraben and the synthesis can finish in a very short period of time. The mechanism of the synthesis under microwaves was explained as the formation of a dipolar transition state that can interact efficiently with microwaves. The study of the synthesis of parabens with different alcohol further proved the mechanism. During the study of various factors on the influence of n-butyl paraben yield, temperature was observed to be critical. The reaction can not be triggered when the temperature is too low but the product will decompose if the temperature is too high. Other factors like microwave power, reactant ratio, the amount of catalyst all significantly affect the n-butyl paraben yield.

A method was developed to visualize the microwave distribution in a microwave cavity. The method uses gypsum plate as carrier and cobalt chloride as indicator. The plate can be placed in the oven horizontally or vertically. After the heating, the locations that absorb more microwave energy will be of a different color than those locations which did not receive energy or receive lower amount of energy.

A simulation program using the finite difference time domain (FDTD) approach was written in programming language C. The E field distribution in either empty microwave cavity or loaded cavity can be simulated. The program is very flexible in terms of simulating cavities with different dimensions and shapes and the locations of a single or multiple power entry port and the simulation of microwaves with different frequencies. Power dissipation into the lossy dielectric loads in the cavity can be analyzed in 3 dimensions. This program was used to assist in designing scaled-up microwave-assisted extraction or synthesis equipments. Through the simulation, it was determined that a cylindrical type of chemical reactor/extractor with multiple magnetron installation along the vertical cylinder can handle up to a few hundred liters of reactants. And it is more practical than the oven type of reactor with multiple magnetrons and glassware inside the cavity.

## **11.2 Contribution to knowledge**

The major contributions to knowledge are:

1. Through the study of various factors on the extraction of peppermint leaves, and the study of comparing different methods on extracting ginsenosides, microwave-assisted extraction was determined to have an acceleration effect on the extraction beyond heating effect.
2. The mechanism of  $\text{ZnCl}_2$  catalyzed microwave-assisted synthesis of parabens were proposed and evidences were observed through the study of the influence of various factors on the synthesis as well as the study of synthesizing different parabens.
3. A visualization method was developed to determine the power distribution in the microwave cavity through experiments.
4. A simulation program was developed in C language by solving the Maxwell's equations using the FDTD approach. The program was used to simulate the scale-up of microwave-assisted chemical reactor or extracting equipment.

### **11.3 Recommendations for future research**

1. Even though acceleration effect was observed when microwave-assisted extraction method was used for the extraction of peppermint and American ginseng, the whole extraction process is in such a short period of time (10-30 min), an economical analysis should be carried out before any effort of scaling up the extraction process.
2. Investigate in a wider range of herbs to find the proper ones for scale-up test. One or a few of the following characteristics should be considered when selecting such type of product to work on:
  - a). long processing time using conventional extraction methods
  - b). special type of target component that is hard to obtain under conventional extraction method
  - c) high value added target components
  - d) large amount of components extracted using conventional extraction methods leading to excess amount of treatment work after the extraction.
3. Similar to the extraction, before the effort of scaling up any microwave-assisted organic synthesis, an economical analysis needs to be performed.
4. Establish a mathematical model that correlate the microwave power density or amount of power absorption with extraction or synthesis processes so that they can be used in the simulation of scale-up process using the simulation program
5. The simulation work presented here did not consider the heat transfer in the heating process, nor was the stirrer agitation considered. In the simulation of any specific microwave assisted extraction or synthesis processes, these factors have to be considered and included in the simulation program.
6. Processes under different frequencies, especially at 915 MHz that has higher penetration depth should be simulated for scale-up.

## REFERENCES

- Abu-Samra, A.; Morris, J.S.; and Koirtyohann, S.R. **1975**. Wet ashing of some biological samples in a microwave oven. *Trace Subst. Environ. Health*. 9: 297-301.
- Alterman, M. and Hallberg, A. **2000**. Fast Microwave-Assisted Preparation of Aryl and Vinyl Nitriles and the Corresponding Tetrazoles from Organo-halides. *Journal of Organic Chemistry* 65(23), 7984-7989.
- Ammann, A.; Hinz, D.C.; Addleman, R. S.; Wai, C.M. and Wenclawiak, B.W. 1999. Superheated water extraction, steam distillation, and SFE of peppermint oil. *Fresenius' Journal of Analytical Chemistry*. 364(7), 650-653.
- Arakawa, T. and Osawa, K. 2000. Pharmacological study and application to food of mint flavor-antibacterial and antiallergic principles. *Aroma Research*. 1(1), 20-23.
- Berg, E.E. Cosmetic creams containing ginseng extract. *Ger. Gebrauchsmusterschrift*. DE 20201550, **2002**; 8 pp.
- Bose, A.K., Jayaraman, M., Okawa, A., Bari, S. S., Robb, E. W., Manhas, M. S. 1996. Microwave-assisted rapid synthesis of  $\alpha$ -amino- $\beta$ -lactams. *Tetrahedron Letters*, 37(39), 6989-6992.
- Bougrin, K., Loupy, A. and Soufiaoui, M. 2005. Microwave-assisted solvent-free heterocyclic synthesis. *Journal of Photochemistry and Photobiology, C: Photochemistry Reviews* 6(2-3), 139-167.
- Bougrin, K., Loupy, A., Petit, A., Daou, B., Soufiaoui, and M. Novel route for synthesis of 2-trifluoromethylarylimidazoles on K10 montmorillonite in a microwave-irradiated "dry medium". *Tetrahedron*. 2001, 57(1), 163-168
- Bousquet, F. **1997**. Preparation of novel plant extracts by organic solvents and microwave radiation. PCT FR96/15078. 13pp.

- Brun, N.; Colson, M.; Perrin, A. and Voirin, B. **1991**. Chemical and morphological studies of the effects of aging on monoterpene composition in menthe-piperita leaves. *Canadian journal of botany*. 69(10), 2271-2278.
- Carmines, E. L. **2002**. Evaluation of the potential effects of ingredients added to cigarettes. Part 1: Cigarette design, testing approach, and review of results. *Food and Chemical Toxicology*. 40(1), 77-91.
- Cesare, L. F. Di; Riva, M.; and Schiraldi, A. **1995**. Microwave extraction of basil aroma compounds. *Dev. Food Sci.* 37A 857-68.
- Chen, X.; Hong, P.; Dai, S. **1993**. Synthesis of nipagin esters with microwave irradiation. *Huaxue Tongbao*. 38-39.
- Chen, S. S. and Spiro, M. **1995**. Kinetics of microwave extraction of rosemary leaves in hexane, ethanol and a hexane + ethanol mixture. *Flavour Fragrance J.* 10(2), 101-12.
- Chen, S. S. and Spiro, M. **1994**. Study of microwave extraction of essential oil constituents from plant materials. *Journal of microwave power and electromagnetic energy*. 29(4), 231-241.
- Craveiro, A. A.; Matos, F. J. A.; Alencar, J. W.; and Plumel, M. M. **1989**. Microwave oven extraction of an essential oil. *Flavour Fragrance J.* 4(1), 43-44.
- Dai, J.; Yaylayan, V.A.; Raghavan, G. S. V.; and Pare, J. R. **1999**. Extraction and colorimetric determination of azadirachtin related limonoids in the neem seed kernel. *J. Agric. Food Chem.* 47, 3738-3742
- Dai, J. and G.S.Vijaya Raghavan, Microwave-assisted synthesis of n-butylparaben using ZnCl<sub>2</sub> as catalyst. In proceeding of 39th Annual Symposium of International Microwave Power Institute, **2005**, Seattle, Washington, USA
- De Leo, R.; Cerri, G.; and Mariani P, V. **1991**. TLM techniques in microwave ovens analysis: numerical and experimental results. *International Conference on computation in Electromagnetics*. Nov. 25-27. In proceeding page: 361 -364.

- Decareau, R.V. **1983**. Microwave food processing: today and tomorrow. *Activities Report of the R & d Associates*. 35 (1) p. 41-49.
- Ding, J.; Ding, Z.; Wu, Y.; and Zhou, J. **1991**. The extraction of aroma constituents from fresh flowers of *Magnolia soulangeana* through microwave oven-absorption. *Yunnan Zhiwu Yanjiu*. 13(3), 344-348.
- Ding, J., Gu, H., Wen, J. and Lin, C. 1994. Dry Reaction under microwave: N-alkylation of saccharin on silica gel. *Synthetic Communications* 24(3), 301-3.
- Dou, D.Q.; Zhang, Y.W.; Zhang, L.; Chen, Y.J.; Yao, X.S. The inhibitory effects of ginsenosides on protein tyrosine kinase activated by hypoxia/reoxygenation in cultured human umbilical vein endothelial cells. *Planta Medica*. 2001, 67, 19-23.
- Duda, R.B.; Kang, S.S.; Archer, S.Y.; Meng, S.; Hodin, R.A. American ginseng transcriptionally activates p21 mRNA in breast cancer cell lines. *Journal of Korean Medical Science* 2001, 16(Suppl) S54-60.
- Dulebohn, J.I. and Carlotti, R. J. 2002. Soy milk-juice beverage. PCT Int. Appl. WO0249459 20 pp.
- Dziezak, J. D. **1986**. Preservatives: antimicrobial agents. *Food Technol*. 40, 104–111.
- ETC web.  
<http://www.etcentre.org/divisions/mapd/english/SLIDES/indsc/indsc08.htm>)
- Fu, W. and Metaxas, A. **1994**. Numerical prediction of three-dimensional power density distribution in a multimode cavity. *J. Microwave Power and Electromagnetic Energy*. 29(2), 67-75.
- Ganzler, K.; Salgo, A.; and Valko, K. **1986**. Microwave extraction: a novel sample preparation method for chromatography.” *Journal of Chromatography*. 371: 299-306.



- Ganzler, K. and Salgo, A. **1987**. Microwave-extraction - a new method superseding traditional Soxhlet extraction. *Z. Lebensm.-Unters. Forsch.* 84(4), 274-6.
- Ganzler, K.; Szinai, I.; and Salgo, A. **1990**. Effective sample preparation method for extracting biologically active compounds from different matrices by a microwave technique. *J. Chromatogr.* 520 257-62.
- Gao, Q. **1997**. Rapid determination of tannic acid in plant samples with microwave extraction. *Fenxi Ceshi Xuebao*. 16(3), 76-78.
- Gedye, R.; Smith, F.; Westaway, K.; Ali, H.; Baldisera, L.; Laberge, L.; and J. Rousell. **1986**. The use of microwave ovens for rapid organic synthesis. *Tetrahedron Lett.* 27(3): 279-82.
- Giguere, R. J., Bray, T. L., Duncan, S. M.; Majetich, G. **1986**. Application of commercial microwave ovens to organic synthesis. *Tetrahedron Letters* 27(41), 4945-8.
- Grieco, P., Campiglia, P., Gomez-monterrey, I., Lama, T., and Novellino, E. 2003. Rapid and efficient methodology to perform macrocyclization reactions in solid-phase peptide chemistry. *Synlett* 14, 2216-2218.
- Guillot, R., Loupy, A., Meddour, A., Pellet, M., and Petit, A.. 2005. Solvent-free condensation of arylacetonitrile with aldehydes. *Tetrahedron* 61(42), 10129-10137.
- Guntert, M.; Krammer, G.; Lambrecht, S.; Sommer, H.; Surburg, H. and Werkhoff, P. **2001**. Flavor chemistry of peppermint oil (*Mentha piperita* L.). ACS Symposium Series. 794 (Aroma Active Compounds in Foods), 119-137.
- Hao, J; Huang, R.; Wang, P; and Deng, X. **2000**. Study on microwave extraction of orris root. *Xiangliao Xiangjing Huazhuangpin*. 4, 12-17.
- Hao, J.Y.; Han, W.; Huang, S.; Xue, B.Y.; Deng, X. **2002**. Microwave-assisted extraction of artemisinin from *Artemisia annua* L. *Separation and Purification Technology*. 28, 191-196.
- Harada, S.; Ohara, H. and Nishimura, O. **2002**. Method for modification of mentha essential oil. *Jpn. Kokai Tokkyo Koho*. JP 2002038187 6 pp.

- Harms, P.H.; Chen, Y.; Mittra, R.; and Shimony, Y. **1996**. Numerical modeling of microwave heating systems. *J. Microwave Power and Electromagnetic Energy*. 31(2), 114-121.
- Hu, C.; Kitts, D.D. **2001**. Free radical scavenging capacity as related to antioxidant activity and ginsenoside composition of Asian and North American ginseng extracts. *Journal of the American Oil Chemists' Society*. 78, 249-255.
- Huang, R.; Hao, J.; and Wang, P. **2000**. Study of microwave extraction of orris root. *Jingxi Huagong*. 17(11), 640-642.
- Hulls, P.J. **1982**. Development of the industrial use of dielectric heating in the United Kingdom. *Journal of Microwave Power*. 17 (1), 29-38.
- Iskander, M.F. **1993**. Computer Modeling and Numerical Simulation of Microwave Heating Systems. *MRS bulletin*. 18(11) 30-36.
- Langa, F., De La Cruz, P., De La Hoz, A., Diaz-Ortiz, A., and Diez-Barra, E. Microwave irradiation: more than just a method for accelerating reactions. *Contemporary Organic Synthesis*, 1997, 4(5), 373-386.
- LeBlanc, G. **1999**. Microwave-accelerated techniques for solid sample extraction. *LC-GC Current trends and developments in sample preparation*. 17(6s), S30-S37.
- Lee, S.; Lee, K. M.; Park, K. A.; and Hong, I. K. **2000**. Microwave assisted solvent extraction (MASE) of rice bran oil. *Kongop Hwahak*. 11(1), 99-104.
- Letellier, M. and Budzinski. **1999**. Microwave assisted extraction of organic compounds. *Analisis*. 27, 259-271.
- Li, T.S.C., Mazza, G., Cottrell, A.C. and Gao, L. **1996**. Ginsenosides in roots and leaves of American ginseng. *J. Agric. Food Chem*. 44, 717-720
- Li, R. Q. and Yan, H. **2005**. A new method for synthesizing 1,4-dihydropyridine under microwave. *Hecheng Huaxue* 13(6), 597-599.
- Li, R. and Jin, M. **2000**. Microwave extraction of Ginkgo biloba flavone glycosides. *Shipin Kexue*. 21(2), 39-41.
- Liao, X.; Raghavan, G.S.V.; and Yaylayan, V.A. **2002**. A novel way to prepare n-

- butylparaben under microwave irradiation. *Tetrahedron Letters*, 43, 45–48.
- Liu, C.; Bai, F.; Feng, P.; Miao, W.; and Su, Z. **2000**. Trehalose extraction from *saccharomyces cerevisiae* after microwave treatment. *Huagong Xuebao (Chin. Ed.)*. 51(6), 810-813.
- Liu, D.; Li, B.; Liu, Y.; Attele, A. S.; Kyle, J. W.; Yuan, C.S. **2001**. Voltage-dependent inhibition of brain Na<sup>+</sup> channels by American ginseng. *European Journal of Pharmacology*. 413, 47-54.
- Ljubojevic, S. **2000**. Antioxidative activity of ethanol extract of mint, sage, vitamin E and synthetic antioxidant BHT. Prague 2000, International Symposium & Exhibition on Environmental Contamination in Central & Eastern Europe, Proceedings, 5th, Prague, Czech Republic, Sept. 12-14, 2000, p1492-1497.
- Loupy, A. **2004**. Solvent-free microwave organic synthesis as an efficient procedure for green chemistry. *Comptes Rendus Chimie* 7(2), 103-112.
- Jean, F. I.; Collin, G. J.; and Lord, D. **1992**. Essential oils and microwave extracts of cultivated plants. *Perfum. Flavor*. 17(3), 35-41.
- Kalra, Y. P.; Maynard, D. G.; and Radford, F. G. **1989**. 16. Microwave digestion of tree foliage for multi-element analysis. *Can. J. For. Res.* 19(8), 981-5.
- Kovacs, A.; Ganzler, K.; and Simon-Sarkadi, L. **1998**. Microwave-assisted extraction of free amino acids from foods. *Z. Lebensm.-Unters. Forsch. A*. 207(1), 26-30.
- Kunz, S.K. and Luebbers, J.R. **1993**. The finite difference time domain method for electromagnetics. CRC press.
- Ma, L.; Paul, D.L. and Potheary, N. **1995**. Experimental validation of combined electromagnetic and thermal FDTD model of a microwave heating process. *IEEE transactions on microwave theory and technologies*. 43(11), 2565 – 2572.
- Maffei, M.; Chialva, F. and Sacco, T. **1989**. Glandular trichomes and essential oils in developing peppermint leaves I. variation of peltate trichome number and terpene distribution within leaves. *New phytologist*. 111(4), 707-716.

- Mattina, M. J. I.; Berger, W. A. I; and Denson, C. L. **1997**. Microwave-Assisted Extraction of Taxanes from Taxus Biomass. *J. Agric. Food Chem.* 45(12), 4691-4696.
- Meybeck, A.; Dumas, M.; Chaudagne, C.; Bonte, F. Cosmetic and pharmaceutical preparations containing Rb1 ginsenosides for stimulating elastin synthesis. *PCT Int. Appl. WO* 9907338, **1999**; 29 pp.
- Meredith, R.J. **1994**. A three axis model of the mode structure of multimode cavities. *J. Microwave Power and Electromagnetic Energy.* 29(1), 31-44.
- Mingos, D.M.P and Baghurst, D.R. **1991**. Application of microwave dielectric heating effects to synthetic problems in chemistry. *Chemical society reviews*, 20: 1.
- Mittra, R. and Harms, P.H. **1993**. A new finite-difference-time-domain (FDTD) algorithm for efficient field computation in resonator narrow-band structures. *IEEE Microwave Guided Wave lett.* 3, 316-318.
- Moghaddam, F., Boeini, H., and Zargarani, D. 2005. Solvent-free synthesis of tri-substituted thiophenes via thio-Claisen rearrangement under microwave irradiation: A convenient route to novel tertiary 2-thienyl amines. *Journal of Sulfur Chemistry* 26(4-5), 331-335.
- Mudgett, R.E. **1989**. Microwave food processing. *Food Technology.* 43 (1), 117-126.
- Nanjunda Swamy, S., Basappa, Sarala, G., Priya, B. S., Gaonkar, S. L., Shashidhara Prasad, J., and Rangappa, K. S. **2006**. Microwave-assisted synthesis of N-alkylated benzotriazole derivatives: Antimicrobial studies. *Bioorganic & Medicinal Chemistry Letters* 16(4), 999-1004.
- Ni, X.; Bai, J.; Sun, X.; Chen, C.; Sha, X.; Yu, D. **2001**. Studies on anti-anxiety effects of saponin extracted from root or stem and leaf of panax ginseng in elevated cross-maze. *Zhongcaoyao (in Chinese).* 32, 238-241.
- Nykqvist, W.E. and Decareau, R.V. **1976**. Microwave meat roasting. *J. Microwave Power.* 11, 3-24.

- Pan, X.; Liu, H.; Jia, G.; and Shu, Y. **2000**. Microwave-assisted extraction of glycyrrhizic acid from licorice root. *Biochem. Eng. J.* 5(3), 173-177. Pan, X.; Niu, G. and Liu, H. Microwave-assisted extraction of tea polyphenols and tea caffeine from green tea leaves. *Chemical Engineering and Processing*. 2003, 42, 129-133.
- Pan, X.; Niu, G. and Liu, H. Comparison of microwave-assisted extraction and conventional extraction techniques for the extraction of tanshinones from *Salvia miltiorrhiza bunge*. *Biochemical Engineering Journal*. 2002, 12, 71-77.
- Pastor, A.; Vazquez, E.; Ciscar, R.; and de la Guardia, M. **1997**. Efficiency of the microwave-assisted extraction of hydrocarbons and pesticides from sediments. *Anal. Chim. Acta*. 344(3), 241-249.
- Paré, J.R.J.; Sigouin, M.; and Lapointe, J. **1991**. *US patent 5 002 784*. (Various international counterparts).
- Pare, J. R. J. and Belanger, J. M. R. **1994**. Microwave-Assisted Process (MAP): a new tool for the analytical laboratory. *Trends Anal. Chem.* 13(4), 176-84.
- Pare, J.R.J. and Belanger, J.M.R. **1997**. Microwave-assisted process (MAP): Principles and Applications. In *Instrumental methods in Food Analysis*; Pare, J.R.J., Belanger, J.M.R., Eds.; Elsevier: Amsterdam, 1997, pp 395-420.
- Pare, J.R.J. **1994**. *US patent 5338557*. Various international counterparts.
- Pare, J.R.J. **1995**. *US patent 548897*. Various international counterparts.
- Pastor, A.; Vazquez, E.; Ciscar, R. and de la Guardia, M. **1997**. Efficiency of the microwave-assisted extraction of hydrocarbons and pesticides from sediments. *Anal. Chim. Acta*. 344(3), 241-249.
- Perreux, L. and Loupy, A. **2001**. A tentative rationalization of microwave effects in organic synthesis according to the reaction medium, and mechanistic considerations. *Tetrahedron* 57(45), 9199-9223.

- Pittler, M. H. and Ernst, E. **1998**. Peppermint Oil for Irritable Bowel Syndrome: A Critical Review and Metaanalysis. *The American journal of gastroenterology*. 93 (7), 1131 – 1135.
- Pino, J. A.; Borges, P.; Martinez, M. A.; Vargas, M.; Flores, H.; Del Campo, S.T. M. and Fuentes, V. **2002**. Essential oil of *Mentha piperita* L. grown in Jalisco. *Journal of Essential Oil Research*. 14(3), 189-190.
- Robach, M. C. **1980**. Use of preservatives to control microorganisms in food. *Food Technol.* 34, 81–84.
- Ren, G. and Chen, F. **1999**. Degradation of Ginsenosides in American Ginseng (*Panax quinquefolium*) Extracts during Microwave and Conventional Heating *J. Agric. Food Chem.* 47, 1501-1505.
- Ribeiro, M. A.; Martins, M. M.; Esquivel, M. M.; Bernardo-Gil, M. G. **2002**. Peppermint supercritical CO<sub>2</sub> extraction. Influence of extraction conditions on the antioxidant activity of the residues. *Informacion Tecnologica*. 13(3), 185-190.
- Ryu, S. K.; Kim, W. S.; Yu, J. H. **1979**. Studies on the extraction of korean ginseng compoment. *Korean J. Food Sci. Technol.* 11, 118-121.
- Ryynane, S. **2002**. Microwave heating uniformity of multicomponent prepared foods. Academic dissertation, University of Helsinki.
- Seifert, P.; Bertram, C.; and Chollet, D. **2000**. Microwave extraction of botanicals. A high tech green approach. *SOFW J.* 126(1/2), 3-4, 6-9.
- Soni, M. G., Burdock, G. A., Taylor, S. L., and Greenberg, N. A. **2001**. Safety assessment of propyl paraben: a review of the published literature. *Food and Chemical Toxicology*, 39(6), 513-532.
- Spiro, M. and Chen, S. S. **1995**. Kinetics of isothermal and microwave extraction of essential oil constituents of peppermint leaves into several solvent systems. *Flavour Fragrance J.* 10(4), 259-72.
- Stangler, H.S.; Hadolin, M.; Knez, Z. and Bauman, D. 2001. Antioxidant and emulsification efficiency of active components of Labiatae. *Zbornik*

Referatov s Posvetovanja Slovenski Kemijski Dnevi, Maribor, Slovenia,  
Sept. 20-21, 2001(Part 2), 856d/1-856d/6.

- Stripp, A. R. and Bogen, C. D. **1989**. The rapid decomposition of biological materials by using a microwave acid digestion bomb. *J. Anal. Toxicol.* 13(1), 57-59.
- Stuerga, D. and Delmotte, M. **2002**. Wave-material interactions, microwave technology and equipment. In *Microwaves in Organic Synthesis*, Ed. Loupy, A. Published by Wiley-VCH Verlag GmbH & Co. KGaA, Weinheim, 2002, pp 1-33.
- Sullivan, M.D. **2000**. Electromagnetic simulation using the FDTD method. IEEE press series on RF and Microwave Technology. New York.
- Sung, H. S.; Yang, J. W. **1986**. Effect of the heating treatment on the stability of saponin in white ginseng. *J. Korean Soc.Food Nutr.* 15,22-26.
- Thompson, J.E.; Simpson, T.L.; Caulfield, J.B. **1978**. Thermographic Tumor Detection Enhancement Using Microwave Heating. *IEEE Transactions on Microwave Theory and Techniques.* 26(8): 573 -580.
- Tulasidas, T.N.; Raghavan, G.S.V.; and Norris, E.R. **1993**. Microwave and convective drying of grapes. *Transactions of the ASAE.* 36 (6) p. 1861-1865.
- van Remmen, H.J.H.; Ponne, T.C.; Nijhuis, H.H.; Bartels, V.N.; and Kerkhof, J.A.M. **1996**. Microwave heating distributions in slabs, spheres, and cylinders with relation to food processing. *J. Food sci.* 61(6) 1105-1113.
- Varma, R. S.; Kumar, D. **1999**. Microwave-Accelerated Solvent-Free Synthesis of Thioketones, Thiolactones, Thioamides, Thionoesters, and Thioflavonoids. *Organic Letters* 1(5), 697-700.
- Vega, J. A., , Senida Cueto, A. R., Vaquero, J. J., Garcfa-Navio, J. L., Alvarez-Builla, J. **1996**., A Microwave Synthesis of the *c/s* and *trans* Isomers of 3-Hydroxy-2-(4-methoxyphenyl)-2,3-dihydro-1,5-benzothiazepin-4(5H)-one: The influence of Solvent and Power Output on the Diastereoselectivity. *Tetrahedron Letters*, 37( 35), 6413-6416.

- Villemin, D., Martin, B., Puciova, M., Toma, S. **1994**. Dry synthesis under microwave irradiation: synthesis of ferrocenylenones. *Journal of Organometallic Chemistry* 484(1-2), 27-31.
- Villemin, D., Martin, B., Khalid, M. **1998**. Dry reaction on KF-alumina: synthesis of 4-arylidene-1,3-(2H,4H)-isoquinolinediones. *Synthetic Communications* 28(17), 3195-3200.
- Wang, X.; Sakuma, T.; Asafu-Adjaye, E. and Shiu, G.K. **1999**. Determination of ginsenosides in plant extracts from *Panax ginseng* and *Panax quinquefolius* L. by LC/MS/MS. *Anal. Chem.* 71, 1579 – 1584.
- Wang, Y.; Bonilla, M.; McNair, H.M.; and Khaled, M. **1997**. Solid phase microextraction associated with microwave assisted extraction of food products. *J. High Resolut. Chromatogr.* 20(4), 213-216.
- Williams, O.J, Raghavan, G.S.V., Orsat V. and Dai, J. Microwave assisted extraction of capsaicinoids from capsicum fruit. *Journal of Food Biochemistry* 2004, 28, 113-122.
- Wu, Jie. **2006**. General microwave-assisted protocols for the expedient synthesis of furo[3,2-c]chromen-4-ones. *Chemistry Letters* 35(1), 118-119.
- Yazdani, D.; Jamshidi, A. H. and Mojab, F. **2002**. Comparison on menthol content of cultivated peppermint at different regions of Iran. *Faslnamah-i Giyahan-i Daruyi.* 1(3), 73-77, 93.
- Yee, K.S. **1996**. Numerical solution of initial boundary value problems involving Maxwell's equations in isotropic media. *IEEE trans. on Antennas and Propagation.* AP-17, 585-589.
- Yuan, C.S.; Wang, X.; Wu, J. A.; Attele, A. S.; Xie, J.T.; Gu, M. **2001**. Effects of *panax quinquefolius* L. on brainstem neuronal activities: Comparison between Wisconsin-cultivated and Illinois-cultivated roots. *Phytomedicine.* 8, 178-183.
- Zhang, Z.; Zhang, M.; Zhan, D.; Wang, A. **1998**. New method for synthesis of p-hydroxybenzoic acid esters. *Huagong Shikan.* 12, 24–25.



- Zhong, Y.L., Zhou, H., Gauthier, D. R. and Askin, D. **2006**. Efficient synthesis of functionalized pyrimidones via microwave-accelerated rearrangement reaction. *Tetrahedron Letters* 47(8), 1315-1317.
- Zhou, L.; Puri, V.M.; Anantheswaran, R.C. and Yeh, G. **1995**. Finite element modeling of heat and mass transfer in food materials during microwave heating – model development and validation. *J. Food Engineering*. 25, 509-529.
- Zhou, D.L.; Kitts, D.D. **2002**. Peripheral blood mononuclear cell production of TNF- $\alpha$  in response o North American ginseng stimulation. *Canadian Journal of Physiology and Pharmacology*. 80, 1030-1033.
- Zhu, R., Hong, P., Dai, S. **1994**. Study on the "dry reaction" without any medium under microwave irradiation. *Synthetic Communications* 24(17), 2417-21.
- Zlotorzynski, A. **1995**. The application of microwave radiation to analytical and environmental chemistry. *Critical reviews in Analytical Chemistry*. 25 (1), 43-76.
- Zuo, X.; Ma, S.; Hou, Z. **2001**. Study on processing of American ginseng-pumpkin health beverage containing Bifidobacteria promoting factor. *Shipin Gongye Keji* (in Chinese)., 22, 70-71.

## Appendix 1.

```
//*****
// Microwave E field and Power dissipation simulation program
//*****
// Program author: Mr. Jianming Dai
//           McGill University
//           Department of Bioresource Engineering
//           21,111 lakeshore road
//           Ste-Anne-de-Bellevue
//           QC, H9X 3V9, Canada
//           Tel. 0514-4571539, jdai@corn-poppy.com
//
// Date of this version: Jan 23, 2006
//
// This program is written for the PhD thesis of Mr. Jianming Dai
// The purpose of this program is to simulate the microwave E field distribution
// as well as the Power dissipation into lossy dielectric materials in a
microwave
// cavity or a waveguide applicator. This program is written in C language and
// compiled with Microsoft visual C++ software.
//
// Part of the code and parameter definition was adopted from 'TOYFDTD',
// the author wishes to acknowledge
// the TOYFDTD group for this.
//*****
... ..
main()
{
.....
ny = 3;
dy = OVEN_WIDTH/ny;
```

```

while(dy >= lambda/25.0)
{
    ny++;
    dy = OVEN_WIDTH/ny;
}

dt = 1.0/(LIGHT_SPEED*sqrt(1/(dx*dx) + 1.0/(dy*dy) + 1.0/(dz*dz)));
// time in seconds that will be simulated by the program:
totalSimulatedTime = MAXIMUM_ITERATION*dt;

ic = (int)(nx/2); //+nx_guide;
jc= (int)(ny/2);

// constants used in the field update equations:
.....
////////////////////////////////////

ca = (double ***)malloc((nx)*sizeof(double **));
for(i=0; i<(nx); i++)
{
    ca[i] = (double **)malloc((ny+1)*sizeof(double *));
    for(j=0; j<(ny+1); j++)
    {
        ca[i][j] = (double *)malloc((nz+1)*sizeof(double));
        for(k=0; k<(nz+1); k++)
        {
            ca[i][j][k]=1.0;
            //sigma[i][j][k] = 0.0;
        }
    }
}
}

```

```

allocatedBytes += ( (nx)*(ny+1)*(nz+1) * sizeof(double));

// allocate the array of relative dielectric constant:
// Allocate memory for the Absorbed Power arrays:
// allocate the array of loss factor:
// allocate the array of Absorbed power:
// Allocate memory for the E field arrays:
// allocate the array of average e:
// allocate the array of ex components:
// allocate the array of ey components:
// allocate the array of ez components:
// Allocate the H field arrays:
// allocate the array of hx components:
// allocate the array of hy components:
// allocate the array of hz components:
//Allocate epsilon_re and sigma vlaues.

//Simulate a plate with one cell thickness located horizontally in the cavity.By
changing the K value and the range of k
//one can make the plate as thick as they wish.

for (k=K; k<K+1; k++) {
    for (j=1; j<ny-1; j++) {
        for (i=1; i<nx-1; i++) {
            ca[i][j][k] = (1-
0.5*(dt*LOSS_FACTOR*OMEGA)/EPSILON_RE)/(1+0.5*(dt*LOSS_FACTOR*O
MEGA)/EPSILON_RE);

            cb[i][j][k]=1/(EPSILON_RE*(1+0.5*(dt*LOSS_FACTOR*OMEGA)/EPSILO
N_RE));

            loss[i][j][k]=LOSS_FACTOR;

```

}}

//Simulate a plate with one cell thickness vertically located in the cavity parallel to the power entry port.

//By changing the K value and the range of k one can make the plate as thick as they wish.

```
/*for (k=0; k<nz; k++) {
    for (j=J; j<J+1; j++) {
        for (i=0; i<nx; i++) {
            ca[i][j][k] = (1-
0.5*(dt*LOSS_FACTOR*OMEGA)/EPSILON_RE)/(1+0.5*(dt*LOSS_FACTOR*O
MEGA)/EPSILON_RE);

            cb[i][j][k]=1/(EPSILON_RE*(1+0.5*(dt*LOSS_FACTOR*OMEGA)/EPSILO
N_RE));

            loss[i][j][k]=LOSS_FACTOR;
        }
    }
} */
```

//Simulate a plate with one cell thickness vertically located in the cavity facing to the power entry port.

//By changing the K value and the range of k one can make the plate as thick as they wish.

```
/*for (k=0; k<nz; k++) {
    for (j=0; j<ny; j++) {
        for (i=l; i<l+1; i++) {
            ca[i][j][k] = (1-
0.5*(dt*LOSS_FACTOR*OMEGA)/EPSILON_RE)/(1+0.5*(dt*LOSS_FACTOR*O
MEGA)/EPSILON_RE);
```

```

        cb[i][j][k]=1/(EPSILON_RE*(1+0.5*(dt*LOSS_FACTOR*OMEGA)/EPSILO
N_RE));

```

```

        loss[i][j][k]=LOSS_FACTOR;

```

```

    }}} */

```

```

/* for (k=0; k<=CYLINDER_HEIGHT; k++) {

```

```

    // for (k=0; k<=nz; k++) {

```

```

        for (j=0; j<ny; j++) {

```

```

            for (i=0; i<nx; i++) {

```

```

                xdist=(ic-i);

```

```

                ydist=(jc-j);

```

```

                dist=sqrt(pow(xdist,2.) + pow(ydist,2.));

```

```

                if(dist<=RADIUS) {

```

```

                    ca[i][j][k] = (1-

```

```

0.5*(dt*LOSS_FACTOR*OMEGA)/EPSILON_RE)/(1+0.5*(dt*LOSS_FACTOR*O
MEGA)/EPSILON_RE);

```

```

        cb[i][j][k]=1/(EPSILON_RE*(1+0.5*(dt*LOSS_FACTOR*OMEGA)/EPSILO
N_RE));

```

```

        loss[i][j][k]=LOSS_FACTOR;}

```

```

    }}}/}*/

```

```

// main loop:

```

```

for(iteration = 0; iteration < MAXIMUM_ITERATION; iteration++)

```

```

{
    // mainloop

```

```

    // Output section:

```

```

    if ( (iteration % PLOT_MODULO) == 0)

```

```

    {

```

```

sprintf(filename, "E%05d.bin", iteration);
sprintf(filename2, "P_abs%05d.bin", iteration);

while ((openFilePointer2 = fopen(filename2, "wb")) == NULL)
{
    // if the file fails to open, print an error message to
    // standard output:
    fprintf(stderr, "Difficulty opening P_abs%05d.bin", iteration);
    perror(" ");
}

for(k=0; k<(nz); k++)
{
    for(j=0; j<(ny); j++)
    {
        for(i=0; i<(nx); i++)
        {
            e[i][j][k]=sqrt(ex[i][j][k]*ex[i][j][k] + ey[i][j][k]*ey[i][j][k] +
ez[i][j][k]*ez[i][j][k]);
            fwrite(&e[i][j][k], sizeof(double), 1, openFilePointer);
            fwrite(&p_absorb[i][j][k], sizeof(double), 1,
openFilePointer2);
        }
    }
    fclose(openFilePointer);
    fclose(openFilePointer2);
} // end output section

//define stimulus
stimulus = 2.92*sin(omega*currentSimulatedTime); //2.92 is
calculated for the 1 KW power
// }

```

```

//define the power entry
    // set all vectors on the x=0 face to the value of stimulus:
    /*  for (i=0; i<(1); i++)
        {
            for(j=0; j<(ny+1); j++)
            {
                for(k=0; k<nz; k++)
                {
                    ez[i][j][k] = stimulus;
                }
            }
        } */

    /*  for (i=0; i<(1); i++)
        {
            for(j=0; j<ny_guide+1; j++)
            {
                for(k=0; k<nz_guide; k++)
                {
                    ez[i][j][k] = 0;
                }
            }
        } */

    for (i=0; i<(1); i++)
    {
        for(j=((int)(ny/2)-8); j<=((int)(ny/2)+8); j++)
        {
            for(k=((int)(nz/2)-4); k<=((int)(nz/2)+4); k++)
            {
                ez[i][j][k] = stimulus;
            }
        }
    }

```



```
} } }
```

```
//ez[0][(int)(ny/2)][(int)(nz/2)] = stimulus;
```

```
// Update the hx values:
```

```
for(i=0; i<nx-1; i++)
{
    for(j=0; j<ny; j++)
    {
        for(k=0; k<nz; k++)
        {
            //hx[i][j][k] += 0.5*((ey[i+1][j][k+1] - ey[i+1][j][k]) -
            // (ez[i+1][j+1][k] - ez[i+1][j][k]));
            hx[i][j][k] += (dtmudz*(ey[i+1][j][k+1] - ey[i+1][j][k]) -
            dtmudy*(ez[i+1][j+1][k] - ez[i+1][j][k]));
        }
    }
}
```

```
// Update the hy values:
```

```
// Update the hz values:
```

```
// Update the ex values:
```

```
// Update the ey values:
```

```
// Update the ez values:
```

```
//calculate the effective e field by taking the sqrt of the three vectorial
components
```

```
for(k=0; k<(nz); k++)
{
```

```

        for(j=0; j<(ny); j++)
        {
            for(i=0; i<(nx); i++)
            {
                e[i][j][k]=sqrt(ex[i][j][k]*ex[i][j][k] + ey[i][j][k]*ey[i][j][k] +
ez[i][j][k]*ez[i][j][k]);
            }
        }

```

//Power absorbed by the lossy dielectric material

```

for(i=0; i<(nx); i++)
{
    for(j=0; j<(ny); j++)
    {
        for(k=0; k<(nz); k++)
        {
            p_absorb[i][j][k]
+=dt*loss[i][j][k]*EPSILON_0*OMEGA*e[i][j][k]*e[i][j][k];
        }
    }
}

```

////////////////////////////////////

// PEC boundary conditions:

// The PEC condition is enforced by setting the tangential E field  
//components on the PEC faces of the mesh to zero every timestep  
//(except the stimulus face). This has been already true through  
//the previous initialization to be zero throughout the working space.  
} // end mainloop

////////////////////////////////////

// Output section:

```

if ( (iteration % PLOT_MODULO) == 0)
{
    sprintf(filename, "E%05d.bin", iteration);
    // open a new data file for this iteration:
    while ((openFilePointer = fopen(filename, "wb")) == NULL)
        {
            // if the file fails to open, print an error message to
            // standard output:
            fprintf(stderr, "Difficulty opening Ez%05d.bin", iteration);
            perror(" ");
        }

    sprintf(filename2, "P_abs%05d.bin", iteration);
    // open a new data file for this iteration:
    while ((openFilePointer2 = fopen(filename2, "wb")) == NULL)
        {
            // if the file fails to open, print an error message to
            // standard output:
            fprintf(stderr, "Difficulty opening P_abs%05d.bin", iteration);
            perror(" ");
        }
    for(k=0; k<(nz); k++)
    {
        for(j=0; j<(ny); j++)
        {
            for(i=0; i<(nx); i++)
            {
                e[i][j][k]=sqrt(ex[i][j][k]*ex[i][j][k] + ey[i][j][k]*ey[i][j][k] +
ez[i][j][k]*ez[i][j][k]);
                fwrite(&e[i][j][k], sizeof(double), 1, openFilePointer);
                fwrite(&p_absorb[i][j][k], sizeof(double), 1,
openFilePointer2);
            }
        }
    }
}

```

```
    }    }    }
```

```
    // close the output file for this iteration:
```

```
    fclose(openFilePointer);
```

```
        fclose(openFilePointer2);
```

```
    }// end bob output section
```

```
// end main
```

## Appendix 2:

```
//*****  
//  Microwave E field and Power dissipation visualization program  
//*****  
//  Program author: Mr. Jianming Dai  
//          McGill University  
//          Department of Bioresource Engineering  
//          21,111 lakeshore road  
//          Ste-Anne-de-Bellevue  
//          QC, H9X 3V9, Canada  
//          Tel. 0514-4571539, jdai@corn-poppy.com  
//  
//  Date of this version: Jan 23, 2006  
//  
//  This program is written for the PhD thesis of Mr. Jianming Dai  
//  The purpose of the program is to get a section in X, Y, Z direction in 2-D  
array.  
//  The 2-D files created are used by the Matlab code to visualize in  
//  graphical method  
//*****  
// the includes  
// the defines  
main()  
{  
//define variables  
    //inpute parameter for files  
    fprintf(stdout, "The iteration number of the file to be read: \n");  
    scanf("%d", &iteration);  
    flushall();
```

```

//open files
sprintf(E_3DFile, "E%05d.bin", iteration);
    sprintf(filename2, "Ez2%05d.dat", iteration);
    // open a new data file for this iteration:
while ((openFilePointer = fopen(E_3DFile, "rb")) == NULL)
{
    // if the file fails to open, print an error message to
        // standard output:
    fprintf(stderr, "Difficulty opening E%05d.bin", iteration);
    perror(" ");
}
//Conversion section
e = (double ***)malloc((Nx+1)*sizeof(double **));
for(i=0; i<(Nx+1); i++)
{
    e[i] = (double **)malloc((Ny+1)*sizeof(double *));
    for(j=0; j<(Ny+1); j++)
    {
        e[i][j] = (double *)malloc((Nz)*sizeof(double));
        for(k=0; k<(Nz); k++)
        {
            e[i][j][k] = 0.0;
        }
    }
}
allocatedBytes += ( (Nx+1)*(Ny+1)*(Nz) * sizeof(double));

p = (double ***)malloc((Nx+1)*sizeof(double **));
for(i=0; i<(Nx+1); i++)
{
    p[i] = (double **)malloc((Ny+1)*sizeof(double *));

```

```

for(j=0; j<(Ny+1); j++)
{
    p[i][j] = (double *)malloc((Nz)*sizeof(double));
    for(k=0; k<(Nz); k++)
    {
        p[i][j][k] = 0.0;
    }
}
}
allocatedBytes += ( (Nx+1)*(Ny+1)*(Nz) * sizeof(double));
... ..
    fclose(openFilePointer);
    ... ..
}

//end main

```

### Appendix 3: matlab code to visualize the E and Power dissipation

```
%//*****
%//  Microwave E field and Power dissipation visualization program
%//*****
%//  Program author: Mr. Jianming Dai
%//      McGill University
%//      Department of Bioresource Engineering
%//      21,111 lakeshore road
%//      Ste-Anne-de-Bellevue
%//      QC, H9X 3V9, Canada
%//      Tel. 0514-4571539, jdai@corn-poppy.com
%//
%//  Date of this version: Jan 23, 2006
%//
%//  This program is written for the PhD thesis of Mr. Jianming Dai
%//  The purpose of the program is to visualize both E field distribution
%//  and the Power dissipation into lossy dielectric material in a
%//  microwave cavity. The data used here are obtained from the
%//  simulation program written in C and converted to 2-D files each one
%//  repreenting one plane in the 3-D space.
%//*****

clear all;
close all;

fprintf('\nVisualize 3D matrices\n');
fprintf('by a slit.\n');

% define the size of the array. The values are the same as obtained by the
% C simulation program
Nx =97;
```



```

fprintf('Number of smaplex in x-direction: Nx = %d\n', Nx);
Ny = 97;
fprintf('Number of smaplex in z-direction: Nz = %d\n', Ny);
Nz = 56;
fprintf('Number of smaplex in z-direction: Nz = %d\n', Nz);

%initialize the arrays
field1 = zeros(Nx,Ny);
field2=zeros(Ny,Nz);
field3=zeros(Nx,Nz);
help1 = zeros(Nx*Ny,1);
help2=zeros(Ny*Nz,1);
help3=zeros(Nx*Nz,1);

field4 = zeros(Nx,Ny);
field5=zeros(Ny,Nz);
field6=zeros(Nx,Nz);
help4 = zeros(Nx*Ny,1);
help5=zeros(Ny*Nz,1);
help6=zeros(Nx*Nz,1);

%read files obtained by the conversion program written in C
fid3 = fopen('E_xz03000_18.bin','rb');
fid2=fopen('E_yz03000_18.bin','rb');
fid1=fopen('E_xy03000_1.bin','rb');

fid6 = fopen('P_xz03000_18.bin','rb');
fid5=fopen('P_yz03000_18.bin','rb');
fid4=fopen('P_xy03000_1.bin','rb');

```

```
% The first Figure has 6 subplots representing the E field distribution and
% power dissipation using 'surfc' command to generate the 3-D surface view
% in XY, YZ, XZ planes.
```

```
fig = figure('Position',[100 100 200 450]);
figure(1);
```

```
subplot(3,2,1);
[help3,nread]=fread(fid3,Nx*Nz,'double');
%fprintf('Number of samples read: Nx*Nz = %d\n', nread);
```

```
for nz=0:Nz-1;
    for nx=1:Nx
        field3(nx, Nz-nz) = help3(nx + nz*Nx,1);
    end
end
```

```
fprintf('%d ',field3);
surfc(field3);
%axis([1 Nz 1 Nx -100 800]);
shading interp;
```

```
title('E density in XZ plane');
colorbar;
grid on;
... ..
```

#### Appendix 4:

```
//*****  
// Microwave power dissipation by layers from the top to bottom and by circular  
// layers in the radius direction.  
//*****  
// Program author: Mr. Jianming Dai  
//           McGill University  
//           Department of Bioresource Engineering  
//           21,111 lakeshore road  
//           Ste-Anne-de-Bellevue  
//           QC, H9X 3V9, Canada  
//           Tel. 0514-4571539, jdai@corn-poppy.com  
//  
// Date of this version: Jan 23, 2006  
//  
// This program is written for the PhD thesis of Mr. Jianming Dai  
// The purpose of this program is to calculate the power dissipation into different  
// layers from the top to bottom and the circular layers from in the radius  
// direction.  
// This program is written in C language and compiled with Microsoft visual  
// C++  
// software.  
//*****  
// includes ...  
//defines ...  
  
main()  
{ //variables  
//allocate memories for arrays  
    P_abs = (double ***)malloc((l)*sizeof(double **));  
    for(i=0; i<(l); i++)
```

```

{
    P_abs[i] = (double **)malloc((J)*sizeof(double *));
    for(j=0; j<(J); j++)
    {
        P_abs[i][j] = (double *)malloc((K)*sizeof(double));
        for(k=0; k<(K); k++)
        {
            P_abs[i][j][k]=0.0;
            //sigma[i][j][k] = 0.0;
        }
    }
}

// allocatedBytes += ( (nx)*(ny+1)*(nz+1) * sizeof(double));

//open files
while ((inFilePointer = fopen("P_abs03000.bin", "rb")) == NULL)
    {
        // if the file fails to open, print an error message to
        // standard output:
        fprintf(stderr, "Difficulty opening P_abs03000.bin");
        perror(" ");
    }

    .....

    //read data files
    for(k=0; k<K; k++)
    {
        P_vertical = 0;
        for(j=0; j<J; j++)
        {
            for(i=0; i<I; i++)
            {
                fread(&P_abs[i][j][k], sizeof(double), 1, inFilePointer);
            }
        }
    }
}

```

```

        fprintf(stdout, "Total power dissipated in the %dth layer is:
%f\n", k, P_abs[i][j][k]);
        P_vertical+=35780000*P_abs[i][j][k];
    }
}

fprintf(outFilePointer1, "Total power dissipated in the %dth layer is:
%f\n", k, P_vertical);

fprintf(stdout, "Total power dissipated in the %dth layer is: %f\n",
k, P_vertical);
}

for (n_circle=1; n_circle < RADIUS; n_circle++)
{
for(k=0; k<K; k++)
{   for(j=0; j<J; j++)
    {
        for(i=1; i<I; i++)
        {
            xdist=(IC-i);
            ydist=(IC-j);
            dist=sqrt(pow(xdist,2.) + pow(ydist,2.));
            if(dist<=n_circle && dist >n_circle-1)
            {
                P_circular+=35780000*P_abs[i][j][k];
            }
        }
    }
}

fprintf(outFilePointer2, "Total power dissipated in the %dth circle is:
%f\n", n_circle, P_circular);

fprintf(stdout, "Total power dissipated in the %dth circle is: %f\n",
n_circle, P_circular);

P_circular =0;
}

```